Oxidized Lipid Species Promote Atherogenic Phenotypes in Innate and Adaptive Cells

By

Brenna Denise Appleton

Dissertation

Submitted to the Faculty of the

Graduate School of Vanderbilt University

in partial fulfillment of the requirements

for the degree of

DOCTOR OF PHILOSOPHY

In

Molecular Pathology & Immunology

December 16, 2023

Nashville, Tennessee

Approved:

Jeffrey C. Rathmell, Ph.D., Chair
Amy S. Major, Ph.D., Advisor
Thomas M. Aune, Ph.D.
Meenakshi S. Madhur, M.D., Ph.D.
Heather H. Pua, M.D., Ph.D.

For my parents, Caryn and John,

who told me it was ok to quit but gave me everything I needed to make sure I didn't.

Acknowledgements

I must begin by acknowledging my Principal Investigator, Dr. Amy S. Major for the training she has provided me with since I joined her lab in 2017. I came to graduate school a tentative student fresh out of undergrad with no formal training in immunology, and through my experiences in her lab I have grown into a self-assured scientist. I am thankful for the endless drafts she has revised and for every early morning harvest she has made possible. Amy has taught me the importance of good leadership and I will take the lessons I learned from her with me for the rest of my professional journey.

My training was also shaped by the members of my thesis committee: Dr. Jeffrey C. Rathmell (Chair), Dr. Thomas M. Aune, Dr. Meenakshi S. Madhur, and Dr. Heather Pua. Thank you for your time, expertise, and patience navigating through multiple project changes. I would like to specifically acknowledge Heather for informally adopting me into her lab during my early training to build my microRNA background, and Jeff for allowing me to practically live on his flow cytometers.

I would also like to thank my lab mates, past (Jillian, Jenny, Lilly, and Harrison) and present (Sydney, Meghan, and Sherry) for helping me through this process and always bringing joy and entertainment to the benches. Jillian and Jenny made up what I think of as my “Phase I” lab, and they were both integral in making me the scientist I am today through their example. Though they have long since left the lab, they have continued to be a part of my life, answering any and all questions I send their way and simply being my friends. My “Phase II” lab of Harrison, Sydney, and Lilly came much later, but was just as impactful to my experience. Though I was meant to be training

them, I think they gave much more, both in terms of their contributions to my work and the joy and good humor they brought to the lab. In particular, I would like to thank Sydney – not only has she directly contributed to every chapter in this thesis, but she is also one of my best friends and has picked me up and had my back more times than I can count through this experience. Sydney and I have recently been joined by Meghan and Sherry to make up the “Phase III” lab, and I’d like to acknowledge them for their encouragement and patience as I’ve worked through these final months of graduate school.

Outside of the laboratory walls, there are many people who helped me through my graduate school experience. Jordan, Bella, and Danielle were the first good friends I made in Nashville and the ones who made it into a home-away-from-home. Jenny, Chris, and Kara made me into a Bachelor(ette) viewer and gave me a great excuse to take a break each week, though I still contend I was more interested in seeing my friends than watching the show. From far away, Jacqueline and Jordan sent constant love and support, and I always looked forward to our phone calls and video chats. My pretend siblings (real people, fake siblings), Nichole, Alex, and Rebeka, all supported me in a multitude of ways whether it was planning one of my coolest vacations ever, or finding me my first apartment in Nashville, or making sure that despite my business I still knew about Squishmallows. Finally, my boyfriend Thomas has been an amazing source of support through the tail end of graduate school, doing everything from filling my fridge with food so I didn’t have to worry about cooking as I worked on this dissertation to making sure I got to scratch Dollywood off my Tennessee bucket list.

I am incredibly fortunate to have a large family – Joanie, Jeff, Jack, Charlie, Kathy, Joe, Janice, Hannah, Alivia, Cash, and Carol – rooting for me on from afar and every word of encouragement has meant so much. Last, but certainly not least, I would like to thank my parents, Caryn and John, for their truly unconditional love and support. My mom is my best friend and has walked beside me through this experience, holding me up at times, even though she was hundreds of miles away. My dad is my biggest cheerleader and always reminds me to be proud of the things I have accomplished and the woman I have become. I learned what hard work and dedication looked like through their example and I could not have done this without them.

Table of Contents

Page

Page

List of Tables

Page

List of Figures

Page

Page

Page

List of Abbreviations

ACLY: ATP citrate lyase

adLN: Aorta draining lymph node

ApoB: Apolipoprotein B

Bcl-2: B-cell lymphoma 2

BMDC: Bone marrow-derived dendritic cell

BMDM: bone marrow-derived macrophages

***C. albicans*:** *Candida albicans*

cDC: Conventional dendritic cell

CHIP-Seq: B-cell lymphoma 2

CLEC9A: C-type lectin domain family 9 member A

CTV: CellTrace Violet

CVD: Cardiovascular disease

DC: Dendritic cell

DUSP6: Dual-specificity phosphatase 6

ECM: Extracellular matrix

ER: Estrogen receptor

FcγR: Fc gamma receptor

GM-CSF: Granulocyte-macrophage colony-stimulating factor

haIC: Heat-aggregated IgG immune complex

HRT: Hormone replacement therapy

IFN-γ: Interferon-γ

IFNγR: IFN-γ receptor

IL: Interleukin

ILC: Innate lymphoid cells

KAP1: KRAB-associated protein 1

KRAB: Krüppel-associated box

LDL: Low-density lipoprotein

***Ldlr*$^{-/-}$:** Low-density lipoprotein receptor deficient

LNA: Locked-nucleic acid

LPS: Lipopolysaccharide

mcDC: Merocytic dendritic cell

MHC: Major histocompatibility complex

miRNA: microRNA

NC: Normal chow

NK: Natural killer cell

NKT: Natural killer T cell

oxLDL-IC: Oxidized low-density lipoprotein immune complex

oxLDL: Oxidized low-density lipoprotein

oxPAPC: Oxidized 1-palmitoyl-2-arachidonoyl-sn-glycero-3-phosphocholine

oxPL: Oxidized phospholipids

PCSK9: Proprotein convertase subtilisin/kexin type 9

pDC: Plasmacytoid dendritic cell

pSTAT1: Phosphorylated STAT1

***Pten*:** Phosphatase and tensin homolog

RA: Rheumatoid arthritis

RNAseq: RNA sequencing

ROS: Reactive oxygen species

SLE: Systemic lupus erythematosus

SMC: Smooth muscle cell

sRNAseq: Small RNA sequencing

T_{FH}: T follicular helper cell

T_{FR}: Regulatory T follicular cell

TGF-β: Transforming growth factor β

Th1: T helper 1

Th17: T helper 17

TLR: Toll-like receptor

TNF: Tumor necrosis factor

T_{reg}: Regulatory T cell

TREM: Triggering receptor expressed on myeloid cells 2

T_{res}: Responder T cell

UTR: Untranslated region

WD: Western diet

CHAPTER 1

Introduction

Portions of this chapter were adapted from the following manuscript published in Current Opinion in Rheumatology and used with permission:
Appleton BD, Major AS. The latest in systemic lupus erythematosus-accelerated atherosclerosis: related mechanisms inform assessment and therapy. *Current Opinion in Rheumatology*. 2021;33(2):211–218.

Atherosclerosis as an Inflammatory Disease

Cardiovascular disease (CVD) is the leading cause of death in the United States, accounting for approximately one million fatalities annually according to the American Heart Association[1]. Moreover, the most recent available data from the World Health Organization identified clinical manifestations of CVD, ischemic heart disease and stroke, as the top two causes of mortality worldwide[2]. Atherosclerosis, one of the most common forms of CVD, is characterized by thickening of the artery walls and is a precursor to these clinical events. Therefore, the need for a better understanding of the mechanisms contributing to atherosclerosis is great.

It is known that hyperlipidemia is a critical driver of atherosclerosis development. The concentrations of cholesterol-transporting low-density lipoproteins (LDL) and triglyceride-rich lipoproteins far exceed what is physiologically necessary in most modern humans, and both their concentration and duration of exposure are positively correlated with disease development[3–8]. Patients with familial hypercholesterolemia have chronically elevated LDL and develop premature atherosclerosis[9,10]. Conversely,

individuals with loss-of-function nonsense mutations in proprotein convertase subtilisin/kexin type 9 (*PCSK9*), a protein that increases LDL titers by causing degradation of LDL receptor, have less circulating LDL and significantly reduced frequency of cardiovascular events[11]. However. LDL directly contributes to the disease process as retention within the intima has been identified as an initiating step in atherosclerosis[12] (Figure 1.1). Therefore, the relationship between lipid levels and atherosclerosis is not just correlative.

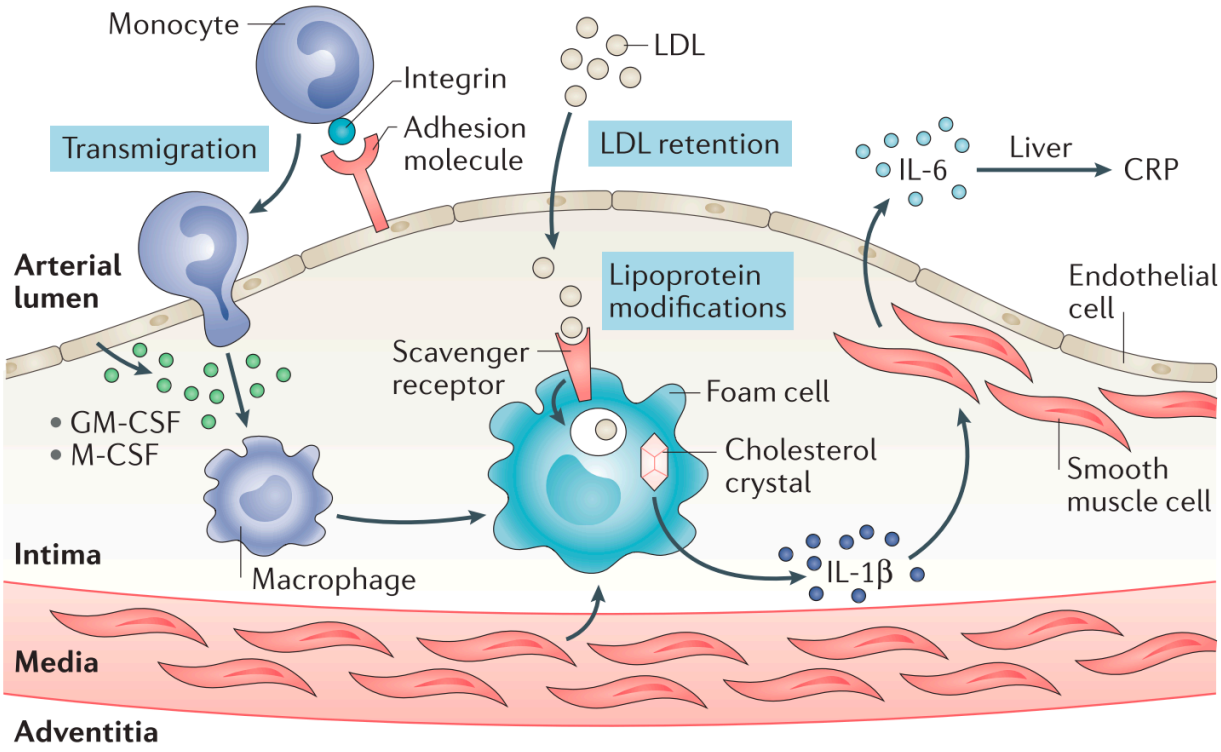

Figure 1.1. Initiation of atherosclerotic inflammation. LDL retention and oxidation within the intima drives monocyte recruitment leading to macrophage differentiation and foam cell formation after lipid loading. From (370). Copyright © Gisterå and Hansson. *Nature Reviews Nephrology*. Volume 13. 2017. Used with permission.

Despite the significant role lipids and lipoproteins play in the development of atherosclerosis, multiple lines of evidence indicate the immune system is a critical

mediator as well. In the 1980s, the inflammation-responsive pentraxin C-reactive protein was shown to be elevated in the plasma of myocardial infarction patients compared to subjects with exercise-induced angina[13], and was later identified as an independent risk factor for atherosclerosis[14,15]. Additionally, immune cells are present at sites of likely plaque development (e.g., aortic intima and fatty streaks) in children and young adults[16], indicating these cells are involved even in early stages of the disease process before formation of a mature plaque. Furthermore, many of the well-known risk factors for atherosclerosis like hypertension and type II diabetes involve activation of immune pathways[17–19]. Interestingly, accelerated atherosclerosis is a common co-morbidity of many autoimmune diseases like systemic lupus erythematosus (SLE), rheumatoid arthritis (RA), and type I diabetes[20](reviewed in [21]). In fact, it is estimated that women with SLE between the ages of 35 and 44 have a 50-fold increased risk of myocardial infarction compared with age- and gender-matched controls[22]. Even excluding pre-menopausal women who are typically protected from CVD[23], post-menopausal women with SLE are still five times more likely to develop atherosclerosis than healthy, age-matched controls[24]. Statin therapy, which significantly reduces LDL cholesterol levels[25], has been shown to provide less cardiovascular protection in SLE patients compared to the general population[26], suggesting that SLE-accelerated atherosclerosis is not entirely lipid dependent and has a significant immune component. Reflecting this, work from our lab has shown that atherosclerosis-susceptible mice have worsened disease with hematopoietic cells derived from a mouse model of SLE, even in the absence of high fat diet[27,28]. Collectively, these studies show atherosclerosis is truly a chronic disease of sterile inflammation.

Atherosclerosis Disease Progression

Initiation of atherosclerosis is generally thought to involve the retention of LDL in the intima where it becomes oxidized (oxLDL) through interaction with myeloperoxidase, lipoxygenase, and reactive oxygen species (ROS) present in the subendothelial space[12,29]. This modified lipoprotein induces the expression of adhesion molecules on endothelial cells causing recruitment of monocytes into the intima[30–32]. Monocytes then differentiate into macrophages that bind and internalize oxLDL through scavenger receptors[31,33]. Due to the high concentration of oxLDL in the environment, these macrophages become lipid-laden foam cells which tend to be stationary and are the basis of early fatty streaks that later develop into full lesions[33,34] (Figure 1.1). These plaque-resident macrophages proliferate, creating a positive feedback loop of increased foam cell accumulation and additional inflammatory cell recruitment[35].

As plaque progress, smooth muscle cells (SMCs) invade the lesion, secreting extracellular matrix (ECM) proteins that begin to form a fibrous cap on the plaque as well as ingesting lipid and contributing to the foam cell population[36,37]. Dendritic cells (DCs) activated in the lesion take up plaque-derived antigens and migrate to aorta draining lymph nodes (adLNs), or sometimes tertiary lymphoid organs that develop in the adventitia, where they activate naive T cells[38–41]. Activated T cells may migrate to the lesion to contribute directly to the inflammatory microenvironment[42,43] or provide help to B cells that will produce antibodies against plaque-specific epitopes like oxLDL[44–47](Figure 1.2). The presence of high oxLDL-specific IgM titers also suggests a T cell-independent B cell response[48].

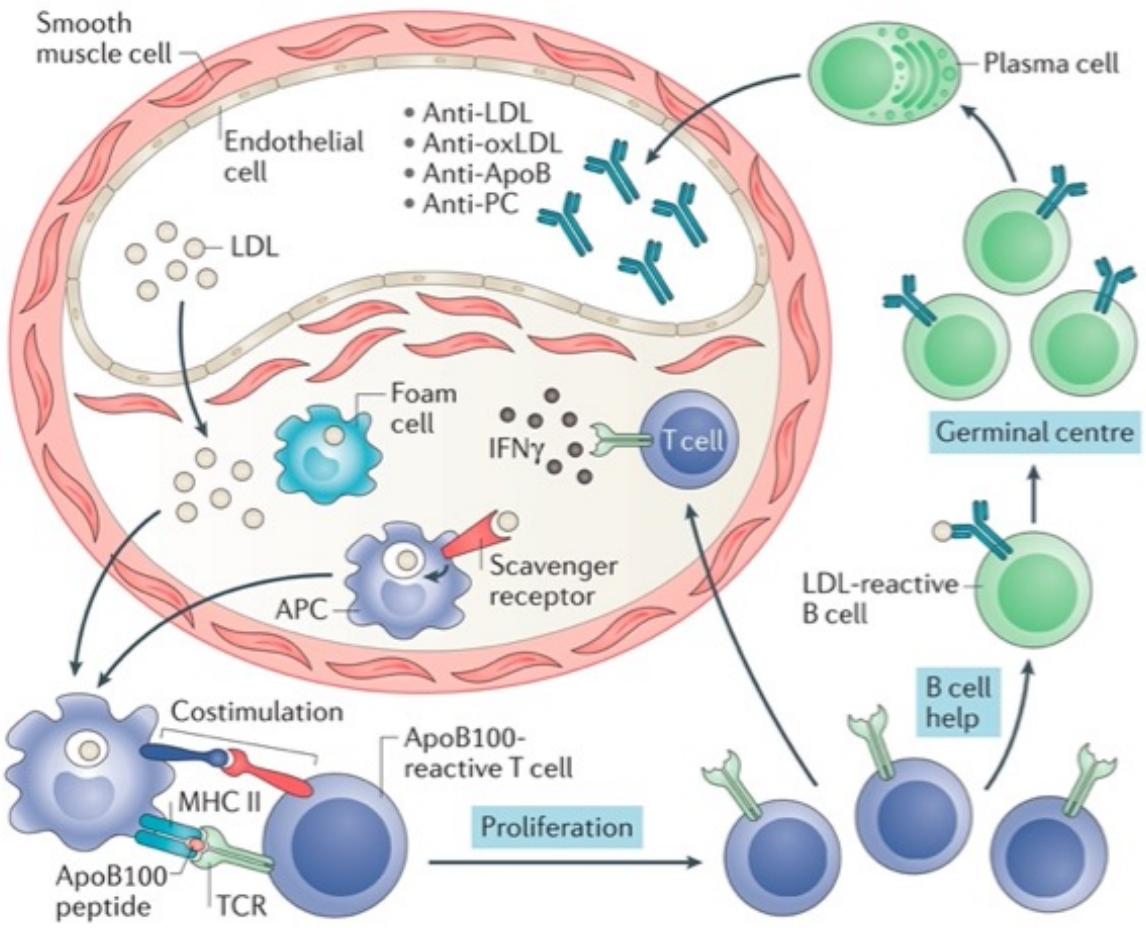

Figure 1.2. Progression of atherosclerotic inflammation. Antigen presenting cells (APCs) present plaque-derived antigens to activate T and B cells in aorta draining lymph nodes or tertiary lymphoid structures. From (373). Copyright © Gisterå and Hansson. *Nature Reviews Nephrology*. Volume 13. 2017. Used with permission.

Macrophages in Atherosclerosis

Macrophages are known to be critical to the development of atherosclerosis with early studies demonstrating that mice lacking macrophage colony stimulating factor are protected from disease[54]. Inflammatory macrophages derived from monocytes are one of the main populations involved in atherogenesis and are not found in non-diseased vessels. These cells are characterized by increased expression of major

histocompatibility complex (MHC) class II molecules, activating Fc gamma receptor (FcγR) I, co-stimulatory molecules CD80 and CD86, nitric oxide synthase 2, and proinflammatory cytokines interleukin (IL)-6, tumor necrosis factor (TNF), and IL-1β[55,56]. Another proinflammatory, atherosclerosis-specific subset known as type I interferon-inducible macrophages also arise from monocytes and have, as the name suggests, increased expression of interferon-inducible genes[55,57–59]. Together these proinflammatory populations aid plaque progression. The lipid-filled foam cells which accumulate in the developing lesions can be defined by triggering receptor expressed on myeloid cells 2 (TREM2)[55]. Counter to some earlier hypotheses about these foam cells, $TREM2^+$ macrophages have low expression of inflammatory genes and appear to have an inflammation resolving function[59,60]. These data were mostly obtained using mouse models, however, transcriptomic studies from human carotid endarterectomy samples suggest similar macrophage populations are present in atherosclerosis patients[61].

Dendritic Cells in Atherosclerosis

There are many different populations of DCs that contribute to atherosclerosis development primarily through modulation of T cell responses. DCs are found in the intimal layer of healthy vessels and under those conditions are thought to induce T cell tolerance by presenting self-antigen without co-stimulation[62,63]. However, during disease progression DC numbers are greatly increased, they are activated by the local atherosclerotic antigens via Toll-like receptors (TLRs) and have altered phenotypes that promote T cell activation and proinflammatory changes[63–66]. The $CD11c^+$ $CD11b^+$ $CD8\alpha^-$

CCL17$^-$ subset is unique to atherosclerotic lesions and is thought to promote inflammation by inhibiting regulatory T cell (T_{reg}) development[66]. C-type lectin domain family 9 member A (CLEC9A)$^+$ CD8α^+ DCs promote atherosclerosis through reduced IL-10 production[67], while CD11b$^-$ CD103$^+$ IRF8^{hi} DCs derived from a CLEC9A$^+$ precursor directly drive proinflammatory T cell activation[68]. However, not all DC subsets are proatherogenic. Some CD103$^+$ DCs have been shown to be atheroprotective through their promotion of T_{regs}[63]. In addition to conventional DC (cDC) populations, plasmacytoid DCs (pDCs) have also been detected in mouse and human arteries, though in low numbers (reviewed in [69]). The role of pDCs in the lesion is unclear with some reports claiming they promote atherosclerosis by enhancing inflammatory T cell responses[70], and others reporting they induce T_{regs} through the production of indoleamine 2,3-dioxygenase[71,72]. Overall, DCs are important modulators of atherosclerosis, but their role in the disease is nuanced.

Additional Innate Immunity in Atherosclerosis

Other innate populations that make up a small proportion of the lesion infiltrate include mast cells, neutrophils, natural killer (NK) cells, and natural killer T (NKT) cells. Mast cells secrete ECM-degrading cytokines and are regularly found at the site of plaque rupture[73], suggesting they contribute to plaque instability. Evidence from mouse models suggests that neutrophils populate the lesion early in development but are missing from later stages of disease[74]. Antibody depletion and adoptive transfer experiments indicate NK cells are atherogenic, but these findings have not been supported by more precise genetic knock out models making their ultimate impact

unclear[75–77]. Studies indicate that the effect of NKT cells is dependent upon the cytokines that they produce[78,79]. Findings from our lab have shown a major subpopulation of NKT cells, termed invariant NKT cells, become intrinsically dysfunctional during atherosclerosis-associated dyslipidemia[80]. Little work has been done to characterize the role of innate lymphoid cells (ILCs) in atherosclerosis. Due to the transcriptional and cytokine overlap with $CD4^+$ T helper subsets, ILCs have been difficult to interrogate with specificity. However, a recent study showed Type-2 ILCs are atheroprotective through their production of IL-5 and IL-13[81]. Collectively, innate immune cells are critical modulators of atherosclerosis.

B Cells in Atherosclerosis

The overall contribution of the adaptive immune system seems to be atherogenic as atherosclerosis-susceptible *Apoe*$^{-/-}$ mice lacking mature T and B cells have reduced disease compared to controls[82], however, the effect of individual adaptive subsets is more complex. B cells are a rarer population in plaques, but they still play a role in atherosclerosis. They are generally divided into two distinct subtypes: B1 B cells which are fetal derived, long-lived, producers of natural antibodies, and B2 B cells that make up the majority of B cells and are activated in secondary lymphoid organs to produce class-switched antibodies (reviewed in [83]). B cells were initially thought to be protective[84,85], but later work demonstrated some B2 B cells and IgG antibodies are proatherogenic[86–88]. Work from our lab and others have shown oxLDL-specific IgG antibodies form immune complexes with antigen (oxLDL-ICs) and induce proinflammatory changes in macrophages and DCs[89–91]. Given this, it is likely the

protective effects from B cells are mediated by B1 B cells producing natural, germline-encoded antibodies as well as IgM isotypes produced prior to B cell class switching[48,92]. More recently, a proatherogenic role for IgE has been described in patients, likely due to IgE-dependent activation of mast cells and macrophages[93]. However, B cell effector functions in atherosclerosis are not mediated entirely through antibody production. B cells have also been shown to directly modulate IL-17 and IFN-γ production from T cells, T follicular helper cell (T_{FH}) activation, and DC maturation[85,86,94–96]. The antigenic targets of B cells and antibodies in atherosclerosis appear to be largely apolipoprotein B (ApoB)-100 derived but also contain epitopes for oxidized phospholipids and other oxidation-specific sites[97–100]. Overall, the impact of adaptive immunity on atherosclerosis largely depends on the cell type and antigen specificity in question.

T Cells in Atherosclerosis

Though T cell populations are altered during atherosclerosis development, the cells can be detected even in the adventitia of control mice[101]. $CD8^+$ T cells are prevalent early in the disease process, but their relative proportion is reduced during progression[102]. Evidence suggests $CD8^+$ T cells are proatherogenic due to their production of inflammatory mediators like interferon-γ (IFN-γ), perforin, and granzyme B, stimulation of cell death, and promotion of monopoiesis[103–105]. However, $CD4^+$ T cells are thought to contribute more strongly to disease outcome[102,106,107]. $CD4^+$ T cells can directly influence the lesion microenvironment through the production of cytokines or can indirectly modulate disease outcome by providing help to B cells (reviewed in [108]). The antigen specificities of $CD4^+$ T cells in atherosclerosis have not yet been completely

identified, but some known epitopes include $ApoB_{978-993}$ and $ApoB_{3501-3516}$ in mice[109–111] and $APOB_{3036-3050}$ in humans[112]. Specific $CD4^+$ T cell subsets and their impact on atherosclerosis will be introduced with greater detail in Chapter 2.

Research Goal and Overview

Given the wealth of immune cells within the unique, hyperlipidemic microenvironment of the plaque, the goal of this work was to determine how oxLDL reshapes innate and adaptive cells. In Chapter 2, I address the gap in knowledge regarding what causes T_{reg} dysfunction in atherosclerosis, and show that oxidized phospholipids (oxPL) within oxLDL, namely oxidized 1-palmitoyl-2-arachidonoyl-sn-glycero-3-phosphocholine (oxPAPC), alters T_{reg} differentiation and inhibits their atheroprotective function. This oxPAPC-driven effect is partially IFN-γ signaling dependent, prompting an investigation of the role of T_{reg} IFN-γ receptor (IFNγR) signaling in a mouse model of atherosclerosis in Chapter 3. This builds on previous work that has shown sex-dependent outcomes for IFN-γ inhibition in atherosclerosis mouse models. In Chapter 4, I demonstrate oxLDL-ICs trigger long-term changes in DCs that are distinct from alterations caused by oxLDL alone, better characterizing how this prevalent atherosclerotic antigen might contribute to chronic inflammation. The summary of these chapters and potential future directions of this work is the focus of Chapter 5. Ultimately, these studies add to our understanding of how oxidized lipids in atherosclerosis modulate the immune responses that are critical to driving or resolving disease.

CHAPTER 2

OxPAPC Alters T_{reg} Differentiation and Decreases their Protective Function in Atherosclerosis

Most of this work is under review at *Arteriosclerosis, Thrombosis, and Vascular Biology*. Used with permission.

Introduction

Atherosclerosis, the underlying cause of many forms of CVD, is characterized by the accumulation of oxidized lipids in the artery wall which can drive immune cell recruitment to the intima. Although macrophages are important in atherogenesis and comprise a large portion of the immune cells in plaques, recent single-cell RNA sequencing of patient carotid plaques demonstrated that T cells make up at least 50% of infiltrating immune cells[113,114]. The importance of T cells to disease progression in animal models has been previously demonstrated by our group[115] and others (reviewed in [108]), but less is known about how T cells are impacted by the oxidized lipid-rich environment of the aorta.

Multiple $CD4^+$ T cell populations have been shown to influence the progression of atherosclerosis (reviewed in [108]). IFN-γ-producing T helper 1 (Th1) cells are generally considered atherogenic due to their ability to stimulate inflammatory cell recruitment to the intima, activate DCs, and promote foam cell formation[116–119]. However, while IFN-γ deficiency is protective in male apolipoprotein E deficient (*Apoe*$^{-/-}$) mice, female mice are not protected[120], suggesting the role of Th1 cells and IFN-γ in atherosclerosis may be more complex. Effects of T helper 17 (Th17) cells in atherosclerosis are even less

concrete with several groups reporting either atherogenic or atheroprotective effects depending on the mouse models used or the disease stage studied[121–124].

Ample evidence suggests T_{regs} are protective in atherosclerosis both through direct interactions with coinhibitory receptors such as CTLA-4 and PD-1, and production of anti-inflammatory cytokines[125,126]. Depletion of T_{regs} from atherosclerosis susceptible mice significantly increases plaque size and progression[125,127]. Additionally, T_{regs} are increased in multiple mouse models of regressing plaques and are required for regression to take place[128].

Studies in both mice and humans have demonstrated reduced T_{reg} numbers as atherosclerosis progresses[129–131]. This loss may be in part due to an increase in T_{reg} apoptosis[131,132]. T_{regs} in atherosclerosis lose stability and convert to exT_{regs}, adopting the phenotype and function of other T helper subtypes like Th1 cells, which are largely thought to be atherogenic[116–119], or T_{FH} cells that have been shown to be both pro- and anti-atherogenic[96,133,134]. Each of these models provides a hypothesis for the overall reduction of T_{regs} during atherosclerosis, but mechanisms underpinning T_{reg} death and loss of stability in the plaque microenvironment remain unknown. Collectively, these findings highlight that T_{regs} are critical mediators for controlling and reversing atherosclerosis.

OxLDL, one of the main oxidized lipoproteins associated with atherosclerosis, is highly abundant in the lesion environment and has been shown to both inhibit T_{reg} differentiation and promote apoptosis *in vitro*[132,133,135,136]. OxLDL is a complex particle made up of the central protein, apoB-100, and a variety of oxidized lipids, including the phospholipid, oxPAPC[137]. Interestingly, several studies have demonstrated that oxPAPC

is the bioactive component of oxLDL, eliciting many of the same effects in innate immune cells as oxLDL despite its reduced molecular size and complexity[138–140]. OxPAPC is also increased in the membrane of apoptotic cells which are abundant in atherosclerotic plaques[141]. However, the effects of oxPAPC have mostly been studied in innate immune cells and its direct impact on T cells is unknown.

In this study we sought to determine if oxPAPC affects T cell differentiation and function to promote atherosclerosis. We report that oxPAPC modulates T_{reg} polarization, inducing surviving T_{regs} to develop a Th1-like phenotype, expressing T-bet and producing IFN-γ. These effects were specific to T_{regs}, as other T helper subtypes were unaffected. OxPAPC-treated T_{regs} had reduced suppressive activity *in vitro* and, when adoptively transferred into hyperlipidemic low-density lipoprotein receptor deficient (*Ldlr*$^{-/-}$) mice, oxPAPC-treated T_{regs} did not inhibit plaque progression compared to control T_{regs}. Overall, our findings demonstrate that oxPAPC inhibits stable T_{reg} polarization and results in a Th1-like T_{reg} phenotype that makes them less protective against plaque progression. Therefore, exposure of differentiating T_{regs} to oxPAPC may be an important mechanism for their dysfunction during atherosclerosis.

Materials and Methods

All sequencing data have been made publicly available at NCBI GEO with accession numbers GSE236226 and GSM7520079-GMS7520086

Mice. C57BL/6J (B6; Stock # 000664), B6.Cg-Tg(TcraTcrb)425Cbn/J (OT-II; Stock # 004194), B6.129S7-Ldlr^{tm1Her}/J (*Ldlr*$^{-/-}$; Stock # 002207), B6.129S7-Ifngr1^{tm1Agt}/J (*Ifngr1*$^{-/-}$; Stock # 003288), B6.Cg-Foxp3^{tm2Tch}/J (B6-FoxP3^{GFP}; Stock # 006772), and B6.PL-

Thy1^{a}/CyJ (Thy1.1; Stock # 000406) mice were originally obtained from the Jackson Laboratory (Bar Harbor, ME). B6-FoxP3^{GFP} and Thy1.1 animals were crossed to generate B6-Thy1.1- FoxP3^{GFP} mice. Animals were maintained and housed at Vanderbilt University. All mice used in these studies were on the C57BL/6J background. Procedures were approved by the Vanderbilt University Institutional Animal Care and Use Committee. Both male and female mice were used for studies as specified.

T Cell Polarization. Spleens from four- to six-week-old mice were processed to single cell suspensions and CD4^{+} T cells were enriched using mouse CD4 (L3T4) Microbeads kit (Miltenyi Biotec Cat # 130-117-043) according to manufacturer instructions. Experiments were performed using both male and female mice. For T_{reg} polarization, CD4^{+} T cells were cultured in α-CD3 (coating concentration was 2μg/ml; Tonbo Cat # 40-0031) coated flat-bottom 96-well plates at a final concentration of 2x10^{6} cells/ml in T Cell Media (TCM; RPMI-1640, 10% fetal bovine serum [FBS], L-glutamine-penicillin-streptomycin [2mM, 100 units, 100μg/ml, respectively], 2mM β-mercaptoethanol, and 1x non-essential amino acids) with 2μg/ml α-CD28 (Tonbo Cat # 70-0281), 50U/ml IL-2 (Tonbo Cat # 21-8021 and Peprotech Cat # 212-12), 10ng/ml TGF-β (Peprotech Cat # 100-21), 2μg/ml α-IFN-γ (Tonbo Cat # 40-7311), and 500ng/ml α-IL-4 (Tonbo Cat # 70-7041) for three days. If culture was continued to day 5, T_{regs} were split, replated, and fed with TCM containing final concentrations of 50U/ml IL-2, 10ng/ml TGF-β, 2μg/ml α-IFN-γ, and 500ng/ml α-IL-4. Media was replaced on day 4 and cells were harvest on day 5. T_{regs} were cultured with or without 5μg/ml oxPAPC (Invivogen Cat # tlrl-oxp1) for the first three days of culture unless otherwise stated. For Th1 polarization, CD4^{+} T cells were cultured in α-CD3 coated flat-bottom 96-well plates at a final concentration of 2x10^{6}

cells/ml in TCM with 2μg/ml α-CD28, 10ng/ml IL-12 (Peprotech Cat # 210-12), and 1μg/ml α-IL-4 for three days. On day 3, cells were split, replated, and fed with TCM containing final concentrations of 20U/ml IL-2, 10ng/ml IL-12, and 1μg/ml α-IL-4. Feeding was repeated on day 4 and cells were harvested on day 5. For Th17 polarization, $CD4^+$ T cells were cultured in α-CD3 coated flat-bottom 96-well plates at a final concentration of $1x10^6$ cells/ml in TCM with 2μg/ml α-CD28, 25ng/ml IL-6 (Peprotech Cat # 216-16), 5ng/ml TGF-β, 2μg/ml α-IFN-γ, and 500ng/ml α-IL-4 for three days. Th1 and Th17 cells were cultured with or without 5μg/ml oxPAPC for the duration of the culture.

For antigen-specific T_{reg} polarization experiments, bone marrow-derived dendritic cells (BMDCs) were generated as previously described[142]. On day 10 of BMDC culture, cells were harvested and irradiated (15 Gy). $1x10^4$ irradiated BMDCs were co-cultured in a round-bottom 96-well plate with $1x10^5$ OT-II $CD4^+$ T cells enriched as above, the same concentrations of IL-2, TGF-β, α-IFN-γ, and α-IL-4 used in non-antigen-specific T_{reg} conditions, and 50μg/ml $OVA_{323-339}$ peptide (Invivogen Cat # vac-isq) in activated conditions. Co-cultures were incubated for three days with or without 5μg/ml oxPAPC.

Flow Cytometry. Flow cytometry was performed on cells obtained *ex vivo* and following *in vitro* cell culture. Cells requiring a viability dye were stained with Viobility Fixable Dye (Miltenyi Biotec) or Ghost Dyes™ (Tonbo) according to the manufacturer protocols. For surface staining, cells were washed in HBSS containing, 1% BSA, 4.17mM sodium bicarbonate, and 3.08mM sodium azide (FACS buffer), followed by a 10-minute room temperature incubation in 1μg/ml Fc block (α-CD16/32; Tonbo Cat # 40-0161) diluted in FACS buffer. Cells were then stained for 30 minutes at 4°C protected from light with the

following antibodies diluted in FACS buffer: α-B220-APCCy7 (Tonbo Cat # 25-0452), α-CD4-PECy7 (Tonbo Cat # 60-0042), α-CD4-PerCp-Cy5.5 (Tonbo Cat # 65-0042), α-CD4-SB600 (eBioscience Cat # 63-0041-82), α-CD8a-APCCy7 (Tonbo Cat # 25-0081), α-CD11b-APCCy7 (BD Biosciences Cat # 557657), α-CD25-FITC (Tonbo Cat # 35-0251), α-CD45.2-PerCp-Cy5.5 (Tonbo Cat # 65-0454), α-CXCR3-APC (BD Biosciences Cat # 562266), α-GITR-FITC (Tonbo Cat # 35-5874), α-ICOS-FITC (eBioscience Cat # 11-9949-82), α-Thy1.1-V450 (BD Biosciences Cat # 561406). Samples not requiring intracellular staining were then washed in FACS buffer and fixed in 2% paraformaldehyde (PFA). Samples with intracellular stains were washed then permeabilized and stained with the following intracellular antibodies according to the FoxP3/Transcription Factor Staining Buffer Set manufacturer protocol (eBioscience Cat # 00-5523-00): α-FoxP3-PECy7 (eBioscience Cat # 25-5773-82), α-IFN-γ-APC (Tonbo Cat # 20-7311), α-IL-4-FITC (eBioscience Cat # 11-7042-82), α-IL-17-PE (BD Biosciences Cat # 559502), α-T-bet-PE (Biolegend Cat # 644810), α-ROR-γt-PerCp-Cy5.5 (eBioscience Cat # 12-6988-82). Isotype controls were used to confirm FoxP3, IFN-γ, and T-bet staining (Rat IgG2a kappa isotype-PECy7 eBioscience Cat # 25-4321-82, Rat IgG1 isotype-APC Tonbo Cat # 20-4301, and Mouse IgG1 kappa isotype-PE Biolegend Cat # 400114, respectively). All samples were washed and resuspended in 2% PFA before analysis. Cells that were stimulated with phorbol myristate acetate (PMA; Sigma Cat # P1585) and ionomycin (Sigma Cat # I9657) prior to staining were treated with either 20ng/ml PMA, 1μg/ml ionomycin, and 1.3μg/ml Golgi Stop (BD Biosciences Cat # 554724) or 500ng/ml PMA, 500ng/ml ionomycin, and 110μg/ml Golgi Plug (BD Biosciences Cat # 555029) in TCM or complete RPMI (cRPMI; RPMI-1640,

10% fetal bovine serum [FBS], L-glutamine-penicillin-streptomycin [2mM, 100 units, 100μg/ml, respectively], and 2mM β-mercaptoethanol) for four-six hours. Apoptosis staining was done using the Annexin V Apoptosis Detection kit (Tonbo Cat # 20-6410) and performed according to manufacturer instruction. Sample acquisition was performed on a MacsQuant Analyzer (Miltenyi Biotec) and data were analyzed using FlowJo Single Cell Analysis software.

RNA Sequencing (RNAseq). $4.5x10^6$ – $7.3x10^6$ live control or oxPAPC-treated T_{regs} were harvested on day 3 of culture and RNA was isolated using Rneasy Plus Mini Kit (Qiagen Cat #: 74134) according to manufacturer instruction. RNA was sent to Vanderbilt Technologies for Advanced Genomics (VANTAGE) core. Libraries were prepared using 200-500ng of total RNA using NEBNext® Poly(A) selection kit and sequenced at Paired-End 150bp on the Illumina NovaSeq 6000 targeting an average of 50M reads per sample. Additional analysis using the resulting demultiplexed FASTQ files containing pass-filter (PF) reads was performed by Vanderbilt Technologies for Advanced Genomics Analysis and Research Design (VANGARD). Sequencing reads were aligned against the mouse GENCODE GRCm38.p6 using STAR software v2.7.8a. Mapped reads were assigned to gene features and quantified using featureCounts v2.0.2. Normalization and differential expression were performed using DESeq2 v1.30.1. Significantly differentially expressed genes (fold change ≥2 and false discovery rate (FDR) ≤0.05) were used for subsequent Gene Set Enrichment Analysis v4.2.2.

Diet Comparison Studies. Eight-week-old male and female *Ldlr*$^{-/-}$ mice were maintained on normal chow or placed on Western diet (21% saturated fat and 0.15% cholesterol; Envigo Cat #: TD.88137) for 16 weeks. After which animals were sacrificed,

and aorta and spleen were collected for flow cytometry analysis. Animals were included in this study based on age, sex, and genotype, and were excluded or removed from the study if they experienced weight loss or a notable physical ailment. Cages were randomly assigned diet treatment.

Tissue Collection. Aortas were processed as previously described[143]. Briefly, aortas were perfused with PBS, cleaned of fat, minced, and digested with 450U/ml Collagenase Type I (Worthington Biochemicals Cat # LS004194), 125U/ml Collagenase Type XI (Sigma Cat # C-7657), 60U/ml Hyaluronidase Type I (Sigma Cat # H-3506), and 60U/ml Dnase I (Millipore Sigma Cat # 69182) in PBS at 37°C for 30-45 minutes. Digested aortas were passed through 70μm cell strainers, and leukocytes washed before use in flow cytometry.

Livers were processed as previously described[144]. Briefly, livers were perfused with PBS, minced, and then digested with 1mg/ml Collagenase Type II (Gibco Cat # 17101-015) in HBSS with calcium and magnesium at 37°C for 30 minutes. Liver tissue was passed through 70μm cell strainers and allowed to settle for 45 minutes on ice. Supernatants were pelleted and resuspended in cold 40% Percoll (Cytiva Cat # 17-0891-01) with a 60% Percoll underlay. Gradients were centrifuged at 2000rpm at 10°C for 20 minutes with no break. Leukocytes were collected from the gradient interface.

T_{reg} Suppression Assay. T_{regs} were skewed as described above. On day 5 of culture, T_{regs} were harvested and an equal number of live cells from each group were replated in cRPMI in flat-bottom 96-well plates at ratios of 3:1, 2:1, 1:1, 1:2, 1:4, and 1:8 with $CD8^+$ T cells enriched using mouse CD8 (Ly-2) Microbeads kit (Miltenyi Biotec Cat # 130-117-044) and labeled with CellTrace Violet (CTV; Invitrogen Cat # C34557), both according

to the manufacturer protocols. Also included in the co-culture, were $2x10^5$ irradiated (30Gy) feeder splenocytes per well and 1μg/ml α-CD3. After 72 hours, T_{reg} suppression was determined by measuring CTV dilution in $CD8^+$ responder cells (T_{res}) via flow cytometry. Percent inhibition was calculated as [100%-((proliferation of given T_{reg}:T_{res} ratio/proliferation of 0:1 T_{reg}:T_{res} group)x100)].

Adoptive Transfers. Adoptive transfer protocol was adapted from Li *et al.*[145]. 15-week-old female *Ldlr*$^{-/-}$ mice were placed on Western diet for 9-11 weeks after which mice were retro-orbitally injected with saline, or $1x10^6$ live day 5 control or oxPAPC-treated T_{regs}. The injections were repeated 4-6 weeks later, and animals were sacrificed 2 weeks after the final injection. Aortas, adLNs, livers, blood, and spleens were collected for flow analysis. Atherosclerosis severity was quantified in the proximal aorta. Animals were included in this study based on age, sex, and genotype, and were excluded or removed from the study if they experienced weight loss or a notable physical ailment. Animals were assigned to treatment groups based on their weight at the time of the first adoptive transfer so that each group had the same average weight.

Atherosclerotic Plaque Analysis. Plaque analysis was performed on cryosections obtained from OCT embedded hearts. Sectioning started at the aortic sinus and proceeded for about 300μm before sample collection began. Sample sections were collected in alternating 10μm and 5μm sizes. Oil-red-O staining of 10μm cryosections was performed as previously described[146]. Trichrome staining (abcam Cat # ab150686) was performed using 10μm cryosections fixed in 10% formalin for 30 minutes according to manufacturer instructions. Immunohistochemistry was performed using 5μm cryosections. Sections were fixed in cold acetone for 10 minutes and blocked at room

temperature in 2% BSA/PBS for 30 minutes. Slides were treated with avidin/biotin block (Vector Cat # SP-2001) for 15 minutes each, and peroxidase activity block (9:1 methanol:30% H_2O_2) for 10 minutes. Macrophages or SMCs were stained using a 1:25 dilution of rat-anti mouse macrophage (Biorad Cat # MCA519G) or 1:2000 dilution of rabbit anti-α-actin (Millipore Sigma Cat # ABT1487), respectively, in 2% BSA/PBS at 4°C overnight. Secondary biotinylated goat anti-rat Ig (BD Bioscience Cat # 554014) was used at 1:200 in 2% BSA/PBS for macrophage staining or biotinylated goat anti-rabbit IgG (BD Biosciences Cat # 550338) was used at 1:30 in 2% BSA/PBS for SMC staining and incubated at 37°C for 30 minutes. Streptavidin peroxidase (Biogenex Cat # HK330) was applied for 20 minutes followed by AEC substrate (Biogenex Cat # HK139-06k) for 1.5 or 1 minutes for macrophage or SMC staining, respectively. Hematoxylin counterstain was applied for 2 minutes and slides were imaged using an Olympus BX41 Phase Contrast & Darkfield microscope and the Olympus cellSens Standard program. Quantification of total lesion area, Oil-red-O and immunohistochemistry staining, and necrotic core area was performed using ImageJ.

Cholesterol and Triglyceride Assays. Mice were fasted for four hours, and blood was collected from the retroorbital sinus and centrifuged to obtain serum. Cholesterol (Millipore Sigma Cat # MAK436-1KT) and triglycerides (Millipore Sigma Cat # MAK266-1KT) were measured using commercially available kits according to the manufacturer instructions.

ELISAs. Cell supernatants were collected following three days in culture and IFN-γ (BD Biosciences Cat # 551866) was measured by ELISA according to the manufacturer instructions. Anti-oxLDL ELISAs were performed as previously described[144]. Briefly,

Nunc Maxisorp 96-well plates (Invitrogen Cat # 44-2404-21) were coated in 1μg/ml oxLDL overnight at 4°C. After washing with 0.05% Tween in PBS and blocking with 3% BSA/PBS, serum samples were applied, and the plate was again incubated overnight. Biotinylated α-IgG (eBioscience Cat # 13-4013-85), α-IgG1 (Southern Biotech Cat # 1070-08), α-IgG2c (Southern Biotech Cat # 1080-08), or α-IgM (Southern Biotech Cat # 1020-08) were incubated for one hour at room temperature, followed by streptavidin-peroxidase (Southern Biotech Cat # 7200-05) for 30 minutes at room temperature. Plates were washed and OptEIA TMB substrate (BD Biosciences Cat # 555214) was applied for 8, 10, 15, and 5 minutes, respectively, before reaction was quenched with 2M HCl. Results were read at 450nm.

Statistical Analyses. All experiments were performed using biological replicates. Normal distribution of data was determined using the Shapiro-Wilk test as described previously[147]. In experiments with two groups, homogenous variance was assessed using an F test. For experiments with three or more groups, homogenous variance was measured using Brown-Forsythe test (< five samples per group) or Bartlett's test (five or more samples per group). Normally distributed data with homogenous variance were analyzed using Student's *t* tests (for two groups) or one-way ANOVAs with Bonferroni post-test (for three or more groups). Non-parametric data were analyzed using Mann-Whitney tests (for two groups). For experiments with two independent variables, two-way ANOVAs with a Tukey's multiple comparison post-test or Šídák's multiple comparisons post-test (for repeated measures) were used. All statistical tests were performed using GraphPad Prism.

Results

OxPAPC alters T_{reg} differentiation but does not impact Th1 or Th17 polarization.

T_{regs} are known to be atheroprotective but are reduced by cell death or loss of stability in atherosclerosis, presumably due to the plaque microenvironment[125,131,133,134]. OxPLs are an abundant component of the lesion environment and can impact the functioning of immune cells[140,148]. To determine whether the oxPLs associated with atherosclerotic lesions, such as oxPAPC, contribute to T_{reg} dysregulation, we performed *in vitro* $CD4^+$ T cell polarization experiments with or without oxPAPC. Skewing T_{regs} in the presence of oxPAPC significantly reduced their viability at day 3 in culture by increasing apoptosis (Figure 2.1A, Figure 2.2A, and Figure 2.3A-E). The proportion of live cells that were $FoxP3^+$ was not affected by oxPAPC (Figure 2.1A, middle panels), but there was an increased proportion of T-bet^+ $FoxP3^+$ cells in oxPAPC-treated cultures (Figure 2.1A, bottom panels, and Figure 2.2A). Interestingly, FoxP3 expression preceded the most significant drop in cell viability and T-bet expression increase observed in oxPAPC-treated T_{regs} (Figure 2.3F). Both cell death and dysregulated transcription factor expression were specific to T_{reg} skewing conditions as oxPAPC treatment had no effect on Th1 or Th17 viability or polarization (Figure 2.1B-C and Figure 2.2B-C).

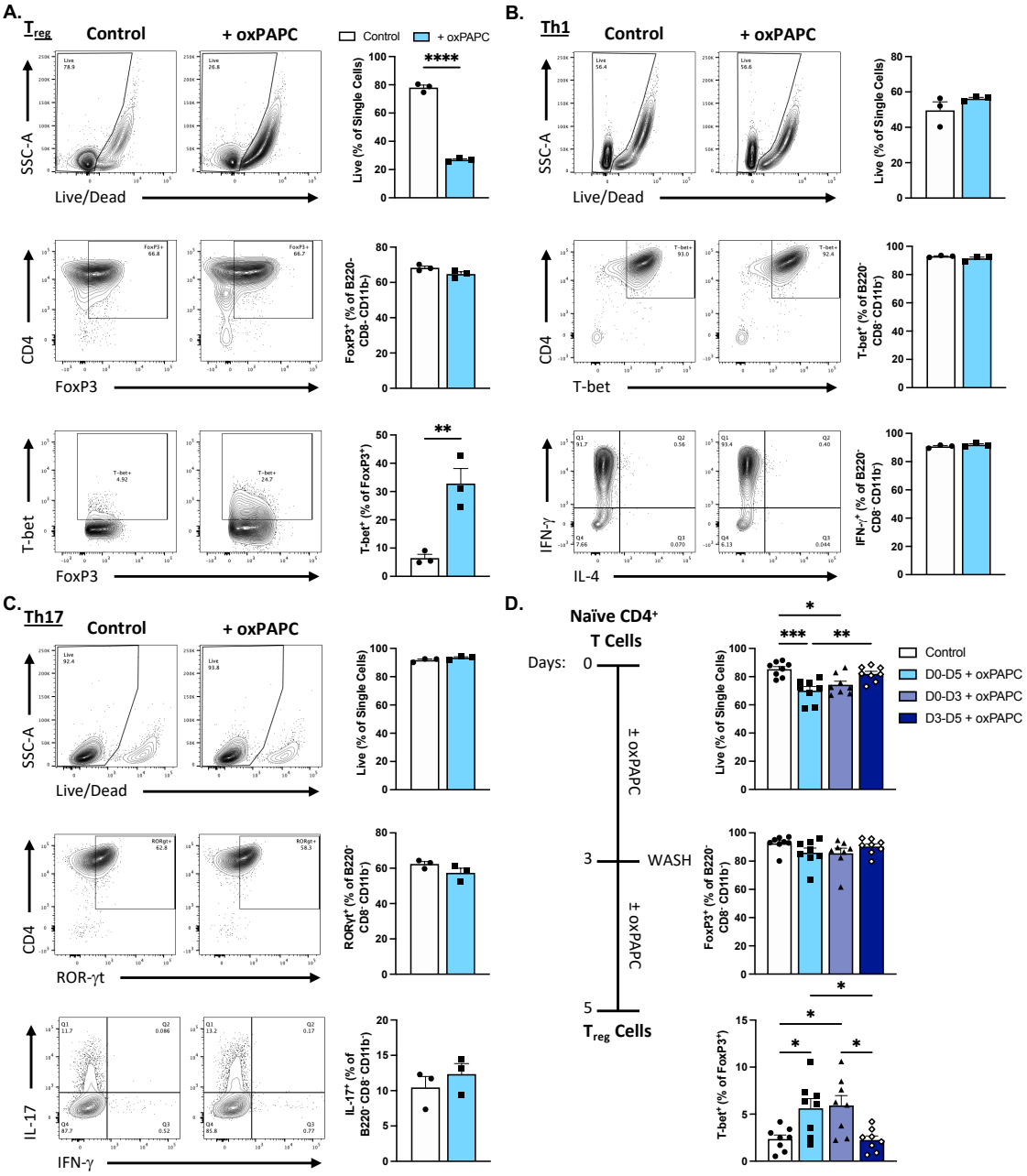

Figure 2.1: OxPAPC specifically alters T_{reg} phenotype. $CD4^+$ T cells were enriched from the spleens of four- to six-week-old B6 mice and skewed to the indicated phenotype for three **(A and C)** or five **(B and D)** days with or without 5μg/ml oxPAPC. T cell phenotype was assessed by flow cytometry directly after harvest **(A,D)** or after a four-hour stimulation with PMA, ionomycin, and Golgi inhibitor **(B,C)**. **(A-C)** Shown is one representative of at least three experiments. ** and **** denote significance $p<0.01$ and $p<0.0001$, respectively, by Student's *t* test. **(D)** T_{reg} phenotype was assessed by flow cytometry directly after harvest on day five of culture. *, **, and *** denote significance $p<0.05$, $p<0.01$, and $p<0.001$, respectively, by one-way ANOVA and Tukey's multiple comparison. Data points represent individual mice and error bars show SEM.

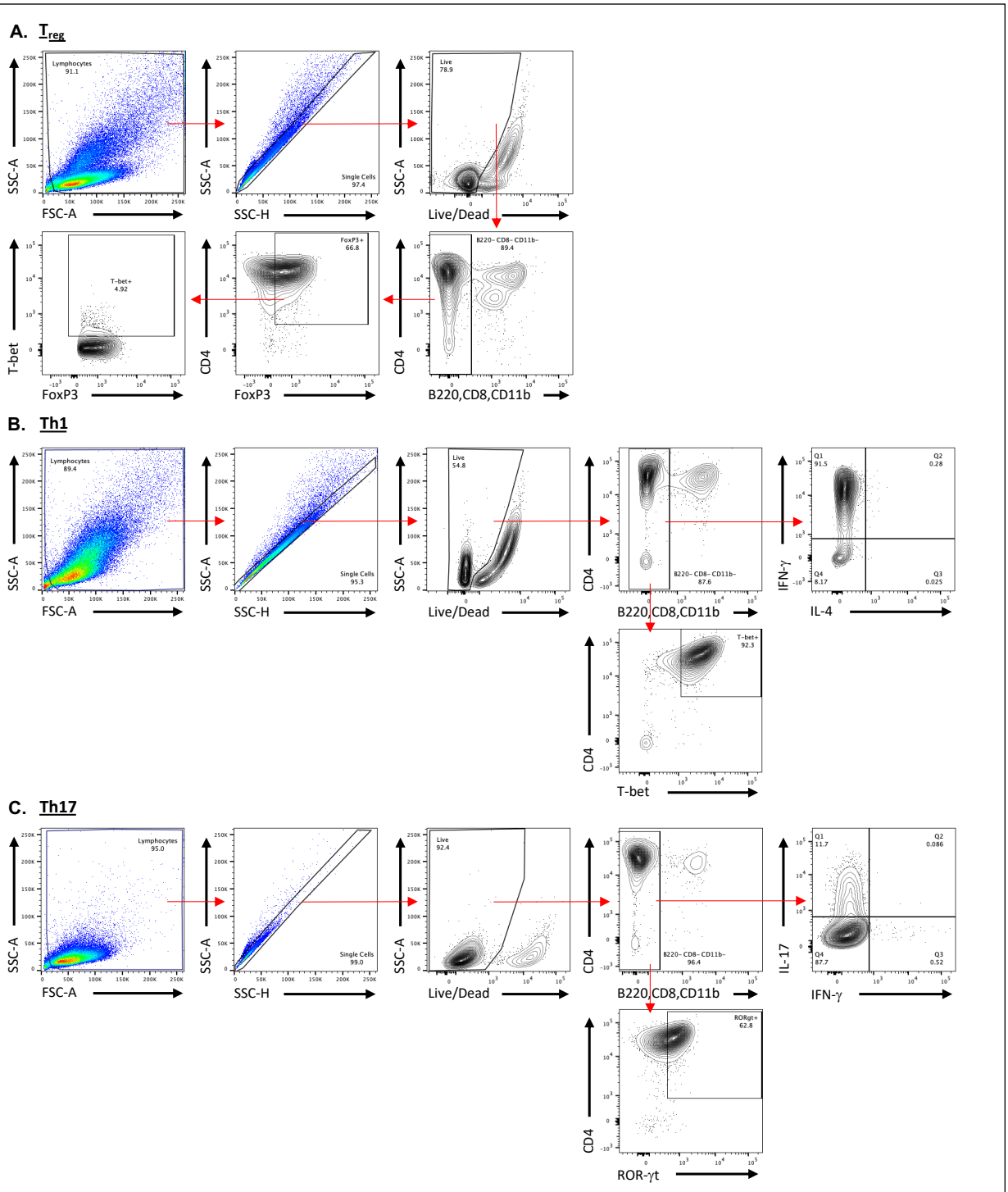

Figure 2.2: Gating strategy for characterization of skewed T_{regs}, Th1, and Th17 cells. (A) Skewed T_{regs} were analyzed by flow cytometry, gating on FSC/SSC, single cells, viability, exclusion of non-$CD4^+$ markers, and then assessed for transcription factors. **(B,C)** Polarized Th1 and Th17 cells were incubated with PMA, ionomycin, and Golgi inhibitor for four hours after which cells were analyzed by flow cytometry, gating on FSC/SSC, single cells, viability, exclusion of non-$CD4^+$ markers, and then assessed for transcription factors and cytokine production.

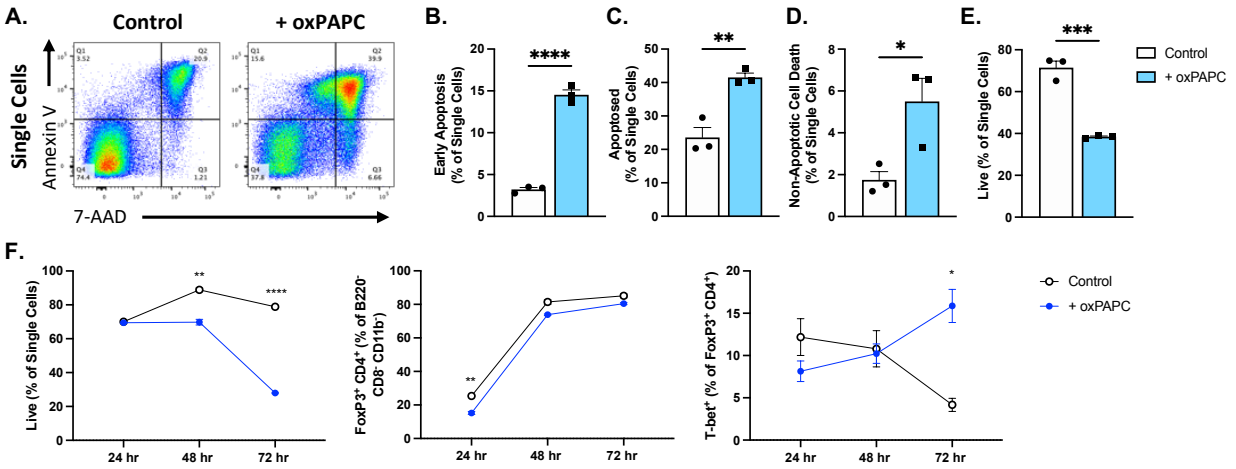

Figure 2.3: OxPAPC induces apoptosis in T_{regs}. $CD4^+$ T cells were enriched from the spleens of four- to six-week-old B6-Thy1.1-$FoxP3^{GFP}$ mice and skewed to a T_{reg} phenotype for three days with or without 5μg/ml oxPAPC. Viability was assessed by flow cytometry. **(A)** Representative flow results. **(B)** Cells in early apoptosis were defined as Annexin V^+ 7-AAD^-. **(C)** Apoptosed cells were Annexin V^+ 7-AAD^+. **(D)** Non-apoptotic cell death was defined as Annexin V^- 7-AAD^+. **(E)** Live cells were Annexin V^- 7-AAD^-. Data points are individual mice and error bars show SEM. *, **, ***, and **** denote significance $p<0.05$, $p<0.01$, $p<0.001$, and $p<0.0001$, respectively, by Student's *t* test. **(F)** $CD4^+$ T cells were skewed to a T_{reg} phenotype as above and harvested at 24-hour intervals for assessment by flow cytometry. Error bars show SEM representing at least three biological replicates. *, **, ***, and **** denote significance $p<0.05$, $p<0.01$, $p<0.001$, and $p<0.0001$, respectively, by repeated measures two-way ANOVA and Šídák's multiple comparisons test.

T_{reg} cultures were extended to five days under resting conditions and oxPAPC was found to be required during differentiation as addition of the phospholipid after day 3, when FoxP3 levels are established, had no effect on cell viability or T-bet expression (Figure 2.1D). To ensure the observed changes in T_{reg} phenotype were not an artifact of the experimental system, T_{regs} were polarized in an antigen-specific manner using OT-II $CD4^+$ T cells co-cultured with $OVA_{323-339}$ peptide and irradiated BMDCs. Under these conditions, oxPAPC still significantly reduced T_{reg} viability, did not alter FoxP3 proportion of live cells, and increased T-bet^+ $FoxP3^+$ cells, though the relative differences were not as dramatic as in the non-antigen-specific conditions (Figure 2.4A-

C). Collectively, these data support oxPL-mediated dysregulation of $CD4^+$ T cell differentiation in a T_{reg}-specific manner.

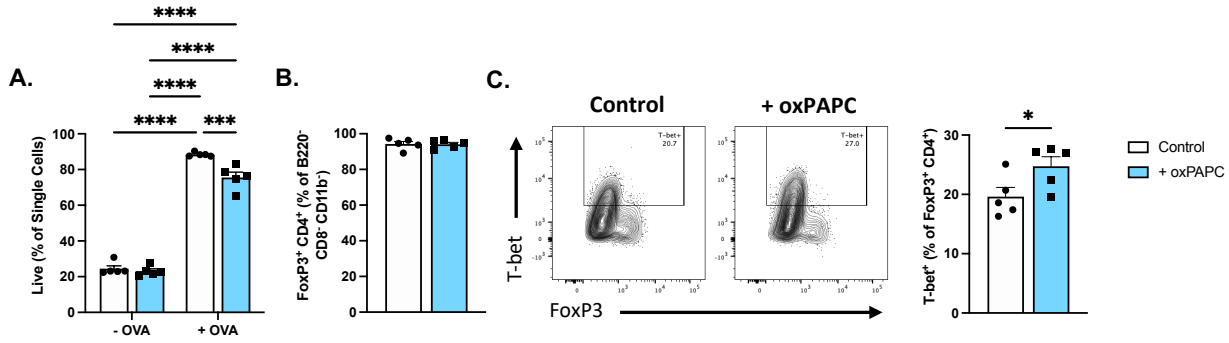

Figure 2.4: OxPAPC-induced changes in T_{regs} are reproduced in an antigen-specific model of polarization. (A-C) $CD4^+$ T cells were enriched from the spleens of four- to six-week-old OT-II mice and co-cultured with irradiated BMDCs, 50μg/ml OVA peptide, and T_{reg} promoting cytokines for three days with or without 5μg/ml oxPAPC. Co-cultures without OVA peptide served as non-activated controls. T cell phenotype was assessed by flow cytometry directly after harvest. **(A)** *** and **** denote significance $p<0.001$ and $p<0.0001$ respectively, by two-way ANOVA and Tukey's multiple comparison. **(B-C)** Polarization results of groups including OVA peptide. * denotes significance of $p<0.05$ by one-tailed t test. Data points represent individual mice and error bars show SEM.

Though surviving oxPAPC-treated T_{regs} had the same overall proportion of $FoxP3^+$ cells as control T_{regs}, the level of FoxP3 expression was altered. When oxPAPC-treated T_{regs} were analyzed on day 3, just following activation and differentiation, FoxP3 expression was significantly higher than in control T_{regs}, and a greater proportion of the cells were $FoxP3^{hi}$ (Figure 2.5A-B). However, on day 5, after resting, oxPAPC-treated T_{regs} did not increase FoxP3 expression as controls did and a greater proportion of oxPAPC-induced T_{regs} were $FoxP3^{lo}$ (Figure 2.5A-B). T_{reg} functional markers (CD25, GITR, and ICOS) were most highly expressed in the $FoxP3^{hi}$ group and Th1-like markers (T-bet, IFN-γ, CXCR3) were observed at the greatest levels in the $FoxP3^{lo}$

population (Figure 2.5C). These data suggest that skewing T_{regs} in the presence of oxPAPC may decrease FoxP3 stability resulting in increased T effector function.

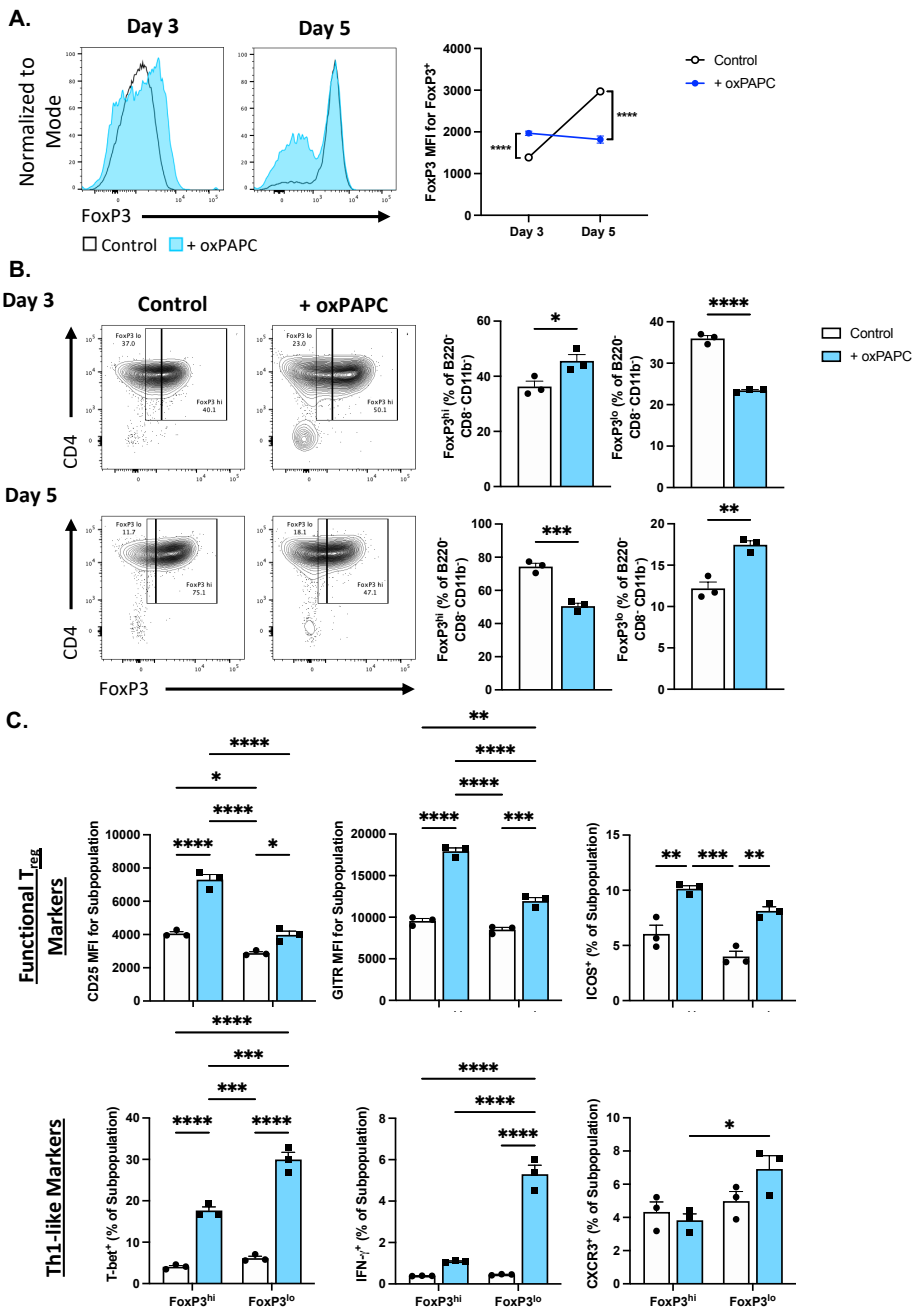

Figure 2.5: FoxP3 expression is altered in oxPAPC-treated T_{regs} and the resulting subpopulations have distinct phenotypic profiles. $CD4^+$ T cells were enriched from the spleens of four- to six-week-old B6 mice and skewed to a T_{reg} phenotype for three or five days with or without 5μg/ml oxPAPC. **(A)** Level of FoxP3 expression was assessed by flow cytometry. **** denotes significance $p<0.0001$ by repeated measures two-way ANOVA and Šídák's multiple comparisons test. **(B)** Proportion of $FoxP3^{hi}$ vs $FoxP3^{lo}$ cells as determined by flow cytometry. *, **, *** and **** denote significance $p<0.05$, $p<0.01$, $p<0.001$, and $p<0.0001$, respectively, by Student's *t* test. **(C)** T_{regs} were polarized as in (A) for three days and T_{reg} and Th1-like markers in FoxP3 subpopulations were assessed by flow cytometry. *, **, ***, and **** denote significance $p<0.05$, $p<0.01$, $p<0.001$, and $p<0.0001$, respectively, by two-way ANOVA and Tukey's multiple comparison. Data points are individual mice and error bars show SEM.

OxPAPC-treated T_{regs} have an IFN-γ enriched genetic signature. Bulk RNAseq was performed on T_{regs} after three days in culture in the presence or absence of oxPAPC. Distinct transcriptional profiles were observed between the two groups (Figure 2.6A) and differential expression analysis identified *Ifng* as the second highest increased gene (Figure 2.6B). Furthermore, gene set enrichment analysis (GSEA) revealed increased expression of genes in the IFN-γ response pathway (Figure 2.6C) as well as the inflammatory response pathway (Figure 2.6D) in oxPAPC-treated $T_{regs.}$ Together these results indicate oxPAPC treatment induces widespread inflammatory changes in the T_{reg} transcriptome identifying response to IFN-γ as a potential mechanism.

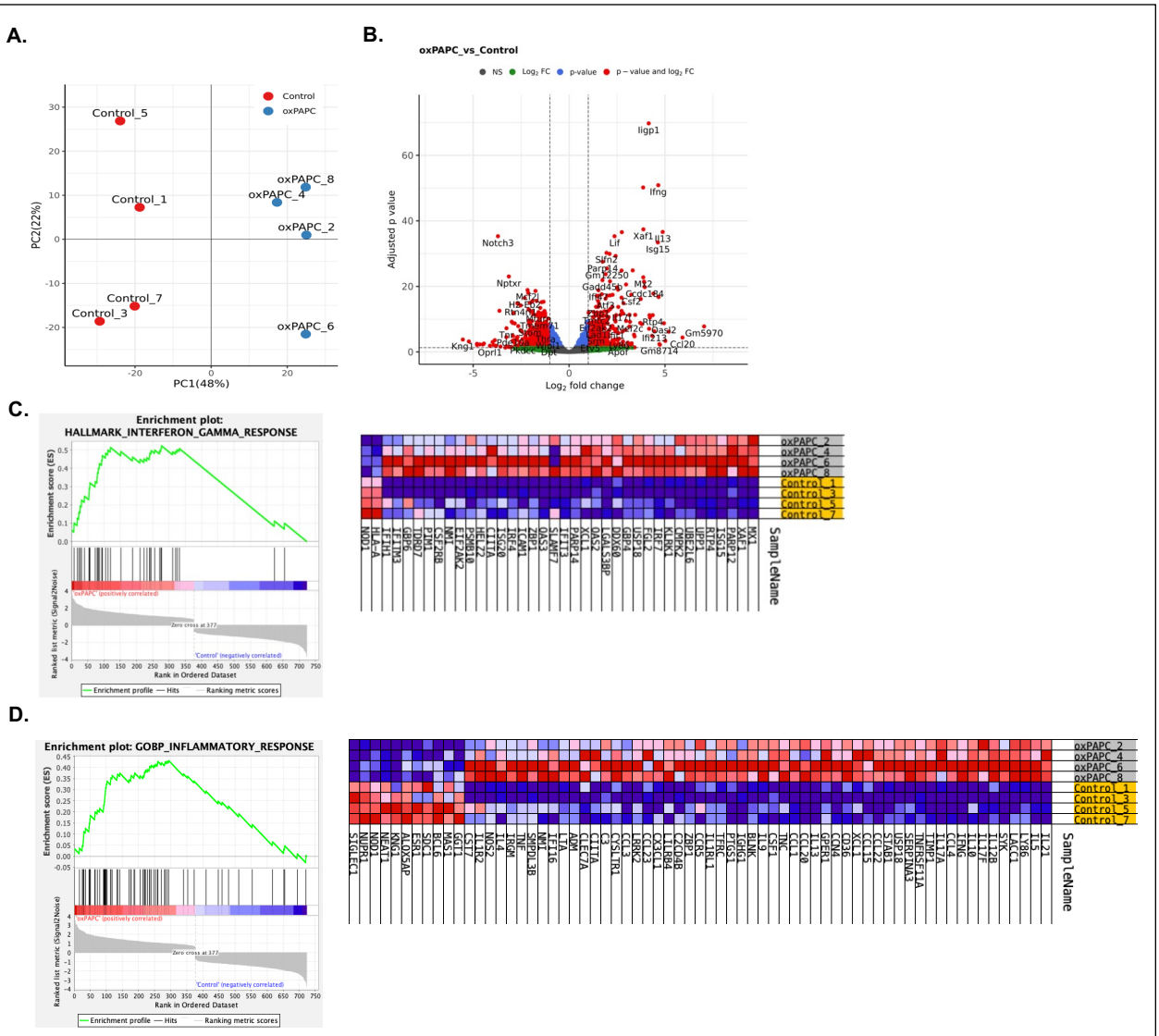

Figure 2.6: OxPAPC-treated T_{regs} increase expression of inflammatory and IFN-γ response genes. $CD4^+$ T cells were enriched from the spleens of four- to six-week-old B6 mice and skewed to a T_{reg} phenotype for three days with or without 5μg/ml oxPAPC before being harvested for bulk RNAseq. N=4 mice per group. Shown is one of two independent experiments. **(A)** Principal component analysis comparing control and oxPAPC-treated T_{regs}. **(B)** Volcano plot showing differentially expressed genes in oxPAPC-treated T_{regs} (significantly enriched = red and right, significantly reduced = red and left). **(C)** GSEA results and heatmap for significantly altered genes in IFN-γ response pathway (red=high, blue= low). **(D)** GSEA results and heatmap for significantly altered genes in inflammatory response pathway (red=high, blue= low).

OxPAPC induces a Th1-like phenotype in surviving T_{regs}. Given the IFN-γ signature identified in oxPAPC-treated T_{regs}, we sought to investigate the expression of the

cytokine and other Th1-associated markers in our oxPAPC treated T_{reg} cultures. Consistent with RNAseq, the proportion of IFN-γ^+ FoxP3$^+$ cells and CXCR3$^+$ FoxP3$^+$ cells were significantly increased in the surviving population of oxPAPC treated cultures (Figure 2.7A), and the concentration of IFN-γ was elevated in the supernatants from oxPAPC treated conditions (Figure 2.7B). The *in vitro* T_{reg} phenotype induced by oxPAPC was consistent with *in vivo* T_{regs} in atherosclerotic mice. We compared T_{regs} from male *Ldlr*$^{-/-}$ mice fed a high fat Western diet (WD) or normal chow (NC) (Figure 2.8A). Consistent with previous studies[134,145] and our *in vitro* results, WD-fed animals had an increased proportion of IFN-γ expressing T_{regs} in the aorta (Figures 2.8B and 2.9A), while the proportion of IFN-γ^+ T_{regs} in the spleen of these mice remained unchanged (Figures 2.8C and 2.9B). Similar results were observed for NC- and WD-fed female *Ldlr*$^{-/-}$ mice (data not shown). Collectively, these data support a role for oxPLs in dysregulation of T_{regs} during differentiation in atherosclerosis.

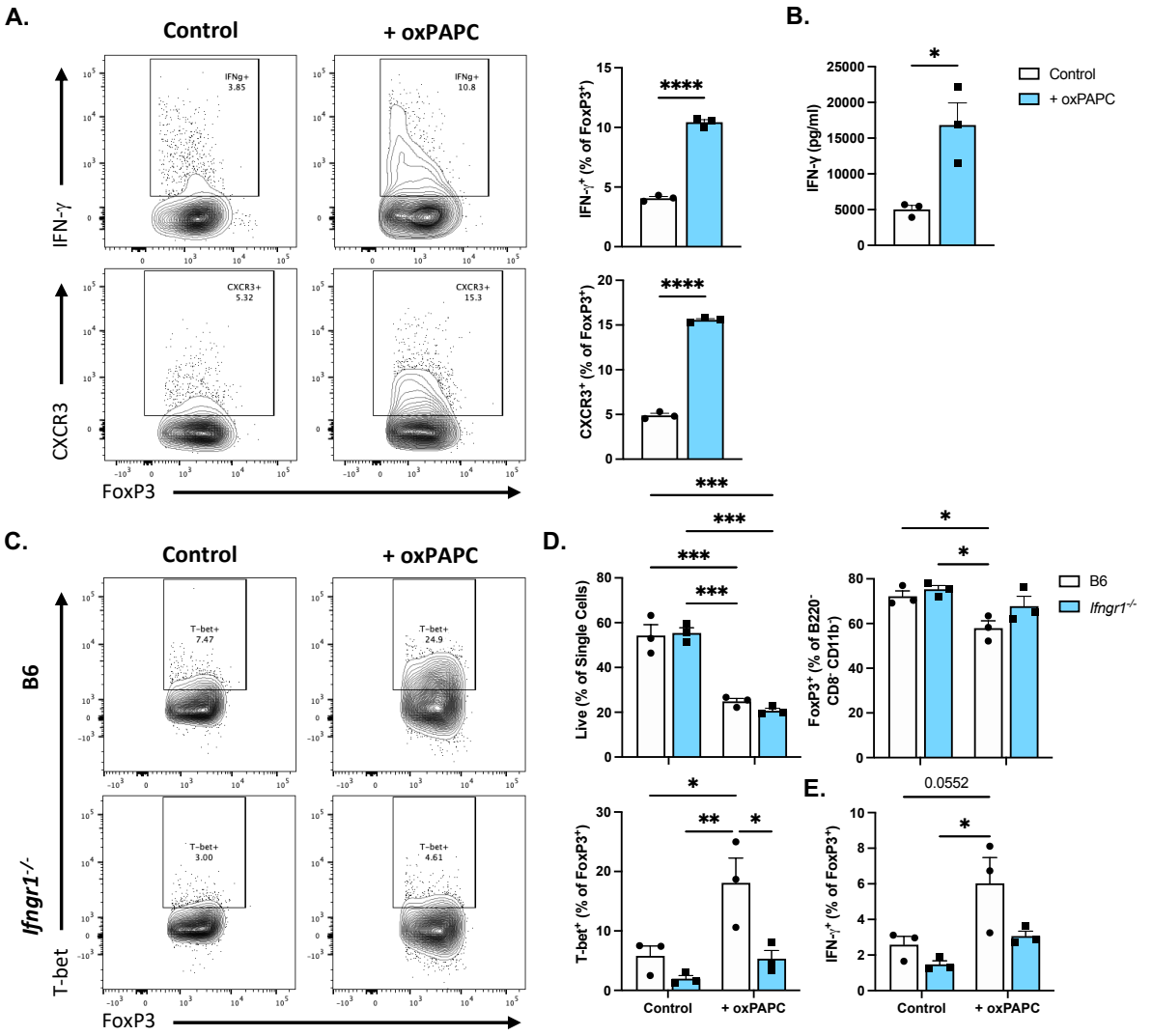

Figure 2.7: OxPAPC treatment increases T_{reg} IFN-γ production through an IFNγR1-dependent mechanism. (A) $CD4^+$ T cells were enriched from the spleens of four- to six-week-old B6 mice and skewed to a T_{reg} phenotype for five days with or without 5μg/ml oxPAPC. Th1 associated cytokines and markers were assessed by flow cytometry after a four-hour stimulation with PMA, ionomycin, and Golgi inhibitor (top) or directly after harvest (bottom). **(B)** T_{regs} were polarized as in (A) for three days. IFN-γ was measured in supernatants by ELISA. * and **** denote significance $p<0.05$ and $p<0.0001$, respectively, by Student's *t* test. **(C-E)** $CD4^+$ T cells were enriched from the spleens of four- to six-week-old B6 or *Ifngr1*$^{-/-}$ mice and skewed to a T_{reg} phenotype for three **(C-D)** or five **(E)** days with or without 5μg/ml oxPAPC. T_{reg} phenotype was assessed by flow cytometry directly at harvest **(C-D)** or after a four-hour stimulation with PMA, ionomycin, and Golgi inhibitor **(E)**. Shown is one representative of at least three experiments. Data points are individual mice and error bars show SEM. *, **, and *** denote significance $p<0.05$, $p<0.01$, and $p<0.001$, respectively, by two-way ANOVA and Tukey's multiple comparison test.

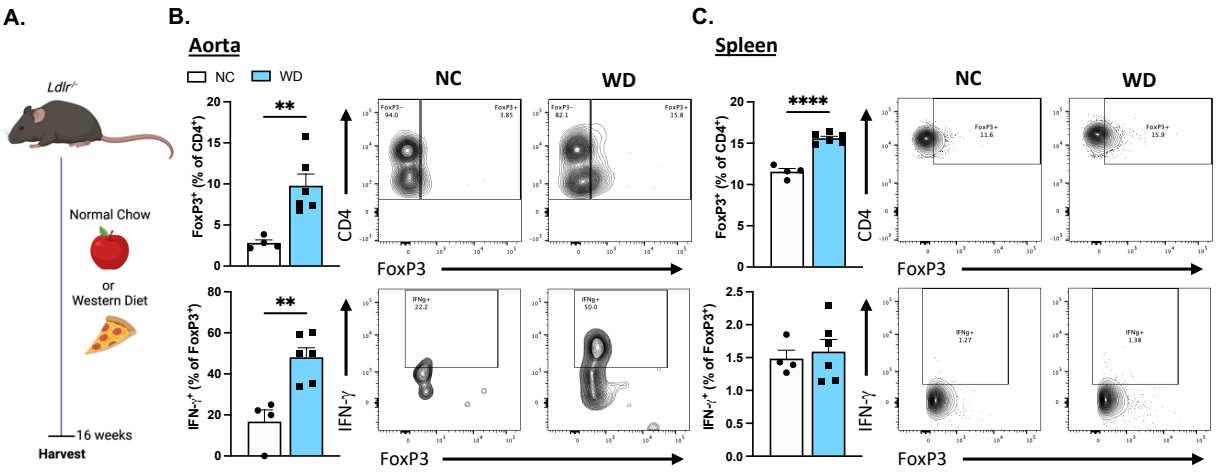

Figure 2.8: IFN-γ$^+$ T$_{regs}$ are increased in oxPL rich atherosclerotic environment. **(A)** Study design (image generated with Biorender). Samples were collected from male *Ldlr*$^{-/-}$ mice maintained as depicted. **(B)** Aortas were enzymatically digested, processed through 70μm strainers, and analyzed by flow cytometry. **(C)** Spleens were processed through 40μm strainers, red blood cells were lysed, and splenocytes were analyzed by flow cytometry. N=4-6 mice per group. Data points represent individual mice and error bars show SEM. ** and **** denote significance $p<0.01$ and $p<0.0001$, respectively, by Student's *t* test.

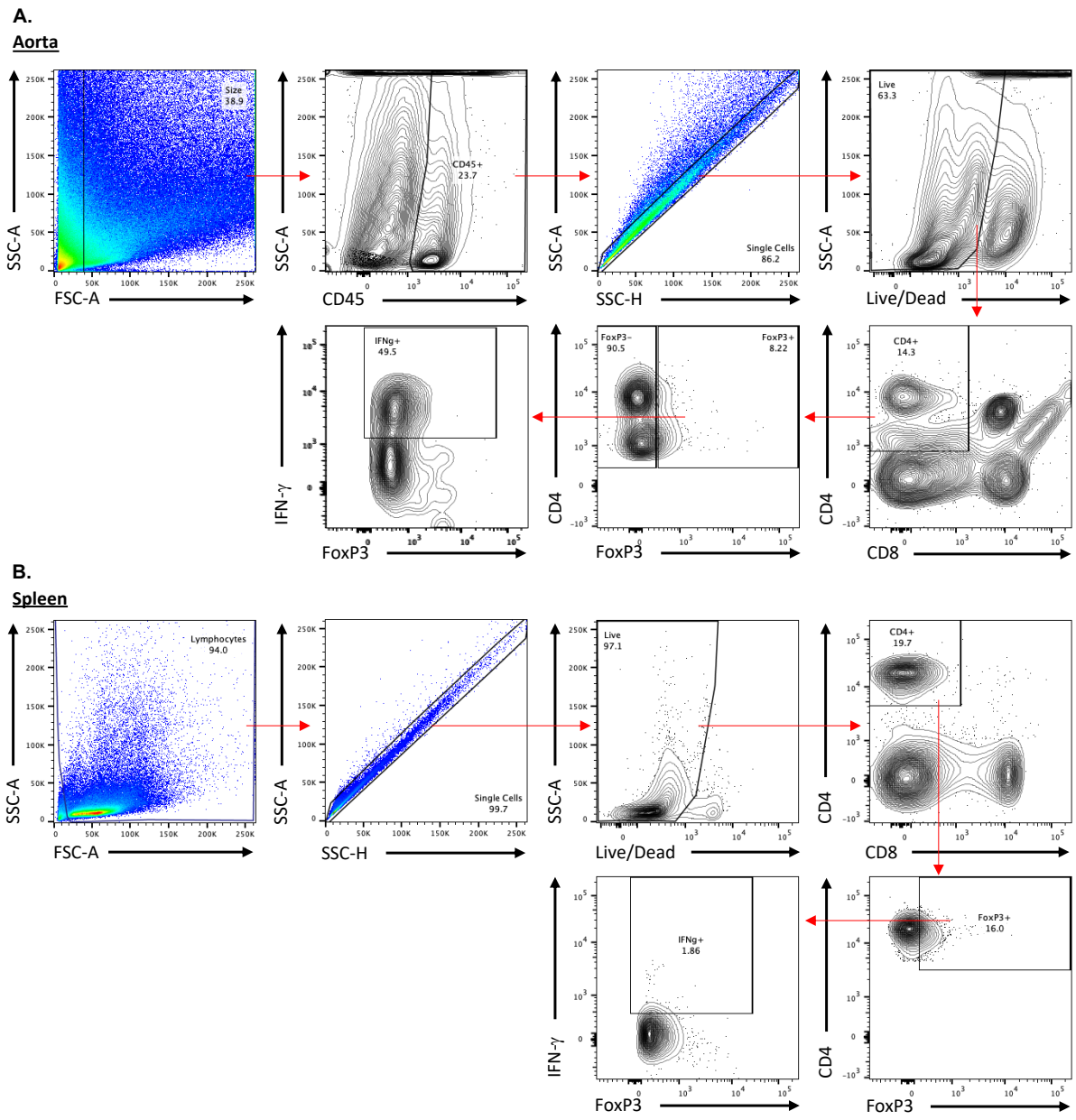

Figure 2.9: Diet comparison gating strategies. Male *Ldlr*$^{-/-}$ mice were maintained on NC or WD for 16 weeks. **(A)** Aortas were enzymatically digested, processed through 70μm strainers, and analyzed by flow cytometry. Cells were gated on size, CD45^{+}, single cells, viability, CD4^{+}, FoxP3^{+}, and then IFN-γ^{+}. Shown is a concatenation of all NC samples. **(B)** Spleens were processed through 40μm strainers, red blood cells were lysed, and splenocytes were analyzed by flow cytometry. Cells were gated on FSC/SSC, single cells, viability, CD4^{+}, FoxP3^{+}, and then IFN-γ^{+}.

IFN-γ signaling and CD36 are required for the Th1-like phenotype of oxPAPC-treated T_{regs}. Due to the elevated production of IFN-γ by surviving oxPAPC-treated T_{regs} and the known autocrine effects of the cytokine, we tested the contribution of IFN-γ signaling to oxPAPC-mediated T_{reg} phenotypes. To do this, naïve $CD4^+$ T cells were purified from spleens of *Ifngr1*$^{-/-}$ mice and skewed to T_{regs} in the presence or absence of oxPAPC. Interestingly, the Th1-like phenotype characterized by increased T-bet$^+$ IFN-γ producing FoxP3$^+$ cells, did not develop in surviving IFNγR1-deficient oxPAPC-treated T_{regs} (Figure 2.7C-E). However, IFNγR1 deficiency did not affect the oxPAPC-induced reduction in viability (Figure 2.7D), suggesting cell death is mediated by a separate mechanism.

To try to determine the mechanism facilitating oxPAPC-induced cell death, we tested the role of known oxPAPC receptors, CD36 and TLR-4[149,150]. To do this, naïve $CD4^+$ T cells were purified from spleens of *Cd36*$^{-/-}$ or *Tlr4*$^{-/-}$ mice and skewed to T_{regs} in the presence or absence of oxPAPC. Like IFNγR1, CD36 deficiency inhibited the development of Th1-like phenotypes in T_{regs} following oxPAPC treatment but did not affect oxPAPC-driven cell death (Figure 2.10A-C). However, TLR-4 deficiency did not alter any oxPAPC-induced T_{reg} phenotypes (Figure 2.11A-B). These data suggest oxPAPC needs multiple receptors to mediate its Th1-like alterations, but that an independent mechanism still exists to reduce T_{reg} viability.

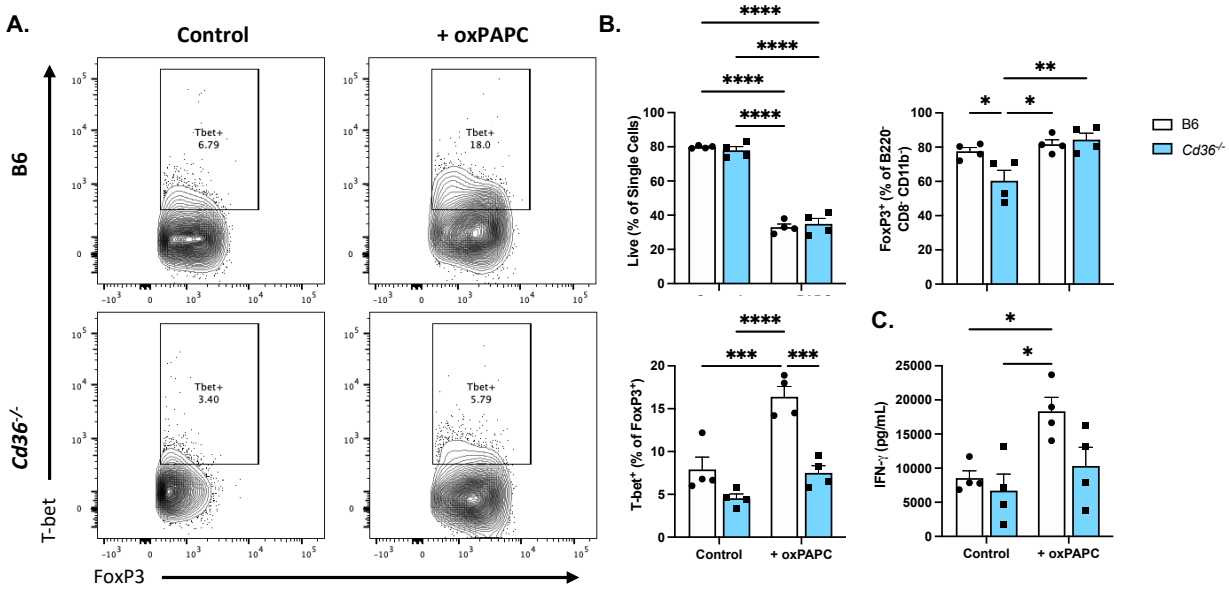

Figure 2.10: CD36 mediates oxPAPC-induced Th1-like phenotypes but does not affect T_{reg} viability. (A-C) $CD4^+$ T cells were enriched from the spleens of four- to six-week-old B6 or *Cd36*$^{-/-}$ mice and skewed to a T_{reg} phenotype for three days with or without 5μg/ml oxPAPC. **(A-B)** T_{reg} phenotype was assessed by flow cytometry directly at harvest. **(C)** IFN-γ concentration was measured in culture supernatants by ELISA. Shown is one representative of at least three experiments. Data points are individual mice and error bars show SEM. *, **, ***, and **** denote significance $p<0.05$, $p<0.01$, $p<0.001$, and $p<0.0001$, respectively, by two-way ANOVA and Tukey's multiple comparison test.

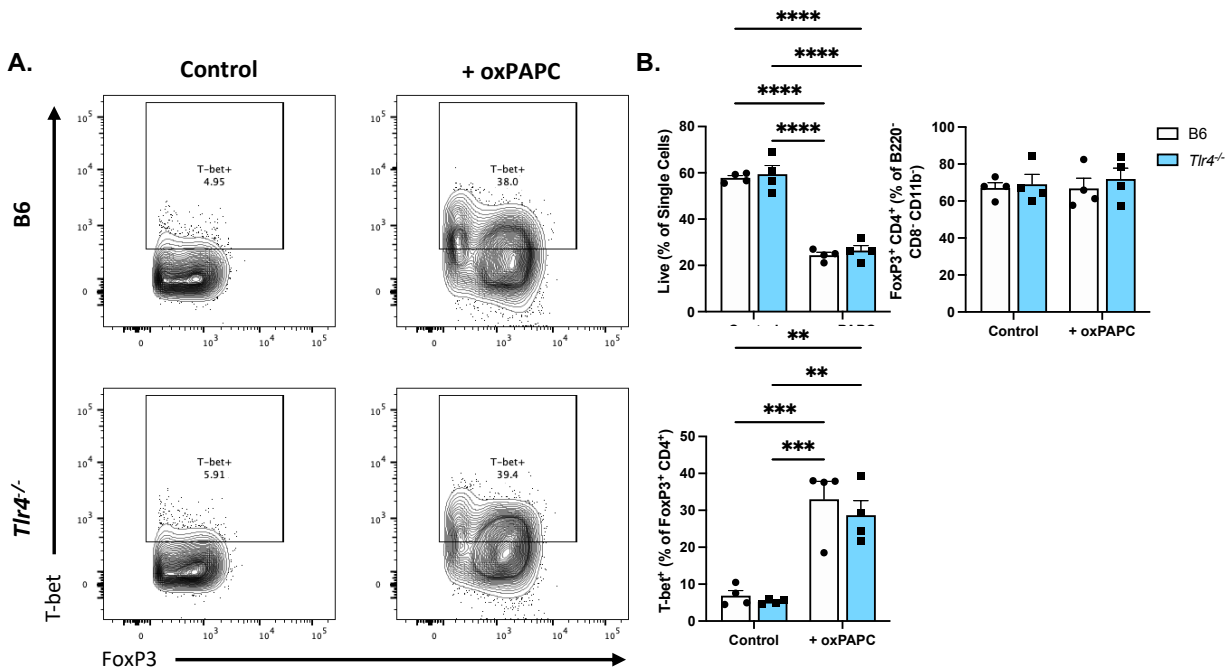

Figure 2.11: TLR-4 is not required for oxPAPC-induced changes in T_{regs}. (A-B) $CD4^+$ T cells were enriched from the spleens of four- to six-week-old B6 or *Tlr4*$^{-/-}$ mice and skewed to a T_{reg} phenotype for three days with or without 5μg/ml oxPAPC. T_{reg} phenotype was assessed by flow cytometry directly at harvest. Shown is one representative of at least two experiments. Data points are individual mice and error bars show SEM. **, ***, and **** denote significance $p<0.01$, $p<0.001$, and $p<0.0001$, respectively, by two-way ANOVA and Tukey's multiple comparison test.

T_{regs} require optimal cytokine concentrations for appropriate polarization and survival[151,152], so T_{reg} skews with and without oxPAPC were performed while titrating T_{reg} promoting cytokines IL-2 and transforming growth factor β (TGF-β). Titration of IL-2 or TGF-β did not have an effect on the oxPAPC-mediated alterations to T_{reg} differentiation (Figure 2.12A-F) indicating that increasing either cytokine could not rescue the oxPAPC-induced viability deficit or Th1-like phenotype.

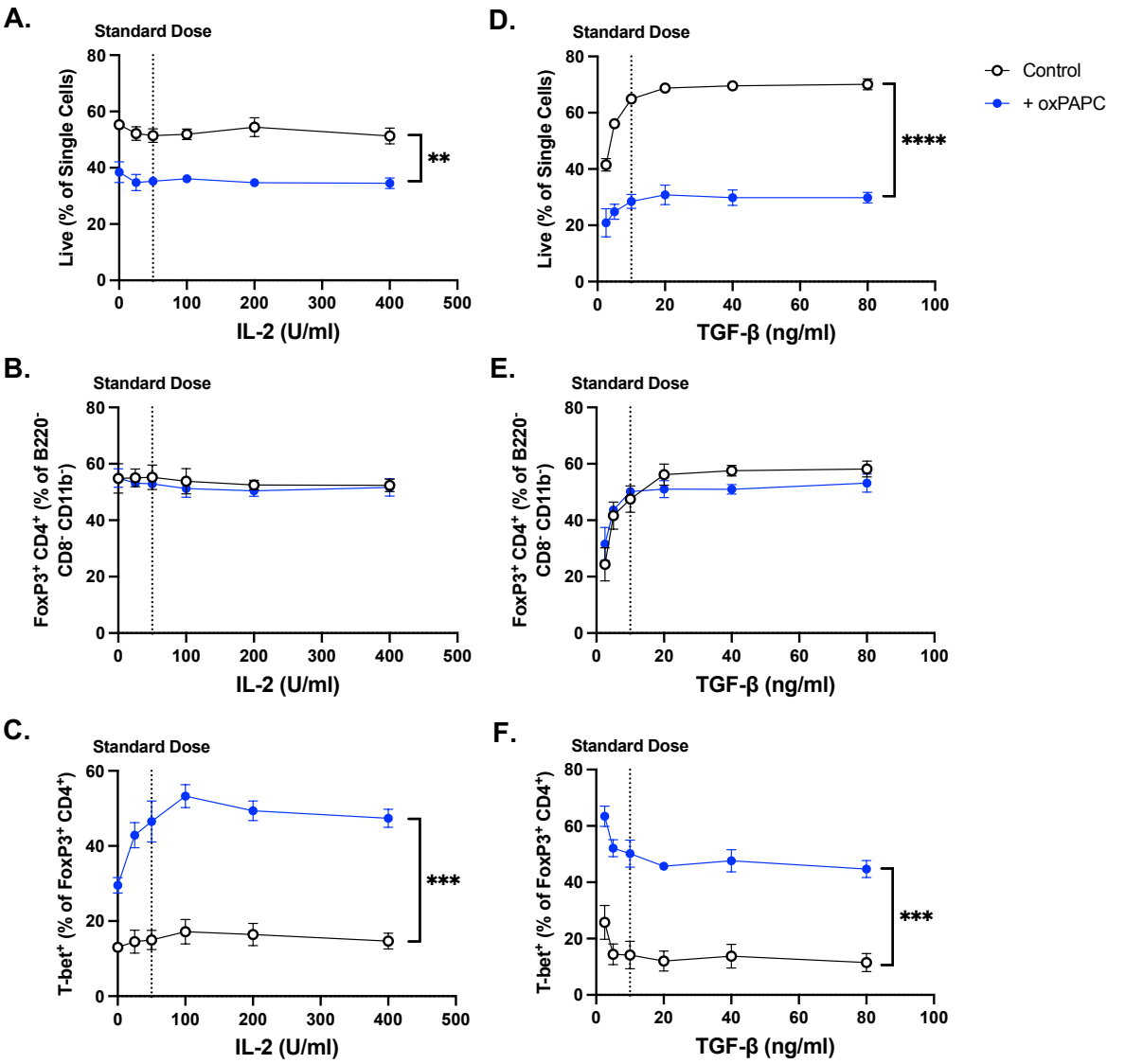

Figure 2.12: Neither IL-2 nor TGF-β titration rescue oxPAPC-induced phenotypes. **(A-F)** $CD4^+$ T cells were enriched from the spleens of four- to six-week-old B6 mice and skewed to a T_{reg} phenotype for three days with or without 5μg/ml oxPAPC. IL-2 **(A-C)** or TGF-β **(D-F)** concentrations were titrated as indicated for the duration of the culture. T_{reg} phenotype was assessed by flow cytometry directly at harvest. Error bars show SEM representing at least three biological replicates. **, ***, and **** denote significance $p<0.01$, $p<0.001$, and $p<0.0001$, respectively, for area under the curve by Student's *t* test.

OxPAPC reduces T_{reg} suppressive capacity in vitro and in vivo. Because T_{regs} have been shown to be impaired in the oxidized lipid-rich microenvironment during

atherosclerosis[131–134], we hypothesized oxPAPC treatment would make T_{regs} less suppressive. Interestingly, surviving oxPAPC-treated T_{regs} expressed higher levels of functional T_{reg} markers at day 3 in culture, but by day 5 these were significantly reduced, in some cases to below control levels (Figure 2.13A). In agreement with these observations, when T_{regs} were cultured for five days and then used for an *in vitro* suppression assay, oxPAPC-treated T_{regs} were less able to suppress $CD8^+$ T cell proliferation than control T_{regs} (Figure 2.13B). This was not simply due to the viability deficit observed in oxPAPC-treated T_{regs}, as suppression assays were conducted using equivalent numbers of live cells. Therefore, results indicate oxPAPC treatment impairs T_{reg} function in surviving cells as well as stable differentiation. These data suggest that presence of oxPL during induction of T_{regs} might affect their suppressive function during atherosclerosis.

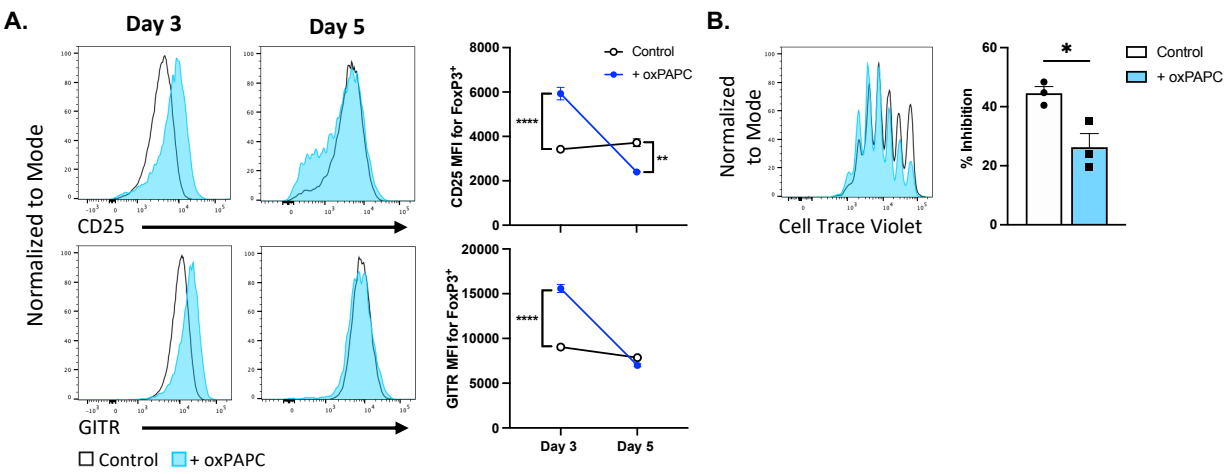

Figure 2.13: OxPAPC-treated T_{regs} are less suppressive. (A) $CD4^+$ T cells were enriched from the spleens of four- to six-week-old B6 mice and skewed to a T_{reg} phenotype for the indicated time with or without 5μg/ml oxPAPC. T_{reg} markers were assessed by flow cytometry. Error bars show SEM. ** and **** denote significance $p<0.01$ and $p<0.0001$, respectively, by repeated measures two-way ANOVA and Šídák's multiple comparisons test. **(B)** $CD4^+$ T cells were enriched from the spleens of four- to six-week-old B6-Thy1.1-$FoxP3^{GFP}$ mice and skewed to a T_{reg} phenotype for five days with or without 5μg/ml oxPAPC. Equal numbers of live T_{regs} were then co-cultured with cell trace violet-labeled $CD8^+$ T cells for three days. Percent inhibition of $CD8^+$ T cell proliferation was assessed by flow cytometry. Shown are the 3:1 T_{reg}:T_{res} ratio results from one representative of at least three experiments. Error bars show SEM. * denote significance $p<0.05$ by Student's *t* test.

To assess the function of oxPAPC-induced T_{regs} in atherosclerosis, T_{regs} were skewed from $Thy1.1^+$ mice in the presence or absence of oxPAPC and equivalent numbers of resulting live T_{regs} were adoptively transferred into *Ldlr*$^{-/-}$ mice with established lesions (Figure 2.14A). Saline injected *Ldlr*$^{-/-}$ mice served as the control. Compared to the saline injected group, mice given control T_{regs} had significantly less atherosclerosis in the proximal aorta. In contrast, oxPAPC-treated T_{regs} were unable to inhibit atherosclerosis progression (Figure 2.14B-C), demonstrating oxPAPC-induced Th1-like T_{regs} are not protective *in vivo*. Adoptive transfer of T_{regs} did not significantly alter the collagen deposition, necrotic area, or SMC or macrophage content in the

lesions (Figure 2.15A-C), indicating adopted T_{regs} were not remodeling the total plaque structure, but slowing progression when functional. Serum cholesterol and triglycerides (Figure 2.16A) were also unchanged in recipient mice, suggesting the changes observed in the plaque were immune mediated rather than a consequence of improved dyslipidemia. OxLDL-specific antibody titers were similar among all groups (Figure 2.16B).

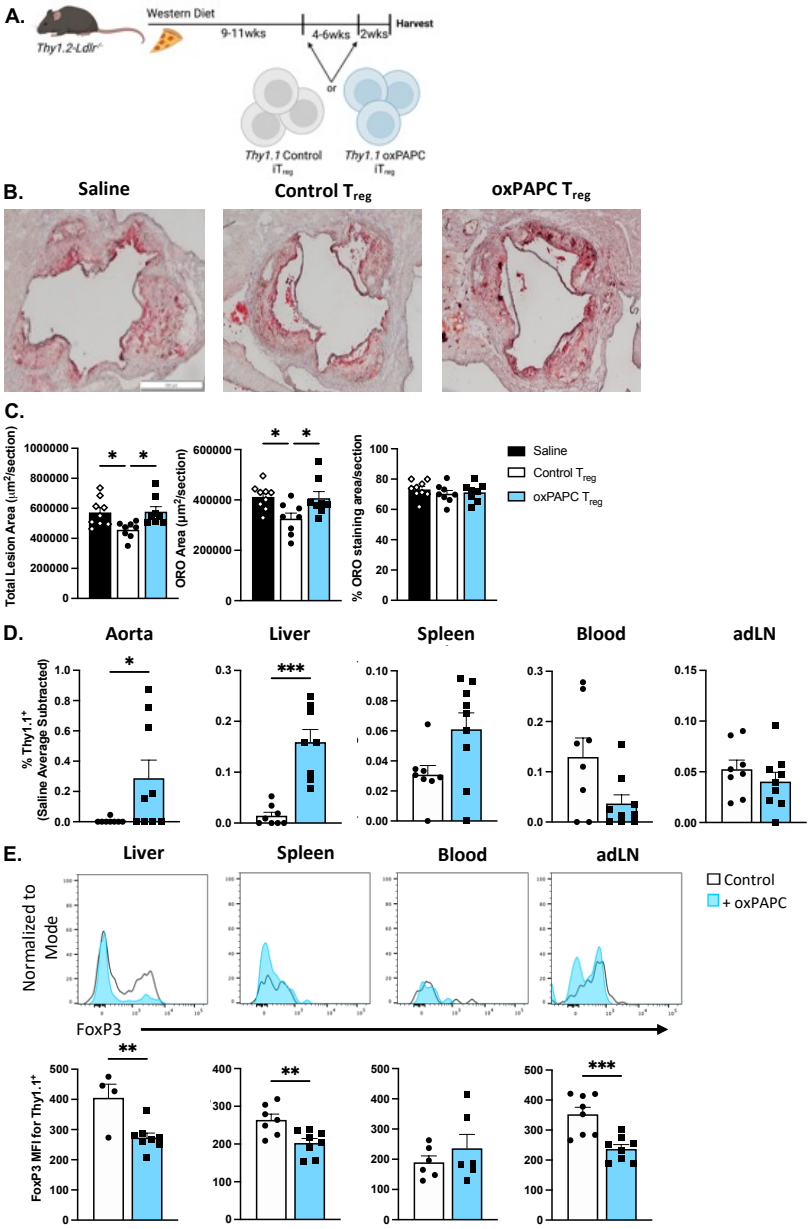

Figure 2.14: OxPAPC-treated T_{regs} are unable to inhibit atherosclerosis progression. (A) Study design (image generated with Biorender). Adoptively transferred T_{regs} were skewed from $CD4^+$ T cells enriched from the spleens of four- to six-week-old B6-Thy1.1-$FoxP3^{GFP}$ mice for five days with or without 5μg/ml oxPAPC. *Ldlr*$^{-/-}$ mice were injected as shown with saline or equal numbers of live control T_{regs} or oxPAPC-treated T_{regs}. **(B)** Representative Oil-Red-O (ORO) stained atherosclerotic lesions from the aortic root (scale bar represents 500μm). **(C)** Quantification of ORO stained lesions by total lesion area, ORO staining area, and percentage of ORO staining in recipient *Ldlr*$^{-/-}$ mice. N=8-9 mice per group, 4 independent experiments. *, **, ***, and **** denote significance $p<0.05$, $p<0.01$, $p<0.001$, and $p<0.0001$, respectively, by one-way ANOVA and Tukey's multiple comparison test. **(D)** Indicated tissues were processed and analyzed by flow cytometry. The average $Thy1.1^+$ signal in saline injected controls was treated as background and subtracted from samples. * and *** denote significance $p<0.05$ and $p<0.001$, respectively, by Mann-Whitney test. **(E)** Adoptively transferred T_{regs} in the indicated tissues were analyzed by flow cytometry. Histogram shows representative samples. *, **, ***, and **** denote significance $p<0.05$, $p<0.01$, $p<0.001$, and $p<0.0001$, respectively, by Student's *t* test. N=8-9 mice per group, 4 independent experiments. Data points represent individual mice and error bars show SEM.

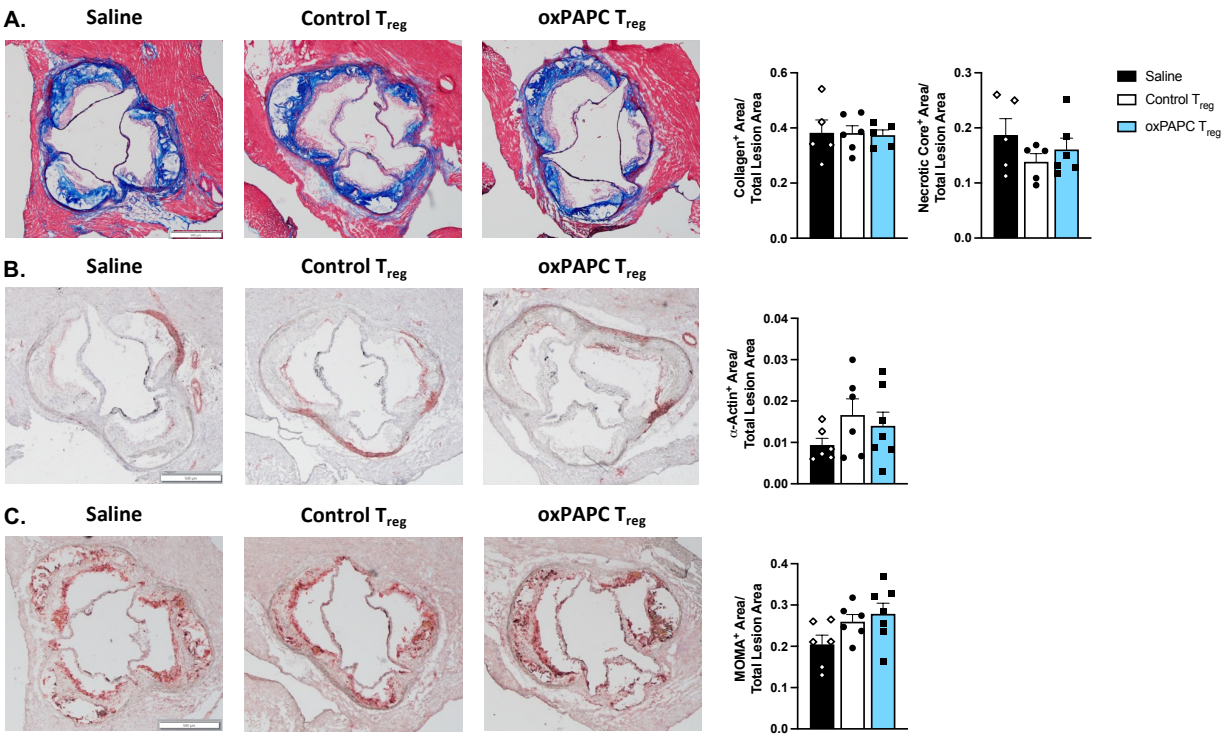

Figure 2.15: Adoptive transfer of *in vitro*-derived T_{regs} does not cause significant plaque remodeling. Adoptively transferred T_{regs} were skewed from $CD4^+$ T cells enriched from the spleens of four- to six-week-old B6-Thy1.1-$FoxP3^{GFP}$ mice for five days with or without 5μg/ml oxPAPC. *Ldlr*$^{-/-}$ mice were injected with saline or equal numbers of live control T_{regs} or oxPAPC-treated T_{regs}. **(A)** Representative trichrome stained atherosclerotic lesions from the aortic root. Quantification of fraction of collagen (blue) staining area of total lesion area (left graph) and fraction of necrotic core area of total lesion area (right graph) in recipient *Ldlr*$^{-/-}$ mice. **(B)** Representative sections of SMC immunohistochemistry as measured by α-actin in atherosclerotic lesions from the aortic root. Quantification of fraction of α-actin (red) staining area of total lesion area in recipient *Ldlr*$^{-/-}$ mice. **(C)** Representative sections of macrophage immunohistochemistry as measured by MOMA staining in atherosclerotic lesions from the aortic root. Quantification of fraction of MOMA (red) staining area of total lesion area in recipient *Ldlr*$^{-/-}$ mice. Scale bar represents 500μm. N=5-7 mice per group, 2 independent experiments.

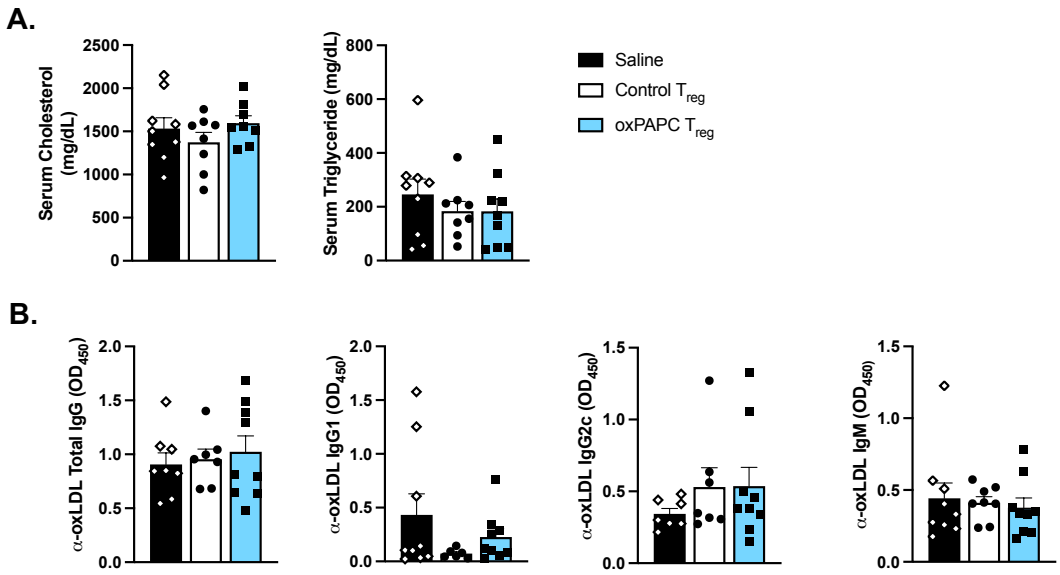

Figure 2.16: Adoptive transfer of control or oxPAPC-treated T_{regs} does not significantly alter serum lipids, α-oxLDL antibodies, or lesion $CD4^+$ T cell content. Adoptively transferred T_{regs} were skewed from $CD4^+$ T cells enriched from the spleens of four- to six-week-old B6-Thy1.1-$FoxP3^{GFP}$ mice for five days with or without 5μg/ml oxPAPC. Cells or saline were then injected into hyperlipidemic *Ldlr*$^{-/-}$ mice. **(A)** Serum cholesterol and triglycerides were determined by commercially available kits. **(B)** Serum α-oxLDL Total IgG, IgG1, IgG2c, and IgM were determined by ELISA at a 1:500, 1:250, 1:250, and 1:8000 dilution, respectively. N=6-9 mice per group, 4 independent experiments. *, **, ***, and **** denote significance $p<0.05$, $p<0.01$, $p<0.001$, and $p<0.0001$ by one-way ANOVA and Tukey's multiple comparison test.

Thy1.1$^+$ cells were detected in every tissue tested in recipient mice (Figure 2.14D and Figure 2.17A-C). All recipients had similar proportions of transferred Thy1.1$^+$ T_{regs} in the adLNs, yet mice injected with oxPAPC-treated T_{regs} had a larger proportion of transferred cells in the aorta, liver, and spleen, but a significant reduction circulating in the blood compared to control T_{reg} recipients (Figure 2.14D). Both control and oxPAPC-treated T_{regs} had reduced FoxP3 expression relative to when they were first injected, but adoptively transferred oxPAPC-induced T_{regs} in the liver, spleen and adLNs expressed significantly less FoxP3 than control T_{regs} by the end of the study (Figure 2.14E). Interestingly, this relative reduction in FoxP3 was not observed in transferred cells found

in the blood (Figure 2.14E). Overall, these data indicate that oxPAPC not only alters T_{reg} differentiation, but also compromises the atheroprotective function of the cells that survive, possibly by reducing T_{reg} stability and changing migration *in vivo*.

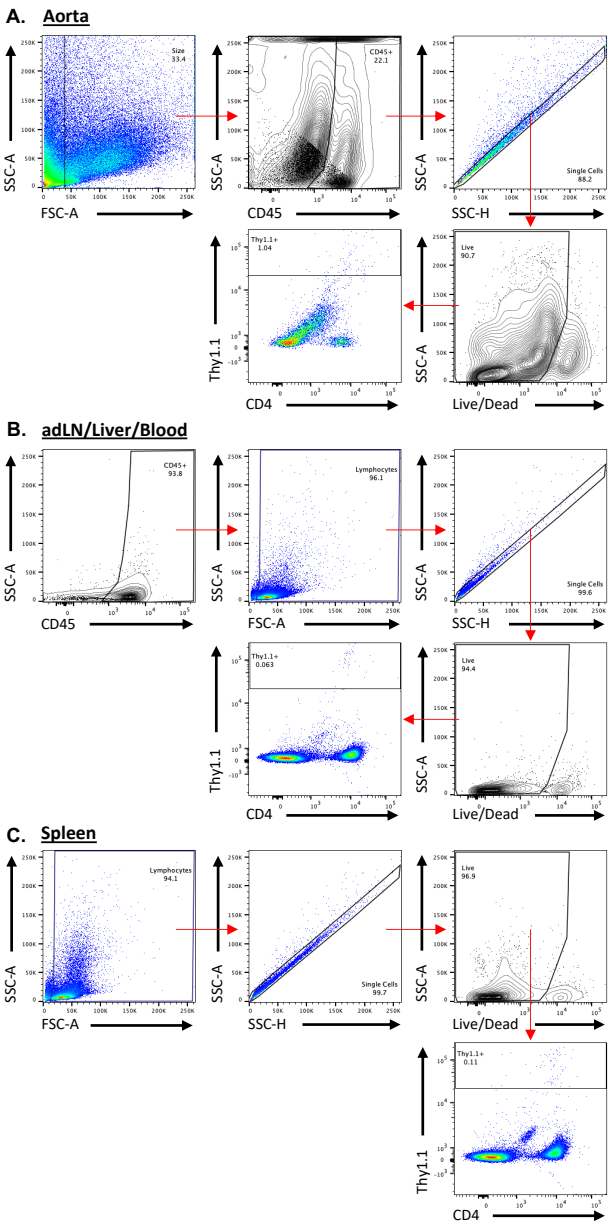

Figure 2.17: Adoptive transfer gating strategies. Female *Ldlr*$^{-/-}$ mice were maintained WD for 15-19 weeks and received two injections of saline, control T_{regs}, or oxPAPC-treated T_{regs}. **(A)** Aortas were enzymatically digested, processed through 70μm strainers, and analyzed by flow cytometry. Cells were gated on size, CD45^{+}, single cells, viability, and then Thy1.1^{+}. Shown is a concatenation of oxPAPC T_{reg} injected samples. **(B)** Aorta draining lymph nodes were processed through 40μm strainers and analyzed by flow cytometry. Cells were gated on CD45^{+}, FSC/SSC, single cells, viability, and then Thy1.1^{+}. The same gating scheme was used for livers and blood samples. **(C)** Spleens were processed through 40μm strainers, red blood cells were lysed, and splenocytes were analyzed by flow cytometry. Cells were gated on FSC/SSC, single cells, viability, and then Thy1.1^{+}.

Discussion

The current study demonstrates that oxPAPC alters T_{reg} differentiation and elicits a Th1-like phenotype in those that survive, compromising their function *in vitro* and *in vivo.* Previous work has shown T_{regs} are reduced in number in atherosclerotic mice and are less suppressive after treatment with oxLDL[126,136], in agreement with our own findings with oxPAPC. However, these prior studies utilized fully differentiated T_{regs} for their experiments meaning they were not able to address what role oxLDL might play during T_{reg} polarization. Gaddis *et al.* skewed naïve *Apoe*$^{-/-}$ $CD4^+$ T cells *in vitro* with TGF-β and reported the inclusion of oxLDL in these cultures inhibited T_{reg} differentiation[133]. However, oxLDL is a rather large, heterogeneous molecule, so this work does not specifically address the role of oxPL in T_{reg} dysregulation. Therefore, our study fills a gap in knowledge regarding how oxPLs, as represented by oxPAPC, impact the differentiation and function of T_{regs}.

It is known that adoptive transfer of T_{regs} into atherogenic mouse models inhibits plaque progression[115,125,126,153]. This is consistent with our current findings which showed transfer of control T_{regs} into WD-fed *Ldlr*$^{-/-}$ mice significantly delayed disease development. However, the adoptive transfer of an equivalent number of live oxPAPC-treated T_{regs} did not result in reduced atherosclerosis suggesting exposure to oxPLs decrease the suppressive capacity of T_{regs} *in vivo* (Figure 2.14). Transferred T_{regs} also demonstrated differential migration in hyperlipidemic mice. While both control and oxPAPC-treated T_{regs} were found in similar proportions in the adLNs of recipient mice, oxPAPC-treated cells were elevated in other tissues (aorta, liver, spleen), whereas the control T_{regs} were enriched in the blood (Figure 2.14). These findings are consistent with

work from Amersfoort *et al.* showing T_{regs} from dyslipidemic mice homed to atherosclerotic lesions and sites of inflammation more than T_{regs} from animals maintained on normal chow[154]. One limitation of our study, however, is the relatively small population of transferred T_{regs} that remained detectable by flow cytometry at the time of harvest (Figure 2.17). Though our altered disease burdens demonstrate that functional adopted T_{regs} played a biologically relevant role in our system, too few transferred cells persisted by the conclusion of the study to fully characterize phenotypic changes. In future studies, recipients may need to be injected with more cells from the start or be sacrificed at an earlier time point to enrich the transferred Thy1.1$^+$ population. Collectively, these results indicate oxPLs directly promote functional and migratory changes in T_{regs} that ultimately undermine their regulatory function and allow for disease progression.

T_{reg} instability is one major hypothesis for T_{reg} loss in atherosclerosis with exT_{regs} developing Th1- or T_{FH}-like phenotypes[133,134]. Here, we demonstrate that oxPAPC treatment leads to a decrease of FoxP3 expression in surviving cells over time in culture. Consistent with potential T_{reg} instability, Th1-like markers (T-bet, IFN-γ, CXCR3) were most increased in FoxP3^{lo} T_{regs}, a population that proportionally increased with oxPAPC treatment, while receptors related to T_{reg} function (CD25, GITR, ICOS) were more associated with FoxP3^{hi} cells (Figure 2.5). Additionally, oxPAPC-treated T_{regs} had reduced expression of FoxP3 compared to control T_{regs} following adoptive transfer into hyperlipidemic *Ldlr*$^{-/-}$ mice (Figure 2.14). This suggests oxPLs, like oxPAPC, may be partly responsible for T_{reg} instability in the plaque. This conclusion is consistent with the findings of Wolf *et al*.[109] and Kimura *et al*.[155] which show T_{regs} specific for the apoB core

of oxLDL have increased expression of T effector-associated markers in mice and humans with atherosclerosis. However, our study does not leverage T_{reg} lineage tracing mouse models, so additional work in these systems will be required in the future to truly determine how oxPLs impact development of exT_{regs}.

The potential for oxPL-induced T_{reg} instability also has implications for atherosclerosis regression. In Sharma *et al.* T_{regs} in progressing atherosclerotic plaques are mostly thymic-derived. However, regressing plaques, in mice where lipid levels were normalized, have a larger T_{reg} population in part due to inducible peripheral T_{regs}[128]. These findings suggest the normalization of oxPLs in circulation allows for altered recruitment, efficient polarization, and/or survival of peripherally induced T_{reg} populations in the plaque. This, in combination with our own findings, suggests a model in which oxPLs modulate T_{reg} differentiation in peripherally derived T_{regs}. Thus one may hypothesize that peripherally induced T_{regs} differentiating *in situ* or migrating to the plaque during disease progression cannot persist as functional T_{regs} due to increased presence of oxPLs.

In addition to T_{reg} instability, T_{reg} numbers are also reduced during atherosclerosis as a result of increased apoptosis[131,132]. Magnato-García *et al*. proposed that the increase in T_{reg} death is due to the altered microenvironment of the plaque[131] and others have shown that oxLDL is capable of inducing apoptosis in T_{regs}[132,136]. Our results demonstrating oxPAPC-treated T_{regs} undergo significantly increased levels of apoptosis compared to control T_{regs} (Figure 2.1 and Figure 2.3), are consistent with these findings and indicate oxPLs are at least one specific component of the lesion microenvironment that may induce T_{reg} apoptosis. Interestingly, there is some conflicting information

regarding T_{reg} numbers in patients with CVD. As stated above, some groups have shown T_{reg} loss with disease progression[132,156], others have found no correlation between T_{reg} number and disease severity[157], and still others have actually measured an increase in apoB-specific T_{regs} in patients[109]. In all these cases, T_{reg} frequencies were measured in peripheral blood, which unfortunately does not precisely reflect the oxPL microenvironment of the lesion.

OxPAPC-induced T_{reg} apoptosis was not mediated by IFNγR1 signaling or CD36 unlike the Th1-like phenotypes (Figure 2.7 and Figure 2.10), suggesting the two effects are decoupled and that IFN-γ signaling and CD36 are only part of the mechanism by which oxPAPC alters T_{regs}. Modulation of TLR-4, IL-2 concentration, and TGF-β levels additionally did not rescue oxPAPC-induced cell death or Th1-like phenotypes (Figure 2.11 and Figure 2.12). T_{reg} death was also not due to an overall toxicity of oxPAPC as neither Th1 nor Th17 cells polarized with oxPAPC had reduced viability (Figure 2.1). Interestingly, the majority of oxPAPC-induced cell death did not occur until after FoxP3 expression was established (Figure 2.3F), suggesting the transcription factor itself may be promoting the apoptosis. This would be consistent with the work of Tai *et al.* which demonstrates FoxP3 expression is proapoptotic during differentiation in the thymus unless countered by additional pro-survival signals[151].

Th1-like T_{regs} such as those we describe here, are not specific to atherosclerosis and have been identified in the literature in various inflammatory conditions. Interestingly, in atherosclerosis, cancer, and vitiligo these cells are described as proinflammatory[134,145,158,159], while in graft-versus-host disease, diabetes, and infection they are anti-inflammatory[160–163]. Therefore, our findings may suggest the ultimate

impact of these Th1-like T_{regs} is disease dependent and perhaps in niches characterized by high levels of oxPL, like atherosclerotic plaques and tumors, Th1-like T_{regs} are dysfunctional. This is consistent with Li *et al*. proposed importance for unidentified "atherosclerosis antigens" to the development of a proinflammatory Th1-like T_{reg} phenotype[145].

In conclusion, our study shows oxPAPC specifically alters T_{reg} differentiation and elicits a Th1-like phenotype in the cells that survive, compromising their suppressive function. Development of the Th1-like T_{reg} phenotype is partially dependent on CD36 and IFN-γ signaling, but a yet to be identified pathway exists to mediate oxPAPC-induced T_{reg} apoptosis. Overall, our findings demonstrate that oxPLs, such as oxPAPC, can directly alter T_{reg} polarization and phenotype and may be relevant to their decreased presence and function in atherosclerosis.

CHAPTER 3

T_{reg} IFNγR Signaling Modulates Atherosclerosis in a Sex-Dependent Manner

Introduction

OxPLs like oxPAPC are highly prevalent in the atherosclerotic plaque as components of oxLDL particles and from apoptotic cells[138,141]. As demonstrated in Chapter 2, T_{reg} exposure to oxPAPC during differentiation promotes the development of Th1-like T-bet^{+} IFN-γ^{+} T_{regs} through an IFNγR-dependent mechanism. While *in vitro*-derived oxPAPC-treated T_{regs} are dysfunctional and incapable of controlling atherosclerosis progression when adoptively transferred (Chapter 2), it is less clear how oxPAPC might impact the development and function of T_{regs} *in vivo.*

Functional T_{regs} are known to be protective in atherosclerosis and genetic deficiency or depletion of T_{regs} significantly enhances plaque development[125,127]. However, T_{regs} are inhibited during disease progression via enhanced cell death and loss of stability[131–134]. The dysregulation induced in T_{regs} in the atherosclerotic microenvironment has been well described (reviewed in [164]), but no published studies interrogate the T_{reg}-intrinsic signals that mediate the dysfunctional phenotypes in atherosclerosis *in vivo*. Therefore, there is a great need to define what specific T_{reg} pathways are being disrupted *in vivo* to induce dysfunction.

In tumor immunology, IFN-γ has been shown to act directly on T_{regs} promoting "fragile" phenotypes in which FoxP3 expression is maintained but function is not[165]. The cytokine has also been described to limit T_{reg} population development[165–168] and promote Th1-like T_{reg} phenotypes, though whether those altered cells are pro- or anti-inflammatory appears to be dependent on the disease context in which they are

found[169,170] (Chapter 2). IFN-γ is generally considered a proatherogenic cytokine due to its role in inflammatory immune cell recruitment, DC activation, foam cell differentiation, and SMC collagen inhibition[116–119,171]. However, Whitman *et al.* have reported that, while full body IFN-γ deficiency in *Apoe*$^{-/-}$ mice is atheroprotective in males, it exerts no change in females[120]. Thus, IFN-γ-mediated regulation of atherosclerosis may be more complex than is generally appreciated.

Using bone marrow chimeras, I show IFNγR1 deficiency specifically on T_{regs} significantly alters atherosclerosis severity in *Ldlr*$^{-/-}$ mice. Surprisingly, whether the receptor deficiency was protective or atherogenic was dependent on sex, with *Ifngr1*$^{fl/fl}$-*Foxp3*$^{Cre+}$ males developing smaller lesions while females of the same genotype established larger lesions than sex-matched controls.

Materials and Methods

Mice. B6.129S7-Ldlr^{tm1Her}/J (*Ldlr*$^{-/-}$; Stock # 002207), C57BL/6N-*Ifngr1*$^{tm1.1Rds}$/J (*Ifngr1*$^{fl/fl}$; Stock # 025394), and B6.129(Cg)-*Foxp3*$^{tm4(YFP/icre)Ayr}$/J (*Foxp3*$^{Cre+}$; Stock # 016959) mice were originally obtained from the Jackson Laboratory (Bar Harbor, ME). *Ifngr1*$^{fl/fl}$ and *FoxP3*$^{Cre+}$ animals were crossed to generate *Ifngr1*$^{WT/WT}$-*FoxP3*$^{Cre+}$ and *Ifngr1*$^{fl/fl}$-*FoxP3*$^{Cre+}$ littermates. Animals were maintained and housed at Vanderbilt University. All mice used in these studies were on the C57BL/6J background. Procedures were approved by the Vanderbilt University Institutional Animal Care and Use Committee. Both male and female mice were used for studies as specified.

Bone Marrow Transplants. Eight- to nine-week-old male and female *Ldlr*$^{-/-}$ mice were lethally irradiated with 900 rad from a ^{137}Cs source. At least four hours after irradiation,

transplant recipients were retro-orbitally injected with $1.6x10^6$ - $2.6x10^6$ live bone marrow cells from four- to eight-week-old sex-matched *Ifngr1*$^{WT/WT}$-*FoxP3*$^{Cre+}$ or *Ifngr1*$^{fl/fl}$-*FoxP3*$^{Cre+}$ littermate donors. Recipients were co-housed and maintained on NC during a four-week reconstitution period. Following this, mice were placed on WD for eight weeks after which animals were sacrificed, and aorta, adLN, and spleen were collected for flow cytometry analysis. Animals were included in this study based on age, sex, and genotype, and were excluded or removed from the study if they experienced weight loss or a notable physical ailment.

Tissue Collection. Aortas were processed as previously described[143]. Briefly, aortas were perfused with PBS, cleaned of fat, minced, and digested with 450U/ml Collagenase Type I (Worthington Biochemicals Cat # LS004194), 125U/ml Collagenase Type XI (Sigma Cat # C-7657), 60U/ml Hyaluronidase Type I (Sigma Cat # H-3506), and 60U/ml Dnase I (Millipore Sigma Cat # 69182) in PBS at 37°C for 30-45 minutes. Digested aortas were passed through 70μm cell strainers, and leukocytes washed before use in flow cytometry.

Flow Cytometry. Flow cytometry was performed on cells obtained *ex vivo*. Cells requiring a viability dye were stained with Ghost Dyes™ (Tonbo) according to the manufacturer protocol. For surface staining, cells were washed in HBSS containing 1% BSA, 4.17mM sodium bicarbonate, and 3.08mM sodium azide (FACS buffer), followed by a 10-minute room temperature incubation in 1μg/ml Fc block (α-CD16/32; Tonbo Cat # 40-0161) diluted in FACS buffer. Cells were then stained for 30 minutes at 4°C protected from light with the following antibodies diluted in FACS buffer: α-CD4-APCCy7 (Tonbo Cat # 25-0041), α-CD11b-Pe (Tonbo Cat # 50-0112), α-CD86-PeCy7

(Tonbo Cat # 60-0862), α-F4/80-APCCy7 (Tonbo Cat # 25-4801), α-IFNγR1-SB600 (BD Biosciences Cat # 745111). Samples not requiring intracellular staining were then washed in FACS buffer and fixed in 2% paraformaldehyde (PFA). Samples with intracellular stains were washed then permeabilized and stained with the following intracellular antibodies according to the FoxP3/Transcription Factor Staining Buffer Set manufacturer protocol (eBioscience Cat # 00-5523-00): α-FoxP3-PECy7 (eBioscience Cat # 25-5773-82), α-IFN-γ-APC (Tonbo Cat # 20-7311). All samples were washed and resuspended in 2% PFA before analysis. Sample acquisition was performed on a MacsQuant Analyzer (Miltenyi Biotec) and data were analyzed using FlowJo Single Cell Analysis software.

Atherosclerotic Plaque Analysis. Plaque analysis was performed on cryosections obtained from OCT embedded hearts. Sectioning started at the aortic sinus and proceeded for about 300μm before sample collection began. Sample sections were collected in alternating 10μm and 5μm sizes. Oil-red-O staining of 10μm cryosections was performed as previously described[146]. Slides were imaged using an Olympus BX41 Phase Contrast & Darkfield microscope and the Olympus cellSens Standard program. Quantification of total lesion area and Oil-red-O staining was performed using ImageJ.

ELISAs. Anti-oxLDL ELISAs were performed as previously described[144]. Briefly, Nunc Maxisorp 96-well plates (Invitrogen Cat # 44-2404-21) were coated in 1μg/ml oxLDL overnight at 4°C. After washing with 0.05% Tween in PBS and blocking with 3% BSA/PBS, serum samples were applied, and the plate was again incubated overnight. Biotinylated α-IgG (eBioscience Cat # 13-4013-85), α-IgG1 (Southern Biotech Cat # 1070-08), α-IgG2c (Southern Biotech Cat # 1080-08), or α-IgM (Southern Biotech Cat #

1020-08) were incubated for one hour at room temperature, followed by streptavidin-peroxidase (Southern Biotech Cat # 7200-05) for 30 minutes at room temperature. Plates were washed and OptEIA TMB substrate (BD Biosciences Cat # 555214) was applied for 8, 10, 15, and 5 minutes, respectively, before reaction was quenched with 2M HCl. Results were read at 450nm.

Statistical Analyses. All experiments were performed using biological replicates. Normally distributed data were analyzed using Student's *t* tests. All statistical tests were performed using GraphPad Prism.

Results

IFN-γ signaling in T_{regs} modulates atherosclerosis severity in a sex-dependent manner. Since IFN-γ is critical for oxPAPC-mediated T_{reg} alterations *in vitro* (Chapter 2), I wanted to test whether IFN-γ signaling in T_{regs} affects atherosclerosis severity *in vivo*. I produced bone marrow chimeras with *Ldlr*$^{-/-}$ recipients and either *Ifngr1*$^{WT/WT}$-*Foxp3*$^{Cre+}$ or *Ifngr1*$^{fl/fl}$-*Foxp3*$^{Cre+}$ littermate donors. Following sufficient time for reconstitution, transplanted mice were fed WD for eight weeks (Figure 3.1A). Consistent with previously published studies[165], IFNγR1 expression was reduced by ~50% in *Ifngr1*$^{fl/fl}$-*Foxp3*$^{Cre+}$ recipients compared to *Ifngr1*$^{WT/WT}$-*Foxp3*$^{Cre+}$ mice (Figure 3.1B). Recipient weight gain and spleen size were unaffected by donor genotype in both sexes (Figure 3.2A-F). Atherosclerosis severity was quantified by total lesion area in the aortic root and Oil-red-O area staining. Consistent with my prediction that IFN-γ signaling in T_{regs} is atherogenic, T_{reg} IFNγR1 deficiency significantly reduced atherosclerosis lesion size in

males (Figure 3.1C). Surprisingly however, inhibiting T_{reg} IFN-γ signaling was atherogenic in female recipients (Figure 3.1C).

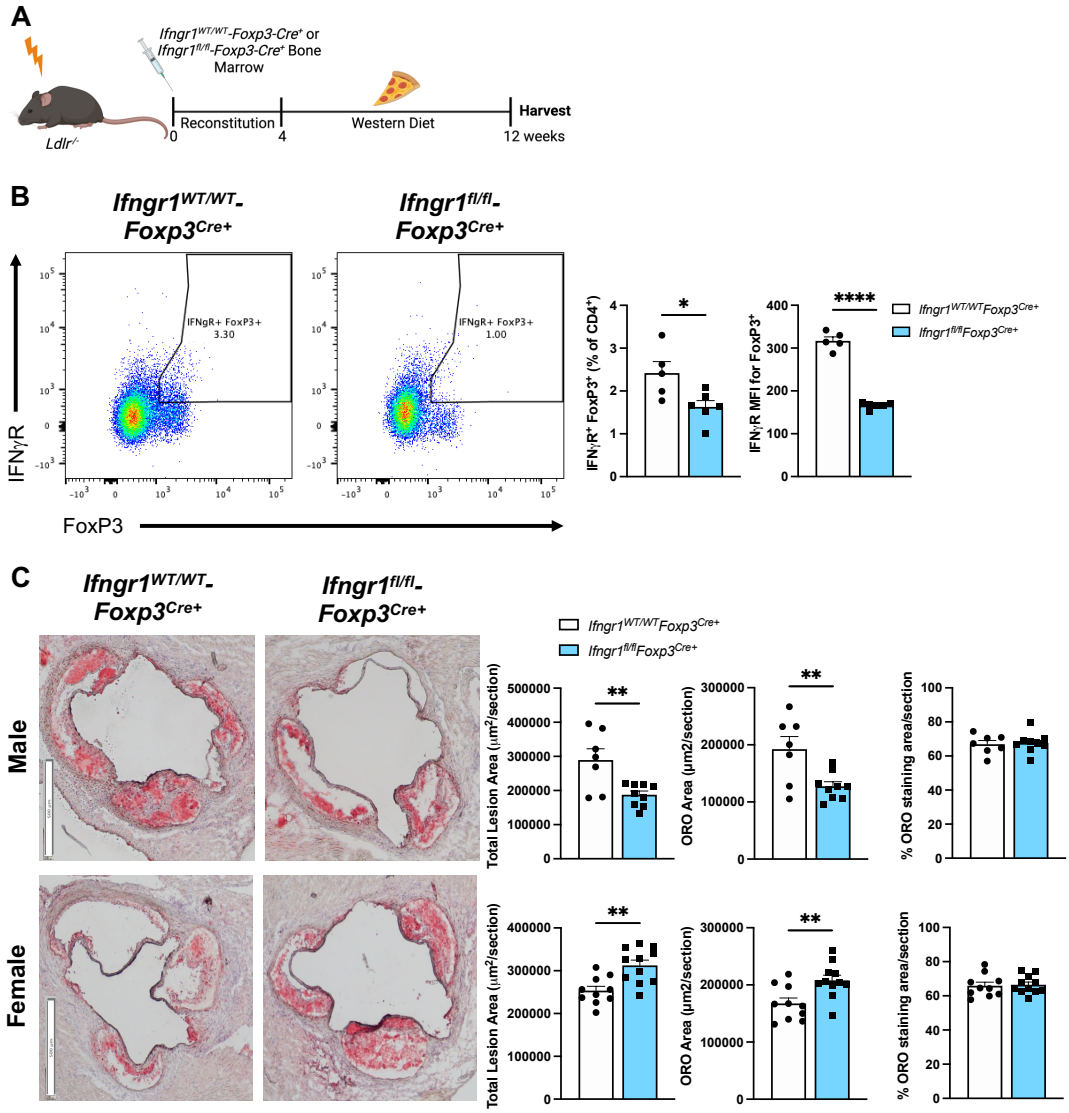

Figure 3.1: Reducing T_{reg} IFN-γ signaling is atheroprotective in male *Ldlr*$^{-/-}$ mice, but atherogenic in females. (A) Study design. Bone marrow from *Ifngr1*$^{WT/WT}$*Foxp3*$^{Cre+}$ and *Ifngr1*$^{fl/fl}$*Foxp3*$^{Cre+}$ was transplanted into lethally irradiated male and female *Ldlr*$^{-/-}$ mice. After four weeks of reconstitution, during which mice are maintained on normal chow, recipients were switched to WD for eight weeks and then harvested. **(B)** Quantification of IFNγR1 expression on T_{regs} in aorta draining lymph nodes from male mice. N=5-6 mice per group. **(C)** Representative Oil-Red-O (ORO) stained atherosclerotic lesions from the aortic root (scale bar represents 500µm) quantified by total lesion area, ORO staining area, and percentage of ORO staining in male and female recipients. N=7-11 mice per group, 2 independent experiments per sex. Data points represent individual mice and error bars show SEM. *, ** and **** denote significance $p<0.05$, $p<0.01$, and $p<0.0001$, respectively, by Student's *t* test.

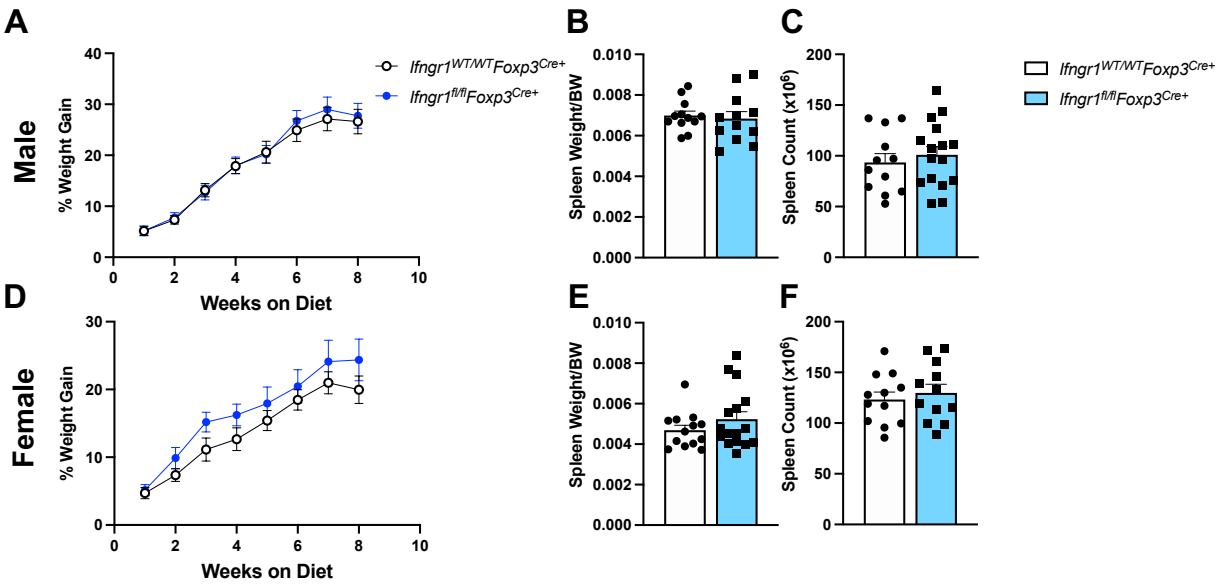

Figure 3.2: T_{reg}-specific IFNγR deficiency does not alter body weight, spleen weight, or lymphocyte counts in male or female recipients. *Ldlr*$^{-/-}$ mice were irradiated and transplanted with *Ifngr1*$^{WT/WT}$*FoxP3*$^{Cre+}$ or *Ifngr1*$^{fl/fl}$*FoxP3*$^{Cre+}$ bone marrow as described in Figure 3.1. **(A and D)** Weight gain over the eight weeks of WD feeding expressed as percent gain since the start of diet. **(B and E)** Spleen weight normalized to body weight. **(C and F)** Spleen cell count. N=12-16 mice per group, 2-3 independent experiments per sex. Data points represent individual mice and error bars show SEM.

Males with T_{reg}-specific IFNγR1 deficiency have increased signs of systemic IFN-γ-mediated inflammation. Though T_{reg} IFNγR1 deficiency significantly reduced atherosclerosis in male *Ifngr1*$^{fl/fl}$*-Foxp3*$^{Cre+}$ recipients compared to male controls (Figure 3.1C), there were not any changes in the proportions of total T_{regs}, IFN-γ$^+$ T_{regs}, or IFN-γ$^+$ CD4$^+$ T cells in the aorta or adLN of these mice (Figure 3.3A and data not shown). There was, however, an increase in IFN-γ$^+$ T_{regs} as well as IFN-γ$^+$ CD4$^+$ T cells in the spleen of male *Ifngr1*$^{fl/fl}$*-Foxp3*$^{Cre+}$ recipients (Figure 3.3B). There was also higher expression of IFNγR1 on non-T_{reg} CD4$^+$ cells in the adLN of male *Ifngr1*$^{fl/fl}$*-Foxp3*$^{Cre+}$ recipients compared to controls (Figure 3.4), possibly indicating more IFN-γ in the environment. B cell responses provided an additional sign of increased systemic IFN-γ.

In comparison to sex-matched controls, male *Ifngr1*$^{fl/fl}$-*Foxp3*$^{Cre+}$ mice had significantly elevated titers of anti-oxLDL IgG2c antibodies (Figure 3.5A), an isotype induced by IFN-γ-mediated B cell class switching. Therefore, while male *Ifngr1*$^{fl/fl}$-*Foxp3*$^{Cre+}$ recipients had reduced disease compared to *Ifngr1*$^{WT/WT}$-*Fox3*$^{Cre+}$ male mice, cellular and humoral changes indicated higher levels of IFN-γ in circulation.

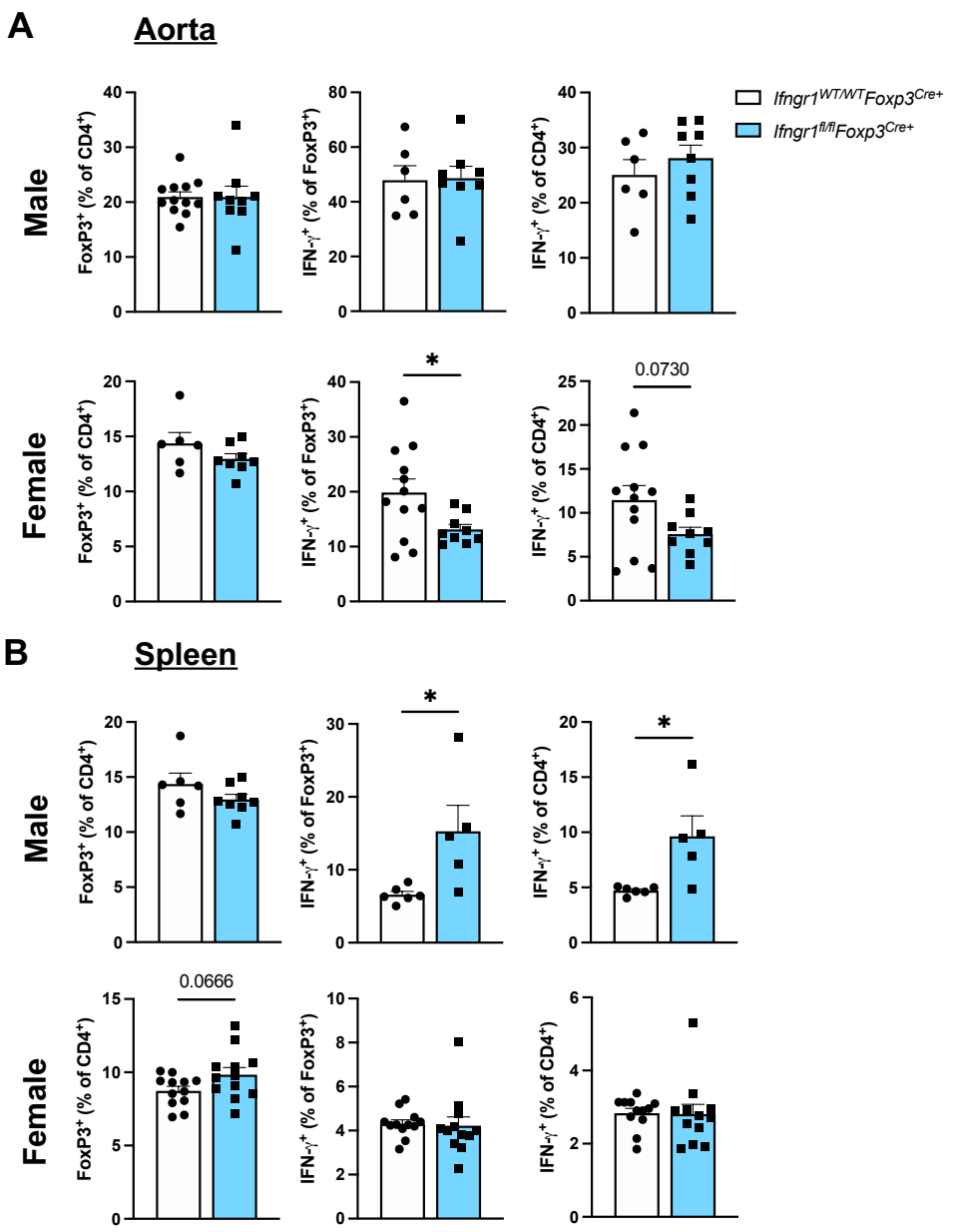

Figure 3.3: T_{reg}-specific IFNγR1 deficiency differentially alters IFN-γ$^+$ CD4$^+$ T cell populations in male and female mice. *Ldlr*$^{-/-}$ mice were irradiated and transplanted with *Ifngr1*$^{WT/WT}$*FoxP3*$^{Cre+}$ or *Ifngr1*$^{fl/fl}$*FoxP3*$^{Cre+}$ bone marrow as described in Figure 3.1. **(A)** Proportion of T_{regs} (left), IFN-γ$^+$ T_{regs} (middle), and IFN-γ$^+$ CD4$^+$ T cells (right) in aorta from male and female mice. **(B)** Proportion of T_{regs} (left), IFN-γ$^+$ T_{regs} (middle), and IFN-γ$^+$ CD4$^+$ T cells (right) in spleen from male and female mice. N=6-12 mice per group, 2 independent experiments per sex. Data points represent individual mice and error bars show SEM. * denotes significance $p<0.05$ by Student's *t* test.

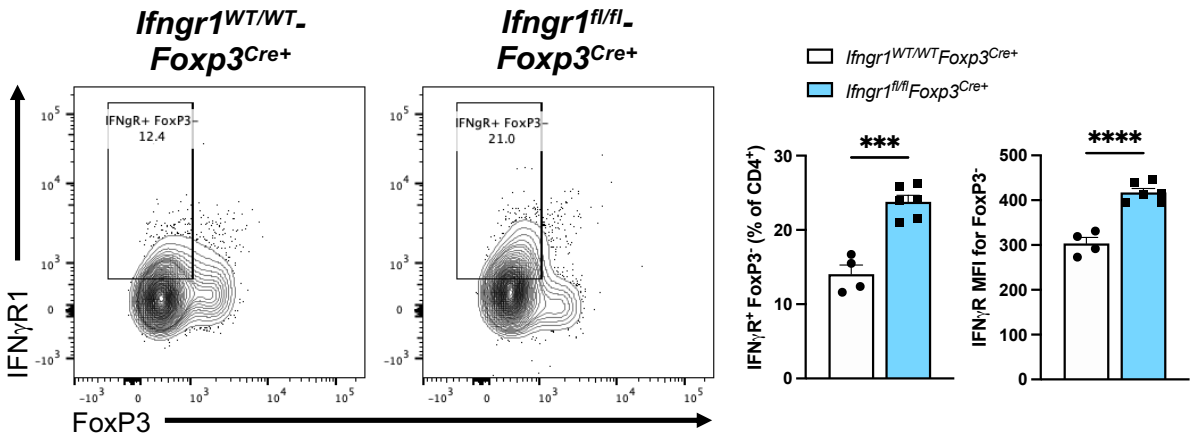

Figure 3.4: Despite reduced atherosclerosis severity, male T_{reg}-specific IFNγR1 deficient mice have increased expression of IFNγR1 on non-T_{reg} CD4⁺ cells. *Ldlr*$^{-/-}$ mice were irradiated and transplanted with *Ifngr1*$^{WT/WT}$*FoxP3*$^{Cre+}$ or *Ifngr1*$^{fl/fl}$*FoxP3*$^{Cre+}$ bone marrow as described in Figure 3.1. Quantification of IFNγR1 expression on non-T_{reg} CD4⁺ cells in aorta draining lymph nodes from male mice. N=5-6 mice per group. Data points represent individual mice and error bars show SEM. *** and **** denote significance $p<0.001$ and $p<0.0001$, respectively, by Student's *t* test.

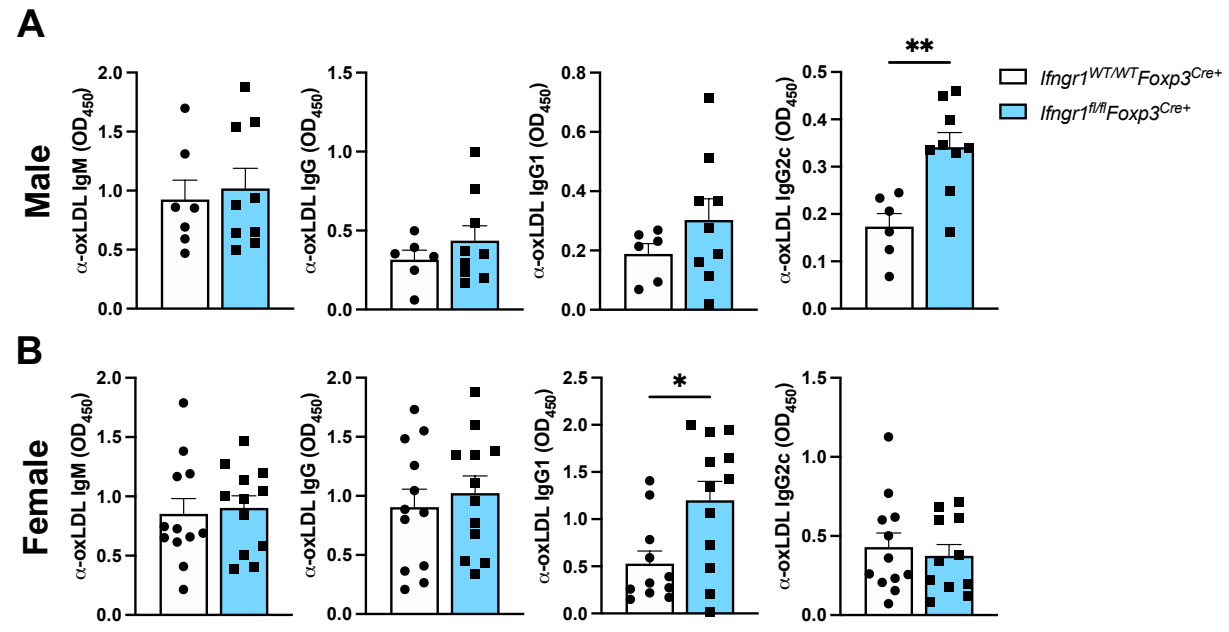

Figure 3.5: T_{reg}-specific IFNγR1 deficient mice have sex dependent increases in circulating α-oxLDL antibodies. *Ldlr*$^{-/-}$ mice were irradiated and transplanted with *Ifngr1*$^{WT/WT}$*FoxP3*$^{Cre+}$ or *Ifngr1*$^{fl/fl}$*FoxP3*$^{Cre+}$ bone marrow as described in Figure 3.1. **(A-B)** Serum α-oxLDL IgM, Total IgG, IgG1, and IgG2c were determined by ELISA at a 1:8000, 1:500, 1:250, and 1:250, respectively. N=6-12 mice per group, 2 independent experiments per sex. Data points represent individual mice and error bars show SEM. * and ** denote significance $p<0.05$ and $p<0.01$, respectively, by Student's *t* test.

Females with T_{reg}-specific IFNγR1 deficiency have increased atherosclerosis, but reduced IFN-γ producing CD4⁺ T cell populations. Like male *Ifngr1$^{fl/fl}$-Foxp3^{Cre+}* recipients, females of the same genotype did not have an altered proportion of total T_{regs} in the aorta compared to sex-matched controls (Figure 3.3A). However, contrary to males, female *Ifngr1$^{fl/fl}$-Foxp3^{Cre+}* mice had significantly decreased proportions of IFN-γ$^+$ T_{regs} and IFN-γ$^+$ CD4$^+$ cells in the aorta despite greater plaque burden (Figure 3.3A). There were again no observed differences in these populations in adLN (data not shown). Interestingly, the reduction in IFN-γ$^+$ T_{regs} and IFN-γ$^+$ CD4$^+$ proportion was also not observed in the spleen (Figure 3.3B). In addition to cellular changes, female *Ifngr1$^{fl/fl}$-Foxp3^{Cre+}* recipients had significantly increased titers of anti-oxLDL IgG1 (Figure 3.5B), an isotype that has been suggested to be protective in mouse models of atherosclerosis[172]. Overall, though plaque size was increased in female *Ifngr1$^{fl/fl}$-Foxp3^{Cre+}* recipients compared to sex-matched controls, cellular and humoral changes were more indicative of an atheroprotective state. Together with the data from the males, this suggests IFNγR1 signaling in T_{regs} mediates changes in atherosclerosis via an indirect mechanism.

Macrophages in males with T_{reg}-specific IFNγR1 have reduced expression of costimulatory molecule, CD86. Prior work has shown that T_{regs} facilitate atherosclerosis regression by remodeling plaque macrophages to more anti-inflammatory, wound healing phenotypes which help shrink the lesion[128]. To determine whether T_{regs} may be working through macrophages to alter atherosclerosis here, I analyzed CD11b$^+$ F4/80$^+$ macrophages by flow cytometry in the adLN of male recipients. While there was no change in the proportion of CD11b$^+$ F4/80$^+$ macrophages

present in the adLN (Figure 3.6A), CD86 expression on these macrophages in *Ifngr1*$^{fl/fl}$-*Foxp3*$^{Cre+}$ recipients was significantly decreased compared to controls (Figure 3.6B). Reduced expression of CD86 on CD11b^{+} F4/80^{+} macrophages in male *Ifngr1*$^{fl/fl}$-*Foxp3*$^{Cre+}$ mice is consistent with their less severe disease as CD86 is an important costimulatory molecule sometimes used to define inflammatory macrophages in atherosclerosis[55]. Additional work will be needed to more robustly phenotype the macrophages in this model and to gather the corresponding data from female recipients, but these results suggest T_{regs} lacking IFNγR may be altering macrophage phenotype to ultimately modulate disease burden.

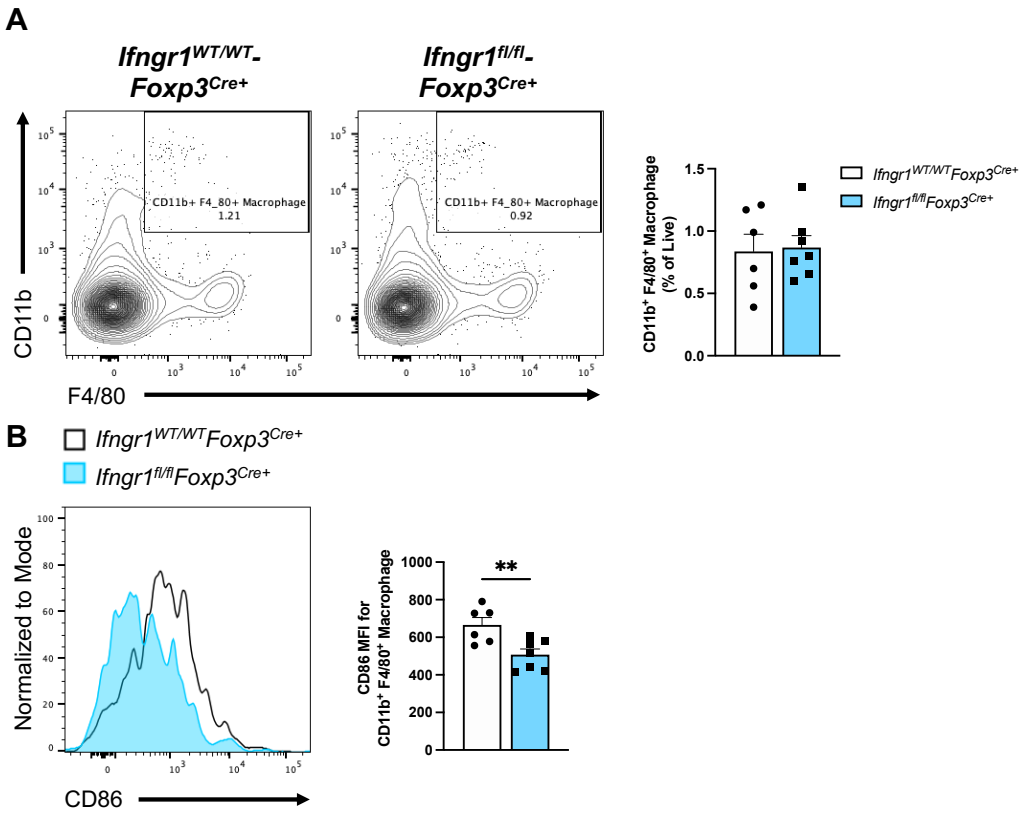

Figure 3.6: Male T_{reg}-specific IFNγR1 deficient mice may have less inflammatory macrophages. *Ldlr*$^{-/-}$ mice were irradiated and transplanted with *Ifngr1*$^{WT/WT}$*FoxP3*$^{Cre+}$ or *Ifngr1*$^{fl/fl}$*FoxP3*$^{Cre+}$ bone marrow as described in Figure 3.1. **(A)** Quantification of CD11b^{+} F4/80^{+} macrophages in aorta draining lymph nodes from male mice. **(B)** Mean fluorescent intensity of CD86 on CD11b^{+} F4/80^{+} macrophages. N=5-6 mice per group. Data points represent individual mice and error bars show SEM. ** denotes significance p<0.01 by Student's t test.

Discussion

Based on the understanding that IFN-γ signaling is critical to oxPAPC-induced Th1-like T_{reg} phenotypes *in vitro* (Chapter 2), I hypothesized that a T_{reg}-specific inhibition of IFNγR1 would be atheroprotective in a *Ldlr*$^{-/-}$ bone marrow transplant model of atherosclerosis. Consistently, there were smaller lesions in male *Ifngr1*$^{fl/fl}$-*Foxp3*$^{Cre+}$ recipients compared to sex-matched *Ifngr1*$^{WT/WT}$-*Foxp3*$^{Cre+}$ controls (Figure 3.1). However, when T_{reg} IFN-γ signaling was reduced in female mice, lesion size was increased relative to sex-matched controls (Figure 3.1). This is contrary to my initial hypothesis but suggests that sex may be a biological variable in our model system. Our lab and others have previously documented significant sex-driven differences in models of atherosclerosis and in patients[144,173,174]. In fact, some work has even suggested sex-dependent changes in IFN-γ signaling in atherosclerosis[117,119,120,175], but there is no current consensus in this regard.

Consistent with the findings of this study, Whitman *et al.* showed whole-animal *Ifng*$^{-/-}$ is atheroprotective in male *Apoe*$^{-/-}$ mice but elicits no change in females[120]. A similar result was described in *T-bet*$^{-/-}$ *Ldlr*$^{-/-}$ mice which have significantly reduced production of IFN-γ[116]. Yet, Buono *et al.* demonstrated both male and female *Ifng*$^{-/-}$ *Ldlr*$^{-/-}$ mice are protected from atherosclerosis compared to *Ldlr*$^{-/-}$ controls[117]. Gupta *et al*. showed female *Apoe*$^{-/-}$ *Ifngr*$^{-/-}$ mice develop less atherosclerosis than *Apoe*$^{-/-}$ controls, but males were not tested[119]. Using a bone marrow chimera model in which hematopoietic cells lacked IFN-γ, Niwa *et al.* demonstrated that IFN-γ deficiency was atherogenic in male mice early in the development of disease, contrary to previous findings[175]. Variability in the body of work may be partially due to the different genetic

backgrounds and deficiency models used, each of which with their own potentially confounding effects (Table 1). However, a great deal of future work will be required to develop a consensus regarding the sex-dependent nature of IFN-γ signaling in atherosclerosis.

Table 1. Sex-specific summary of results from IFN-γ studies in atherosclerosis mouse models. * indicates the results from this work.

Deficiency Model	Strain Background	Affect in Males	Affect in Females	Ref.
Whole body *Ifng*$^{-/-}$	*Apoe*$^{-/-}$	Atheroprotective	No Change	[120]
Whole body *T-bet*$^{-/-}$	*Ldlr*$^{-/-}$	Atheroprotective	No Change	[116]
Whole body *Ifng*$^{-/-}$	*Ldlr*$^{-/-}$	Atheroprotective	Atheroprotective	[117]
Whole body *Ifngr*$^{-/-}$	*Apoe*$^{-/-}$	Not Tested	Atheroprotective	[119]
Ifng$^{-/-}$ Bone Marrow Chimera	*Ldlr*$^{-/-}$	Atherogenic	Not Tested	[175]
*T_{reg}-specific *Ifngr1*$^{-/-}$ Bone Marrow Chimera	*Ldlr*$^{-/-}$	Atheroprotective	Atherogenic	-

In addition to observing sex-specific alterations in disease burden in the presence of T_{reg} IFNγR1 deficiency, there were also shifts in immune populations and circulating anti-oxLDL antibody titers. Male *Ifngr1*$^{fl/fl}$-*Foxp3*$^{Cre+}$ recipients had elevated proportions of IFN-γ$^+$ CD4$^+$ Th1 cells and IFN-γ$^+$ T_{regs} in the spleen compared to sex-matched controls, but there were no observed changes in these populations in the aorta or adLN (Figure 3.3 and data not shown). Surprisingly, female *Ifngr1*$^{fl/fl}$-*Foxp3*$^{Cre+}$ mice had significantly reduced proportions of Th1 cells and IFN-γ$^+$ T_{regs} in the aorta compared to female controls, but no differences in these populations in the adLN or spleen (Figure 3.3 and data not shown). These results were again counter to my initial hypothesis that IFN-γ$^+$ T_{regs} would be dysfunctional and not protective. This hypothesis was based on our oxPAPC work (Chapter 2) as well as that of others describing Th1-like T_{regs} as atherogenic[134,145]. However, the conclusions of this prior work were drawn using

adoptive transfer of *ex vivo* and *in vitro*-derived Th1-like T_{regs}. Therefore, the differing results from this study may indicate that the impact of Th1-like T_{regs} differ depending on their source (exogenous addition or endogenous manipulation).

Accompanying changes in Th1 cells and T_{regs}, male *Ifngr1*$^{fl/fl}$-*Foxp3*$^{Cre+}$ mice had significantly increased IFNγR1 expression on non-T_{reg} CD4$^+$ cells and higher circulating anti-oxLDL IgG2c than male controls (Figure 3.4 and Figure 3.5), indicating elevated levels of systemic IFN-γ despite their reduced disease burden. Furthermore, female *Ifngr1*$^{fl/fl}$-*Foxp3*$^{Cre+}$ recipients, which had larger lesions compared to female controls, did not have these indications of increased systemic IFN-γ. In fact, female *Ifngr1*$^{fl/fl}$-*Foxp3*$^{Cre+}$ mice had significantly more anti-oxLDL IgG1 (Figure 3.5) which has been suggested to be atheroprotective[172]. IFN-γ is regularly described as an atherogenic cytokine[116–119,171], but this work suggests its role may be context dependent in atherosclerosis.

As the modulation of atherosclerosis severity in T_{reg}-specific IFNγR1 deficient mice did not appear to be directly mediated by T cells, I investigated the macrophage phenotype in male recipients. Prior findings from Sharma *et al*. showed T_{regs} are required for the enrichment and function of atheroprotective M2-macrophages in regressing plaques[128], highlighting a direct connection between the two cell types in atherosclerosis. While the proportion of CD11b$^+$ F4/80$^+$ macrophages was unchanged in *Ifngr1*$^{fl/fl}$-*Foxp3*$^{Cre+}$ male mice, macrophage expression of CD86 was significantly reduced compared to male controls (Figure 3.6). CD86 is a co-stimulatory molecule required on antigen presenting cells for T cell activation and is generally elevated on inflammatory macrophages[55,176]. Therefore, reduced CD86 expression on macrophages

may suggest IFNγR1 deficient T_{regs} are remodeling them to a less atherogenic state. This, in turn, could result in reduced disease in male *Ifngr1*$^{fl/fl}$-*Foxp3*$^{Cre+}$ recipients. However, a more in-depth analysis of this macrophage phenotype will be required in the future as well as investigation of the corresponding population in female recipients.

In conclusion, this study demonstrates that T_{reg} IFN-γ signaling plays a critical, but sex-dependent role in atherosclerosis development. The induced changes in disease severity do not appear to be directly T cell mediated. Rather, I hypothesize T_{reg} IFNγR expression is required for reshaping macrophages that ultimately modulate plaque size. Overall, these results reveal a nuance to IFN-γ signaling in atherosclerosis that can sometimes be overlooked but will be critical to understand for the development of better therapeutics.

CHAPTER 4

OxLDL Immune Complexes Induce Long-Term Alterations in Dendritic Cell Population

Introduction

During the development of atherosclerosis, LDL in the vessel wall becomes oxidized and causes local tissue damage and recruitment of immune cells which produce antibodies specific to oxLDL[101,177]. Studies show that approximately 95% of circulating oxLDL is bound to antibody forming oxLDL-ICs[178]. OxLDL-specific antibodies and immune complexes are present in mouse models of atherosclerosis[89,179,180], there is a positive correlation between titers of oxLDL-ICs and atherosclerosis disease severity[178-181], and titers are increased in patients that have autoimmune diseases associated with accelerated disease like SLE, diabetes, and RA[182,183]. This suggests oxLDL-ICs are not only a biomarker of disease, but actively promote inflammation.

Prior work from our laboratory shows oxLDL-ICs cooperatively signal through FcγRs, CD36, and TLR-4 in BMDCs to prime the Nlrp3 inflammasome causing increased secretion of IL-1β compared to BMDCs stimulated with oxLDL[89]. This demonstrates that oxLDL-ICs are distinct from free oxLDL and elicit unique biological effects. It is significant that oxLDL-ICs are capable of modulating DCs as these cells are critical mediators shaping the vessel microenvironment by activating other immune cells[63–66]. As atherosclerosis is a chronic disease of sterile inflammation, it is critical to understand what, if any, long-term changes oxLDL-ICs might induce in DCs.

Though classic immunological dogma states that innate immune cells are efficient, broad responders to danger signals while adaptive immunity is antigen-specific

and has lasting memory, work from the last decade has demonstrated that some pathogens can impart long-lasting changes on innate immune cells, altering their response upon subsequent activation (reviewed in [184]). This is a concept called trained immunity and it is mediated by ligand binding to pattern recognition receptors which triggers metabolic and epigenetic changes (reviewed in [184]). Fungal pathogen *Candida albicans* (*C. albicans*) and its cell wall component, β-glucan, are some of the most well studied triggers of trained immunity[185–187]. Interestingly, the inflammatory pathway utilized by oxLDL-ICs closely mimics that of fungal signaling through Dectin1 and TLRs to activate the Syk-dependent NF-κB pathway[89,188]. Free oxLDL has also been shown to induce trained immunity in monocytes and macrophages[189] and WD feeding of *Ldlr*$^{-/-}$ mice induces immune training in macrophage precursors in the bone marrow through an Nlrp3 inflammasome-dependent mechanism[190]. Altogether, these data suggest oxLDL-ICs may be capable of immune training.

Prior to the start of my work on this project, the rabbit α-ApoB-100 polyclonal antibody we had used for the formation of oxLDL-ICs in the past[89] was discontinued with no viable direct replacement. Therefore, in this study, I developed a new method of oxLDL-IC treatment in BMDCs in which oxLDL-IC conditions are achieved by incubating cells with free oxLDL and heat-aggregated IgG immune complexes (haIC) simultaneously to recapitulate the signaling of antigen-specific oxLDL-ICs. Using this system, I demonstrate oxLDL-ICs induce trained immunity in BMDCs *in vitro*, both augmenting their cytokine response upon secondary, non-specific stimulation and shifting them towards a more glycolytic metabolism. Additionally, WD feeding of *Ldlr*$^{-/-}$ mice significantly increased the proportion of DC precursor populations *in vivo* and

BMDCs derived from differentially fed mice had altered responses to stimuli. Overall, these findings demonstrate that oxLDL-ICs can induce long-term changes in DCs and may, therefore, be a driving force in the chronic inflammation observed in atherosclerosis.

Materials and Methods

Mice. C57BL/6J (B6; Stock # 000664) and B6.129S7-Ldlr^{tm1Her}/J (*Ldlr*$^{-/-}$; Stock # 002207), mice were originally obtained from the Jackson Laboratory (Bar Harbor, ME). Animals were maintained and housed at Vanderbilt University. All mice used in these studies were on the C57BL/6J background. Procedures were approved by the Vanderbilt University Institutional Animal Care and Use Committee.

Bone Marrow-derived Dendritic Cells. BMDCs were generated as previously described[142]. Briefly, bone marrow was flushed from hind legs with BMDC media (RPMI 1640, 10% FBS, 10mM HEPES, and L-glutamine-penicillin-streptomycin [2mM, 100 units, and 100μg, respectively]). Cells were plated at 2×10^5 cells/ml in 10ml of the above media with 20ng/ml recombinant granulocyte-macrophage colony-stimulating factor (rGM-CSF; Peprotech Cat # 315-03) in 100mm^2 petri dishes. 10ml of media was added on day 3 then removed and replaced on day 6, and cells were harvested days 8-10.

oxLDL and haICs. LDL oxidation methods were adapted from those previously described[89,191]. OxLDL was made by dialyzing 250μg/ml human LDL (Kalen Biomedical Cat # 770200) for 36 hours against sterile 0.9M NaCl at 4°C. This was followed by dialysis against sterile 0.9M NaCl containing 20μM freshly prepared sterile $CuSO_4$ for 6 hours at 37°C. Oxidation was terminated by dialysis against sterile 0.9M NaCl

containing 1mM EDTA for 18 hours at 4°C. Extent of oxidation was determined by TBARS assay (Bioassay Systems Cat # DTBA-100) with the target range of 9-14nmol MDA/mg LDL. HaICs were generated as described previously[192]. Briefly, 250μg/ml sterile mouse IgG (Innovative Research Cat # IR-MS-GF-ED) was incubated at 63°C for 12 minutes. Following heating, aggregated antibody was centrifuged at 10,000xg for five minutes and supernatant containing soluble haICs was collected and diluted to 1mg/ml for use in assays.

Inflammasome Assay. Inflammasome assay was adapted from those previously described[89]. Briefly, BMDCs (1×10^5 cells/well in a 96-well round bottom plate) were primed with 10μg/ml oxLDL or 10μg/ml oxPAPC, 40μg/ml haIC, a combination of 10μg/ml of the appropriate oxidized lipid and 40μg/ml haICs (oxLDL-IC or oxPAPC-IC), or BMDC media alone for three hours. The primed BMDCs were then activated with 5mM adenosine triphosphate (ATP; Sigma Cat # A6419) for two more hours. Supernatants were collected and used for IL-1β ELISAs (eBioscience Cat # 88-7013-88 or Biolegend Cat # 432601) performed according to the manufacturer instructions.

RNA Sequencing (RNAseq). BMDCs were treated with 25μg/ml oxLDL or a combination of 25μg/ml oxLDL and 100μg/ml haIC (oxLDL-ICs) for two hours before harvest and RNA was isolated using Rneasy Plus Mini Kit (Qiagen Cat #: 74134) according to manufacturer instruction. RNA was sent to Vanderbilt Technologies for Advanced Genomics (VANTAGE) core. Libraries were prepared using 200-500ng of total RNA using NEBNext® Poly(A) selection kit and sequenced at Paired-End 150bp on the Illumina NovaSeq 6000 targeting an average of 50M reads per sample. Additional analysis using the resulting demultiplexed FASTQ files containing PF reads

was performed by Vanderbilt Technologies for Advanced Genomics Analysis and Research Design (VANGARD). Sequencing reads were aligned against the mouse GENCODE GRCm38.p6 using STAR software v2.7.8a. Mapped reads were assigned to gene features and quantified using featureCounts v2.0.2. Normalization and differential expression were performed using DESeq2 v1.30.1. Significantly differentially expressed genes (fold change $\geq$2 and FDR $\leq$0.05) were used for subsequent Gene Set Enrichment Analysis v4.2.2.

BMDC Training. Trained immunity assays were adapted from those previously described[189]. BMDCs (1×10^5 cells/well in a 96-well flat bottom plate) were treated with a primary stimulus of 20ng/ml lipopolysaccharide (LPS), 50μg/ml oxLDL, 200μg/ml haICs, a combination of 50μg/ml oxLDL and 200μg/ml haICs (oxLDL-IC), or BMDC media alone for 24 hours. All treatment groups also included 20ng/ml rGM-CSF. Following primary stimulation, BMDCs were washed and cells were rested in fresh BMDC media supplemented with 20ng/ml rGM-CSF for four days. After which, media was replaced with a secondary stimulus of 20ng/ml LPS or BMDC media alone (without rGM-CSF) before incubating for 24 hours. IL-1β, IL-6 (BD Biosciences Cat # 555240), and TNF-α (BD Biosciences Cat # 558534) were measured in culture supernatants by ELISA according to the manufacturer's instruction.

Flow Cytometry. Flow cytometry was performed on cells obtained *ex vivo* and following *in vitro* cell culture. Cells requiring a viability dye were stained with Viobility Fixable Dye (Miltenyi Biotec) according to the manufacturer protocols. For surface staining, cells were washed in HBSS containing, 1% BSA, 4.17mM sodium bicarbonate, and 3.08mM sodium azide (FACS buffer), followed by a 10-minute room temperature incubation in

1μg/ml Fc block (α-CD16/32; Tonbo Cat # 40-0161) diluted in FACS buffer. Fc block was omitted for DC precursor staining in the bone marrow. Cells were then stained for 30 minutes at 4°C protected from light with the following antibodies diluted in FACS buffer: α-B220-Pe (BD Biosciences Cat # 553089), α-CD2-Pe (Tonbo Cat # 50-0021), α-CD3e-Pe (invitrogen Cat # 12-0031), α-CD4-Pe (Tonbo Cat # 50-0042), α-CD8a-Pe (BD Biosciences Cat # 553033), α-CD11b-APCCy7 (BD Biosciences Cat # 557657), α-CD11b-Vioblue (Tonbo Cat # 75-0112), α-CD11c-PeCy7 (Tonbo Cat # 60-0114), α-CD11c-Viogreen (Biolegend Cat # 117337), α-CD16/32-SB600 (Invitrogen Cat # 63-0161-80), α-CD19-Pe (BD Biosciences Cat # 557399), α-CD34-APC (BD Biosciences Cat # 560233), α-CD45.2-APCCy7 (Tonbo Cat # 25-0454), α-CD80-APC (Tonbo Cat # 20-0801), α-CD86-PeCy7 (Tonbo Cat # 60-0862), α-c-kit-Vioblue (Invitrogen Cat # 48-1171-80), α-CX3CR1-FITC (Biolegend Cat # 149019), α-F4/80-APCCy7 (Tonbo Cat # 25-4801), α-Ly6C-FITC (Biolegend Cat # 128005), α-Ly6G-Pe (Tonbo Cat # 50-5931), α-MHC Class II I-Ab-PerCp-Cy5.5 (Invitrogen Cat # 46-5320-82), α-Sca-1-PerCp (Invitrogen Cat # 15-5981-81), α-TER-119/Ly76-Pe (Invitrogen Cat # 12-5921-81). Samples were then washed in FACS buffer and fixed in 2% paraformaldehyde (PFA). Sample acquisition was performed on a MacsQuant Analyzer (Miltenyi Biotec) and data were analyzed using FlowJo Single Cell Analysis software.

Glycolysis Stress Test. Seahorse XF Glycolysis Stress Test (Agilent Cat # 103020-100) was performed according to manufacturer instructions. Seahorse plate was coated with Cell-Tak solution (Corning Cat # 354240) for 30 minutes at room temperature before seeding 2×10^5 BMDCs/well with a minimum of five technical replicates per

sample. Plated cells were treated with BMDC media alone, 20ng/ml LPS, 25μg/ml oxLDL, 100μg/ml haIC, or a combination of 25μg/ml oxLDL and 100μg/ml haICs (oxLDL-ICs) for 24 hours. Final counts of each well were acquired by bright field imaging using a BioTek Cytation5 imager for data normalization. The glycolysis stress test was performed using 10mM glucose, 1.5μM oligomycin A, and 50mM 2-deoxy-D-glucose (2-DG) final concentrations. Analysis was performed with the Agilent Seahorse XFe96 Analyzer.

Diet Comparison Studies. 9-12-week-old male *Ldlr*$^{-/-}$ mice were maintained on NC or placed on WD (21% saturated fat and 0.15% cholesterol; Envigo Cat # TD.88137) for 4 weeks. After which animals were sacrificed and bone marrow, blood, and spleen were collected for further analyses.

Quantitative Polymerase Chain Reaction (qPCR). BMDCs were treated with media alone or 20ng/ml LPS for two hours and total RNA was isolated from cells using Norgen Total RNA Purification Kits (Norgen Biotek Cat # 37500). RNA concentrations were normalized to the least concentrated sample and RNA was reverse transcribed using a High-Capacity cDNA Reverse Transcription Kit (Applied Biosystems Cat # 4368814). mRNA expression was measured with the following TaqMan™ probes: *Il1b* (Thermo Fisher Scientific Cat # Mm00434228), *Il12a* (Thermo Fisher Scientific Cat # Mm00434169), *Il12b* (Thermo Fisher Scientific Cat # Mm01288989), and *Il23a* (Thermo Fisher Scientific Cat # Mm00518984). Quantitative real-time PCR was performed using the Thermo Fisher Scientific QuantStudio 6 Flex Real-Time PCR System. The cycling threshold (C_T) value for each gene was normalized to the housekeeping gene *Ppia*

(Thermo Fisher Scientific Cat # Mm02342430) and relative expression was calculated by the change in C_T method ($\Delta\Delta C_T$).

Statistical Analyses. Normally distributed data was analyzed using Student's *t* tests (for two groups) or one-way ANOVAs with Bonferroni post-test (for three or more groups). All statistical tests were performed using GraphPad Prism.

Results

Combination treatment of oxLDL and haICs elicits similar effects in BMDCs as antigen-specific oxLDL-ICs. Prior work from our laboratory has shown that oxLDL-ICs prime the Nlrp3 inflammasome and result in increased production of IL-1β from BMDCs compared to free oxLDL[89]. The oxLDL-ICs used for these studies were formed by incubating oxLDL and α-ApoB100 polyclonal antibody together before removing unbound antibody from formed immune complexes via size exclusion centrifugation (Figure 4.1)[89]. Due to the polyclonal nature of the antibody, antigen-specific oxLDL-ICs are likely composed of multiple α-ApoB100 antibodies bound to individual oxLDL particles, and possibly are amassed clusters of multiple antibodies and particles together. This is important as it would allow for the cooperative signaling through FcγRs, CD36, and TLR-4 that is required for oxLDL-IC priming of the inflammasome[89]. However, the α-ApoB100 polyclonal antibody was discontinued prior to this work so I hypothesized that an alternative non-specific immune complex could trigger inflammasome activation in BMDCs providing there was coordinated signaling through FcγRs, CD36, and TLR-4.

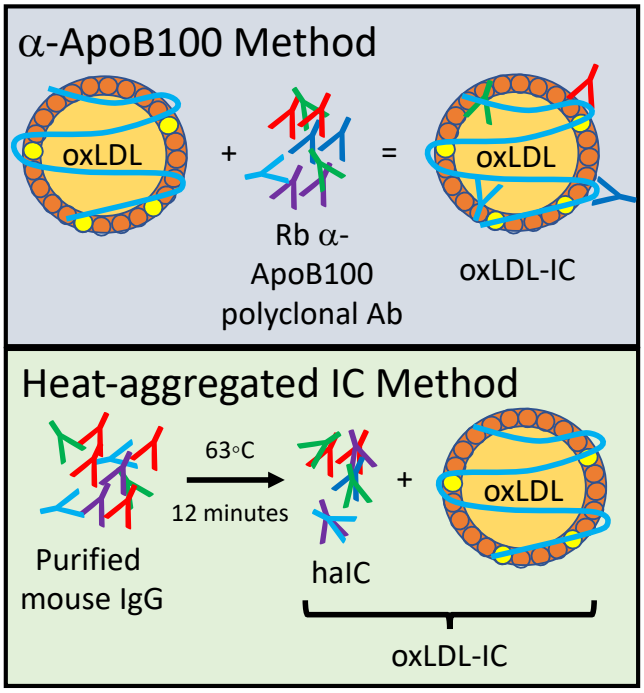

Figure 4.1. Comparison of antigen-specific and heat-aggregated oxLDL-IC formation. Antigen-specific oxLDL-ICs are prepared by incubating oxLDL and α-ApoB100 polyclonal antibody together before removing unbound antibody from formed immune complexes via size exclusion centrifugation. With this method, antibody is directly bound to the oxLDL particle. OxLDL-ICs produced with the haIC method use dual treatment of oxLDL and haICs to mimic the signaling of antigen-specific complexes.

To test this, haICs were formed from purified mouse IgG as in Gamberale *et al.*[192] and BMDCs were primed with free oxLDL, haICs alone, or a combination of oxLDL and haICs in an *in vitro* inflammasome assay (Figures 4.1 and 4.2A-B). Consistent with Rhoads *et al.* free oxLDL alone did not elicit IL-1β release from BMDCs above the control level[89]. Some IL-1β was produced from BMDCs treated with haICs alone, however, the IL-1β concentration was highest in supernatants from BMDCs given oxLDL and haICs together, suggesting the combination treatment primed the inflammasome as effectively as antigen-specific oxLDL-ICs[89]. The concentration of IL-1β produced following treatment with oxLDL and haICs together (herein referred to as

oxLDL-ICs) was greater than the sum of IL-1β concentrations from free oxLDL and haIC groups alone suggesting the observed increase in IL-1β from oxLDL-IC-treated BMDCs was not simply an additive effect, but bona fide cooperative signaling.

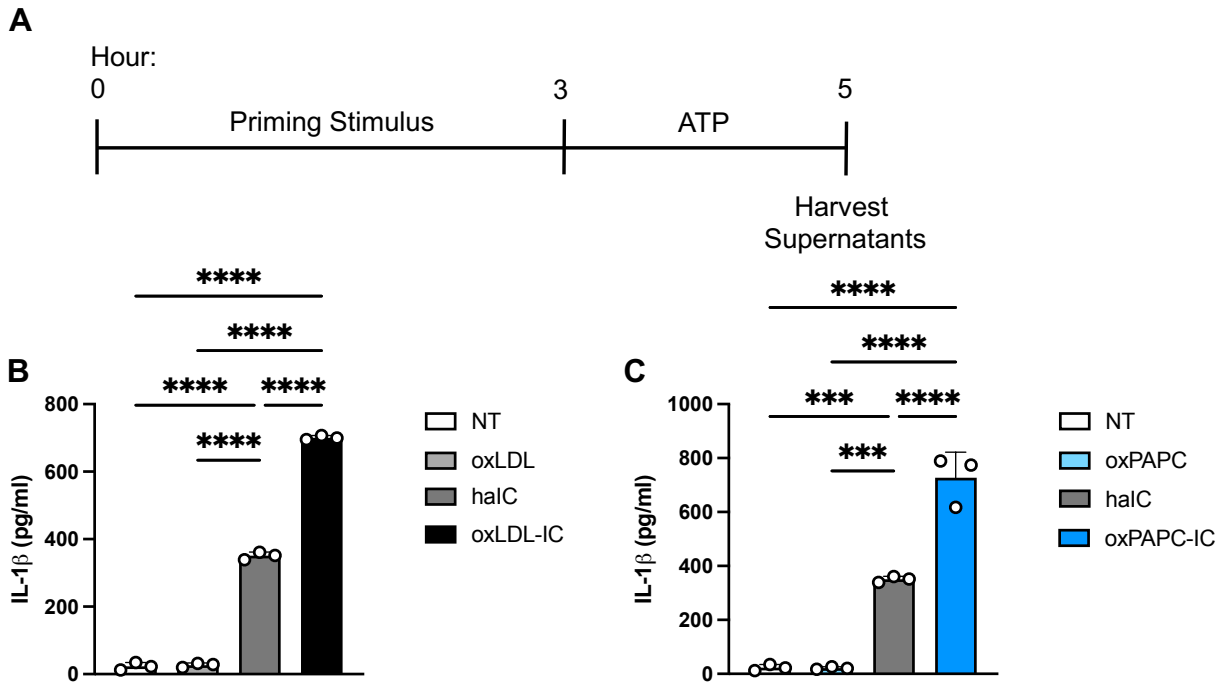

Figure 4.2. Combined treatment of oxidized lipid and haICs induce inflammasome activation similar to antigen-specific immune complexes. (A) Inflammasome assay design. BMDCs were treated with 10μg/ml oxidized lipid, 40μg/ml haICs or a combination of 10μg/ml oxidized lipid and 40μg/ml haICs (ox-IC) for three hours after which 5mM ATP was added for two additional hours. IL-1β was measured in supernatant by ELISA. **(B)** IL-1β concentrations following inflammasome assay using oxLDL. **(C)** IL-1β concentrations following inflammasome assay using oxPAPC. Shown is one representative of at least three experiments. Data points are technical replicates and error bars show SD. *** and **** denote significance $p<0.001$ and $p<0.0001$, respectively, by one-way ANOVA and Tukey's multiple comparison test.

Leveraging this combination haIC and oxLDL method allowed for testing of other types of immune complexes. As discussed in Chapter 2, oxPAPC is a mixture of oxidized phospholipid species that is present in the oxLDL particle as well as cell membranes[141,193]. As oxPAPC has been shown to be the bioactive component of

oxLDL[138–140], I hypothesized oxPAPC-ICs would prime the inflammasome in much the same way as oxLDL-ICs. Consistent with this, free oxPAPC did not trigger IL-1β concentrations above no treatment, but BMDCs primed with oxPAPC and haICs together (oxPAPC-ICs) produced significantly more IL-1β (Figure 4.2C). Again, the level of IL-1β released from oxPAPC-IC-treated BMDCs was not simply the sum of the IL-1β elicited by oxPAPC and haICs alone, suggesting oxPAPC-ICs can prime the inflammasome just as oxLDL-ICs can. Overall, these results suggest combined treatment of haICs and oxLDL are a sufficient alternative to antigen-specific oxLDL-ICs in BMDCs, and they will be the primary form of oxLDL-IC used throughout the remainder of this chapter.

OxLDL-ICs trigger long-term immune training in BMDCs. Bulk RNAseq was performed on BMDCs treated with free oxLDL or oxLDL-ICs for two hours to further characterize changes induced by oxLDL-IC treatment and distinct transcriptional profiles were observed between the two groups (Figure 4.3A). Additionally, of the top 10 KEGG pathways as determined by number of gene changes, three pathways (shown in red) were consistent with the known mechanism for oxLDL-IC signaling in BMDCs (Figure 4.3B)[89]. Interestingly, "C-type Lectin Receptor Signaling Pathway" was also one of the top 10 KEGG pathways identified (Figure 4.3B) which was significant as it is one that is required for the induction of trained immunity by fungal pathogens like *C. albicans*[188]. OxLDL-IC signaling has other mechanistic similarities with *C. albicans* in that it is TLR, Syk, and NF-κB mediated[89,188]. This, combined with the fact that oxLDL can also cause immune training[189], suggested that oxLDL-ICs may be novel triggers of trained immunity.

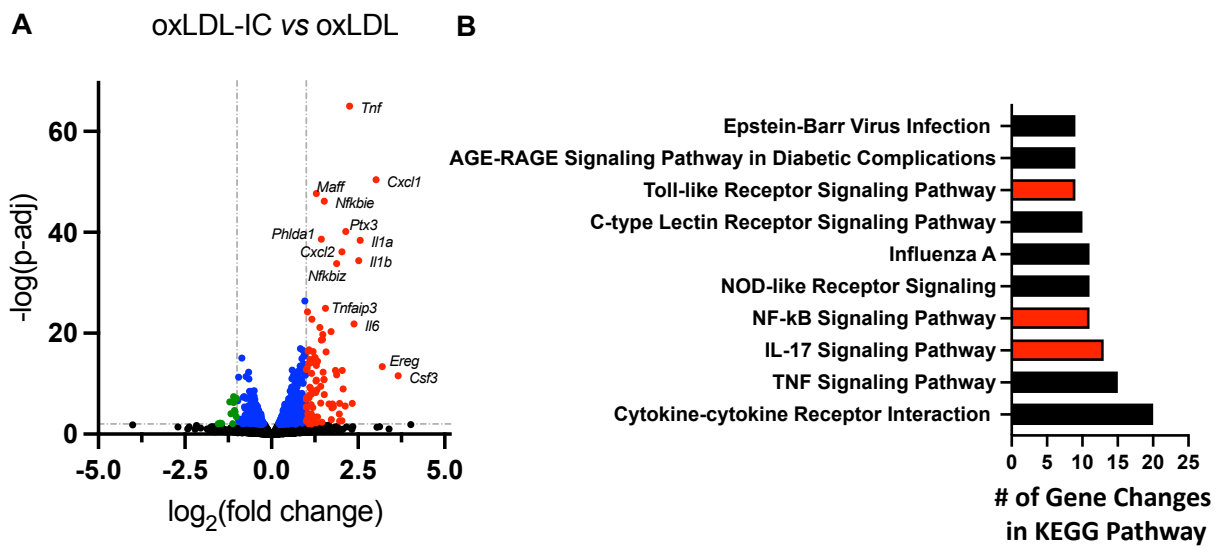

Figure 4.3. OxLDL-IC-treated BMDCs are transcriptionally distinct from oxLDL-treated BMDCs. BMDCs were treated with 25μg/ml oxLDL or oxLDL-ICs (100μg/ml haIC + 25μg/ml oxLDL) for 2hrs before being harvested for bulk RNAseq. N=3 mice per group. **(A)** Volcano plot showing differentially expressed genes in oxLDL-IC-treated BMDCs relative to oxLDL-treated BMDCs (significantly enriched = red, significantly reduced green). **(B)** Top 10 most altered KEGG pathways in oxLDL-IC-treated BMDCs based on the number of differentially expressed genes in the pathway. Red bars indicate pathways that align with the oxLDL-IC signaling mechanism.

To investigate the training potential of oxLDL-ICs *in vitro*, BMDCs were exposed to a primary stimulus for 24 hours before being washed and rested in media supplemented with granulocyte-macrophage colony-stimulating factor (GM-CSF) for four days. Afterwards, BMDCs were restimulated with LPS for 24 hours and then cells and culture supernatants were collected for analysis (Figure 4.4A). BMDC viability was unaffected by the different primary stimuli (Figure 4.4B), but BMDCs initially treated with oxLDL-ICs produced more IL-1β upon secondary, non-specific stimulation than even those receiving oxLDL for a primary stimulus (Figure 4.4C). Of the cytokines tested, oxLDL-IC training only enhanced the production of IL-1β as IL-6 and TNF-α levels were unchanged in response (Figure 4.4C). TNF-α production was significantly reduced by

primary treatment with LPS, but this is consistent with prior work showing high levels of LPS can tolerize cells to further exposure (Figure 4.4C)[194]. Overall, these results support the hypothesis that oxLDL-ICs can induce trained immunity in BMDCs.

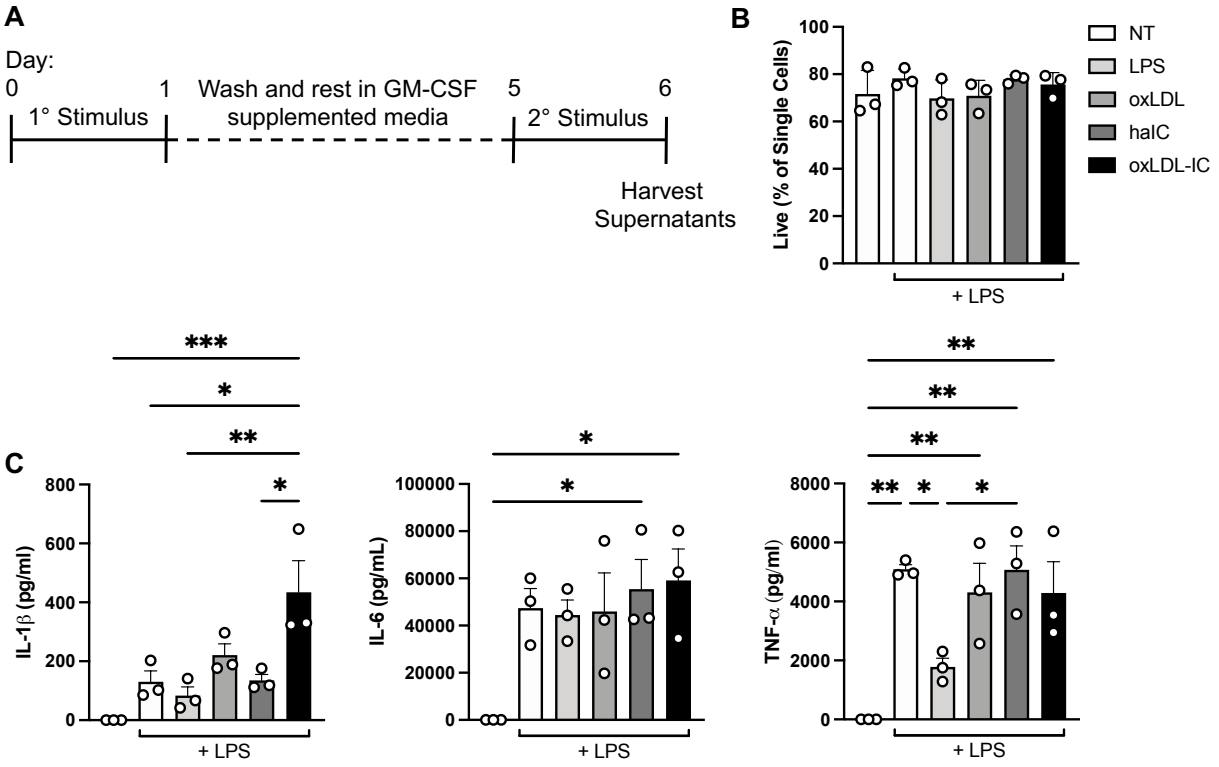

Figure 4.4. OxLDL-ICs induce trained immunity in BMDCs. (A) Trained immunity assay design. Primary stimuli included media alone (NT), 20ng/ml LPS, 50µg/ml oxLDL, 200µg/ml haIC, or a combination of 50µg/ml oxLDL and 200µg/ml haIC (oxLDL-IC). Secondary stimuli were media alone or 20ng/ml LPS. **(B-C)** BMDCs were trained as described in (A). Cell viability was assessed by flow cytometry **(B)** and supernatant cytokines were measured by ELISA **(C)**. Data points are individual mice and error bars show SEM. *, **, and *** denote significance $p<0.05$, $p<0.01$, and $p<0.001$, respectively, by one-way ANOVA and Tukey's multiple comparison test.

OxLDL-IC immune training is associated with increased glycolytic metabolism.

Immune training is mediated by metabolic shifts in the cell which ultimately lead to epigenetic alterations[186]. To investigate whether the metabolism of oxLDL-IC-treated BMDCs was changed, the cells were subjected to extracellular flux analyses after

primary stimulation. BMDC training with both free oxLDL and oxLDL-ICs significantly increased extracellular acidification rate (ECAR) following exposure to glucose and oligomycin, suggesting increased glycolysis and glycolytic capacity, respectively (Figure 4.5A-C). Interestingly, BMDCs receiving a primary stimulus of oxLDL-ICs were even more glycolytic than those treated with oxLDL alone (Figure 4.5A-C), indicating that the training induced by oxLDL-ICs may be distinct from that which was previously described for oxLDL[189].

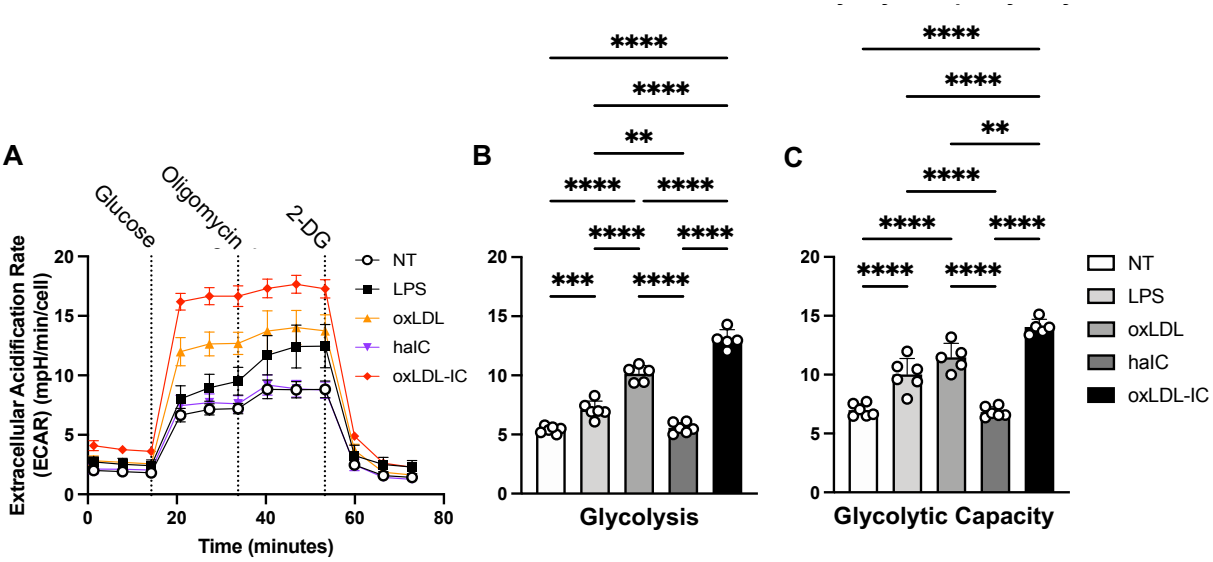

Figure 4.5. OxLDL-ICs enhance glycolytic metabolism. BMDCs were treated with media alone, 20ng/ml LPS, 25μg/ml oxLDL,100μg/ml halC, or a combination of 25μg/ml oxLDL and 100μg/ml halC (oxLDL-IC) for 24hrs before extracellular acidification rate (ECAR) was measured with Seahorse XF Glycolysis Stress Test **(A)**. Level of glycolysis **(B)** and glycolytic capacity **(C)** were determined by calculating ECAR rate change after addition of glucose or oligomycin, respectively. Shown is one representative of at least three experiments. Data points are technical replicates and error bars show SD. **, ***, and **** denote significance $p<0.01$, $p<0.001$, and $p<0.0001$, respectively, by one-way ANOVA and Tukey's multiple comparison test.

Feeding an atherogenic diet to susceptible mice alters DC populations in vivo. To begin to determine whether atherogenic conditions might induce long-term changes in DCs *in vivo* like oxLDL-ICs *in vitro*, male *Ldlr*$^{-/-}$ were maintained on NC or WD for four

weeks before various tissues were harvested for analysis (Figure 4.6A). In this system, WD feeding significantly reduced cell number in the bone marrow compared to mice on NC (Figure 4.6B). WD significantly increased the proportion of hematopoietic stem cells (HSCs) in the bone marrow, consistent with what has been previously described[190,195,196]. However, these past studies did not analyze the full DC developmental lineage. Results indicated WD feeding significantly elevated the frequency of the pre-DC population, the last DC precursor population before the cell leaves the bone marrow (Figure 4.6C). WD feeding also shifted the proportions of mature DC populations including pDCs that secrete high levels of type I interferons[197], CD8α^+ cDCs which can cross-present exogenous antigen on MHC class I molecules (reviewed in [198]), CD11b$^+$ cDCs that are migratory and present antigen to CD4$^+$ T cells (reviewed in [199]), and merocytic DCs (mcDCs) which have been shown to break immune tolerance[200]. However, these alterations were tissue dependent with different patterns emerging in the bone marrow, blood, and spleen (Figure 4.7A-C). Collectively, these results suggest WD reshapes DC population frequencies.

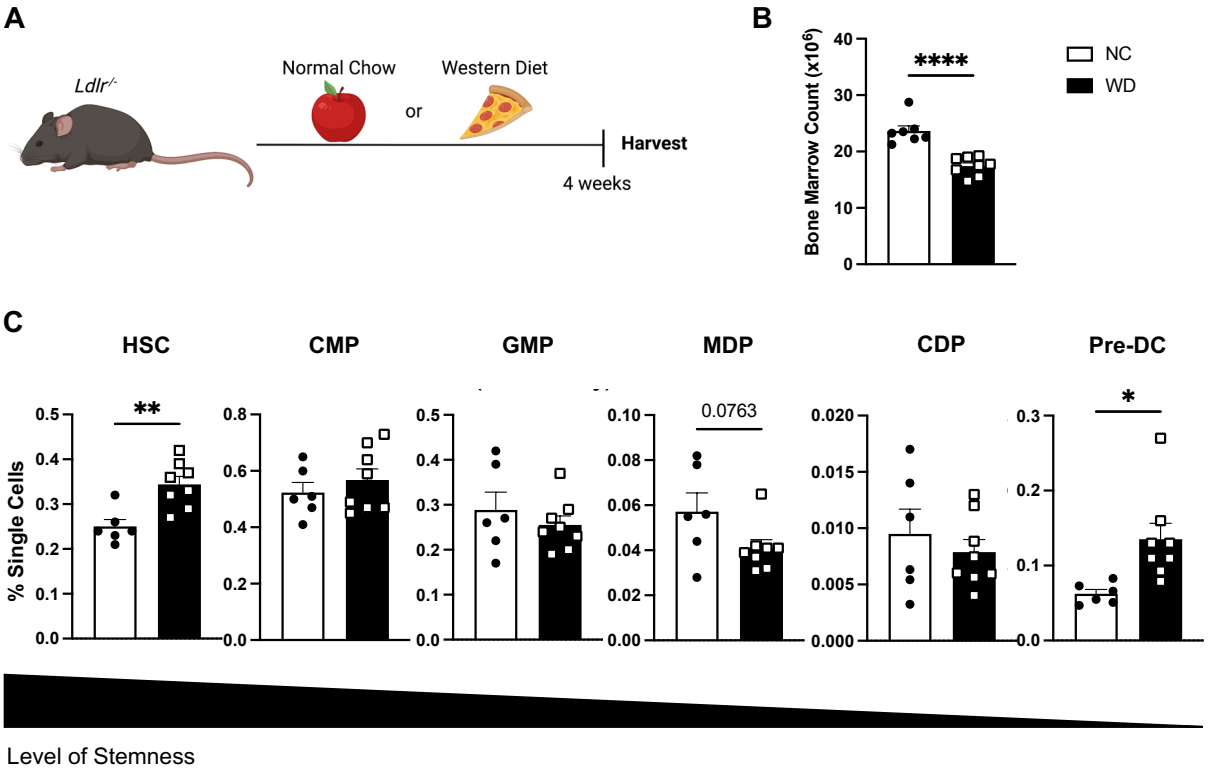

Figure 4.6. Western diet feeding of atherosclerosis-susceptible mice reduces bone marrow compartment and enhances select pre-dendritic cell populations. **(A)** Study design (image generated with Biorender). Bone marrow was collected from male *Ldlr*$^{-/-}$ mice fed as depicted, counted **(B)**, and analyzed by flow cytometry **(C)**. HSC= Lin^{-} c-kit^{+} Sca-1^{+} CD34^{+}, CMP= Lin^{-} c-kit^{+} Sca-1^{-} CD16/32^{low} CD34^{+}, GMP= Lin^{-} c-kit^{+} Sca-1^{-} CD16/32^{hi} CD34^{+}, MDP= Lin^{-} c-kit^{+} Sca-1^{-} CD16/32^{hi} CX3CR1^{+} CD11b^{-}, CDP= Lin^{-} c-kit^{int} Sca-1^{-} CD16/32^{lo} CX3CR1^{+} CD11b^{-}, and Pre-DC= Lin^{-} c-kit^{-} CD16/32^{-} CX3CR1^{+} CD11c^{int} CD11b^{+}. N=6-8 mice per group, 2 independent experiments. Data points represent individual mice and error bars show SEM. *, **, and **** denote significance $p<0.05$, $p<0.01$, and $p<0.0001$, respectively, by Student's *t* test.

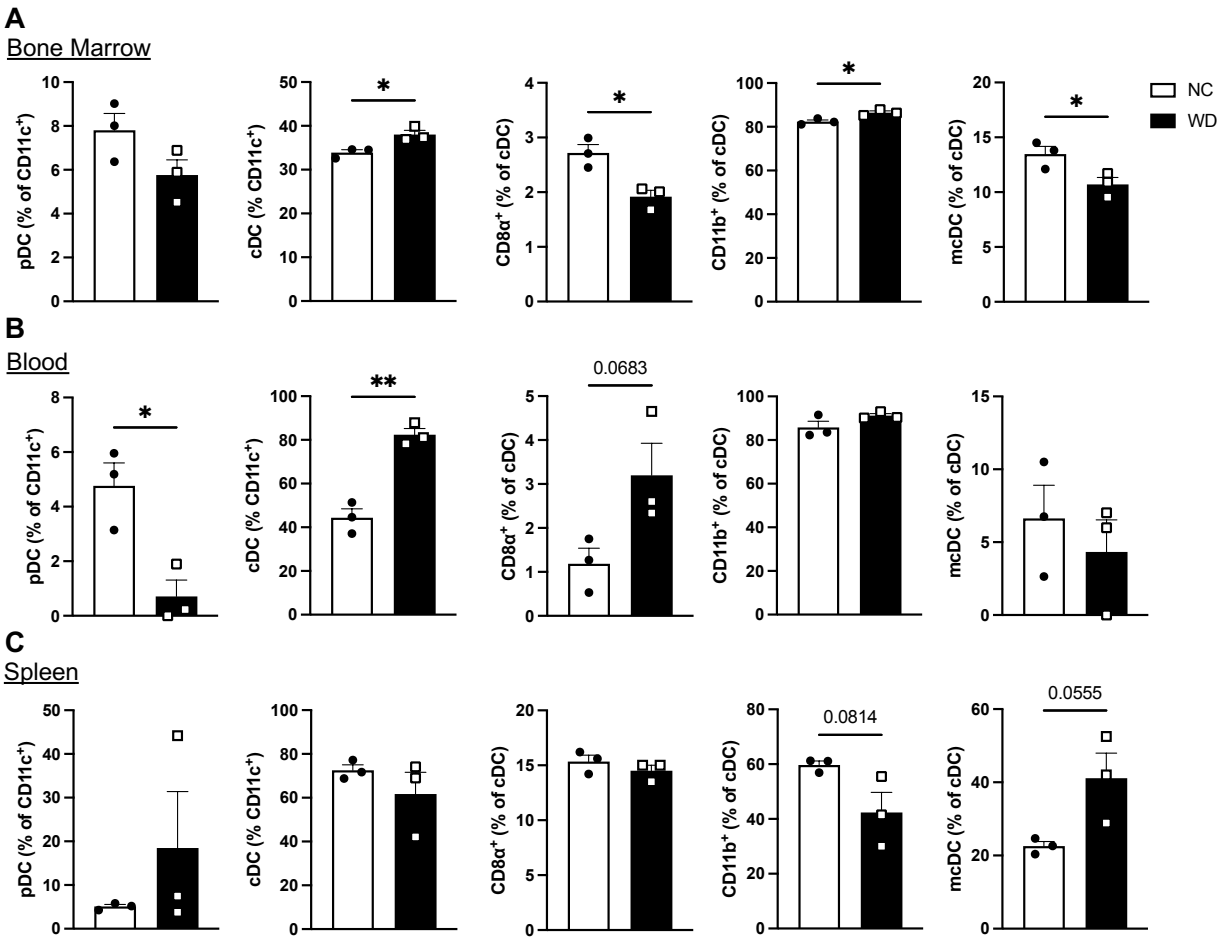

Figure 4.7. Western diet feeding of atherosclerosis-susceptible mice alters mature dendritic cell populations. Male *Ldlr*$^{-/-}$ mice fed were maintained on NC or WD for four weeks before bone marrow **(A)**, blood **(B)**, and spleen **(C)** were harvested and analyzed by flow cytometry to assess various DC populations. pDC= CD11c^{+} PDCA1^{+} B220^{+}, cDC= CD11c^{+} PDCA1^{-} B220^{-}, CD8α cDC= CD8a^{+} CD11b^{-} cDC, CD11b^{+} cDC= CD8a^{-} CD11b^{+} cDC, mcDC= CD8a^{-} CD11b^{-} cDC. N=3 mice per group. Data points represent individual mice and error bars show SEM. * and ** denote significance $p<0.05$ and $p<0.01$, respectively, by Student's *t* test.

WD-induced alterations in the bone marrow lead to long-term changes after DC development. Given the trained phenotype observed *in vitro*, I sought to determine whether the altered frequencies of DC precursor populations in the bone marrow would translate to lasting functional changes in DCs. To evaluate this, I collected bone marrow from differentially fed mice and cultured the cells for nine days in the presence of GM-

CSF to obtain BMDCs (Figure 4.8A). There was no significant difference in cell yield between the two groups (Figure 4.8B). Following differentiation, BMDCs were stimulated with LPS, harvested for RNA, and gene expression was analyzed by qPCR. Interestingly, BMDCs from WD-fed mice had reduced expression of *Il1b*, *Il12a*, and *Il12b* upon stimulation compared to NC-fed cells (Figure 4.8C). Additionally, when BMDC metabolism was investigated, cells from WD-fed animals trended towards elevated glycolysis and glycolytic capacity compared to those from NC-fed mice (Figure 4.8D-F), consistent with the metabolic changes observed in response to oxLDL-IC treatment *in vitro*. Overall, the data from these diet comparison studies suggest WD, which promotes the development of oxLDL-ICs *in vivo*, induces long-term changes in DCs.

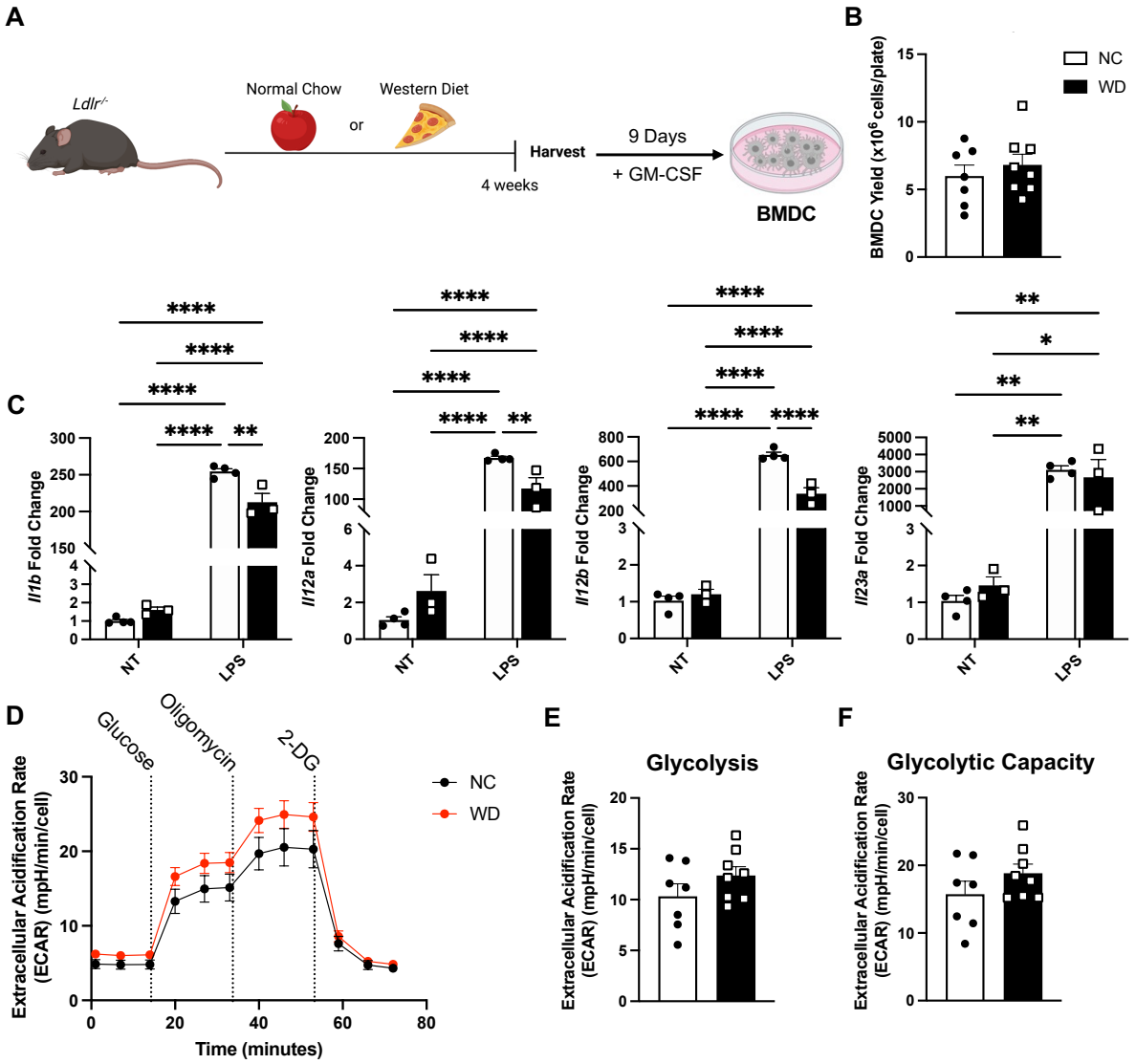

Figure 4.8. BMDCs generated from alternatively fed mice respond differently to stimuli. (A) Study design (image generated with Biorender). Bone marrow was collected from male *Ldlr*$^{-/-}$ mice fed as depicted and differentiated to BMDCs. **(B)** BMDCs were counted and average number per plate calculated. N=7-8 mice per group, 2 independent experiments. **(C)** BMDCs were stimulated with media alone (NT) or 20ng/ml LPS for 2hrs before RNA was purified and used for qPCR analysis. N=3-4 mice per group. Data points represent individual mice and error bars show SEM. *, **, and **** denote significance $p<0.05$, $p<0.01$, and $p<0.0001$, respectively, by two-way ANOVA and Tukey's multiple comparison test. **(D)** Extracellular acidification rate (ECAR) was measured with Seahorse XF Glycolysis Stress Test. Level of glycolysis **(E)** and glycolytic capacity **(F)** were determined by calculating ECAR rate change after addition of glucose or oligomycin, respectively. N=7-8 mice per group, 2 independent experiments. Data points represent individual mice and error bars show SEM.

Discussion

The current study indicates oxLDL-ICs are a novel inducer of trained immunity in BMDCs. I show that cells treated with oxLDL-ICs produce significantly more IL-1β upon secondary stimulation with LPS (Figure 4.4). Additionally, these BMDCs shift their metabolism towards glycolysis following the primary stimulation (Figure 4.5). This is consistent with findings from previous groups which have shown glycolysis is increased and required for innate immune training[186,201]**.** Metabolic alteration is thought to be directly tied to the epigenetic modifications in trained cells as glycolysis leads to a high NAD^+:NADH ratio that in turn reduces expression of sirtuin 1 histone deacetylases[186]. However, future work will be required to characterize the potential epigenic modifications induced by oxLDL-IC treatment in BMDCs.

At this point, most trained immunity studies have been focused on monocytes and macrophages. I used BMDCs for this work, providing more information about immune training in a less studied cell type, but with the important caveat that BMDCs are known to be heterogenous and sometimes monocyte-like[202]. Interestingly, prior work characterizing immune training in DCs did not observe robust cytokine production in response to secondary stimulation with an unrelated antigen[203], contrary to the results of the present study. The experiment in Hole *et a*l. is not a perfect comparison as it uses *ex vivo* sorted DCs restimulated with a variety of antigens following training by *in vivo* exposure to modified *Candida neoformans*. However, the fact that our BMDCs significantly increased cytokine output in response to non-specific secondary stimulation may suggest oxLDL-ICs have some unique properties in immune training.

Prior work from Christ *et al*. has shown that WD feeding of *Ldlr*$^{-/-}$ mice induced inflammatory changes in monocytic precursors and mature macrophages that persisted even when normal lipid levels were restored[190]. This, in combination with the *in vitro* findings that WD-associated oxLDL-ICs can train BMDCs, prompted the study of DC precursors *in vivo* following feeding with NC or WD. Some of these results were consistent with what has been previously described including a significant increase in HSCs[190,195,196], while changes in the pre-DC population have not been studied before (Figure 4.6). Interestingly, I observed an overall reduction in bone marrow cell number in WD-fed animals (Figure 4.6). This was somewhat surprising given a prior study in B6 mice fed a high-fat diet showed an increase in bone marrow cell numbers[204]. This discrepancy could be due to mouse strain or diet differences and would require more follow-up studies.

In addition to looking at DC precursor populations, I also examined mature DC populations in the bone marrow, blood, and spleen (Figure 4.7). The most notable changes were in pDCs, which have been described as both pro- and antiatherogenic[70,72], and CD8α^+ cDCs that have been suggested to be atherogenic[68]. In response to WD feeding pDCs were significantly diminished in the blood and trended towards reduction in the bone marrow. This could indicate a general shrinking of the population or a migration of these cells to the plaque and draining lymph nodes. Similarly, CD8α^+ cDCs are thought to seed tissues directly from the bone marrow[198] so their proportional decrease in the marrow with WD feeding could mean loss of the cell type or increased emigration out of the bone marrow. It is difficult to draw conclusions from these data about the impact of the observed population changes on

atherosclerosis as the tissues studied are not necessarily representative of the plaque. Future studies should directly sample the aorta and adLN to assess DC changes in the microenvironments most important to disease development.

To assess whether WD-induced changes in the DC precursor population had long-lasting functional significance, I generated BMDCs from the marrow of differentially fed mice using GM-CSF (Figure 4.8). There was precedence to suggest that trained phenotypes could persist even through cytokine directed differentiation of the bone marrow as Edgar *et al*. had shown bone marrow-derived macrophages (BMDMs) produced from hyperglycemic mice had increased cytokine production upon restimulation after seven days in culture compared to BMDMs from normoglycemic mice[205]. In the current study, BMDCs generated from WD-fed animals trended towards a more glycolytic metabolic signature compared to cells from NC-fed mice (Figure 4.8). This was exciting as it mirrored the enhanced glycolysis observed with oxLDL-IC treatment *in vitro*. However, the metabolic differences from the *in vivo* experiment were much less dramatic than in the *in vitro* assays, but that is understandable given the increased complexity of the whole animal system. A somewhat surprising finding was the decreased expression of inflammatory cytokine transcripts, *Il1b*, *Il12a*, and *Il12b*, from WD-derived BMDCs restimulated with LPS (Figure 4.8). Given the data obtained *in vitro*, the prediction was that there would at least be an increase in *Il-1b* levels. One important caveat is that this is gene expression data whereas protein changes were measured *in vitro*, so this discrepancy could be due to differing RNA and protein kinetics. However, if the reduced cytokine expression was supported by additional assays, it could potentially be consistent with the body of work showing increased

susceptibility to infection in patients with obesity (reviewed in [206]). Additional experiments will be required to better characterize the long-term changes induced in DCs by WD.

The results of this study agree with work from others which suggest trained immunity is an important player in the progression of atherosclerosis. Interestingly, the modification of LDL appears to be critical for making it an antigen capable of immune training. OxLDL and acetylated LDL both train human primary monocytes *in vitro*, but native LDL does not[189]. Additionally, van der Valk *et al.* have shown lipoprotein(a) induces trained immunity in human monocytes via its oxPLs[207]. Furthermore, when tested *in vitro* statins, drugs commonly used for the treatment of atherosclerosis, prevented training in monocytes by β-glucan or oxLDL[208]. However, three months of statin treatment in atherosclerosis patients did not reduce elevated cytokine production from monocytes nor H3K4me3 marks observed on the *TNF* promoter[209], suggesting the modulation of trained immunity *in vivo* is more complex. To effectively counter the inflammatory effects of trained immunity in atherosclerosis, treatments need to be developed that can reverse the epigenetic alterations once they have been established. It is not enough to rely on inhibitors of the initial training event, especially in the context of chronic diseases like atherosclerosis. This may be especially important for other chronic conditions like SLE that accelerate atherosclerosis, but do not robustly respond to lipid lowering treatments[26].

In conclusion, this study identifies oxLDL-ICs as a new trigger of trained immunity in BMDCs. Training with oxLDL-ICs results in increased release of IL-1β upon secondary stimulation and enhances the glycolytic metabolism of the cell, which may

potentially lead to downstream epigenetic remodeling. This effect is distinct from that triggered by oxLDL, which is known to induce trained immunity. Translating these findings *in vivo*, atherogenic mice on WD have altered proportions of precursor and mature DCs compared to NC-fed controls. Finally, BMDCs derived from these differentially fed mice have altered responses to inflammatory and metabolic stimuli, indicating WD can induce long-term changes in DCs. Overall, these findings suggest oxLDL-ICs are not only involved in acute events in atherosclerosis but may also contribute to the chronic inflammation that is characteristic of the disease.

Chapter 5

Conclusions and Future Directions

Together, the data presented in this dissertation demonstrate how critical oxidized lipids are to modulating the immune response in atherosclerosis. The accumulation of LDL in the artery wall is an initiating event in the disease where it is oxidized through enzymatic modification, free ROS, or metal ions in the environment[12,29]. OxLDL and its oxidized phospholipid components are capable of directly modulating immune cells [44,89,136,148] and studying these responses is necessary for complete understanding of atherosclerosis pathogenesis.

The Mechanism and Impact of oxPAPC-Induced Th1-like T_{regs}

In Chapter 2, I showed the oxidized phospholipid, oxPAPC, alters T_{reg} differentiation, significantly reducing T_{reg} viability and promoting a Th1-like phenotype with T-bet and IFN-γ expression. This was specific to T_{reg} polarization, as Th1 and Th17 differentiation are unaffected by the inclusion of oxPAPC. I showed oxPAPC-treated T_{regs} have a reduced suppressive capacity *in vitro* and that they cannot inhibit atherosclerosis progression when adoptively transferred into hyperlipidemic *Ldlr*$^{-/-}$ mice. Overall, the results of Chapter 2 demonstrate that oxPAPC induces dysfunction in T_{regs} that make them less protective in the atherosclerotic environment and could thereby be one of the factors inhibiting T_{reg} function in atherosclerosis.

A major future direction of this work will be to determine the full mechanism by which oxPAPC is altering T_{reg} differentiation. In Chapter 2, I showed development of T-

bet and IFN-γ expression in oxPAPC-treated T_{regs} is dependent on CD36 and IFN-γ signaling but is independent of TLR-4, IL-2 concentration, and TFG-β levels in the culture media. However, none of these modulations significantly altered the oxPAPC-induced loss of T_{reg} viability, suggesting cell death is mediated by a separate mechanism. Preliminary findings from another member of the lab indicate oxPAPC may be acting in an ATP citrate lyase (ACLY)-dependent manner to impact both Th1-like phenotypes as well as viability. ACLY is an enzyme responsible for converting cytosolic citrate to acetyl-coenzyme A for use in fatty acid synthesis and histone acetylation, and its enzymatic activity has been shown to be reduced during T_{reg} differentiation[210]. Given its ties to epigenetic modifications, an ACLY-dependent mechanism could also provide an explanation for the lasting impact oxPAPC has on T_{regs}. As demonstrated in Chapter 2, T_{regs} differentiated in the presence of oxPAPC for only the first three days of culture remain phenotypically altered on day 5 and are less suppressive when placed in co-culture even though oxPAPC is no longer present in those conditions. Additionally, dysfunction seems to persist for much longer as adoptive transfer of oxPAPC-treated T_{regs} does not reduce plaque burden like adoptive transfer of control T_{regs}.

Another mechanistic future direction is to determine whether FoxP3 is acting in a proapoptotic manner in oxPAPC-treated T_{regs}. As shown in Chapter 2, the time of oxPAPC-induced cell death coincides with the expression of FoxP3, suggesting they could be connected. Tai *et al.* has previously shown that FoxP3 expression is apoptotic during T_{reg} differentiation in the thymus unless counterbalanced by the appropriate pro-survival signals[151]. This apoptosis occurs because of FoxP3 increasing the expression of the proapoptotic protein Puma, enhancing the activity of the proapoptotic protein Bim

by directly downregulating dual-specificity phosphatase 6 (DUSP6) and therefore increasing the activity of Bim-phosphorylating jun N-terminal kinase, and by reducing the expression of the prosurvival protein B-cell lymphoma 2 (Bcl-2) [151]. To test whether FoxP3 is promoting apoptosis in oxPAPC-treated T_{regs}, an initial experiment would be to perform chromatin immunoprecipitation assays with sequencing (CHIP-Seq) in control and oxPAPC-treated T_{regs} to evaluate the binding sites of FoxP3 in each condition. If FoxP3 is causing oxPAPC-linked apoptosis, I would expect CHIP-Seq results to indicate FoxP3 enhancing activity at the Puma promoter and downregulating activity at the DUSP6 and Bcl-2 promoters. To test if compromising the function of FoxP3 improved oxPAPC-induced cell death, T_{regs} could be polarized from B6 or heterozygous B6xSurfy mice each with a FoxP3-driven Thy1.1 reporter transgene in the presence or absence of oxPAPC. Heterozygous B6xScurfy mice have unstable FoxP3 protein[151], so if FoxP3 activity is directly mediating the cell death caused by oxPAPC treatment, I would expect the B6xSurfy T_{regs} to have improved viability. If FoxP3 is indeed promoting cell death in oxPAPC-treated T_{regs}, the next line of investigation will be to determine how oxPAPC is making treated cells vulnerable to this effect when control cells are not.

In addition to interrogating the mechanism behind oxPAPC-induced alterations, another important future direction will be to determine whether the Th1-like phenotypes developed with oxPAPC treatment directly cause T_{reg} dysfunction. OxPAPC reduces T_{reg} viability and leads to the development of Th1-like phenotypes but through separate mechanisms. Though these oxPAPC-treated T_{regs} are dysfunctional, it has not yet determined if this is dependent of the development of Th1-like phenotypes. To test this, T_{regs} deficient for receptors I have already shown to be required for the development of

Th1-like phenotypes, such as CD36 and IFNγR1, will be used in *in vitro* suppression assays and *in vivo* adoptive transfer experiments like those in Chapter 2. These studies will be distinct from those shown in Chapter 3 in that they will evaluate the impact inhibition of these pathways has on functional changes induced only by oxPAPC. The bone marrow chimera experiments test the consequences of T_{reg} IFN-γ signaling inhibition in the whole atherosclerotic microenvironment of which oxPAPC is a part. Studies have shown Th1-like T_{regs} have compromised function in atherosclerosis[134,145], therefore, I predict the Th1-like phenotype induced by oxPAPC treatment is directly responsible for T_{reg} dysfunction observed in Chapter 2 and is not just correlative. In accordance with this, I anticipate *Cd36*$^{-/-}$ and *Ifngr1*$^{-/-}$ T_{regs} will be more functional *in vitro* and *in vivo*. Understanding the specifics of the mechanism behind oxPAPC-induced dysfunction is critical for developing therapeutics that might counter these effects *in vivo* to promote atheroprotective T_{regs}.

The Complex Role of T_{reg} Intrinsic IFN-γ Signaling

In Chapter 3, I built on findings from Chapter 2 which showed IFN-γ signaling was required for the development of oxPAPC-induced Th1-like phenotypes. To investigate the effect of T_{reg} IFN-γ signaling in a mouse model of atherosclerosis, I performed bone marrow transplants into male and female *Ldlr*$^{-/-}$ mice using sex-matched donors that had a T_{reg}-specific deficiency for IFNγR1 (*Ifngr1*$^{fl/fl}$-*Foxp3*$^{Cre+}$) or were wild-type for the receptor (*Ifngr1*$^{WT/WT}$-*Foxp3*$^{Cre+}$). T_{reg} IFNγR1 deficiency impacted atherosclerosis severity in a sex-dependent manner, with disease improving in T_{reg} IFNγR1 deficient males compared to sex-matched controls, and it worsening in T_{reg} IFNγR1 deficient

females compared to sex-matched controls. Interestingly, the systemic immunological changes observed appear to be inconsistent with the disease outcome. *Ifngr1*$^{fl/fl}$-*Foxp3*$^{Cre+}$ male recipients had significantly increased Th1 and IFN-γ^+ T_{reg} proportions in the spleen as well as elevated anti-oxLDL IgG2c titers. Inversely, *Ifngr1*$^{fl/fl}$-*Foxp3*$^{Cre+}$ female recipients had a lower proportion of Th1 cells and IFN-γ^+ T_{regs} in the aorta and increased circulating anti-oxLDL IgG1. Consistent with their reduced disease, macrophages in the adLN of male *Ifngr1*$^{fl/fl}$-*Foxp3*$^{Cre+}$ mice appeared less activated than in sex-matched controls. Overall, the results of this study show IFN-γ signaling in T_{regs} significantly impacts atherosclerosis development but does so in a sex-dependent manner, highlighting that the role of IFN-γ is not as straightforward as is sometimes described. To my knowledge, this is the first investigation of a T_{reg}-specific deficiency in a mouse model of atherosclerosis and its nuanced results suggest the need for more moving forward.

One future direction of this work is to determine if macrophages are in fact directly modulating atherosclerosis levels in *Ifngr1*$^{fl/fl}$-*Foxp3*$^{Cre+}$ recipients. To start, this aim will require a much more sophisticated analysis of the macrophage population than that done in Chapter 3. Using flow cytometry and immunohistochemistry M1- and M2-associated markers (Table 2) will be quantified in male and female *Ifngr1*$^{fl/fl}$-*Foxp3*$^{Cre+}$ and *Ifngr1*$^{WT/WT}$-*Foxp3*$^{Cre+}$ recipients. M1-like macrophages are more inflammatory and atherogenic while M2-like macrophages promote tissue repair and inflammation resolution (reviewed in [211]). If IFNγR deficient T_{regs} are reshaping macrophage phenotypes as hypothesized, I would expect to see increased expression of M1-associated markers in female *Ifngr1*$^{fl/fl}$-*Foxp3*$^{Cre+}$ mice and elevated expression of M2-

associated markers in male *Ifngr1*$^{fl/fl}$-*Foxp3*$^{Cre+}$ recipients compared to sex-matched controls based on the observed changes in lesion size. If changes in M1 or M2 marker expression were observed, the direct effect of these macrophages could then be assessed in our bone marrow chimeras using neutralizing antibodies or pharmacological inhibitors of the functional M1 or M2 receptors, as has been shown previously[212,213].

Table 2. M1/M2 macrophage phenotyping markers.

Macrophage Phenotype	Marker	Function	Ref.
M1	CD86	Costimulatory molecule	55
	Inducible nitric oxide synthase	Produces nitric oxide	214
	CXCL9/10/11	Chemokines	215
M2	Arginase 1	Hydrolyzes l-arginine	128
	G-protein receptor 18	Specialized proresolving mediator receptor	128,212
	Formyl peptide receptor 2	Specialized proresolving mediator receptor	128
	Chemokine-like receptor 1	Specialized proresolving mediator receptor	128
	Mannose receptor 1	Endocytosis and phagocytosis	128

On a broader scale, another future direction of this work will be to determine how biological sex drives differential responses to T_{reg} IFNγR signaling. In humans, premenopausal females are protected from atherosclerosis compared to age-matched males [216]. However, the atherosclerosis risk in post-menopausal females is equal to and eventually surpasses that of age-matched males[216], suggesting an important role for sex hormones in modulating disease. Many observational and preclinical studies have demonstrated atheroprotective effects of estrogen [23,217], though some post-menopausal hormone replacement therapy (HRT) randomized trials have demonstrated that treatment with estrogen is only protective if initiated before the development of

advanced atherosclerosis[218–220]. If introduced too late, HRT may even lead to adverse outcomes due to estrogen's prothrombotic effects[221,222]. In male mice, testosterone has also been shown to be atheroprotective early in disease due to its conversion to estradiol, a form of estrogen, by aromatase[223]. There is also a low, but biologically relevant level of estrogen that circulates in males and deficiency of this estrogen increases testosterone levels[224].

Sex hormones also have a role in promoting T_{reg} function. Estrogen signaling through estrogen receptor (ER)-β on T_{regs} has been shown to promote T_{reg} differentiation and function in mouse models of pneumonia and chronic intestinal inflammation[225,226]. Estrogen has also been shown to significantly increase IFN-γ production from mouse splenocytes[227] and treatment of ovariectomized mice with exogenous estrogen increased Th1 differentiation *in vivo*[228]. Together, these results demonstrate that while estrogen does promote functional T_{regs} it also enhances IFN-γ production in non-T_{reg} $CD4^+$ cells. Along the same lines, work from Fijak *et al.* suggests testosterone treatment expands T_{regs} and promotes their protective function *in vitro* and *in vivo*[229] and Gandhi *et al.* demonstrates androgen receptor signaling promotes T_{reg} function in a model of allergic airway inflammation[230]. Testosterone and other androgens have also been shown to reduce Th1 cell differentiation, thereby exerting the opposite effect of estrogen on non-T_{reg} $CD4^+$ cells[231].

Given all this information and the phenotypes observed in my bone marrow chimera experiments, I hypothesize that T_{reg} IFNγR1 deficiency is leading to a significant reduction of estrogen in both male and female mice. Normal ER activity is required by both sexes for cardiovascular homeostasis[224,232–234]. Loss of estrogen in

female recipients would be consistent with the observed increase in plaque size in *Ifngr1*$^{fl/fl}$-*Foxp3*$^{Cre+}$ recipients as estrogen has been shown to be atheroprotective [23,217], and it could also explain the reduced proportion of IFN-γ^+ T cells since the hormone is known to promote such responses [227,228]. On the other hand, limiting endogenous estrogens in males has been shown to significantly increase testosterone level [224], which is protective in atherosclerosis due to its conversion to estradiol [223]. The reduced plaque size observed in male *Ifngr1*$^{fl/fl}$-*Foxp3*$^{Cre+}$ recipients would be consistent with this, while the elevated percentage of IFN-γ^+ T cells could be the result of increased testosterone-derived estradiol as well. The first step to testing this would be quantifying estrogen levels in circulation in the bone marrow chimera recipients. If my hypothesis holds true, a critical aim will be to determine how IFNγR1 expression specifically on T_{regs} is influencing estrogen levels. There is a great deal of work published studying how estrogen influences T_{reg} responses [225,226,235,236], but nothing regarding how T_{regs} impact estrogen yet these results suggest it is an important avenue of future investigation.

The Future of ICs in the Pathogenesis of Atherosclerosis

In Chapter 4, I demonstrate that oxLDL-ICs induce trained immunity in BMDCs *in vitro*, increasing their pro-inflammatory cytokine response upon restimulation and promoting a more glycolytic metabolism. Free oxLDL was previously shown to train monocytes[189], but the alterations triggered by oxLDL-IC treatment were significantly different from those caused by oxLDL alone. To my knowledge, this is the first evidence of oxLDL-ICs inducing trained immunity. I additionally show that WD feeding of *Ldlr*$^{-/-}$ mice increased the proportion of DC precursor populations in the bone marrow. BMDCs

generated from WD-fed marrow also had altered responses to stimuli compared to NC-fed BMDCs, suggesting the atherogenic diet induced long-term changes in DCs *in vivo* as oxLDL-ICs did *in vitro*.

One important avenue of future investigation will be determining if the long-term changes observed in the DC population with WD feeding are a direct result of ICs. Prior work from our lab has shown oxLDL-ICs signal through TLR-4, CD36, and FcγRs on BMDCs to prime the inflammasome, with FcγRs binding the antibody portion while TLR-4 and CD36 couple to the oxLDL within the complex [89]. This work additionally hypothesized FcγR1 and FcγRIV were the primary FcγRs mediating oxLDL-IC signaling based on their expression levels on BMDCs[89]. Therefore, to study the effect of inhibition of IC signaling on DC phenotypes in atherogenic models, bone marrow chimeras using CD11c-specific FcγR1 or FcγRIV deficient donors could be generated as in Marvin *et al.*[144] and maintained on NC or WD as in Chapter 4. Inversely, to study the effect of amplification of IC signaling on DC phenotypes, a diet comparison study like that in Chapter 4 could be used with animals on each diet being treated with or without exogenous oxLDL-ICs. If oxLDL-ICs directly contribute to WD-induced DC alterations, I would expect the phenotypes (increased proportions of pre-DCs in the bone marrow and altered response to stimuli in resulting BMDCs) to be reduced in the FcγR deficient bone marrow chimeras and elevated in mice supplemented with additional exogenous oxLDL-ICs.

An additional future direction of this work will be to determine whether other types of ICs are capable of immune training. Previously, ICs formed from bovine milk IgG and the respiratory syncytial virus preF protein were shown to induce immune training in

human monocytes[237]. Additionally, autoantibodies and IgG ICs from RA patients have been shown to cause training in human monocytes, enhancing their production of TNF-α[238,239]. ICs are involved in the pathogenesis of multiple autoimmune diseases including SLE, RA, Type 1 diabetes, systemic sclerosis, and multiple sclerosis (reviewed in [240]). In SLE, ICs contain nucleic acid and nucleoprotein antigens, and have been shown to signal through TLR- or FcγR-dependent mechanisms[241,242], similar to oxLDL-ICs. However, the TLRs mediating SLE IC signaling are intracellular which could be significant if immune training like that observed in Chapter 4 requires the cooperative signaling that has previously been described with oxLDL-ICs[89]. Nonetheless, SLE patients display some signs of trained immunity, like the biasing of bone marrow precursor cells to myeloid lineages[243], suggesting SLE ICs may be capable of immune training. Overall, trained immunity could be playing a significant role in many chronic immune diseases and investigation of immune complexes as triggers of training warrants further investigation.

Implications for Treatment

While preventing the oxidation of LDL would seemingly alleviate most of the pathological processes described in this dissertation, it may not be a feasible therapeutic goal as oxidation of lipids is an early event in atherosclerosis that occurs long before the manifestation of clinical symptoms [12,29]. In accordance with this, clinical trials testing the use of antioxidants to treat atherosclerosis have not had great success, though variations in timing, dose, and antioxidant type are still under consideration (reviewed in [244]). Treatments capable of inhibiting the downstream inflammatory

responses to oxidized lipids, such as those studied here, are likely more realistic targets, but this too comes with challenges.

IFN-γ has long been considered an atherogenic cytokine because of its ability to activate and recruit other inflammatory immune cells [116–119,171]. For this reason, pentoxifylline, a phosphodiesterase inhibitor approved for use as a vasodilator, is currently being tested in a phase II clinical trial for treatment of atherosclerosis based on its Th1 inhibitory effects[245,246]. While the work developed in Chapter 2 of this dissertation might agree with the therapeutic benefit of such a treatment, the results of Chapter 3 indicate that IFN-γ inhibition may not be entirely atheroprotective. Based on my findings the success of this treatment will likely depend on the cell types most effected by the drug and the biological sex of the patient.

Canakinumab, a monoclonal antibody targeting IL-1β, is currently under study in a phase III clinical trial, and results so far indicate that it significantly reduces atherosclerosis but also increases the risk of fatal infection [246,247]. Treatment with canakinumab would seemingly counter the inflammation induced by oxLDL-ICs due to their demonstrated ability to prime the inflammasome[89] and induce training which leads to elevated levels of IL-1β when stimulated in the long term. However, in targeting IL-1β, canakinumab is treating the result of oxLDL-IC induced inflammation, not the process. Given my findings that oxLDL-ICs induce trained immunity in DCs, it would be interesting to pursue inhibitors of training in the future, possibly in combination with treatments like canakinumab to try to maximize benefit while eliminating adverse side effects. Though my work did not define the mechanism of oxLDL-IC immune training, it is typically mediated through epigenetic alterations and the observed shift to a more

glycolytic metabolism with oxLDL-IC treatment supports this [186]. Epigenetic inhibitors are already widely used in cancer treatment and preclinical studies with the FDA-approved histone deacetylase inhibitor, suberoylanilide hydroxamic acid, have demonstrated a beneficial effect in atherosclerosis models[248–250]. Therefore, this seems like it could be a promising treatment strategy in atherosclerosis patients.

The findings in this dissertation do not necessarily indicate a new druggable target for future investigation. However, as described above, there is much more mechanism to be investigated in the future. Additionally, all of this work was studied in the context of atherosclerosis progression, and it is equally as important to determine how oxidized lipids might modulate immune cells during regression. It is known that T_{regs} are critical for regression and that they remodel other immune cells in the process[128]. Therefore, it would be particularly interesting to investigate T_{reg} intrinsic signals, as in Chapter 3, in the context of disease regression.

Overall, the work presented in this dissertation highlights the integral role played by oxidized lipid species in the modulation of immune-mediated effects on atherosclerosis. I show that oxPAPC directly and specifically dysregulates T_{regs}, promoting the loss of function that is typically observed in these cells in atherosclerosis. I also demonstrate that the deficiency of IFNγR1, a receptor required for oxPAPC-induced T_{reg} phenotypes *in vitro*, specifically in T_{regs} modulates atherosclerosis severity *in vivo* but does so in a sex dependent manner. Finally, I describe a novel immune training capability of oxLDL-ICs. These findings not only progress our understanding of the immune dysregulation by oxidized lipids in atherosclerosis, but also have

implications for other inflammatory conditions in which such lipids are enriched, like obesity, cancer, RA, and SLE.

APPENDIX A

MicroRNA-22-3p Promotes T_{reg} Dysfunction and Enhances Kidney Disease Associated with Systemic Lupus Erythematosus

This appendix includes work that was performed prior to my start in the laboratory and therefore was not facilitated directly by me. A pre-print of the original study without my contributions can be found on bioRxiv[251]. Here, I have added the data I generated for this project (highlighted in figures with an *) and reshaped the narrative accordingly.

Introduction

SLE is characterized by loss of tolerance to self, which leads to increased circulating antibodies and activation of lymphocytes[252]. The disease can affect nearly any organ, but nephritis is a major cause of morbidity and mortality in SLE patients[253]. MicroRNAs (miRNAs) are small endogenous post-transcriptional regulators of gene expression that repress protein coding gene (mRNA) translation by binding to their target 3' untranslated region (UTR). Critical genes in lymphocyte biology have been shown to be modulated by miRNAs and studies have reported that altered miRNA activity contributes to T cell and B cell dysregulation in SLE[254–256]. For example, miR-146a was found to repress T cell pro-inflammatory AP-1 transcription factor activity and therefore IL-2 production following T cell receptor engagement[257], but this miRNA is reduced in blood lymphocytes from SLE patients[258]. MiR-24 was reported to directly target *FOXP3*, a master transcription factor for T_{regs}[259], a critical anti-inflammatory T cell population. Studies by Xiao *et al*. demonstrated that miRNAs in the miR-17-92 cluster promoted autoimmunity in mice through inhibition of activation-induced cell death in T

cells[260]. A follow up study by Jiang *et al.* expanded on these findings and reported that the miR-17-92 cluster also supported inflammatory IFN-γ^+ $CD4^+$ Th1 responses and antagonized T_{reg} differentiation[261], promoting conditions like those observed in SLE. Many immune cell-associated miRNAs were also found to be altered in serum/plasma of SLE subjects and have been postulated as potential biomarkers for autoimmune disorders, including miR-223-3p, miR-92a-3p, and miR-20a-5p[262,263]. These studies clearly demonstrate a role for miRNAs in SLE pathogenesis, but this topic needs further exploration to better understand disease mechanism.

Here, small RNA sequencing (sRNAseq) was used to quantify miRNA changes in plasma from human SLE subjects, and miR-22-3p was identified as one of the most highly abundant and differentially altered species in the samples. MiR-22-3p was also found to be enriched in multiple immune cell types in a mouse model of SLE. When miR-22-3p was inhibited in B6.SLE mice using locked-nucleic acids targeting the miRNA (LNA-22), it significantly decreased T cell activation and early anti-double-stranded DNA (dsDNA) autoantibody titers compared to scramble (LNA-Scr) treated control mice. Inhibition of miR-22-3p *in vivo* ultimately reduced lupus nephritis severity. Though LNA-22 treatments decreased the frequency of Th1 cells in the spleen and Th1 signaling in the kidney, *in vitro* polarization experiments showed miR-22-3p did not directly impact Th1 differentiation. However, both LNA-22 treatment and *in vitro* modulation of miR-22-3p levels regulated T_{reg} IL-10 expression, and T_{regs} deficient for miR-22-3p were better suppressors of cytokine production in co-culture. Collectively, these data suggest that miR-22-3p is pathogenic in SLE by inhibiting of T_{reg} function, thereby indirectly driving inflammatory T cell responses which promote lupus nephritis.

Materials and Methods

Subjects. Clinical data and stored plasma from SLE (n=12) and healthy (n=12) subjects matched for age, race and sex were used for this study (Table 3). These subjects represent a subset of participants from two prior studies which were concurrently enrolled; study procedures were previously reported[264,265]. Studies were conducted under approved Vanderbilt IRB protocols and written informed consent was obtained from all subjects. Disease activity was measured in SLE subjects using the Systemic Lupus Erythematosus Disease Activity Index (SLEDAI), as modified for the SELENA trial[266]. Disease damage was assessed by the Systemic Lupus International Collaborating Clinics/American College of Rheumatology damage index (SLICC)[267].

Table 3. Subject characteristics.

	SLE (N=12)	Control (N=12)	P
Age, years	48 ± 11	49 ±11	0.77
Race, #Caucasian	12 (100)	12 (100)	0.99
Sex, #female	7 (58)	7 (58)	0.99
Creatinine, mg/dl	1.0±0.33	0.9±0.3	0.46
SLEDAI score, units	4 [0, 6]	-	-
SLICC score, units	1 [0, 3]	-	-
Lupus nephritis (ever), #	1 (8)	-	-
Hydroxychloroquine, #	7 (58)	-	-
Methotrexate, #	1 (8)	-	-
Mycophenolate mofetil, #	1 (8)	-	-
Azathioprine, #	2 (17)	-	-
Prednisone, #	6 (50)	-	-
miR-22-3p, Ct	27.0 ± 2.0	30.7 ± 1.4	0.0003
miR-22-3p, pM (3- spike)	0.33 ± 0.29	0.015±0.012	0.0003

Continuous data are presented as mean ± standard deviation. Categorical data are presented as number (percentage). Difference was determined by Mann Whitney U for continuous and Chi square for categorical data. Medications are listed as current use.

sRNAseq. To quantify miRNAs in human plasma, high-throughput sRNA-seq was performed[268,269]. Briefly, total RNA was isolated from ethylenediaminetetraacetic acid (EDTA)-collected plasma using Total RNA Purification Kits (Norgen Biotek Cat #

37500). Small RNA (cDNA) sequencing libraries were generated by TruSeq Small RNA Library Preparation Kits (Illumina). Libraries were size-selected using a Pippin Prep (Sage Science) and sequenced using the NextSeq500 platform (Illumina) at the Vanderbilt Technologies for Advanced Genomics (VANTAGE) DNA sequencing core facility. sRNA-seq data were analyzed using the TIGER (Tools for Integrative Genome Analysis of Extracellular sRNAs) pipeline[269]. MiRNA aligned read counts were normalized to the total number of high-quality reads per sample and reported as Reads Per Million total reads (RPM). Differential expression analysis for miRNAs was performed by DESeq2 with adjustment for batch effects[270].

qPCR. Plasma miR-22-3p concentrations were validated in each sample by qPCR. For normalization of RNA extraction efficiency, plasma RNA samples were spiked with a standard of three exogenous single-stranded miRNA oligonucleotides (cel-miR-39, cel-miR-54, and cel-miR238; Qiagen) after the initial lysis step. A qScript microRNA cDNA synthesis kit (Quantabio) was used to prepare plasma cDNA and a miR-22-3p PCR assay (Quantabio) and PerfeCTa SYBR green supermix for iQ (Quantabio) were used for qPCR. Plasma miR-22-3p concentrations were derived from a standard dilution series of a known concentration of a DNA mimetic of the target miRNA sequence and normalized to the spike-in standards. For cellular miRNA and mRNA analyses, individual immune populations were enriched from spleen using $CD4^+$ T Cell Isolation Kit mouse (Miltenyi Cat # 130-104-454), B Cell Isolation Kit mouse (Miltenyi Cat # 130-090-862), CD11c Microbeads Ultrapure mouse (Miltenyi Cat # 130-125-835), or $CD4^+$ $CD25^+$ Regulatory T Cell Isolation Kit mouse (Miltenyi Cat # 130-091-041) according to manufacturer instructions. Total RNA was isolated from cells using Total RNA

Purification Kits. RNA samples to be used for miRNA quantification were diluted to 5ng/μl. All others were normalized to the least concentrated sample. RNA was reverse transcribed using a High-Capacity cDNA Reverse Transcription Kit (Applied Biosystems Cat # 4368814) with miR-22-3p (Thermo Fisher Scientific Cat # 000398) and U6 (Thermo Fisher Scientific Cat # 001973)-specific primers utilized for miRNA samples. mRNA or miRNA expression was measured with the following TaqMan™ probes: *Cxcr3* (Thermo Fisher Scientific Cat # Mm00438259), miR-22-3p (Thermo Fisher Scientific Cat # 000398), *Il10* (Thermo Fisher Scientific Cat # Mm01288386), *Il21* (Thermo Fisher Scientific Cat # Mm00517640), and *Ptpn1* (Thermo Fisher Scientific Cat # Mm00448427). Quantitative real-time PCR was performed using the Thermo Fisher Scientific QuantStudio 6 Flex Real-Time PCR System. The cycling threshold (C_T) value for each mRNA gene was normalized to the housekeeping gene *Ppia* (Thermo Fisher Scientific Cat # Mm02342430) and each miRNA to U6 (Thermo Fisher Scientific Cat # 001973). Relative expression was calculated by the change in C_T method ($\Delta\Delta C_T$).

Mice. B6.Cg-Foxp3^{tm2Tch}/J mice (B6.FoxP3^{GFP}; Stock # 006772) were bred to B6.SLE1.2.3 mice originally obtained from Ward Wakeland (UTSW, Dallas, TX) and maintained in our colony. These were used for LNA injection studies and are here after referred to as B6 and B6.SLE, respectively. Additional strains use for *in vitro* experiments include C57BL/6J (B6; Stock # 000664) and B6J.129S7(Cg)-*Mir22*$^{tm1.1Arod}$/J (*mir-22-3p*$^{-/-}$; Stock # 027992). Animals were maintained and housed at Vanderbilt University. All mice used in these studies were on the C57BL/6J background. Procedures were approved by the Vanderbilt University Institutional Animal Care and

Use Committee. Due to the female sex bias observed with SLE, only females were used in experiments.

LNA Injection Study. Female B6.SLE mice were retro-orbitally injected with 10 mg/kg of LNA-miR-22-3p (LNA-22; Qiagen Cat # 339204 YCI0202012-FZA) or scrambled control (LNA-Scr; Qiagen Cat # 339204 YCI0202015-FZA) beginning at 10-12 weeks of age, before the onset of disease. Animals were treated every two weeks for 10 weeks and were euthanized one week after the final injection. Age-matched B6 mice functioned as untreated wild-type controls. Blood was collected before the start of the study, at the midpoint, and at the time of sacrifice for autoantibody measurement. Additionally, spleen, lymph nodes, and kidneys were harvested for analyses.

Flow Cytometry. Flow cytometry was performed on cells obtained *ex vivo* and following *in vitro* cell culture. Cells requiring a viability dye were stained with Viobility Fixable Dye (Miltenyi Biotec) according to the manufacturer protocols. For surface staining, cells were washed in HBSS containing, 1% BSA, 4.17mM sodium bicarbonate, and 3.08mM sodium azide (FACS buffer), followed by a 10-minute room temperature incubation in 1μg/ml Fc block (α-CD16/32; Tonbo Cat # 40-0161) diluted in FACS buffer. Cells were then stained for 30 minutes at 4°C protected from light with the following antibodies diluted in FACS buffer: α-B220-APCCy7 (Tonbo Cat # 25-0452), α-CD4-APC (Tonbo Cat # 20-0042), α-CD4-PECy7 (Tonbo Cat # 60-0042), α-CD4-PerCp-Cy5.5 (Tonbo Cat # 65-0042), α-CD8a-APCCy7 (Tonbo Cat # 25-0081), α-CD11b-APCCy7 (BD Biosciences Cat # 557657), α-CD25-APC (Tonbo Cat # 20-0251), α-CD44-APCCy7 (Tonbo Cat # 25-0441), α-CD62L-Pe (BD Biosciences Cat # 553151), α-CD69-Vioblue (BD Biosciences Cat # 560690), α-CD138-PeCy7 (Biolegend Cat # 560690), α-CXCR5-

PeCy7 (BD Biosciences Cat # 560617), α-GL7-Vioblue (Biolegend Cat # 144613), α-IgD-FITC (BD Biosciences Cat # 553439), α-PD-1-Pe (Tonbo Cat # 50-9985), α-TCR-β-PerCp-Cy5.5 (Tonbo Cat # 65-5961), α-TCR-β-Vioblue (Tonbo Cat # 75-5961). Samples not requiring intracellular staining were then washed in FACS buffer and fixed in 2% paraformaldehyde (PFA). Samples with intracellular stains were washed then permeabilized and stained with the following intracellular antibodies according to the FoxP3/Transcription Factor Staining Buffer Set manufacturer protocol (eBioscience Cat # 00-5523-00): α-IFN-γ-APC (Tonbo Cat # 20-7311), α-IL-4-Pe (Tonbo Cat # 50-7041), α-IL-10-Vioblue (BD Biosciences Cat # 561429), α-IL-17-PE (BD Biosciences Cat # 559502), α-T-bet-PE (Biolegend Cat # 644810). All samples were washed and resuspended in 2% PFA before analysis. Sample acquisition was performed on a MacsQuant Analyzer (Miltenyi Biotec) and data were analyzed using FlowJo Single Cell Analysis software.

ELISA. Anti-dsDNA IgG in mouse serum was measured as previously described[28,271]. Nunc Maxisorp 96-well plates (Invitrogen Cat # 44-2404-21) were pre-coated with 100μg/ml methylated BSA (Sigma Cat # A1009) diluted in 1x PBS for 30 minutes at 37°C. Plates were then washed twice with 1x PBS and coated with 50 μg/ml Calf Thymus dsDNA (Sigma Cat #D476-4) in 1x PBS for 30 minutes at 37°C. Plates were washed twice with 1x PBS and blocked overnight at 4°C in blocking buffer (3% BSA, 3mM EDTA, 0.1% gelatin in 1x PBS). After washing twice with 1x PBS, serum samples were applied diluted 1:1000 in serum diluent (2% BSA, 3mM EDTA, 0.05% Tween, and 0.1% gelatin in 1x PBS) and incubated for two hours at room temperature on an orbital shaker. Plates were washed twice with PBS-Tween (PBS-T; 0.05% Tween in PBS)

followed by two washes with 1x PBS. IgG HRP (Promega Cat # W4021) diluted 1:5000 in secondary diluent (1% BSA and 0.05% Tween in 1x PBS) was applied to plates and incubated overnight at 4°C. Plates were washed twice with PBS-T and twice with 1x PBS before being developed with OptEIA TMB Substrate (BD Biosciences Cat # 555214). Reaction was quenched with 2N hydrochloric acid and plates were read at 450nm. IFN-γ ELISAs were performed according to manufacturer's instructions (BD Biosciences Cat # 551866).

Kidney Pathology Assessment. Severity of glomerulonephritis was assessed using hematoxylin and eosin (H&E) stained, paraffin embedded kidney sections. Scoring was determined by an independent blinded pathologist at the Vanderbilt Translational Pathology Shared Resource core. A score of 0 indicated no pathology, 1 represented a mild increase in basement membrane thickness and mild hypercellularity, 2 signified moderate basement membrane and capillary loop thickening and moderate hypercellularity, 3 indicated marked thickening of the basement membrane and capillary loops, marked hypercellularity, and necrosis, and 4 signified severe basement membrane thickening and capillary loop thickening, severe hypercellularity and inflammation, and obsolescence. For fluorescent immunohistochemistry staining, 5μm cryosections were incubated with goat-anti-Ig, anti-IgG1, or anti-IgG2c diluted 1:50 in 5% normal goat serum for 1 hour at 37ºC. Sections were washed and incubated with biotinylated rabbit anti-goat-Ig for 30 minutes (diluted 1:100) at 37ºC. Sections were washed and incubated with either avidin-FITC or avidin-Texas Red and visualized by fluorescent microscopy.

Western Blotting. Whole kidney lysates were made by homogenizing tissue in RIPA buffer. 50μg of total protein was loaded on a 4-12% SDS-polyacrylamide gel under denaturing and reducing conditions. Proteins were transferred to nitrocellulose and subjected to Western blotting using rabbit anti-STAT1 antibodies (Cell Signaling) recognizing STAT1 (polyclonal) or pSTAT1^{Tyr701} (clone 58D6). Membranes were incubated with anti-rabbit IgG-IRDye 700nm (LiCor) and bands were visualized using the Odyssey system. Semi-quantitative analysis of Western Blots was conducted using the free software Image Studio Lite.

T Cell Polarization. Spleens from four- to six-week-old mice were processed to single cell suspensions and CD4$^+$ T cells were enriched using mouse CD4 (L3T4) Microbeads kit (Miltenyi Biotec Cat # 130-117-043) according to manufacturer instructions. For Th1 polarization, CD4$^+$ T cells were cultured in α-CD3 (coating concentration was 2μg/ml; Tonbo Cat # 40-0031) coated flat-bottom 96-well plates at a final concentration of 2x10^6 cells/ml in TCM with 2μg/ml α-CD28 (Tonbo Cat # 70-0281), 10ng/ml IL-12 (Peprotech Cat # 210-12), and 1μg/ml α-IL-4 (Tonbo Cat # 70-7041) for three days. On day 3, cells were split, replated, and fed with TCM containing final concentrations of 20U/ml IL-2 (Tonbo Cat # 21-8021 and Peprotech Cat # 212-12), 10ng/ml IL-12, and 1μg/ml α-IL-4. Feeding was repeated on day 4 and cells were harvested on day 5. For T_{reg} polarization, CD4$^+$ T cells were cultured in α-CD3 coated flat-bottom 96-well plates at a final concentration of 2x10^6 cells/ml in TCM with 2μg/ml α-CD28, 50U/ml IL-2, 10ng/ml TGF-β (Peprotech Cat # 100-21), 2μg/ml α-IFN-γ (Tonbo Cat # 40-7311), and 500ng/ml α-IL-4 for three days. On day 3, T_{regs} were split, replated, and fed with TCM containing final concentrations of 50U/ml IL-2, 10ng/ml TGF-β, 2μg/ml α-IFN-γ, and 500ng/ml α-IL-

4. Media was replaced on day 4 and cells were harvested on day 5. For Th17 polarization, $CD4^+$ T cells were cultured in α-CD3 coated flat-bottom 96-well plates at a final concentration of $1x10^6$ cells/ml in TCM with 2μg/ml α-CD28, 25ng/ml IL-6 (Peprotech Cat # 216-16), 5ng/ml TGF-β, 2μg/ml α-IFN-γ, and 500ng/ml α-IL-4 for three days. During miR-22-3p overexpression experiments, 500nM miR-22-3p mimic (Dharmacon Cat # C-310516-05-0002) or negative control (Dharmacon Cat # CN-002000-01-05) was transfected on days 1 and 4 (Th1 and T_{reg}) or day 2 (Th17) of culture via electroporation using the Neon Transfection System (Invitrogen Cat # MPK10096) as previously described[272]. Mock transfected controls underwent electroporation without any miRNA present.

T_{reg} Suppression Assay. T_{regs} were skewed as described above. On day 5 of culture, T_{regs} were harvested and an equal number of live cells from each group were replated in cRPMI in flat-bottom 96-well plates at ratios of 3:1, 2:1, 1:1, 1:2, 1:4, and 1:8 with $CD8^+$ T cells enriched using mouse CD8 (Ly-2) Microbeads kit (Miltenyi Biotec Cat # 130-117-044) and labeled with CTV (Invitrogen Cat # C34557), both according to the manufacturer protocols. Also included in the co-culture, were $2x10^5$ irradiated (30Gy) feeder splenocytes per well and 1μg/ml α-CD3. After 72 hours, T_{reg} suppression was determined by measuring CTV dilution in $CD8^+$ T_{res} via flow cytometry and by measuring IFN-γ concentration in the co-culture supernatant by ELISA. Percent inhibition was calculated as [100%-((proliferation of given T_{reg}:T_{res} ratio/proliferation of 0:1 T_{reg}:T_{res} group)x100)].

Statistical Analyses. Normally distributed data were analyzed using Student's *t* tests (for two groups), one-sample *t* test (for comparing a single group to a known value), or

one-way ANOVAs with Bonferroni post-test (for three or more groups). For non-parametric data, a Mann-Whitney non-parametric test was used for comparison. All statistical tests were performed using GraphPad Prism.

Results

MiR-22-3p levels are increased in plasma from SLE subjects. To quantify changes in plasma miRNAs associated with SLE in human subjects, sRNAseq was performed with RNA isolated from plasma collected from human SLE patients (n=12) and age- and sex-matched healthy control subjects (n=12). Remarkably, we found that total plasma miRNAs were elevated in SLE compared to control subjects, as 182 miRNAs were significantly increased and only 4 miRNAs were significantly decreased in SLE plasma compared to control plasma (Figure A1.1A and Table 4). From the list of significantly increased miRNAs in SLE plasma, miR-22-3p was one of the most abundant. To validate these sRNAseq results, qPCR was used to quantify miR-22-3p concentration in plasma from SLE and control subjects, and we confirmed that miR-22-3p was significantly increased in SLE plasma (Figure A1.1B). This was consistent with prior findings which identified miR-22-3p as one of three miRNAs that were increased in circulating B cells isolated from SLE patients[273]. To determine whether miR-22-3p was also increased in immune cells from a mouse model of SLE, $CD4^+$ T cells, $CD19^+$ B cells, and $CD11c^+$ DCs were isolated from age-matched B6 and B6.SLE mice. MiR-22-3p levels were determined by qPCR and were elevated in B6.SLE immune cells compared to B6 in all cell types tested (Figure A1.1C-E*). Together, these results suggest miR-22-3p may play a role in SLE pathogenesis.

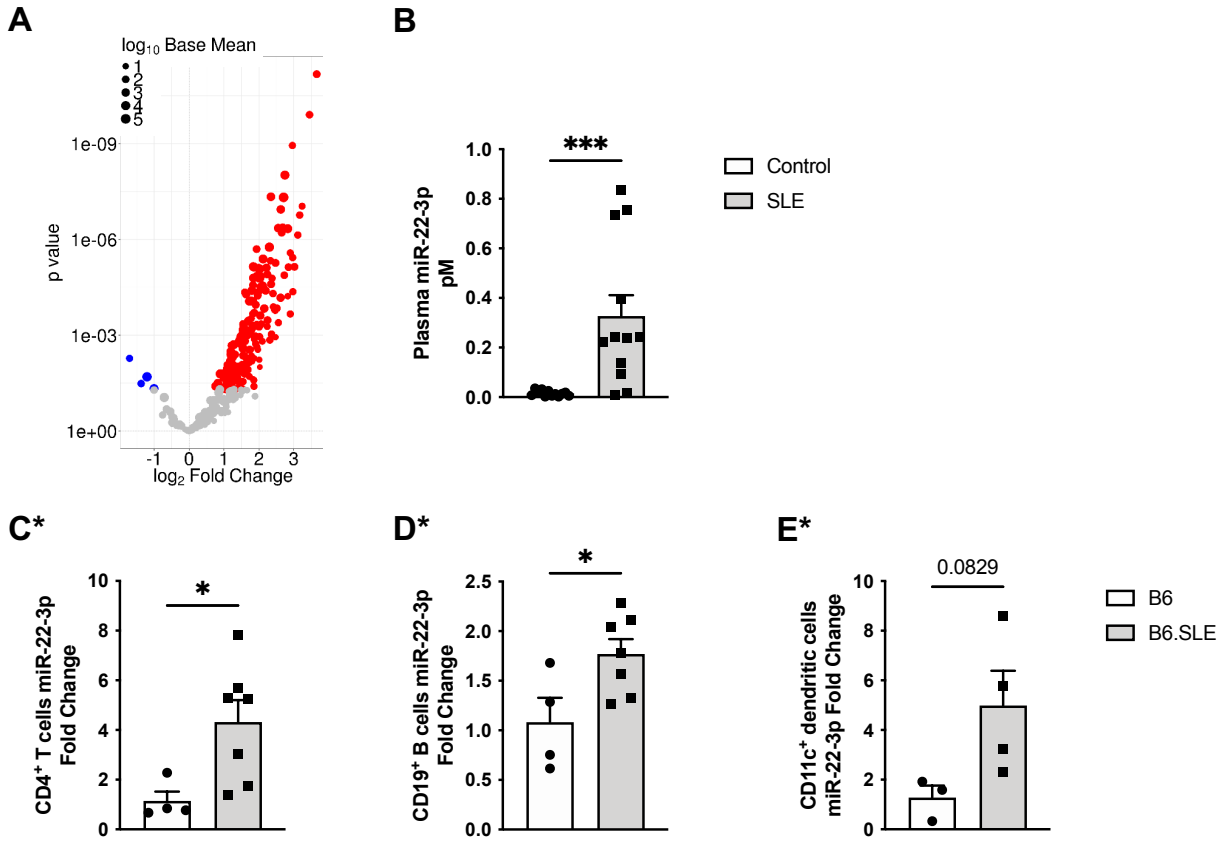

Figure A1.1. MiR-22-3p levels are increased in plasma from human SLE subjects and in immune cells from B6.SLE mice. (A) Significant differentially abundant miRNAs in plasma from SLE and healthy control subjects. Volcano plot. Red, significantly increased; blue, significantly decreased miRNAs. **(B)** qPCR of miR-22-3p levels in plasma from SLE and healthy control subjects. N=12. Data points represent individual subjects and error bars show SEM. *** denotes significance $p<0.001$ by Mann-Whitney non-parametric test. $CD4^+$ T cells **(C)**, $CD19^+$ B cells **(D)**, and $CD11c^+$ DCs **(E)** were enriched from the spleens of 11-16-week-old B6 or B6.SLE mice. MiR-22-3p levels were determined by qPCR and fold change was determined relative to age-matched B6 control. N=3-7 per group. Data points represents individual mice and error bars show SEM. * denotes significance $p<0.05$ by Student's *t* test.

Table 4. Significant differentially abundant plasma miRNAs in SLE.

miRNA	Fold Change	p-value (SLE_vs_Control)	baseMean (SLE_vs_Control)
hsa-miR-24-3p	12.61	6.60E-12	217.50
hsa-miR-1307-3p	10.93	1.23E-10	117.68
hsa-miR-210-3p	9.44	9.05E-08	33.16
hsa-miR-6852-5p	9.00	1.72E-07	78.69
hsa-miR-625-5p	8.66	7.24E-07	72.37

hsa-miR-411-5p	8.11	7.17E-06	212.52
hsa-miR-425-3p	7.86	4.33E-05	58.18
hsa-miR-181c-3p	7.81	3.69E-06	66.90
hsa-miR-500a-3p	7.78	1.13E-09	55.92
hsa-miR-454-5p	7.46	2.63E-06	44.29
hsa-miR-221-5p	7.46	2.15E-04	59.24
hsa-miR-431-5p	7.20	7.37E-06	154.89
hsa-miR-185-3p	7.10	5.97E-05	12.83
hsa-miR-146a-5p	7.10	4.58E-07	6344.84
hsa-miR-30e-5p	6.70	9.59E-09	11482.47
hsa-miR-134-5p	6.62	1.32E-05	154.71
hsa-miR-22-3p	6.53	4.77E-08	97046.53
hsa-miR-21-3p	6.42	4.20E-07	443.21
hsa-miR-345-5p	6.29	6.12E-07	206.29
hsa-miR-143-3p	6.18	1.14E-07	1910.62
hsa-miR-146b-5p	6.15	6.68E-05	980.16
hsa-miR-301b-3p	5.90	4.03E-04	53.45
hsa-miR-140-3p	5.87	4.40E-07	1818.36
hsa-miR-136-3p	5.70	1.43E-04	241.67
hsa-miR-199a-5p	5.56	5.43E-06	258.53
hsa-miR-760	5.56	1.15E-03	10.26
hsa-miR-199b-5p	5.54	1.70E-04	16.63
hsa-miR-493-5p	5.46	1.59E-04	42.80
hsa-miR-191-3p	5.33	1.29E-04	47.29
hsa-miR-181d-5p	5.29	4.94E-05	101.56
hsa-miR-548k	5.19	1.64E-05	56.52
hsa-miR-381-3p	5.14	9.29E-04	152.93
hsa-miR-98-5p	5.09	2.50E-05	431.54
hsa-miR-221-3p	5.08	4.58E-08	2498.37
hsa-miR-671-3p	5.04	4.66E-06	98.39
hsa-miR-485-5p	4.98	1.41E-03	90.16
hsa-miR-191-5p	4.92	1.74E-06	22914.91
hsa-miR-654-3p	4.74	3.38E-04	387.04
hsa-miR-30e-3p	4.72	1.24E-05	370.34
hsa-miR-125b-2-3p	4.71	5.32E-04	33.17
hsa-miR-744-5p	4.65	7.66E-06	925.24
hsa-miR-301a-3p	4.58	4.00E-05	438.77
hsa-miR-409-3p	4.45	1.45E-04	1197.08
hsa-miR-28-5p	4.37	3.12E-05	314.80
hsa-let-7i-5p	4.34	4.07E-06	6739.94
hsa-miR-222-3p	4.30	2.81E-05	2345.46
hsa-miR-1468-5p	4.28	1.55E-03	26.15
hsa-miR-625-3p	4.19	4.46E-04	71.83

hsa-let-7d-5p	4.14	1.43E-05	1500.35
hsa-miR-223-3p	4.11	2.42E-04	1143.97
hsa-miR-769-5p	4.11	3.00E-05	93.60
hsa-miR-3143	4.08	9.90E-03	5.40
hsa-miR-30d-5p	4.06	8.37E-06	16256.23
hsa-miR-628-3p	4.06	1.11E-03	65.98
hsa-miR-26a-5p	4.05	1.61E-05	47499.08
hsa-miR-5189-5p	4.02	5.84E-03	10.80
hsa-miR-223-5p	4.02	5.45E-04	124.55
hsa-miR-151a-3p	3.98	8.04E-06	7600.43
hsa-miR-29c-3p	3.96	4.38E-05	246.28
hsa-miR-99b-3p	3.91	2.81E-03	17.09
hsa-miR-181c-5p	3.90	5.74E-05	235.64
hsa-miR-148a-5p	3.83	4.59E-04	69.55
hsa-miR-93-5p	3.83	1.40E-05	1338.34
hsa-miR-340-3p	3.83	2.33E-03	64.43
hsa-miR-106b-3p	3.82	2.00E-06	195.15
hsa-miR-454-3p	3.75	1.85E-03	67.26
hsa-miR-15b-5p	3.75	1.11E-04	374.52
hsa-miR-130b-5p	3.75	1.07E-03	91.62
hsa-miR-941	3.68	1.08E-03	138.74
hsa-miR-17-5p	3.65	1.99E-04	512.34
hsa-miR-502-3p	3.64	1.33E-03	19.79
hsa-miR-7706	3.63	5.30E-03	19.00
hsa-miR-493-3p	3.63	3.98E-02	49.26
hsa-miR-494-3p	3.61	2.55E-02	37.97
hsa-miR-27b-3p	3.61	7.23E-06	11086.46
hsa-miR-589-5p	3.59	7.04E-06	163.93
hsa-miR-130a-3p	3.58	1.61E-05	2671.06
hsa-miR-26b-5p	3.58	5.19E-04	3806.41
hsa-miR-103a-3p	3.57	7.05E-06	4336.64
hsa-miR-339-3p	3.56	2.67E-05	188.01
hsa-miR-140-5p	3.55	2.38E-02	11.27
hsa-miR-423-3p	3.53	8.64E-05	7796.96
hsa-miR-17-3p	3.52	2.11E-04	21.77
hsa-miR-1273h-3p	3.48	6.56E-04	69.02
hsa-miR-151a-5p	3.48	4.00E-05	3948.58
hsa-miR-487b-3p	3.46	6.40E-03	81.57
hsa-miR-374b-5p	3.46	4.53E-03	36.06
hsa-miR-3615	3.45	6.31E-04	329.10
hsa-miR-424-3p	3.44	2.97E-04	39.11
hsa-miR-28-3p	3.38	8.28E-05	4939.38
hsa-miR-361-3p	3.34	7.30E-04	101.54

hsa-miR-30b-5p	3.33	2.86E-03	689.15
hsa-miR-18a-5p	3.31	7.17E-03	35.41
hsa-miR-369-5p	3.31	1.96E-02	29.60
hsa-miR-148b-3p	3.30	8.64E-05	2332.29
hsa-miR-224-5p	3.30	6.94E-03	122.79
hsa-miR-145-5p	3.26	7.36E-03	31.86
hsa-miR-25-3p	3.25	3.59E-04	5197.71
hsa-miR-197-3p	3.24	6.22E-03	43.39
hsa-miR-24-2-5p	3.23	1.20E-02	48.29
hsa-miR-29a-3p	3.17	9.96E-04	738.88
hsa-miR-122-5p	3.11	7.26E-03	68.14
hsa-miR-1260b	3.11	5.08E-03	84.13
hsa-miR-130b-3p	3.10	5.21E-05	721.22
hsa-miR-652-3p	3.03	4.52E-05	170.97
hsa-let-7b-5p	3.02	1.51E-03	1037.95
hsa-miR-330-3p	3.01	1.64E-02	64.15
hsa-miR-942-5p	3.01	4.38E-03	49.22
hsa-miR-16-5p	2.96	6.18E-04	26559.23
hsa-miR-548e-3p	2.94	1.50E-02	36.36
hsa-miR-107	2.94	4.51E-04	1139.21
hsa-miR-548e-5p	2.94	8.83E-03	17.81
hsa-miR-196b-5p	2.93	4.94E-02	26.76
hsa-miR-19b-3p	2.93	4.32E-03	380.48
hsa-miR-142-5p	2.92	2.59E-03	8555.94
hsa-miR-335-3p	2.92	2.84E-02	72.40
hsa-miR-361-5p	2.91	1.59E-03	235.74
hsa-miR-128-3p	2.91	6.76E-04	1044.76
hsa-miR-374a-5p	2.91	1.02E-02	40.48
hsa-miR-27a-3p	2.90	1.30E-03	1790.96
hsa-miR-425-5p	2.88	9.33E-04	897.79
hsa-miR-26b-3p	2.86	8.34E-03	88.17
hsa-miR-146b-3p	2.82	2.77E-02	24.92
hsa-miR-23a-3p	2.79	1.08E-03	915.75
hsa-miR-30d-3p	2.77	1.91E-03	86.41
hsa-miR-543	2.77	3.91E-02	39.13
hsa-miR-126-5p	2.74	1.42E-03	22661.52
hsa-miR-195-5p	2.66	1.15E-02	19.75
hsa-miR-142-3p	2.65	9.59E-03	518.50
hsa-miR-128-1-5p	2.63	2.02E-02	11.91
hsa-miR-1260a	2.63	1.45E-02	37.85
hsa-miR-574-3p	2.62	1.45E-02	74.41
hsa-miR-148b-5p	2.62	1.60E-02	87.57
hsa-miR-15b-3p	2.60	1.93E-02	30.94

hsa-miR-4433b-5p	2.59	2.61E-02	581.06
hsa-miR-181a-2-3p	2.59	1.22E-02	114.38
hsa-miR-30c-5p	2.59	1.10E-02	3236.63
hsa-miR-505-3p	2.56	2.77E-02	47.25
hsa-miR-3928-3p	2.56	4.82E-02	16.18
hsa-miR-133a-3p	2.55	2.53E-02	195.37
hsa-miR-331-5p	2.53	4.55E-02	8.30
hsa-miR-155-5p	2.50	4.02E-03	187.44
hsa-miR-152-3p	2.47	1.04E-02	99.45
hsa-miR-19a-3p	2.47	1.96E-02	155.68
hsa-miR-148a-3p	2.43	1.97E-03	11205.29
hsa-miR-181a-3p	2.41	1.53E-02	70.31
hsa-miR-106b-5p	2.40	1.06E-02	208.42
hsa-miR-126-3p	2.38	8.51E-03	3424.87
hsa-miR-192-5p	2.36	4.68E-02	3466.23
hsa-miR-92a-3p	2.35	4.82E-03	90706.57
hsa-miR-410-3p	2.34	2.07E-02	810.35
hsa-miR-20a-5p	2.33	3.17E-02	328.43
hsa-miR-199a-3p	2.32	9.43E-03	6588.09
hsa-miR-23b-3p	2.32	2.09E-03	196.55
hsa-miR-186-5p	2.32	4.37E-03	3992.83
hsa-miR-532-5p	2.31	1.69E-02	111.09
hsa-miR-21-5p	2.30	3.95E-03	28450.51
hsa-miR-584-5p	2.29	3.25E-03	3359.22
hsa-let-7e-5p	2.27	1.99E-02	1222.96
hsa-miR-16-2-3p	2.25	6.51E-03	554.01
hsa-miR-1304-3p	2.25	3.65E-02	128.04
hsa-miR-4446-3p	2.23	2.34E-02	133.40
hsa-miR-151b	2.20	1.41E-02	59.87
hsa-miR-484	2.16	1.33E-02	1467.47
hsa-miR-183-5p	2.16	4.34E-02	40.83
hsa-miR-421	2.15	1.21E-02	552.44
hsa-miR-320b	2.15	8.57E-03	660.56
hsa-miR-99b-5p	2.14	1.18E-02	877.68
hsa-miR-363-3p	2.12	1.12E-02	680.15
hsa-miR-92b-3p	2.10	1.64E-02	988.09
hsa-miR-326	2.09	2.85E-02	85.81
hsa-let-7f-5p	2.08	1.46E-02	33309.49
hsa-miR-451a	2.06	4.76E-02	8025.97
hsa-miR-501-3p	2.06	4.79E-02	56.41
hsa-miR-139-5p	2.05	4.20E-02	34.99
hsa-miR-497-5p	2.05	4.86E-02	59.75
hsa-miR-5010-5p	2.04	4.38E-02	47.91

hsa-miR-1307-5p	1.99	4.21E-02	316.03
hsa-miR-328-3p	1.99	2.12E-02	335.65
hsa-miR-181a-5p	1.86	1.62E-02	19018.25
hsa-miR-15a-5p	1.77	3.19E-02	4837.08
hsa-miR-320a	1.70	3.94E-02	5539.67
hsa-miR-150-5p	0.50	4.67E-02	4540.85
hsa-miR-10b-5p	0.43	2.00E-02	31913.03
hsa-miR-205-5p	0.39	3.27E-02	90.49
hsa-miR-204-5p	0.31	5.29E-03	44.42

MiR-22-3p inhibition reduces splenomegaly and lymphadenopathy in B6.SLE mice. To test the role of miR-22-3p in B6.SLE mice, we used LNA inhibitors against miR-22-3p (LNA-22) or scrambled control (LNA-Scr) which were injected intravenously (i.v.) into animals starting before disease onset. Animals were treated with 10mg/kg LNA-22 or LNA-Scr control every 2 weeks for 10 weeks, and then sacrificed 1 week after the last injection (Figure A1.2A). Cellular levels of miR-22-3p were significantly reduced in both splenic $CD4^+$ T cells and $CD19^+$ B cells following treatment with LNA-22 compared to LNA-Scr controls (Figure A1.2B-C), thus demonstrating LNA-22 effectively suppressed cellular miR-22-3p levels. To demonstrate that LNA-22 also altered miR-22-3p activity in lymphocytes, qPCR was used to quantify the mRNA levels of an experimentally validated miR-22-3p target gene, phosphatase and tensin homolog (*Pten*)[274,275]. Accordingly, *Pten* levels were significantly increased in splenic $CD4^+$ T cells and $CD19^+$ B cells from LNA-22 treated animals compared to LNA-Scr treated B6.SLE mice (Figure A1.2D-E).

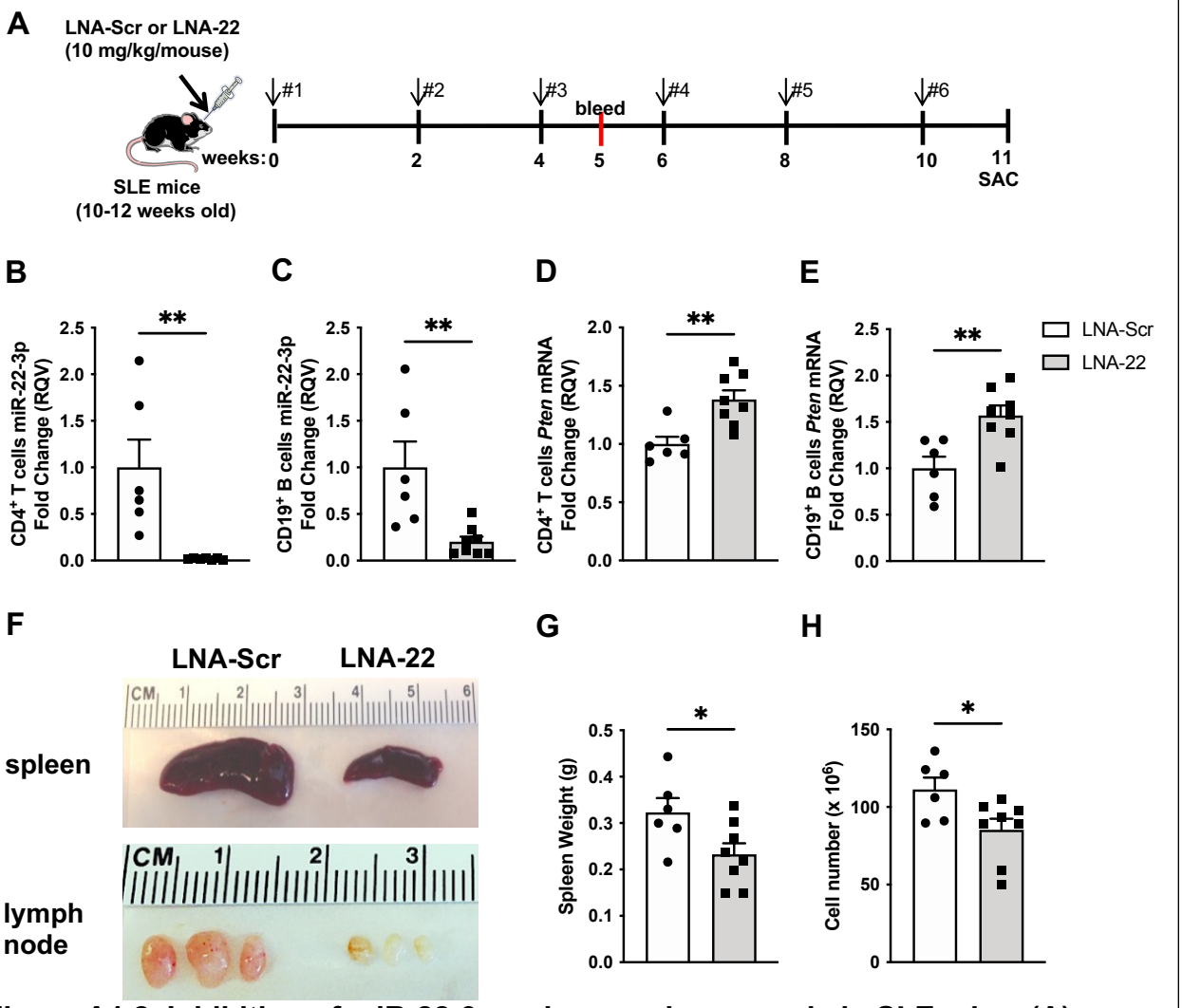

Figure A1.2. Inhibition of miR-22-3p reduces splenomegaly in SLE mice. (A) Schematic of experimental design for LNA injections. SLE mice were i.v. injected at the retro-orbital site with 10 mg/kg of either LNA-22 or LNA-Scr once every 2 weeks for 10 weeks, and mice were euthanized (SAC) 1 week following last injection. (**B-E**) Results from qPCR studies in splenic CD4$^+$ T cells and CD19$^+$ B cells. Fold change was determined relative to LNA-Scr treated control. MiR-22-3p levels in CD4$^+$ T cells **(B)** and CD19$^+$ B cells **(C)**. *Pten* mRNA levels in CD4$^+$ T cells **(D)** and CD19$^+$ B cells **(E)**. Representative spleens and lymph nodes from SLE mice treated with either LNA-22 or LNA-Scr **(F).** Spleen weights **(G)** and total spleen cell numbers **(H)** for SLE mice treated with LNA-22 or LNA-Scr. N=6-8. Data points represents individual mice and error bars show SEM. * and ** denote significance $p<0.05$ and $p<0.01$, respectively, by unpaired Student's *t*-tests.

To assess the impact of miR-22-3p inhibition on gross SLE-induced pathology, secondary lymphoid organs were examined in LNA-Scr and LNA-22 treated B6.SLE

mice. Strikingly, LNA-22 dramatically reduced the splenomegaly and lymphadenopathy normally associated with disease[271] as compared to LNA-Scr treatments (Figure A1.2F). In response to miR-22-3p inhibition, spleen weights and cell numbers were also reduced compared to LNA-Scr controls (Figure A1.2G-H)**.** There was not a significant difference in total body weight between LNA-22 and LNA-Scr-treated mice (data not shown). Collectively, these data suggest that miR-22-3p promotes splenomegaly and lymphadenopathy in B6.SLE mice, and inhibition of miR-22-3p may be a viable strategy to limit the effects of SLE on the spleen and lymph nodes.

Inhibition of miR-22-3p lessens CD4$^+$ T cell activation in B6.SLE mice. CD4$^+$ T cells in SLE can be hyperactive and proinflammatory[115,276], driving disease pathogenesis. Interestingly, when B6.SLE mice were treated with LNA-22 they had a significant increase in the percent of un-activated, naive CD4$^+$ T cells (CD44^{lo}CD62L^{hi}) in the spleen compared to those treated with LNA-Scr (Figure A1.3A-B). Moreover, LNA-22 treated B6.SLE mice had a significantly reduced proportion of CD4$^+$ T_{EM} cells (CD44^{hi}CD62L^{lo}) and a significantly elevated percentage of CD4$^+$ T_{CM} cells (CD44^{hi}CD62L^{hi}) compared to LNA-Scr treated controls (Figure A1.3A and Figure A1.3C-D).

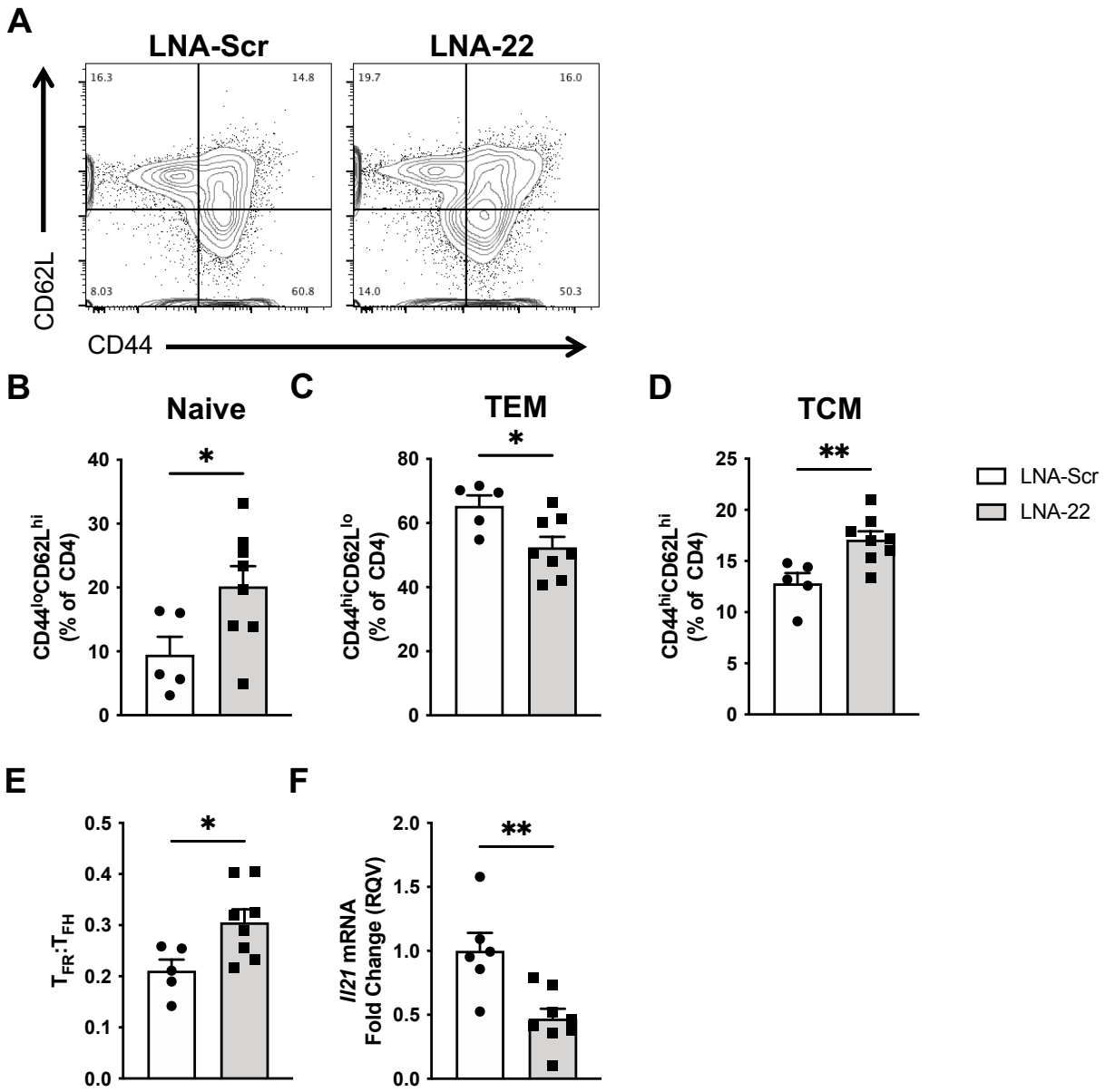

Figure A1.3. Inhibition of miR-22-3p diminishes signs of T cell activation in SLE mice. (A-D) Splenic CD4$^+$ T cells from SLE mice treated with LNA-22 or LNA-Scr as described in Figure A1.2 were analyzed for activation phenotypes via expression of CD44 and CD62L by flow cytometry. **(A)** Representative flow plots of results. **(B-D)** Percent CD4$^+$ T cells expressing CD44 and CD62L levels indicative of (**B**) naïve T cells (CD44^{lo} CD62L^{hi}), (**C**) T_{EM} (CD44^{hi} CD62L^{lo}), or (**D**) T_{CM} (CD44^{hi} CD62L^{hi}). **(E)** Ratio of T_{FR} to T_{FH} in the spleen. T_{FR}= CD4$^+$ PD-1$^+$ CXCR5$^+$ FoxP3$^+$ and T_{FH}= CD4$^+$ PD-1$^+$ CXCR5$^+$ FoxP3$^-$. **(F)** *Il21* expression in enriched CD4$^+$ T cells as measured by qPCR. Fold change was determined relative to LNA-Scr treated control. N=5-8. Data points represents individual mice and error bars show SEM. * and ** denote significance $p<0.05$ and $p<0.01$, respectively, by unpaired Student's *t*-tests.

T_{FH} cells and the IL-21 they produce are critical for germinal center formation, the site of high-affinity autoantibody production by B cells[277,278]. They been shown to correlate with disease severity and autoantibody titer in SLE patients and are expanded in mouse models of the disease[279,280]. A subset of T_{regs} known as follicular regulatory T cells (T_{FR}), restrain autoantibody production by inhibiting T_{FH} and B cell interaction in the germinal center[281]. Here, the ratio of protective T_{FR} to pathogenic T_{FH} was significantly increased in LNA-22 treated B6.SLE mice, suggesting reduced T_{FH} activation in these animals as well (Figure A1.3E). This was supported by a significant reduction in *Il21* expression in $CD4^+$ T cells from LNA-22 treated mice compared to LNA-Scr control animals (Figure A1.3F). Together these data indicate LNA-22 treatment reduces $CD4^+$ T cell activation in B6.SLE mice.

Inhibition of miR-22-3p delays dsDNA autoantibody development. Titers of autoantibodies targeting dsDNA are a central biomarker for lupus activity[282]. Therefore, serum antibodies against dsDNA were measured in B6.SLE mice treated with LNA-22 or LNA-Scr control at baseline when the animals were 10-12 weeks old, at the study mid-point (5 weeks post first injection) when animals were 15-17 weeks old, and at the conclusion of the study (11 weeks post first injection) when mice were 21-23 weeks old (Figure A1.2A). Anti-dsDNA antibody titers were similar between groups at baseline (Figure A1.4A) and were relatively low as the animals had not yet broken tolerance. Interestingly, after 5 weeks of treatment, the LNA-22-treated mice had significantly lower anti-dsDNA antibody titers compared to mice treated with LNA-Scr control (Figure A1.4B), consistent with the reduced germinal center activity suggested by the observed greater T_{FR} to T_{FH} ratio (Figure A1.3E). However, this difference was not maintained at

the end of the study when mice were 21-23 weeks of age (Figure A1.4C). Consistent with this, there was no difference in the proportions of plasma cells or germinal center B cells at time of sacrifice (Figure A1.5A-D). Therefore, we conclude that although LNA-22 treatments can delay the onset of SLE as defined by anti-dsDNA antibody production, it does not completely prevent the break in B cell tolerance in our mouse model of SLE.

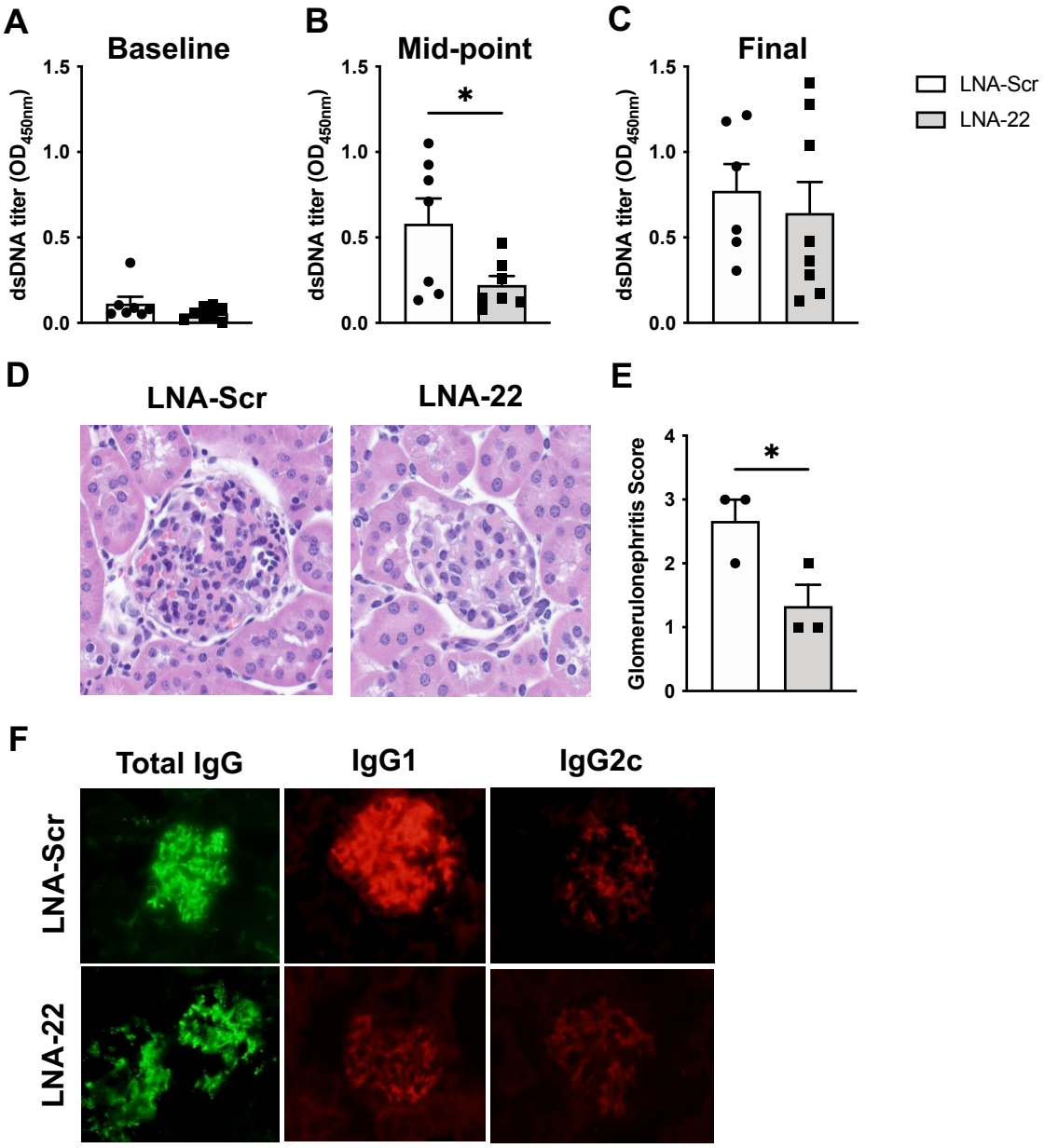

Figure A1.4. MiR-22-3p promotes lupus nephritis in SLE mice. SLE mice were treated with LNA-22 or LNA-Scr as described in Figure A1.2. **(A-C)** Circulating levels of a-dsDNA autoantibodies were measured by ELISA at baseline **(A)**, five weeks after the first treatment **(B)**, and at the end of the study **(C)**. N=5-8. **(D)** Representative H&E staining of paraffin embedded kidney from LNA-Scr or LNA-22 treated SLE mice. **(E)** Glomerulonephritis scores as determined by an independent, blinded pathologist. **(F)** Total IgG, IgG1, and IgG2c deposition in kidney from LNA-Scr and LNA-22 treated SLE mice as measured by fluorescent immunohistochemistry. Data points represents individual mice and error bars show SEM. * denotes significance $p<0.05$ by unpaired Student's *t*-tests.

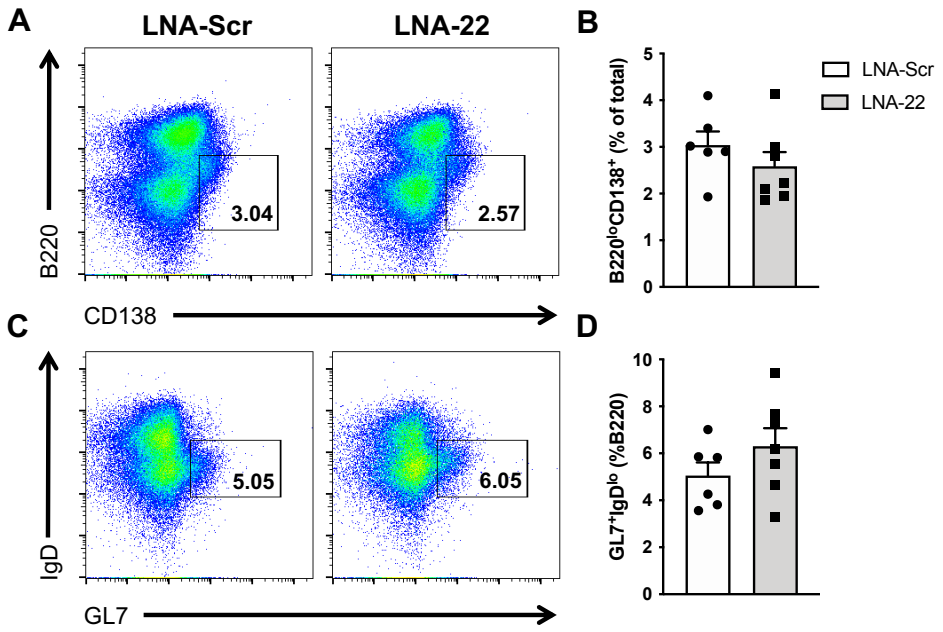

Figure A1.5. Inhibition of miR-22-3p does not alter B cell subset proportions in SLE mice. SLE mice were treated with LNA-22 or LNA-Scr as described in Figure A1.2. **(A)** Representative flow plots defining splenic plasma B cells ($B220^{lo}$ $CD138^{+}$). **(B)** Quantification plasma cells as proportion of total splenocytes. **(C)** Representative flow plots of splenic germinal center B cells ($GL7^{+}$ IgD^{int}). **(D)** Quantification of germinal center B cell a percentage of total splenocytes. N=6-7. Data points represents individual mice and error bars show SEM.

MiR-22-3p inhibition reduces SLE-associated kidney disease. Renal damage associated with lupus nephritis is one of the most detrimental co-morbidities of SLE[283]. To determine if miR-22-3p contributes to SLE-associated kidney disease, kidneys were collected from B6.SLE mice treated with LNA-22 or LNA-Scr. Inhibition of miR-22-3p dramatically reduced glomerulonephritis severity in B6.SLE mice compared to controls, as determined by H&E staining and scoring by a blinded pathologist (Figure A1.4D-E). In LNA-Scr treated mice, almost all glomeruli were diffusely affected, showing increased cellularity, increased eosinophilic hyaline material expanding the glomerular tuft, thickening of capillary loops, and occasional presence of single cell death (Figure

A1.4D). Kidneys from LNA-22-treated B6.SLE mice showed significantly decreased disease severity (mean score of 1.5 indicating mild glomerulonephritis) with the few glomeruli that were affected having a mild segmental increase in eosinophilic hyaline material in the glomerular tuft (Figure A1.4D). To determine if the observed reduction in glomerulonephritis severity was linked to reduced antibody deposition in the kidney, fluorescence-immunohistochemistry was used to assess IgG in the glomeruli. Strikingly, we found that total IgG, as well as IgG1 and IgG2c isotypes, were decreased in glomeruli of LNA-22-treated B6.SLE mice compared to age-matched LNA-Scr-treated mice (Figure A1.4F). Collectively, these data demonstrate that inhibition of miR-22-3p *in vivo* significantly decreased kidney pathology, specifically glomerulonephritis, in a mouse model of SLE.

Inhibition of miR-22-3p in B6.SLE mice decreases Th1-associated inflammation. To determine what cellular changes were underlying the observed improvement in lupus nephritis in LNA-22 treated B6.SLE mice, we assessed the Th1 cell population in our cohort. Th1 cells are important for SLE pathogenesis[284] and they have additionally been shown to infiltrate the glomeruli in lupus nephritis[285]. To determine the impact of miR-22-3p inhibition on Th1 cells, $CD4^+$ T cells from LNA-Scr and LNA-22 treated B6.SLE mice were cultured under stimulating conditions for three days before the cells were used for intracellular flow cytometry and the supernatants for ELISA. Stimulated $CD4^+$ T cells from LNA-22 treated mice had a significantly smaller proportion of IFN-γ^+ cells and produced significantly less IFN-γ in culture compared to cells from LNA-Scr treated mice (Figure A1.6A-C). Of note, we did not observe differences in IL-17 and IL-4 production by $CD4^+$ T cells (data not shown). Additionally, $CD4^+$ cells from LNA-22 treated animals

had significantly reduced expression of *Cxcr3* (Figure A1.6D), a Th1-associated gene important for migration to inflamed tissue[286]. Together, these results indicate inhibition of miR-22-3p reduces Th1 inflammation in the spleen.

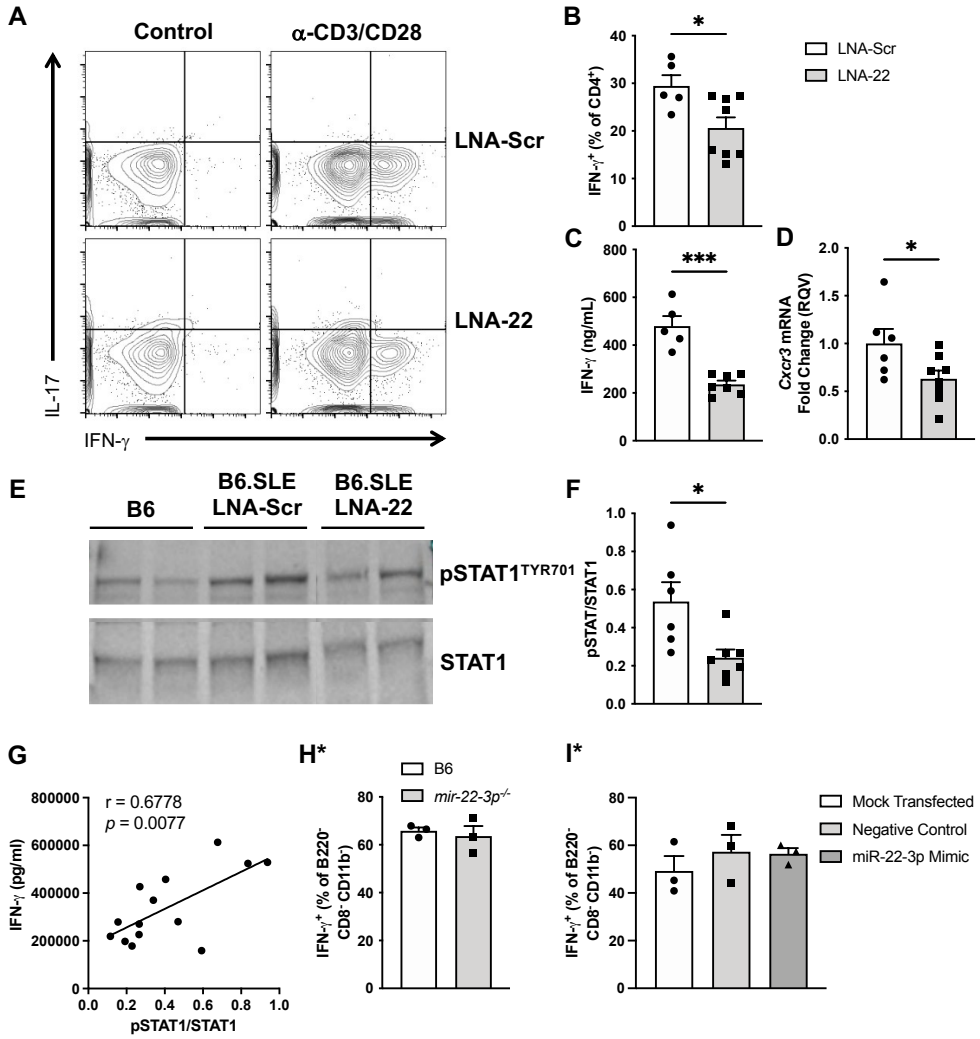

Figure A1.6. Inhibition of miR-22-3p decreases Th1-mediated inflammation in SLE mice, but modulation of miR-22-3p in *vitro* does not directly alter Th1 polarization. (A-G) SLE mice were treated with LNA-22 or LNA-Scr as described in Figure A1.2. N=5-8. **(A-C)** Enriched CD4$^+$ cells from treated mice were cultured for three days with or without 2μg/ml a-CD3 and a-CD28 stimulation. **(A)** Representative flow plots of results. **(B)** Proportion of CD4$^+$ T cells producing IFN-g as measured by flow cytometry. **(C)** IFN-g was measured in culture supernatants by ELISA. **(D)** *Cxcr3* expression in splenic CD4$^+$ cells from treated mice as measured by qPCR and fold change was determined relative LNA-Scr treated control. **(E)** Western blotting of STAT1 phosphorylation (pSTAT^{TYR701}) in whole kidney lysates from treated mice. **(F)** Ratio of pSTAT^{TYR701} to STAT1. * and *** denote significance $p<0.05$ and $p<0.001$, respectively, by unpaired Student's *t*-tests. **(G)** Correlation between IFN-g production by CD4$^+$ T cells in the spleen and pSTAT1 levels in the kidney of treated mice. Significance determined by Pearson correlation coefficients and two-tailed *t* test. **(H)** CD4$^+$ T cells were enriched by the spleens of four- to six-week-old B6 or *mir-22-3p*$^{-/-}$ mice and skewed to a Th1 phenotype for five days. Th1 phenotype as determined by IFN-g production was assessed by flow cytometry after a four-hour stimulation with PMA, ionomycin, and Golgi inhibitor. **(I)** Th1 cells were polarized from B6 mice and assessed as described in (H). On days 1 and 4 of culture, T cells were transfected via electroporation with 500nM miR-22-3p mimic, negative control, or mock treatment. N=3. Data points represents individual mice and error bars show SEM.

Given the decrease in Th1 activity in spleens and that IFN-γ signaling is involved in lupus-associated kidney pathology[287], IFN-γ signaling was assessed in the kidneys of LNA-Scr or LNA-22 treated B6.SLE mice. To do this, STAT1 activation was assessed by immuno-blotting phosphorylated STAT1 (pSTAT1) in whole kidney lysates. Consistent with the Th1 changes observed in the spleen, pSTAT1 levels were found to be significantly decreased in kidneys of LNA-22 treated B6.SLE mice compared to LNA-Scr control when normalized to total STAT1 protein levels (Figure A1.6E-F). Furthermore, the levels of pSTAT1 positively correlated to IFN-γ secretion in splenic T cells (Figure A1.6G). These data suggest that miR-22-3p is important for modulating pathogenic Th1 responses in SLE.

MiR-22-3p does not directly alter Th1 differentiation. Based on these data, one potential hypothesis was that miR-22-3p was directly promoting Th1 polarization. To test the effect of miR-22-3p deficiency on Th1 differentiation, we performed *in vitro* Th1 skewing experiments using naïve B6 or *mir-22-3p*$^{-/-}$ CD4^{+} T cells and observed no difference in the resulting IFN-γ^{+} Th1 population (Figure A1.6H* and Figure A1.7A*). *In vitro* Th1 polarization experiments were also performed under miR-22-3p overexpression conditions. On day 1 and day 4 of Th1 skewing culture, B6 CD4^{+} T cells were transfected with a miR-22-3p mimic, negative control, or a mock treatment. Results again showed no change in the proportion of IFN-γ^{+} Th1 cells from culture (Figure A1.6I* and Figure A1.7D*). These data suggest that although inhibition of miR-22-3p modulates Th1 responses in B6.SLE mice, it does not directly alter Th1 polarization and thereby must be acting through an indirect mechanism.

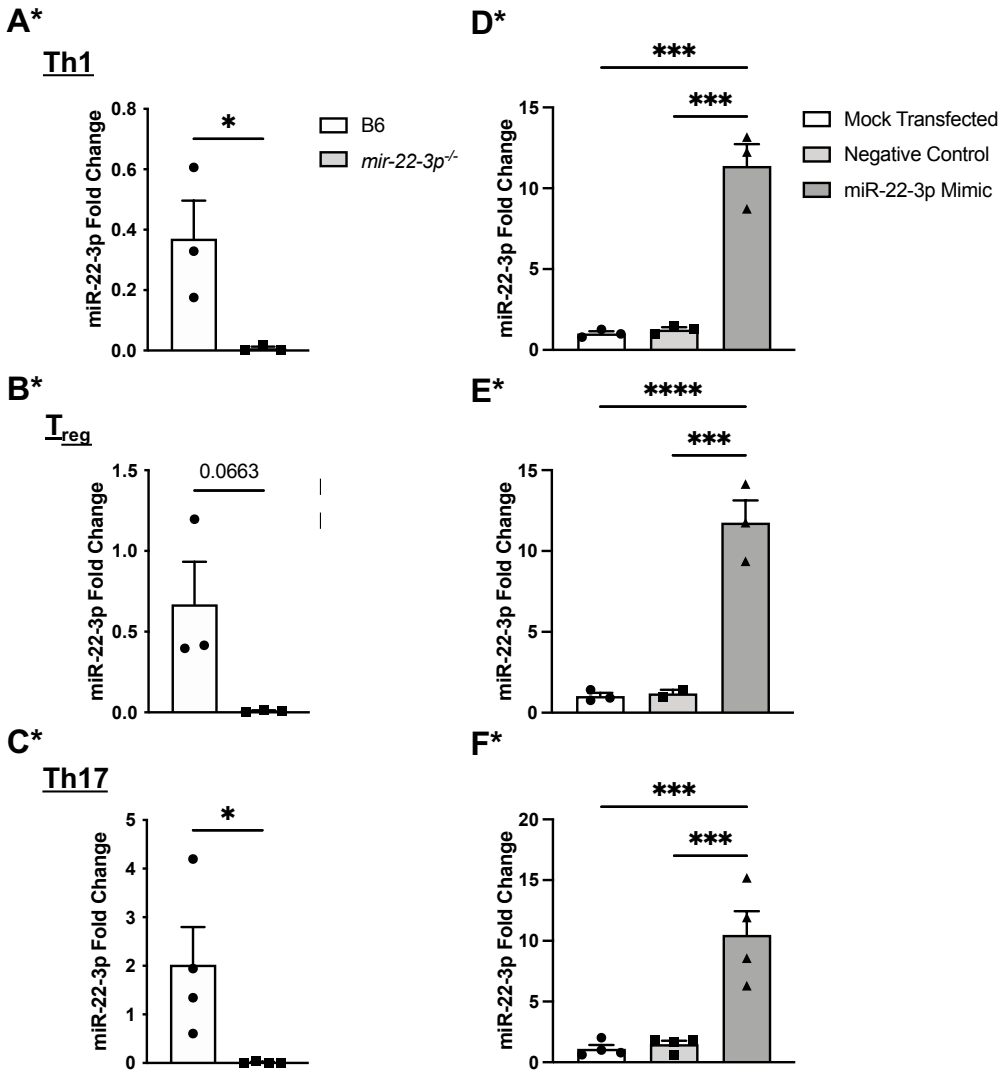

Figure A1.7. Efficacy of miR-22-3p genetic knock out and mimic overexpression. **(A-C)** CD4$^+$ T cells were enriched from spleens of four- to six-week-old B6 or *mir-22-3p*$^{-/-}$ mice and skewed to the indicated phenotype. MiR-22-3p level was determined by qPCR and fold change was determined relative to a B6 non-skewed control. **(D-F)** B6 CD4$^+$ T cells were collected and skewed as in (A). On days 1 (Th1 and T_{reg}), 2 (Th17), and 4 (Th1 and T_{reg}) of culture, T cells were transfected with 500nM miR-22-3p mimic, negative control, or mock treatment. (A-F) MiR-22-3p level was determined by qPCR and fold change was determined relative to mock transfected control. N=3-4. Data points represents individual mice and error bars show SEM. * denotes significance $p<0.05$ by unpaired Student's *t*-tests **(A-C)**. *** and **** denote significance $p<0.001$ and $p<0.0001$, respectively, by one-way ANOVA and Tukey's multiple comparison test **(D-F)**.

MiR-22-3p inhibits T_{reg} function. As T_{regs} can regulate Th1 responses, we sought to determine whether miR-22-3p might be exerting its effects through them. To first establish whether miR-22-3p was increased in T_{regs} in our mouse model, $CD4^+$ $CD25^+$ cells were isolated from age-matched B6 and B6.SLE mice. MiR-22-3p levels were measured by qPCR and were significantly elevated in B6.SLE T_{regs} compared to B6 T_{regs} (Figure A1.8A*). When miR-22-3p was inhibited in B6.SLE mice, the number of splenic T_{regs} and proportion of activated T_{regs} were unchanged (Figure A1.8B-C), but interestingly the proportion of T_{regs} expressing IL-10 was significantly increased (Figure A1.8D).Consistent with this, inhibition or overexpression of miR-22-3p *in vitro* during T_{reg} polarization did not alter differentiation (Figure A1.8E-F*, Figure A1.7B*, and Figure A1.7E*), but overexpression of miR-22-3p significantly reduced *Il10* transcript in skewed T_{regs}. These results suggest that while miR-22-3p is not directly influencing the polarization of T_{regs} it may be impacting their function by negatively regulating cytokine production.

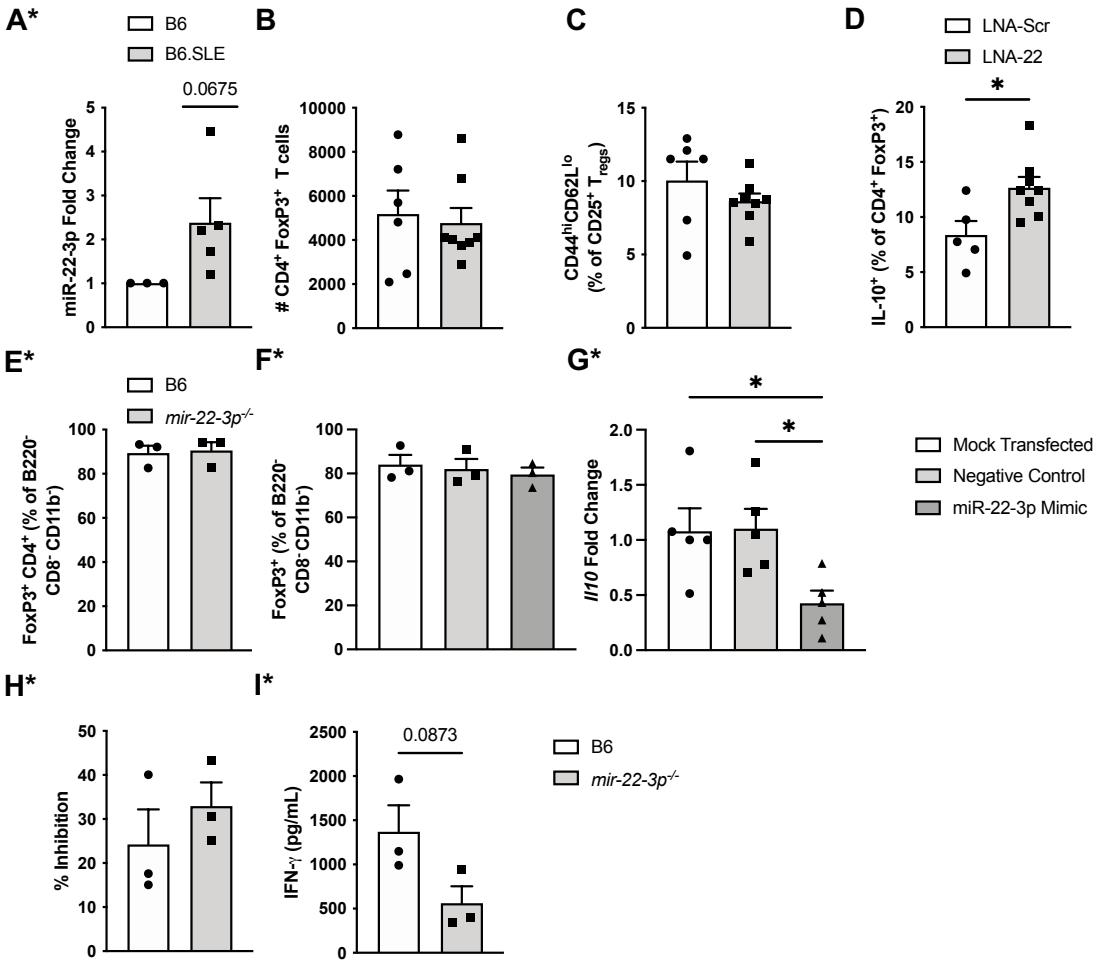

Figure A1.8. MiR-22-3p does not alter T_{reg} polarization but does inhibit function. (A) $CD25^+$ $CD4^+$ $FoxP3^+$ T_{regs} were enriched from the spleens of 11-16-week-old B6 or B6.SLE mice. MiR-22-3p levels were determined by qPCR and fold change was determined relative to age-matched B6 control. N=3-5 per group. Significance determined by one-sample *t* test. **(B-D)** SLE mice were treated with LNA-22 or LNA-Scr as described in Figure A1.2 and splenocytes were analyzed by flow cytometry. N=5-8. **(B)** Number of $CD4^+$ $FoxP3^+$ T_{regs}. **(C)** Proportion of activated $CD25^+$ $CD4^+$ $FoxP3^+$ T_{regs}. **(D)** Proportion of IL-10 producing $CD4^+$ $FoxP3^+$ T_{regs}. * denotes significance $p<0.05$ by unpaired Student's *t*-test. **(E)** $CD4^+$ T cells were enriched by the spleens of four- to six-week-old B6 or *mir-22-3p*$^{-/-}$ mice and skewed to a T_{reg} phenotype for five days. T_{reg} phenotype as determined by FoxP3 expression was assessed by flow cytometry at harvest. **(F)** T_{regs} were polarized from B6 mice and assessed as described in (E). On days 1 and 4 of culture, T cells were transfected via electroporation with 500nM miR-22-3p mimic, negative control, or mock treatment. **(G)** *Il10* expression as measured by qPCR following T_{reg} polarization described in (F) and fold change was determined relative mock transfected control. N=3-4. * denotes significance $p<0.05$ by one-way ANOVA and Tukey's multiple comparison test. **(H-I)** T_{regs} were skewed as described in (E). Equal numbers of live T_{regs} were then co-cultured with cell trace violet-labeled $CD8^+$ T cells for three days. **(H)** Percent inhibition of $CD8^+$ T cell proliferation was assessed by flow cytometry. Shown are the 3:1 T_{reg}:T_{res} ratio results. **(I)** IFN-g concentration in co-culture supernatants was determined by ELISA. Shown are the 2:1 T_{reg}:T_{res} ratio results. N=3. Significance determined by unpaired Student's *t* test. Data points represents individual mice and error bars show SEM.

Another known T cell source of IL-10 is non-pathogenic Th17 cells[288] so we became interested in whether miR-22-3p expression might regulate this population as well. When non-pathogenic Th17 cells were skewed from miR-22-3p deficient $CD4^+$ T cells, there was a slight increase in the proportion of the differentiated population, as measured by IL-17 expression, compared to controls (Figure A1.9A* and Figure A1.7C*). Conversely, when non-pathogenic Th17 cells were polarized with miR-22-3p overexpression, there was a significant reduction in the population size with miR-22-3p mimic treatment compared to mock and negative controls (Figure A1.9B* and Figure A1.7F*). These findings suggest miR-22-3p may be enhancing systemic inflammation by reducing cellular sources of IL-10.

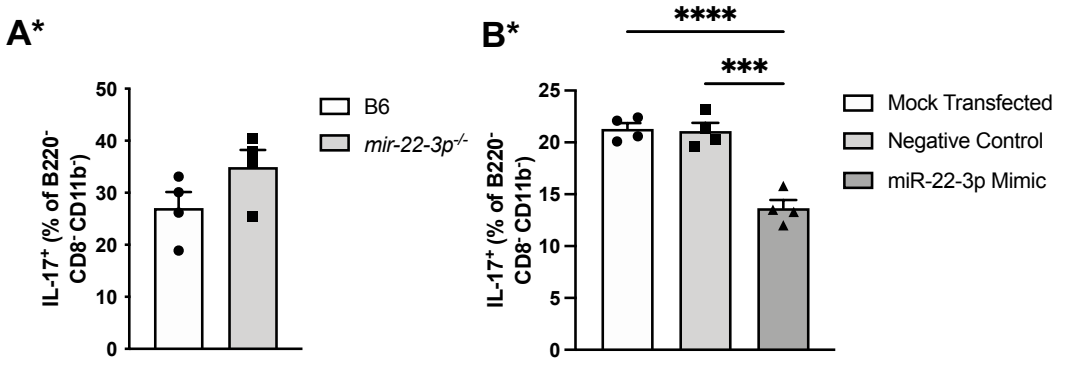

Figure A1.9. Overexpression of miR-22-3p in vitro reduces Th17 polarization. (A) $CD4^+$ T cells were enriched by the spleens of four- to six-week-old B6 or *mir-22-3p*$^{-/-}$ mice and skewed to a Th17 phenotype for three days. Th17 phenotype as determined by IL-17 production was assessed by flow cytometry after a four-hour stimulation with PMA, ionomycin, and Golgi inhibitor. **(B)** Th17 cells were polarized from B6 mice and assessed as described in (A). On day 2 of culture, T cells were transfected via electroporation with 500nM miR-22-3p mimic, negative control, or mock treatment. *** and **** denote significance $p<0.001$ and $p<0.0001$, respectively, by one-way ANOVA and Tukey's multiple comparison test. N=4. Data points represents individual mice and error bars show SEM.

IL-10 is considered anti-inflammatory in the context of many different autoimmune diseases, but studies have shown both proinflammatory and anti-

inflammatory roles for IL-10 in SLE [286,289–293]. To determine whether miR-22-3p-induced modulation of IL-10 expression altered T_{reg} function, control and miR-22-3p deficient T_{regs} were compared in an *in vitro* suppression assay. B6 and *mir-22-3p*$^{-/-}$ *in vitro*-derived T_{regs} were co-cultured for three days with CTV-labeled $CD8^+$ T cells. After co-culturing, $CD8^+$ T cells from the two conditions had similarly proliferated (Figure A1.8H). However, supernatants from co-cultures with *mir-22-3p*$^{-/-}$ T_{regs} had a significantly reduced concentration of IFN-γ compared to control T_{reg} co-cultures (Figure A1.8I). These results suggest miR-22-3p overexpression inhibits T_{reg} control of T_{eff} cytokine production. Taken together, our data indicate increased miR-22-3p compromises T_{reg} function, leading to enhanced Th1 responses and greater disease severity in the context of SLE.

Discussion

Mir-22-3p has previously been associated with SLE[273,294,295], but results from this study demonstrate enrichment of miR-22-3p directly enhances disease pathogenesis and lupus nephritis. We report that inhibition of miR-22-3p *in vivo* reduces characteristic SLE pathologies including splenomegaly and lymphadenopathy, anti-dsDNA autoantibody titers, glomerulonephritis, and T cell hyperactivation. Typically, alteration of a single miRNA produces milder phenotypic changes than those we observe suggesting a potentially novel quality of miR-22-3p[296,297].

Anti-dsDNA antibody titers are a hallmark for SLE disease activity, and, excitingly, miR-22-3p inhibition significantly decreased anti-dsDNA antibody titers at the study midpoint compared to the LNA-Scr control treatments (Figure A1.4). However, at

the terminal time point, no significant differences in anti-dsDNA titers were found between the treatments (Figure A1.4). These results suggest that miR-22-3p inhibition delays the onset of SLE but does not fully prevent the break in B cell tolerance. This is consistent with the activity of other miRNAs in SLE. For example, inhibition of miR-21 dramatically reduced splenomegaly and lymphocyte proliferation but failed to affect anti-dsDNA titers after 12 weeks of LNA-21 treatments[298]. Furthermore, increased miR-326 was found to enhance B cell autoantibody production as soon as 1 week after lentiviral overexpression *in vivo*[299]. These results suggest that miR-22-3p, along with other miRNAs, contribute to early titer production, but do not completely regulate autoantibody production.

Lupus nephritis is one of the most common and severe complications in SLE and is a critically important predictor of morbidity and mortality. The condition is characterized by an increase in Th1 signaling and deposition of immune complexes in the kidneys[300]. In our study, blinded pathological scoring was used to assess renal pathology and LNA-22 treatments were found to significantly reduce glomerulonephritis severity (Figure A1.4). This was also accompanied by a lower level of IgG in the kidneys (Figure A1.4) which suggests a possible reduction in immune complex deposition in the tissue. Limiting immune complex deposit in the kidneys is vital to preventing and treating lupus nephritis, as localization of immune complexes within the glomeruli can lead to complement activation and complement-mediated damage[301]. Moreover, immune complex deposition in the kidney promotes recruitment and activation of neutrophils and myeloid cells via their Fc-receptors[302,303]. Activated immune cells secrete chemokines and cytokines which recruit additional immune cells that further

exacerbate glomerular damage and lead to a pro-inflammatory environment in the kidney. Contrary to these reduced antibody levels, B cell populations were not altered by miR-22-3p inhibition when they were analyzed at the conclusion of the study (Figure A1.5). It is possible that B cell subtypes differed earlier during treatment, similar to the anti-dsDNA antibody titers, but future experiments will need to confirm that. Additionally, changes in antibody deposition may have been indirectly modulated by T cells altering B cell activity as LNA-22 treated mice had an increased ratio of T_{FR} to T_{FH} cells (Figure A1.3), suggesting greater control of germinal center formation. Overall, these results demonstrate miR-22-3p promotes lupus nephritis and indicates transient regulation of B cell activity.

During SLE, T cells can become hyperactive[115,280] and adopt T_{EM} phenotypes, which allow them to migrate to inflamed tissues and rapidly produce cytokines [304,305]. Our results show inhibition of miR-22-3p increased the naïve T cell population (Figure A1.3), suggesting lessened T cell activation. Additionally, the proportion of $CD4^+$ T_{EM} cells was significantly reduced following LNA-22 treatment in B6.SLE mice (Figure A1.3). In contrast, T_{CM} cells, which have only a small cytokine-secreting capacity[305], were elevated following LNA-22 treatment (Figure A1.3). These findings are consistent with human data showing SLE patients have more T_{EM} cells and less T_{CM} cells in circulation compared to healthy controls[305]. Together, these results suggest miR-22-3p promotes long-lasting T cell-mediated inflammation in SLE, providing another possible avenue by which miR-22-3p drives pathogenesis.

In addition to altering $CD4^+$ memory populations and generally limiting T cell activation, inhibition of miR-22-3p also reduced Th1 responses in the spleens of our

SLE mouse model (Figure A1.6). In agreement with this, we showed significantly less pSTAT1 in kidneys from LNA-22 treated B6.SLE mice (Figure A1.6). Phosphorylation of STAT1 increases its transcriptional activity and leads to the upregulation of IFN-inducible genes[306]. For instance, pSTAT1 has been shown to transactivate T-bet, the canonical transcription factor for Th1 cells that drives IFN-γ production[307,308]. Therefore, these results suggest miR-22-3p-enhanced glomerulonephritis is associated with Th1 activation in the kidneys of B6.SLE mice. IFN-γ producing Th1 cells are known to be major proinflammatory effectors in SLE[284,309] and have been shown to infiltrate the kidneys in lupus nephritis[285]. Elevated IFN-γ is observed in several lupus mouse models, particularly in the MRL-*Fas*^{lpr} strain, and is associated with immune complex deposition in kidneys[310]. Several other miRNAs have previously been shown to regulate Th1 and IFN-γ signaling, including the miR-17-92 cluster[261], miR-125b[311], and miR-29[312]. However, in this study, we present a novel relationship between miR-22-3p and the Th1 population during SLE and lupus nephritis. Interestingly, *in vitro* Th1 polarization experiments testing miR-22-3p deficiency and overexpression suggest varying levels miR-22-3p does not directly affect Th1 differentiation, leading to the hypothesis that the observed alterations in the Th1 population *in vivo* are the result of indirect miR-22-3p control.

Due to their role in regulating the rest of the immune system, we hypothesized miR-22-3p might be modulating T_{regs} and thereby indirectly altering inflammatory responses of other T cells. In SLE patients, T_{regs} have been reported to be decreased in number and function compared to healthy controls[313–315]. Additionally, T_{regs} from lupus mice have an altered functional phenotype compared to B6 controls, however, the

degree to which that is T_{reg} intrinsic or mediated by lupus T effector (T_{eff}) cell resistance to suppression is unclear[115,316–318]. MiR-22-3p has previously been shown to be increased in T_{regs} compared to conventional $CD4^+$ cells[319] and in T_{regs} from relapsing-remitting multiple sclerosis patients[320], and we found miR-22-3p was significantly increased in T_{regs} from B6.SLE mice compared to those from controls (Figure A1.8). Interestingly, neither T_{reg} number nor T_{reg} activation was altered by LNA-22 treatment in B6.SLE mice, but the proportion of IL-10^+ T_{regs} was significantly increased relative to LNA-Scr treated controls (Figure A1.8). Mirroring this, the differentiation of T_{regs} *in vitro*, as defined by proportion of FoxP3 expression, was unaffected by miR-22-3p deficiency or overexpression, but T_{regs} treated with a miR-22-3p mimic had reduced levels of *Il10* mRNA (Figure A1.8). IL-10 is considered anti-inflammatory in many different autoimmune diseases but has been ascribed both proinflammatory and anti-inflammatory roles in SLE [286,289–293] where the ultimate impact of the cytokine seems dependent on the cellular source. To evaluate whether miR-22-3p deficient T_{regs} had altered suppressive function, B6 and *mir-22-3p*$^{-/-}$ *in vitro*-derived T_{regs} were co-cultured with CTV-labeled $CD8^+$ T cells. MiR-22-3p sufficient and deficient T_{regs} suppressed $CD8^+$ T cell proliferation to a similar degree, but *miR-22-3p*$^{-/-}$ co-cultures had significantly less IFN-γ in the supernatants (Figure A1.8). These results indicate inhibition of miR-22-3p improves T_{reg} function and suggests the corresponding increase in IL-10 production is directly protective.

While investigating the effect of miR-22-3p deficiency and overexpression on Th1 and T_{reg} polarization, we also tested these variables under Th17 skewing conditions. Interestingly, miR-22-3p overexpression significantly reduced Th17 differentiation, while

deficiency resulted in a trending increase in Th17 polarization (Figure A1.9). These results were somewhat surprising given Th17 populations were not changed by LNA-22 treatment in B6.SLE mice (data not shown). MiR-22-3p has been previously described in relation to Th17 differentiation and function, with some sources suggesting it promotes Th17 responses while others suggest it inhibits[321–324]. Work in recent years have divided the Th17 population into pathogenic and non-pathogenic subtypes. Pathogenic Th17 cells are characterized by the expression of IL-17, IL-21, IL-22, and GM-CSF and are thought to be induced by IL-6, IL1-β, and IL-23, whereas non-pathogenic Th17 populations producing IL-17 and IL-10 and are promoted by TFG-β and IL-6[288,325–327]. Therefore, the described heterogeneity in the role of miR-22-3p in Th17 cells may be at least partially due to the population's variability. Of note, the Th17 polarizing conditions used in this study promote the formation of non-pathogenic Th17. Thus, our Th17 results could be consistent with the T_{reg} findings described above, suggesting elevation of miR-22-3p promotes inflammation by reducing IL-10 and potential sources thereof.

One limitation of this work is the lack of a defined miR-22-3p target gene or genes that is leading to the observed functional changes in T_{regs}. Given the inverse correlation between miR-22-3p and *Il10* expression (Figure A1.8), one might hypothesize that the former directly inhibits the latter. However, there is no predicted miR-22-3p binding site in the 3' UTR of the *Il10* gene[328,329]. Work from Shrestha *et al.* has shown T_{regs} deficient for the known miR-22-3p target gene, *Pten*[274,275], lose stability and allow for the expansion for Th1 and T_{FH} cells[330]. This is not entirely consistent with our own findings as we do not see any alteration in the proportion of T_{regs} when miR-22-

3p is inhibited, but still warrants further investigation. Interestingly, there is a predicted binding site in *Krab1*[328,329], which encodes Krüppel-associated box (KRAB), a zinc finger binding protein that acts as a scaffold for KRAB-associated protein 1 (KAP1)[331]. KAP1 is an important FoxP3 cofactor and T_{regs} deficient for the protein have been shown to be less suppressive with reduced IL-10 production[332], mirroring our own results following miR-22-3p modulation. Therefore, future work should investigate *Krab1* as a promising candidate target gene in T_{regs} hypothesizing that miR-22-3p would induce dysfunction through inhibition of important T_{reg} cofactors.

In conclusion, results from this study show miR-22-3p is significantly elevated in both in SLE patients and B6.SLE mice, compared to controls. Inhibition of miR-22-3p *in vivo* reduced splenomegaly and lymphadenopathy, delayed the development of anti-dsDNA autoantibody titers, and limited antibody deposition in the kidneys. Perhaps most strikingly, treatment with LNA-22 significantly decreased glomerulonephritis severity in B6.SLE mice. This reduced pathology was associated with lessened T cell activation and decreased systemic Th1 responses, but modulation of miR-22-3p *in vitro* did not directly alter Th1 differentiation. Instead, miR-22-3p acted in T_{regs} to reduce IL-10 expression, and deficiency of miR-22-3p improved T_{reg} suppression *in vitro*. Collectively, we demonstrate miR-22-3p plays a pathogenic role in SLE and could have great potential as a novel drug target to reduce glomerulonephritis and SLE pathophysiology.

References

1. Tsao CW, Aday AW, Almarzooq ZI, Anderson CAM, Arora P, Avery CL, Baker-Smith CM, Beaton AZ, Boehme AK, Buxton AE, Commodore-Mensah Y, Elkind MSV, Evenson KR, Eze-Nliam C, Fugar S, et al. *Heart Disease and Stroke Statistics - 2023 Update: A Report from the American Heart Association*.; 2023.
2. Anon. *World health statistics 2023: monitoring health for the SDGs, Sustainable Development Goals*.; 2023.
3. Goldstein JL, Brown MS. A Century of Cholesterol and Coronaries: From Plaques to Genes to Statins. *Cell*. 2015;161(1):161–172.
4. Hopstock LA, Bønaa KH, Eggen AE, Grimsgaard S, Jacobsen BK, Løchen ML, Mathiesen EB, Njølstad I, Wilsgaard T. Longitudinal and secular trends in total cholesterol levels and impact of lipid-lowering drug use among Norwegian women and men born in 1905-1977 in the population-based Tromsø Study 1979-2016. *BMJ Open*. 2017;7(8):1–9.
5. Schreiner PJ, Jacobs DR, Wong ND, Kiefe CI. Twenty-Five Year Secular Trends in Lipids and Modifiable Risk Factors in a Population-Based Biracial Cohort: The Coronary Artery Risk Development in Young Adults (CARDIA) Study, 1985-2011. *Journal of the American Heart Association*. 2016;5(7):1–11.
6. Raal FJ, Pilcher GJ, Waisberg R, Buthelezi EP, Veller MG, Joffe BI. Low-density lipoprotein cholesterol bulk is the pivotal determinant of atherosclerosis in familial hypercholesterolemia. *The American Journal of Cardiology*. 1999;83(9):1330–1333.
7. Ference BA, Yoo W, Alesh I, Mahajan N, Mirowska KK, Mewada A, Kahn J, Afonso L, Williams KA, Flack JM. Effect of Long-Term Exposure to Lower Low-Density Lipoprotein Cholesterol Beginning Early in Life on the Risk of Coronary Heart Disease. *Journal of the American College of Cardiology*. 2012;60(25):2631–2639.
8. Nordestgaard BG. Triglyceride-Rich Lipoproteins and Atherosclerotic Cardiovascular Disease: New Insights from Epidemiology, Genetics, and Biology. *Circulation Research*. 2016;118(4):547–563.
9. Cuchel M, Bruckert E, Ginsberg HN, Raal FJ, Santos RD, Hegele RA, Kuivenhoven JA, Nordestgaard BG, Descamps OS, Steinhagen-Thiessen E, Tybjaerg-Hansen A, Watts GF, Averna M, Boileau C, Boren J, et al. Homozygous familial hypercholesterolaemia: new insights and guidance for clinicians to improve detection and clinical management. A position paper from the Consensus Panel on Familial Hypercholesterolaemia of the European Atherosclerosis Society. *European Heart Journal*. 2014;35(32):2146–2157.
10. Nordestgaard BG, Chapman MJ, Humphries SE, Ginsberg HN, Masana L, Descamps OS, Wiklund O, Hegele RA, Raal FJ, Defesche JC, Wiegman A, Santos RD, Watts GF, Parhofer KG, Hovingh GK, et al. Familial hypercholesterolaemia is underdiagnosed and undertreated in the general population: guidance for clinicians to prevent coronary heart disease: Consensus Statement of the European Atherosclerosis Society. *European Heart Journal*. 2013;34(45):3478–3490.
11. Cohen JC, Boerwinkle E, Mosley TH, Hobbs HH. Sequence Variations in PCSK9, Low LDL, and Protection against Coronary Heart Disease. *New England Journal of Medicine*. 2006;354(12):1264–1272.

12. Skålén K, Gustafsson M, Knutsen Rydberg E, Hultén LM, Wiklund O, Innerarity TL, Boren J. Subendothelial retention of atherogenic lipoproteins in early atherosclerosis. *Nature*. 2002;417(6890):750–754.
13. de Beer FC, Hind CRK, Fox KM, Allan RM, Maseri A, Pepys MB. Measurement of serum C-reactive protein concentration in myocardial ischaemia and infarction. *British Heart Journal*. 1982;47(3):239–243.
14. Liuzzo G, Biasucci LM, Gallimore JR, Grillo RL, Rebuzzi AG, Pepys MB, Maseri A. The Prognostic Value of C-Reactive Protein and Serum Amyloid A Protein in Severe Unstable Angina. *New England Journal of Medicine*. 1994;331(7):417–424.
15. Hirschfield GM, Gallimore JR, Kahan MC, Hutchinson WL, Sabin CA, Benson GM, Dhillon AP, Tennent GA, Pepys MB. Transgenic human C-reactive protein is not proatherogenic in apolipoprotein E-deficient mice. *Proceedings of the National Academy of Sciences of the United States of America*. 2005;102(23):8309–8314.
16. Xu Q, Oberhuber G, Gruschwitz M, Wick G. Immunology of atherosclerosis: Cellular composition and major histocompatibility complex class II antigen expression in aortic intima, fatty streaks, and atherosclerotic plaques in young and aged human specimens. *Clinical Immunology and Immunopathology*. 1990;56(3):344–359.
17. Kranzhöfer R, Browatzki M, Schmidt J, Kübler W. Angiotensin II activates the proinflammatory transcription factor nuclear factor-κB in human monocytes. *Biochemical and Biophysical Research Communications*. 1999;257(3):826–828.
18. Sam S, Haffner S, Davidson MH, D'Agostino RB, Feinstein S, Kondos G, Perez A, Mazzone T. Relation of abdominal fat depots to systemic markers of inflammation in type 2 diabetes. *Diabetes Care*. 2009;32(5):932–937.
19. McMaster WG, Kirabo A, Madhur MS, Harrison DG. Inflammation, Immunity, and Hypertensive End-Organ Damage. *Circulation Research*. 2015;116(6):1022–1033.
20. Van Halm VP, Peters MJL, Voskuyl AE, Boers M, Lems WF, Visser M, Stehouwer CDA, Spijkerman AMW, Dekker JM, Nijpels G, Heine RJ, Bouter LM, Smulders YM, Dijkmans BAC, Nurmohamed MT. Rheumatoid arthritis versus diabetes as a risk factor for cardiovascular disease: A cross-sectional study, the CARRÉ Investigation. *Annals of the Rheumatic Diseases*. 2009;68(9):1395–1400.
21. Appleton BD, Major AS. The latest in systemic lupus erythematosus-accelerated atherosclerosis: related mechanisms inform assessment and therapy. *Current Opinion in Rheumatology*. 2021;33(2):211–218.
22. Manzi S, Selzer F, Sutton-Tyrrell K, Fitzgerald SG, Rairie JE, Tracy RP, Kuller LH. Prevalence and risk factors of carotid plaque in women with systemic lupus erythematosus. *Arthritis and rheumatism*. 1999;42(1):51–60.
23. Mendelsohn ME, Karas RH. Molecular and cellular basis of cardiovascular gender differences. *Science*. 2005;308(5728):1583–1587.
24. Urowitz MB, Bookman AA, Koehler BE, Gordon DA, Smythe HA, Ogryzlo MA. The bimodal mortality pattern of systemic lupus erythematosus. *The American journal of medicine*. 1976;60(2):221–5.
25. Baigent C, Blackwell L, Emberson J, Holland LE, Reith C, Bhala N, Peto R, Barnes EH, Keech A, Simes J, Collins R, De Lemos J, Braunwald E, Blazing M, Murphy S, et al. Efficacy and

safety of more intensive lowering of LDL cholesterol: A meta-analysis of data from 170 000 participants in 26 randomised trials. *The Lancet*. 2010;376(9753):1670–1681.
26. Petri MA, Kiani AN, Post W, Christopher-Stine L, Magder LS. Lupus Atherosclerosis Prevention Study (LAPS). *Annals of the rheumatic diseases*. 2011;70(5):760–5.
27. Braun N, Wade N, Wakeland E, Major A. Accelerated atherosclerosis is independent of feeding high fat diet in systemic lupus erythematosus–susceptible LDLr−/− mice. *Lupus*. 2008;17(12):1070–1078.
28. Stanic AK, Stein CM, Morgan AC, Fazio S, Linton MF, Wakeland EK, Olsen NJ, Major AS. Immune dysregulation accelerates atherosclerosis and modulates plaque composition in systemic lupus erythematosus. *Proceedings of the National Academy of Sciences of the United States of America*. 2006;103(18):7018–23.
29. Palinski W, Rosenfeld ME, Yla-Herttuala S, Gurtner GC, Socher SS, Butler SW, Parthasarathy S, Carew TE, Steinberg D, Witztum JL. Low density lipoprotein undergoes oxidative modification in vivo. *Proceedings of the National Academy of Sciences of the United States of America*. 1989;86(4):1372–1376.
30. Cybulsky MI, Gimbrone MA. Endothelial Expression of a Mononuclear Leukocyte Adhesion Molecule During Atherogenesis. *Science*. 1991;251(4995):788–791.
31. Swirski FK, Libby P, Aikawa E, Alcaide P, Luscinskas FW, Weissleder R, Pittet MJ. Ly-6Chi monocytes dominate hypercholesterolemia-associated monocytosis and give rise to macrophages in atheromata. *Journal of Clinical Investigation*. 2007;117(1):195–205.
32. Tacke F, Alvarez D, Kaplan TJ, Jakubzick C, Spanbroek R, Llodra J, Garin A, Liu J, Mack M, Van Rooijen N, Lira SA, Habenicht AJ, Randolph GJ. Monocyte subsets differentially employ CCR2, CCR5, and CX3CR1 to accumulate within atherosclerotic plaques. *Journal of Clinical Investigation*. 2007;117(1):185–194.
33. Kunjathoor V V., Febbraio M, Podrez EA, Moore KJ, Andersson L, Koehn S, Rhee JS, Silverstein R, Hoff HF, Freeman MW. Scavenger receptors class A-I/II and CD36 are the principal receptors responsible for the uptake of modified low density lipoprotein leading to lipid loading in macrophages. *Journal of Biological Chemistry*. 2002;277(51):49982–49988.
34. Young MP, Febbraio M, Silverstein RL. CD36 modulates migration of mouse and human macrophages in response to oxidized LDL and may contribute to macrophage trapping in the arterial intima. *Journal of Clinical Investigation*. 2009;119(1):136–145.
35. Robbins CS, Hilgendorf I, Weber GF, Theurl I, Iwamoto Y, Figueiredo JL, Gorbatov R, Sukhova GK, Gerhardt LMS, Smyth D, Zavitz CCJ, Shikatani EA, Parsons M, Van Rooijen N, Lin HY, et al. Local proliferation dominates lesional macrophage accumulation in atherosclerosis. *Nature Medicine*. 2013;19(9):1166–1172.
36. Feil S, Fehrenbacher B, Lukowski R, Essmann F, Schulze-Osthoff K, Schaller M, Feil R. Transdifferentiation of vascular smooth muscle cells to macrophage-like cells during atherogenesis. *Circulation Research*. 2014;115(7):662–667.
37. Shankman LS, Gomez D, Cherepanova OA, Salmon M, Alencar GF, Haskins RM, Swiatlowska P, Newman AAC, Greene ES, Straub AC, Isakson B, Randolph GJ, Owens GK. KLF4-dependent phenotypic modulation of smooth muscle cells has a key role in atherosclerotic plaque pathogenesis. *Nature Medicine*. 2015;21(6):628–637.
38. Llodrá J, Angeli V, Liu J, Trogan E, Fisher EA, Randolph GJ. Emigration of monocyte-derived cells from atherosclerotic lesions characterizes regressive, but not progressive, plaques.

Proceedings of the National Academy of Sciences of the United States of America. 2004;101(32):11779–84.
39. Bobryshev Y V., Lord RSA. Mapping of vascular dendritic cells in atherosclerotic arteries suggests their involvement in local immune-inflammatory reaction. *Cardiovascular Research*. 1998;37(3):799–810.
40. Gräbner R, Lötzer K, Döpping S, Hildner M, Radke D, Beer M, Spanbroek R, Lippert B, Reardon CA, Getz GS, Fu YX, Hehlgans T, Mebius RE, Van Wall M Der, Kruspe D, et al. Lymphotoxin β receptor signaling promotes tertiary lymphoid organogenesis in the aorta adventitia of aged ApoE -/- mice. *Journal of Experimental Medicine*. 2009;206(1):233–248.
41. M W, A S, Y S, M Y, M T-S, M S, Y. I. Distribution of Inflammatory Cells in Adventitia Changed with Advancing Atherosclerosis of Human Coronary Artery. *Journal of atherosclerosis and Thrombosis*. 2007;14(6):325–331.
42. Zhou X, Stemme S, Hansson GK. Evidence for a local immune response in atherosclerosis: CD4+ T cells infiltrate lesions of apolipoprotein-E-deficient mice. *American Journal of Pathology*. 1996;149(2):359–366.
43. Hansson GK, Holm J, Jonasson L. Detection of activated T lymphocytes in the human atherosclerotic plaque. *American Journal of Pathology*. 1989;135(1):169–175.
44. Bui MN, Sack MN, Moutsatsos G, Lu DY, Katz P, McCown R, Breall JA, Rackley CE. Autoantibody titers to oxidized low-density lipoprotein in patients with coronary atherosclerosis. *American Heart Journal*. 1996;131(4):663–667.
45. Wu R, Huang YH, Elinder LS, Frostegård J. Lysophosphatidylcholine is involved in the antigenicity of oxidized LDL. *Arteriosclerosis, Thrombosis, and Vascular Biology*. 1998;18(4):626–630.
46. Fredrikson GN, Hedblad B, Berglund G, Alm R, Ares M, Cercek B, Chyu KY, Shah PK, Nilsson J. Identification of immune responses against aldehyde-modified peptide sequences in apoB associated with cardiovascular disease. *Arteriosclerosis, Thrombosis, and Vascular Biology*. 2003;23(5):872–878.
47. Stemme S, Faber B, Holm J, Wiklund O, Witztum JL, Hansson GK. T lymphocytes from human atherosclerotic plaques recognize oxidized low density lipoprotein. *Proceedings of the National Academy of Sciences of the United States of America*. 1995;92(9):3893–3897.
48. Shaw PX, Hörkkö S, Chang MK, Curtiss LK, Palinski W, Silverman GJ, Witztum JL. Natural antibodies with the T15 idiotype may act in atherosclerosis, apoptotic clearance, and protective immunity. *Journal of Clinical Investigation*. 2000;105(12):1731–1740.
49. Schrijvers DM, De Meyer GRY, Kockx MM, Herman AG, Martinet W. Phagocytosis of apoptotic cells by macrophages is impaired in atherosclerosis. *Arteriosclerosis, Thrombosis, and Vascular Biology*. 2005;25(6):1256–1261.
50. Thorp E, Cui D, Schrijvers DM, Kuriakose G, Tabas I. Mertk receptor mutation reduces efferocytosis efficiency and promotes apoptotic cell accumulation and plaque necrosis in atherosclerotic lesions of Apoe-/- mice. *Arteriosclerosis, Thrombosis, and Vascular Biology*. 2008;28(8):1421–1428.
51. Ovchinnikova OA, Folkersen L, Persson J, Lindeman JHN, Ueland T, Aukrust P, Gavrisheva N, Shlyakhto E, Paulsson-Berne G, Hedin U, Olofsson PS, Hansson GK. The collagen cross-linking enzyme lysyl oxidase is associated with the healing of human atherosclerotic lesions. *Journal of Internal Medicine*. 2014;276(5):525–536.

52. Van Der Wal AC, Becker AE, Van Der Loos CM, Das PK. Site of intimal rupture or erosion of thrombosed coronary atherosclerotic plaques is characterized by an inflammatory process irrespective of the dominant plaque morphology. *Circulation*. 1994;89(1):36–44.
53. Kubo T, Imanishi T, Takarada S, Kuroi A, Ueno S, Yamano T, Tanimoto T, Matsuo Y, Masho T, Kitabata H, Tsuda K, Tomobuchi Y, Akasaka T. Assessment of Culprit Lesion Morphology in Acute Myocardial Infarction. Ability of Optical Coherence Tomography Compared With Intravascular Ultrasound and Coronary Angioscopy. *Journal of the American College of Cardiology*. 2007;50(10):933–939.
54. Smith JD, Trogan E, Ginsberg M, Grigaux C, Tian J, Miyata M. Decreased atherosclerosis in mice deficient in both macrophage colony-stimulating factor (op) and apolipoprotein E. *Proceedings of the National Academy of Sciences of the United States of America*. 1995;92(18):8264–8268.
55. Cochain C, Vafadarnejad E, Arampatzi P, Pelisek J, Winkels H, Ley K, Wolf D, Saliba AE, Zernecke A. Single-cell RNA-seq reveals the transcriptional landscape and heterogeneity of aortic macrophages in murine atherosclerosis. *Circulation Research*. 2018;122(12):1661–1674.
56. Winkels H, Ehinger E, Vassallo M, Buscher K, Dinh HQ, Kobiyama K, Hamers AAJ, Cochain C, Vafadarnejad E, Saliba AE, Zernecke A, Pramod AB, Ghosh AK, Michel NA, Hoppe N, et al. Atlas of the immune cell repertoire in mouse atherosclerosis defined by single-cell RNA-sequencing and mass cytometry. *Circulation Research*. 2018;122(12):1675–1688.
57. King KR, Aguirre AD, Ye YX, Sun Y, Roh JD, Ng RP, Kohler RH, Arlauckas SP, Yoshiko V, Savo A, Sadreyev RI, Kelly M, Fitzgibbons TP, Fitzgerald KA, Mitchison T, et al. IRF3 and type i interferons fuel a fatal response to myocardial infarction. *Nature Medicine*. 2017;23(12):1481–1487.
58. Lin J Da, Nishi H, Poles J, Niu X, Mccauley C, Rahman K, Brown EJ, Yeung ST, Vozhilla N, Weinstock A, Ramsey SA, Fisher EA, Loke P. Single-cell analysis of fate-mapped macrophages reveals heterogeneity, including stem-like properties, during atherosclerosis progression and regression. *JCI insight*. 2019;4(4).
59. Kim K, Shim D, Lee JS, Zaitsev K, Williams JW, Kim KW, Jang MY, Jang HS, Yun TJ, Lee SH, Yoon WK, Prat A, Seidah NG, Choi J, Lee SP, et al. Transcriptome analysis reveals nonfoamy rather than foamy plaque macrophages are proinflammatory in atherosclerotic murine models. *Circulation Research*. 2018;123(10):1127–1142.
60. Spann NJ, Garmire LX, McDonald JG, Myers DS, Milne SB, Shibata N, Reichart D, Fox JN, Shaked I, Heudobler D, Raetz CRH, Wang EW, Kelly SL, Sullards MC, Murphy RC, et al. Regulated accumulation of desmosterol integrates macrophage lipid metabolism and inflammatory responses. *Cell*. 2012;151(1):138–152.
61. Depuydt MAC, Prange KHM, Slenders L, Örd T, Elbersen D, Boltjes A, De Jager SCA, Asselbergs FW, De Borst GJ, Aavik E, Lönnberg T, Lutgens E, Glass CK, Den Ruijter HM, Kaikkonen MU, et al. Microanatomy of the Human Atherosclerotic Plaque by Single-Cell Transcriptomics. *Circulation Research*. 2020;127(11):1437–1455.
62. Ma-Krupa W, Jeon MS, Spoerl S, Tedder TF, Goronzy JJ, Weyand CM. Activation of Arterial Wall Dendritic Cells and Breakdown of Self-tolerance in Giant Cell Arteritis. *Journal of Experimental Medicine*. 2004;199(2):173–183.

63. Choi JH, Cheong C, Dandamudi DB, Park CG, Rodriguez A, Mehandru S, Velinzon K, Jung IH, Yoo JY, Oh GT, Steinman RM. Flt3 signaling-dependent dendritic cells protect against atherosclerosis. *Immunity*. 2011;35(5):819–831.
64. Yilmaz A, Lochno M, Traeg F, Cicha I, Reiss C, Stumpf C, Raaz D, Anger T, Amann K, Probst T, Ludwig J, Daniel WG, Garlichs CD. Emergence of dendritic cells in rupture-prone regions of vulnerable carotid plaques. *Atherosclerosis*. 2004;176(1):101–110.
65. Björkbacka H, Kunjathoor VV, Moore KJ, Koehn S, Ordija CM, Lee MA, Means T, Halmen K, Luster AD, Golenbock DT, Freeman MW. Reduced atherosclerosis in MyD88-null mice links elevated serum cholesterol levels to activation of innate immunity signaling pathways. *Nature Medicine*. 2004;10(4):416–421.
66. Subramanian M, Thorp E, Hansson GK, Tabas I. Treg-mediated suppression of atherosclerosis requires MYD88 signaling in DCs. *Journal of Clinical Investigation*. 2013;123(1):179–188.
67. Haddad Y, Lahoute C, Clément M, Laurans L, Metghalchi S, Zeboudj L, Giraud A, Loyer X, Vandestienne M, Wain-Hobson J, Esposito B, Potteaux S, Ait-Oufella H, Tedgui A, Mallat Z, et al. The Dendritic Cell Receptor DNGR-1 Promotes the Development of Atherosclerosis in Mice. *Circulation Research*. 2017;121(3):234–243.
68. Clément M, Haddad Y, Raffort J, Lareyre F, Newland SA, Master L, Harrison J, Ozsvar-Kozma M, Bruneval P, Binder CJ, Taleb S, Mallat Z. Deletion of IRF8 (Interferon Regulatory Factor 8)-dependent dendritic cells abrogates proatherogenic adaptive immunity. *Circulation Research*. 2018;122(6):813–820.
69. Zernecke A. Dendritic Cells in Atherosclerosis. *Arteriosclerosis, Thrombosis, and Vascular Biology*. 2015;35(4):763–770.
70. Sage AP, Murphy D, Maffia P, Masters LM, Sabir SR, Baker LL, Cambrook H, Finigan AJ, Ait-Oufella H, Grassia G, Harrison JE, Ludewig B, Reith W, Hansson GK, Reizis B, et al. MHC Class II-restricted antigen presentation by plasmacytoid dendritic cells drives proatherogenic T cell immunity. *Circulation*. 2014;130(16):1363–1373.
71. Yun TJ, Lee JS, Machmach K, Shim D, Choi J, Wi YJ, Jang HS, Jung IH, Kim K, Yoon WK, Miah MA, Li B, Chang J, Bego MG, Pham TNQ, et al. Indoleamine 2,3-Dioxygenase-Expressing Aortic Plasmacytoid Dendritic Cells Protect against Atherosclerosis by Induction of Regulatory T Cells. *Cell Metabolism*. 2016;23(5):852–866.
72. Daissormont ITMN, Christ A, Temmerman L, Millares SS, Seijkens T, Manca M, Rousch M, Poggi M, Boon L, Van Der Loos C, Daemen M, Lutgens E, Halvorsen B, Aukrust P, Janssen E, et al. Plasmacytoid dendritic cells protect against atherosclerosis by tuning T-cell proliferation and activity. *Circulation Research*. 2011;109(12):1387–1395.
73. Kovanen PT, Kaartinen M, Paavonen T. Infiltrates of activated mast cells at the site of coronary atheromatous erosion or rupture in myocardial infarction. *Circulation*. 1995;92(5):1084–1088.
74. Drechsler M, Megens RTA, Van Zandvoort M, Weber C, Soehnlein O. Hyperlipidemia-triggered neutrophilia promotes early atherosclerosis. *Circulation*. 2010;122(18):1837–1845.
75. Whitman SC, Rateri DL, Szilvassy SJ, Yokoyama W, Daugherty A. Depletion of natural killer cell function decreases atherosclerosis in low-density lipoprotein receptor null mice. *Arteriosclerosis, Thrombosis, and Vascular Biology*. 2004;24(6):1049–1054.

76. Selathurai A, Deswaerte V, Kanellakis P, Tipping P, Toh BH, Bobik A, Kyaw T. Natural killer (NK) cells augment atherosclerosis by cytotoxic-dependent mechanisms. *Cardiovascular Research*. 2014;102(1):128–137.
77. Nour-Eldine W, Joffre J, Zibara K, Esposito B, Giraud A, Zeboudj L, Vilar J, Terada M, Bruneval P, Vivier E, Ait-Oufella H, Mallat Z, Ugolini S, Tedgui A. Genetic Depletion or Hyperresponsiveness of Natural Killer Cells Do Not Affect Atherosclerosis Development. *Circulation Research*. 2018;122(1):47–57.
78. Tupin E, Nicoletti A, Elhage R, Rudling M, Ljunggren HG, Hansson GK, Berne GP. CD1d-dependent Activation of NKT Cells Aggravates Atherosclerosis. *Journal of Experimental Medicine*. 2004;199(3):417–422.
79. Van Puijvelde GHM, Van Wanrooij EJA, Hauer AD, De Vos P, Van Berkel TJC, Kuiper J. Effect of natural killer T cell activation on initiation of atherosclerosis. *Thrombosis and Haemostasis*. 2009;102(2):223–230.
80. Braun NA, Mendez-Fernandez Y V, Covarrubias R, Porcelli SA, Savage PB, Yagita H, Van Kaer L, Major AS. Development of spontaneous anergy in invariant natural killer T cells in a mouse model of dyslipidemia. *Arteriosclerosis, thrombosis, and vascular biology*. 2010;30(9):1758–65.
81. Newland SA, Mohanta S, Clément M, Taleb S, Walker JA, Nus M, Sage AP, Yin C, Hu D, Kitt LL, Finigan AJ, Rodewald HR, Binder CJ, McKenzie ANJ, Habenicht AJ, et al. Type-2 innate lymphoid cells control the development of atherosclerosis in mice. *Nature Communications*. 2017;8(May 2016):1–11.
82. Zhou X, Nicoletti A, Elhage R, Hansson GK. Transfer of CD4 + T Cells Aggravates Atherosclerosis in Immunodeficient Apolipoprotein E Knockout Mice. *Circulation*. 2000;102(24):2919–2922.
83. Tsiantoulas D, Diehl CJ, Witztum JL, Binder CJ. B Cells and Humoral Immunity in Atherosclerosis. *Circulation Research*. 2014;114(11):1743–1756.
84. Major AS, Fazio S, Linton MF. B-lymphocyte deficiency increases atherosclerosis in LDL receptor-null mice. *Arteriosclerosis, Thrombosis, and Vascular Biology*. 2002;22(11):1892–1898.
85. Ait-Oufella H, Herbin O, Bouaziz JD, Binder CJ, Uyttenhove C, Laurans L, Taleb S, Van Vré E, Esposito B, Vilar J, Sirvent J, Van Snick J, Tedgui A, Tedder TF, Mallat Z. B cell depletion reduces the development of atherosclerosis in mice. *Journal of Experimental Medicine*. 2010;207(8):1579–1587.
86. Kyaw T, Tay C, Khan A, Dumouchel V, Cao A, To K, Kehry M, Dunn R, Agrotis A, Tipping P, Bobik A, Toh B-H. Conventional B2 B Cell Depletion Ameliorates whereas Its Adoptive Transfer Aggravates Atherosclerosis. *The Journal of Immunology*. 2010;185(7):4410–4419.
87. Kyaw T, Tay C, Hosseini H, Kanellakis P, Gadowski T, MacKay F, Tipping P, Bobik A, Toh B-H. Depletion of B2 but Not B1a B Cells in BAFF Receptor-Deficient ApoE−/− Mice Attenuates Atherosclerosis by Potently Ameliorating Arterial Inflammation. Schmidt HHHW, ed. *PLoS ONE*. 2012;7(1):e29371.
88. Tay C, Liu YH, Kanellakis P, Kallies A, Li Y, Cao A, Hosseini H, Tipping P, Toh BH, Bobik A, Kyaw T. Follicular B Cells Promote Atherosclerosis via T Cell-Mediated Differentiation Into Plasma Cells and Secreting Pathogenic Immunoglobulin G. *Arteriosclerosis, thrombosis, and vascular biology*. 2018;38(5):e71–e84.

89. Rhoads JP, Lukens JR, Wilhelm AJ, Moore JL, Mendez-Fernandez Y, Kanneganti T-D, Major AS. Oxidized Low-Density Lipoprotein Immune Complex Priming of the Nlrp3 Inflammasome Involves TLR and FcγR Cooperation and Is Dependent on CARD9. *The Journal of Immunology*. 2017;198(5):2105–2114.
90. Saad AF, Virella G, Chassereau C, Boackle RJ, Lopes-Virella MF. OxLDL immune complexes activate complement and induce cytokine production by MonoMac 6 cells and human macrophages. *Journal of Lipid Research*. 2006;47(9):1975–1983.
91. Lennartz MR, Aggarwal A, Michaud TM, Feustel PJ, Jones DM, Brosnan MJ, Keller RS, Loegering DJ, Kreienberg PB. Ligation of macrophage Fcγ receptors recapitulates the gene expression pattern of vulnerable human carotid plaques. *PLoS ONE*. 2011;6(7).
92. Kyaw T, Tay C, Krishnamurthi S, Kanellakis P, Agrotis A, Tipping P, Bobik A, Toh BH. B1a B lymphocytes are atheroprotective by secreting natural IgM that increases IgM deposits and reduces necrotic cores in atherosclerotic lesions. *Circulation Research*. 2011;109(8):830–840.
93. Guo X, Yuan S, Liu Y, Zeng Y, Xie H, Liu Z, Zhang S, Fang Q, Wang J, Shen Z. Serum IgE levels are associated with coronary artery disease severity. *Atherosclerosis*. 2016;251:355–360.
94. Ponnuswamy P, Joffre J, Herbin O, Esposito B, Laurans L, Binder CJ, Tedder TF, Zeboudj L, Loyer X, Giraud A, Zhang Y, Tedgui A, Mallat Z, Ait-Oufella H. Angiotensin II synergizes with BAFF to promote atheroprotective regulatory B cells. *Scientific Reports*. 2017;7(1):1–10.
95. Hilgendorf I, Theurl I, Gerhardt LMS, Robbins CS, Weber GF, Gonen A, Iwamoto Y, Degousee N, Holderried TAW, Winter C, Zirlik A, Lin HY, Sukhova GK, Butany J, Rubin BB, et al. Innate response activator b cells aggravate atherosclerosis by stimulating t helper-1 adaptive immunity. *Circulation*. 2014;129(16):1677–1687.
96. Nus M, Sage AP, Lu Y, Masters L, Lam BYH, Newland S, Weller S, Tsiantoulas D, Raffort J, Marcus D, Finigan A, Kitt L, Figg N, Schirmbeck R, Kneilling M, et al. Marginal zone B cells control the response of follicular helper T cells to a high-cholesterol diet. *Nature Medicine*. 2017;23(5):601–610.
97. Vallejo J, Dunér P, Fredrikson GN, Nilsson J, Bengtsson E. Autoantibodies against aldehyde-modified collagen type IV are associated with risk of development of myocardial infarction. *Journal of Internal Medicine*. 2017;282(6):496–507.
98. Engelbertsen D, Vallejo J, Quách TD, Fredrikson GN, Alm R, Hedblad B, Björkbacka H, Rothstein TL, Nilsson J, Bengtsson E. Low Levels of IgM Antibodies against an Advanced Glycation Endproduct–Modified Apolipoprotein B100 Peptide Predict Cardiovascular Events in Nondiabetic Subjects. *The Journal of Immunology*. 2015;195(7):3020–3025.
99. Cambridge G, Acharya J, Cooper JA, Edwards JC, Humphries SE. Antibodies to citrullinated peptides and risk of coronary heart disease. *Atherosclerosis*. 2013;228(1):243–246.
100. Zou J, Wang G, Li H, Yu X, Tang C. IgM natural antibody T15/E06 in atherosclerosis. *Clinica Chimica Acta*. 2020;504(November 2019):15–22.
101. Galkina E, Kadl A, Sanders J, Varughese D, Sarembock IJ, Ley K. Lymphocyte recruitment into the aortic wall before and during development of atherosclerosis is partially L-selectin dependent. *The Journal of experimental medicine*. 2006;203(5):1273–82.
102. Elhage R, Gourdy P, Brauchet L, Jawien J, Fouque MJ, Fiévet C, Huc X, Barreira Y, Couloumiers JC, Arnal JF, Bayard F. Deleting TCRαβ+ or CD4+ T lymphocytes leads to opposite effects on site-specific atherosclerosis in female apolipoprotein E-deficient mice. *American Journal of Pathology*. 2004;165(6):2013–2018.

103. Kyaw T, Winship A, Tay C, Kanellakis P, Hosseini H, Cao A, Li P, Tipping P, Bobik A, Toh BH. Cytotoxic and proinflammatory CD8+ T lymphocytes promote development of vulnerable atherosclerotic plaques in ApoE-deficient mice. *Circulation*. 2013;127(9):1028–1039.
104. Seijkens TTP, Poels K, Meiler S, Van Tiel CM, Kusters PJH, Reiche M, Atzler D, Winkels H, Tjwa M, Poelman H, Slütter B, Kuiper J, Gijbels M, Kuivenhoven JA, Matic LP, et al. Deficiency of the T cell regulator Casitas B-cell lymphoma-B aggravates atherosclerosis by inducing CD8 + T cell-mediated macrophage death. *European Heart Journal*. 2019;40(4):372–382.
105. Cochain C, Koch M, Chaudhari SM, Busch M, Pelisek J, Boon L, Zernecke A. CD8+ T Cells Regulate Monopoiesis and Circulating Ly6Chigh Monocyte Levels in Atherosclerosis in Mice. *Circulation Research*. 2015;117(3):244–253.
106. Emeson EE, Shen ML, Bell CGH, Qureshi A. Inhibition of atherosclerosis in CD4 T-cell-ablated and nude (nu/nu) C57BL/6 hyperlipidemic mice. *American Journal of Pathology*. 1996;149(2):675–685.
107. Olofsson PS, Söderström LÅ, Wågsäter D, Sheikine Y, Ocaya P, Lang F, Rabu C, Chen L, Rudling M, Aukrust P, Hedin U, Paulsson-Berne G, Sirsjö A, Hansson GK. CD137 is expressed in human atherosclerosis and promotes development of plaque inflammation in hypercholesterolemic mice. *Circulation*. 2008;117(10):1292–1301.
108. Saigusa R, Winkels H, Ley K. T cell subsets and functions in atherosclerosis. *Nature Reviews Cardiology*. 2020;3050.
109. Wolf D, Gerhardt T, Winkels H, Michel NA, Pramod AB, Ghosheh Y, Brunel S, Buscher K, Miller J, McArdle S, Baas L, Kobiyama K, Vassallo M, Ehinger E, Dileepan T, et al. Pathogenic Autoimmunity in Atherosclerosis Evolves from Initially Protective Apolipoprotein B100-Reactive CD4+T-Regulatory Cells. *Circulation*. 2020:1279–1293.
110. Shaw MK, Tse KY, Zhao X, Welch K, Eitzman DT, Thipparthi RR, Montgomery PC, Thummel R, Tse HY. T-cells specific for a self-peptide of ApoB-100 exacerbate aortic atheroma in murine atherosclerosis. *Frontiers in Immunology*. 2017;8(FEB).
111. Tse K, Gonen A, Sidney J, Ouyang H, Witztum JL, Sette A, Tse H, Ley K. Atheroprotective vaccination with MHC-II restricted peptides from ApoB-100. *Frontiers in Immunology*. 2013;4(DEC):1–10.
112. Kimura T, Kobiyama K, Winkels H, Tse K, Miller J, Vassallo M, Wolf D, Ryden C, Orecchioni M, Dileepan T, Jenkins MK, James EA, Kwok WW, Hanna DB, Kaplan RC, et al. Regulatory CD4 + T Cells Recognize Major Histocompatibility Complex Class II Molecule–Restricted Peptide Epitopes of Apolipoprotein B. *Circulation*. 2018;138(11):1130–1143.
113. Fernandez DM, Rahman AH, Fernandez NF, Chudnovskiy A, Amir ED, Amadori L, Khan NS, Wong CK, Shamailova R, Hill CA, Wang Z, Remark R, Li JR, Pina C, Faries C, et al. Single-cell immune landscape of human atherosclerotic plaques. *Nature Medicine*. 2019;25(10):1576–1588.
114. Depuydt MAC, Prange KHM, Slenders L, Örd T, Elbersen D, Boltjes A, de Jager SCA, Asselbergs FW, de Borst GJ, Aavik E, Lönnberg T, Lutgens E, Glass CK, den Ruijter HM, Kaikkonen MU, et al. Microanatomy of the Human Atherosclerotic Plaque by Single-Cell Transcriptomics. *Circulation Research*. 2020:1437–1455.
115. Wilhelm AJ, Rhoads JP, Wade NS, Major AS. Dysregulated CD4+ T cells from SLE-susceptible mice are sufficient to accelerate atherosclerosis in LDLr-/- mice. *Annals of the Rheumatic Diseases*. 2015;74(4):778–785.

116. Buono C, Binder CJ, Stavrakis G, Witztum JL, Glimcher LH, Lichtman AH. T-bet deficiency reduces atherosclerosis and alters plaque antigen-specific immune responses. *Proceedings of the National Academy of Sciences*. 2005;102(5):1596–1601.
117. Buono C, Come CE, Stavrakis G, Maguire GF, Connelly PW, Lichtman AH. Influence of interferon-γ on the extent and phenotype of diet-induced atherosclerosis in the LDLR-deficient mouse. *Arteriosclerosis, Thrombosis, and Vascular Biology*. 2003;23(3):454–460.
118. Whitman SC, Ravisankar P, Elam H, Daugherty A. Exogenous Interferon-γ Enhances Atherosclerosis in Apolipoprotein E−/− Mice. *The American Journal of Pathology*. 2000;157(6):1819–1824.
119. Gupta S, Pablo AM, Jiang XC, Wang N, Tall AR, Schindler C. IFN-gamma potentiates atherosclerosis in ApoE knock-out mice. *Journal of Clinical Investigation*. 1997;99(11):2752–2761.
120. Whitman SC, Ravisankar P, Daugherty A. IFN-γ deficiency exerts gender-specific effects on atherogenesis in apolipoprotein E−/− mice. *Journal of Interferon and Cytokine Research*. 2002;22(6):661–670.
121. Erbel C, Chen L, Bea F, Wangler S, Celik S, Lasitschka F, Wang Y, Böckler D, Katus HA, Dengler TJ. Inhibition of IL-17A Attenuates Atherosclerotic Lesion Development in ApoE-Deficient Mice. *The Journal of Immunology*. 2009;183(12):8167–8175.
122. van Es T, van Puijvelde GHM, Ramos OH, Segers FME, Joosten LA, van den Berg WB, Michon IM, de Vos P, van Berkel ThJC, Kuiper J. Attenuated atherosclerosis upon IL-17R signaling disruption in LDLr deficient mice. *Biochemical and Biophysical Research Communications*. 2009;388(2):261–265.
123. Smith E, Prasad K-MR, Butcher M, Dobrian A, Kolls JK, Ley K, Galkina E. Blockade of Interleukin-17A Results in Reduced Atherosclerosis in Apolipoprotein E–Deficient Mice. *Circulation*. 2010;121(15):1746–1755.
124. Taleb S, Romain M, Ramkhelawon B, Uyttenhove C, Pasterkamp G, Herbin O, Esposito B, Perez N, Yasukawa H, van Snick J, Yoshimura A, Tedgui A, Mallat Z. Loss of SOCS3 expression in T cells reveals a regulatory role for interleukin-17 in atherosclerosis. *Journal of Experimental Medicine*. 2009;206(10):2067–2077.
125. Ait-Oufella H, Salomon BL, Potteaux S, Robertson A-KL, Gourdy P, Zoll J, Merval R, Esposito B, Cohen JL, Fisson S, Flavell RA, Hansson GK, Klatzmann D, Tedgui A, Mallat Z. Natural regulatory T cells control the development of atherosclerosis in mice. *Nature Medicine*. 2006;12(2):178–180.
126. Mor A, Planer D, Luboshits G, Afek A, Metzger S, Chajek-Shaul T, Keren G, George J. Role of naturally occurring CD4+CD25+ regulatory T cells in experimental atherosclerosis. *Arteriosclerosis, Thrombosis, and Vascular Biology*. 2007;27(4):893–900.
127. Klingenberg R, Gerdes N, Badeau RM, Gisterå A, Strodthoff D, Ketelhuth DFJ, Lundberg AM, Rudling M, Nilsson SK, Olivecrona G, Zoller S, Lohmann C, Lüscher TF, Jauhiainen M, Sparwasser T, et al. Depletion of FOXP3+ regulatory T cells promotes hypercholesterolemia and atherosclerosis. *Journal of Clinical Investigation*. 2013;123(3):1323–1334.
128. Sharma M, Schlegel MP, Afonso MS, Brown EJ, Rahman K, Weinstock A, Sansbury BE, Corr EM, Van Solingen C, Koelwyn GJ, Shanley LC, Beckett L, Peled D, Lafaille JJ, Spite M, et al. Regulatory T cells license macrophage pro-resolving functions during atherosclerosis regression. *Circulation Research*. 2020;127(3):335–353.

129. Dietel B, Cicha I, Voskens CJ, Verhoeven E, Achenbach S, Garlichs CD. Decreased numbers of regulatory T cells are associated with human atherosclerotic lesion vulnerability and inversely correlate with infiltrated mature dendritic cells. *Atherosclerosis*. 2013;230(1):92–99.
130. George J, Schwartzenberg S, Medvedovsky D, Jonas M, Charach G, Afek A, Shamiss A. Regulatory T cells and IL-10 levels are reduced in patients with vulnerable coronary plaques. *Atherosclerosis*. 2012;222(2):519–523.
131. Maganto-García E, Tarrio ML, Grabie N, Bu DX, Lichtman AH. Dynamic changes in regulatory T cells are linked to levels of diet-induced hypercholesterolemia. *Circulation*. 2011;124(2):185–195.
132. Zhang WC, Wang J, Shu YW, Tang TT, Zhu ZF, Xia N, Nie SF, Liu J, Zhou SF, Li JJ, Xiao H, Yuan J, Liao MY, Cheng LX, Liao YH, et al. Impaired thymic export and increased apoptosis account for regulatory T cell defects in patients with non-ST segment elevation acute coronary syndrome. *Journal of Biological Chemistry*. 2012;287(41):34157–34166.
133. Gaddis DE, Padgett LE, Wu R, McSkimming C, Romines V, Taylor AM, McNamara CA, Kronenberg M, Crotty S, Thomas MJ, Sorci-Thomas MG, Hedrick CC. Apolipoprotein AI prevents regulatory to follicular helper T cell switching during atherosclerosis. *Nature Communications*. 2018;9(1).
134. Butcher MJ, Filipowicz AR, Waseem TC, McGary CM, Crow KJ, Magilnick N, Boldin M, Lundberg PS, Galkina E V. Atherosclerosis-Driven Treg Plasticity Results in Formation of a Dysfunctional Subset of Plastic IFNγ + Th1/Tregs. *Circulation Research*. 2016;119(11):1190–1203.
135. Glass CK, Witztum JL. Atherosclerosis: The Road Ahead. *Cell*. 2001;104(4):503–516.
136. Mor A, Luboshits G, Planer D, Keren G, George J. Altered status of CD4+CD25+ regulatory T cells in patients with acute coronary syndromes. *European Heart Journal*. 2006;27(21):2530–2537.
137. Miller YI, Shyy JYJ. Context-Dependent Role of Oxidized Lipids and Lipoproteins in Inflammation. *Trends in Endocrinology and Metabolism*. 2017;28(2):143–152.
138. Watson AD, Leitinger N, Navab M, Faull KF, Hörkkö S, Witztum JL, Palinski W, Schwenke D, Salomon RG, Sha W, Subbanagounder G, Fogelman AM, Berliner JA. Structural identification by mass spectrometry of oxidized phospholipids in minimally oxidized low density lipoprotein that induce monocyte/endothelial interactions and evidence for their presence in vivo. *Journal of Biological Chemistry*. 1997;272(21):13597–13607.
139. Awasthi D, Nagarkoti S, Kumar A, Dubey M, Singh AK, Pathak P, Chandra T, Barthwal MK, Dikshit M. Oxidized LDL induced extracellular trap formation in human neutrophils via TLR-PKC-IRAK-MAPK and NADPH-oxidase activation. *Free Radical Biology and Medicine*. 2016;93:190–203.
140. Chu LH, Indramohan M, Ratsimandresey RA, Gangopadhyay A, Morris EP, Monack DM, Dorfleutner A, Stehlik C. The oxidized phospholipid oxPAPC protects from septic shock by targeting the non-canonical inflammasome in macrophages. *Nature Communications*. 2018;9(1).
141. Chang MK, Binder CJ, Miller YI, Subbanagounder G, Silverman GJ, Berliner JA, Witztum JL. Apoptotic cells with oxidation-specific epitopes are immunogenic and proinflammatory. *Journal of Experimental Medicine*. 2004;200(11):1359–1370.

142. Lutz MB, Kukutsch N, Ogilvie ALJ, Rößner S, Koch F, Romani N, Schuler G. An advanced culture method for generating large quantities of highly pure dendritic cells from mouse bone marrow. *Journal of Immunological Methods*. 1999;223(1):77–92.
143. Gjurich BN, Taghavie-Moghadam PL, Galkina E V. Flow cytometric analysis of immune cells within murine aorta. *Methods in Molecular Biology*. 2015;1339(3):161–175.
144. Marvin J, Rhoads JP, Major AS. FcγRIIb on CD11c + cells modulates serum cholesterol and triglyceride levels and differentially affects atherosclerosis in male and female Ldlr −/− mice. *Atherosclerosis*. 2019;285(April):108–119.
145. Li J, McArdle S, Gholami A, Kimura T, Wolf D, Gerhardt T, Miller J, Weber C, Ley K. CCR5 + T-bet + FoxP3 + Effector CD4 T Cells Drive Atherosclerosis. *Circulation Research*. 2016;118(10):1540–1552.
146. Paigen B, Morrow A, Holmes PA, Mitchell D, Williams RA. Quantitative assessment of atherosclerotic lesions in mice. *Atherosclerosis*. 1987;68(3):231–240.
147. Royston P. Remark AS R94: A Remark on Algorithm AS 181: The W-test for Normality. *Applied Statistics*. 1995;44(4):547.
148. di Gioia M, Spreafico R, Springstead JR, Mendelson MM, Joehanes R, Levy D, Zanoni I. Endogenous oxidized phospholipids reprogram cellular metabolism and boost hyperinflammation. *Nature Immunology*. 2020;21(1):42–53.
149. Rao X, Zhong J, Maiseyeu A, Gopalakrishnan B, Villamena FA, Chen LC, Harkema JR, Sun Q, Rajagopalan S. CD36-dependent 7-ketocholesterol accumulation in macrophages mediates progression of atherosclerosis in response to chronic air pollution exposure. *Circulation Research*. 2014;115(9):770–780.
150. Erridge C, Kennedy S, Spickett CM, Webb DJ. Oxidized phospholipid inhibition of Toll-Like Receptor (TLR) signaling is restricted to TLR2 and TLR4: Roles for CD14, LPS-binding protein, and MD2 as targets for specificity of inhibition. *Journal of Biological Chemistry*. 2008;283(36):24748–24759.
151. Tai X, Erman B, Alag A, Mu J, Kimura M, Katz G, Guinter T, McCaughtry T, Etzensperger R, Feigenbaum L, Singer DS, Singer A. Foxp3 Transcription Factor Is Proapoptotic and Lethal to Developing Regulatory T Cells unless Counterbalanced by Cytokine Survival Signals. *Immunity*. 2013;38(6):1116–1128.
152. Selvaraj RK, Geiger TL. A kinetic and dynamic analysis of Foxp3 induced in T cells by TGF-β. *The Journal of Immunology*. 2007;179(2):1390–1390.
153. Mallat Z, Gojova A, Brun V, Esposito B, Fournier N, Cottrez F, Tedgui A, Groux H. Induction of a regulatory T cell type I response reduces the development of atherosclerosis in apolipoprotein E-knockout mice. *Circulation*. 2003;108(10):1232–1237.
154. Amersfoort J, Schaftenaar FH, Douna H, Van Santbrink PJ, Van Puijvelde GHM, Slütter B, Foks AC, Harms A, Moreno-Gordaliza E, Wang Y, Hankemeier T, Bot I, Chi H, Kuiper J. Diet-induced dyslipidemia induces metabolic and migratory adaptations in regulatory T cells. *Cardiovascular Research*. 2021;117(5):1309–1324.
155. Kimura T, Kobiyama K, Winkels H, Tse K, Miller J, Vassallo M, Wolf D, Ryden C, Orecchioni M, Dileepan T, Jenkins MK, James EA, Kwok WW, Hanna DB, Kaplan RC, et al. Regulatory CD4+ T cells recognize major histocompatibility complex class II molecule-restricted peptide epitopes of apolipoprotein B. *Circulation*. 2018;138(11):1130–1143.

156. Cheng X, Yu X, Ding Y jun, Fu Q qing, Xie J jiao, Tang T ting, Yao R, Chen Y, Liao Y hua. The Th17/Treg imbalance in patients with acute coronary syndrome. *Clinical Immunology*. 2008;127(1):89–97.
157. Olson NC, Sitlani CM, Doyle MF, Huber SA, Landay AL, Tracy RP, Psaty BM, Delaney JA. Innate and adaptive immune cell subsets as risk factors for coronary heart disease in two population-based cohorts. *Atherosclerosis*. 2020;300(1):47–53.
158. Overacre-Delgoffe AE, Chikina M, Dadey RE, Yano H, Brunazzi EA, Shayan G, Horne W, Moskovitz JM, Kolls JK, Sander C, Shuai Y, Normolle DP, Kirkwood JM, Ferris RL, Delgoffe GM, et al. Interferon-γ Drives Treg Fragility to Promote Anti-tumor Immunity. *Cell*. 2017;169(6):1130-1141.e11.
159. Chen J, Wang X, Cui T, Ni Q, Zhang Q, Zou D, He K, Wu W, Ma J, Wang Y, Guo W, Li C, Li S. Th1-like Treg in vitiligo : An incompetent regulator in immune tolerance. *Journal of Autoimmunity*. 2022;131(30):102859.
160. Koenecke C, Lee C-W, Thamm K, Föhse L, Schafferus M, Mittrücker H-W, Floess S, Huehn J, Ganser A, Förster R, Prinz I. IFN-γ Production by Allogeneic Foxp3 + Regulatory T Cells Is Essential for Preventing Experimental Graft-versus-Host Disease. *The Journal of Immunology*. 2012;189(6):2890–2896.
161. Tan TG, Mathis D, Benoist C. Singular role for T-BET + CXCR3 + regulatory T cells in protection from autoimmune diabetes. *Proceedings of the National Academy of Sciences*. 2016;113(49):14103–14108.
162. Levine AG, Mendoza A, Hemmers S, Moltedo B, Niec RE, Schizas M, Hoyos BE, Putintseva E v, Chaudhry A, Dikiy S, Fujisawa S, Chudakov DM, Treuting PM, Rudensky AY. Stability and function of regulatory T cells expressing the transcription factor T-bet. *Nature*. 2017;546(7658):421–425.
163. Koch MA, Tucker-Heard G, Perdue NR, Killebrew JR, Urdahl KB, Campbell DJ. The transcription factor T-bet controls regulatory T cell homeostasis and function during type 1 inflammation. *Nature Immunology*. 2009;10(6):595–602.
164. Baardman J, Lutgens E. Regulatory T cell metabolism in atherosclerosis. *Metabolites*. 2020;10(7):1–15.
165. Overacre-Delgoffe AE, Chikina M, Dadey RE, Yano H, Brunazzi EA, Shayan G, Horne W, Moskovitz JM, Kolls JK, Sander C, Shuai Y, Normolle DP, Kirkwood JM, Ferris RL, Delgoffe GM, et al. Interferon-γ Drives Treg Fragility to Promote Anti-tumor Immunity. *Cell*. 2017;169(6).
166. Deligne C, Metidji A, Fridman WH, Teillaud JL. Anti-CD20 therapy induces a memory Th1 response through the IFN-γ/IL-12 axis and prevents protumor regulatory T-cell expansion in mice. *Leukemia*. 2015;29(4):947–957.
167. Olalekan SA, Cao Y, Hamel KM, Finnegan A. B cells expressing IFN-γ suppress Treg-cell differentiation and promote autoimmune experimental arthritis. *European Journal of Immunology*. 2015;45(4):988–998.
168. Visperas A, Shen B, Min B. γδ T cells restrain extrathymic development of Foxp3+-inducible regulatory T cells via IFN-γ. *European Journal of Immunology*. 2014;44(8):2448–2456.
169. Gocher-Demske AM, Cui J, Szymczak-Workman AL, Vignali KM, Latini JN, Pieklo GP, Kimball JC, Avery L, Cipolla EM, Huckestein BR, Hedden L, Meisel M, Alcorn JF, Kane LP, Workman CJ, et al. IFNγ-induction of TH1-like regulatory T cells controls antiviral responses. *Nature Immunology*. 2023.

170. Koch MA, Thomas KR, Perdue NR, Smigiel KS, Srivastava S, Campbell DJ. T-bet+ Treg Cells Undergo Abortive Th1 Cell Differentiation due to Impaired Expression of IL-12 Receptor β2. *Immunity*. 2012;37(3):501–510.
171. Amento EP, Ehsani N, Palmer H, Libby P. Cytokines and growth factors positively and negatively regulate interstitial collagen gene expression in human vascular smooth muscle cells. *Arteriosclerosis, Thrombosis, and Vascular Biology*. 1991;11(5):1223–1230.
172. Duan R, Liu Y, Tang D, Lin R, Huang J, Zhao M. IgG1 Is the Optimal Subtype for Treating Atherosclerosis by Inducing M2 Macrophage Differentiation, and Is Independent of the FcγRIIA Gene Polymorphism. *International Journal of Molecular Sciences*. 2023;24(6):5932.
173. Marek I, Canu M, Cordasic N, Rauh M, Volkert G, Fahlbusch FB, Rascher W, Hilgers KF, Hartner A, Menendez-Castro C. Sex differences in the development of vascular and renal lesions in mice with a simultaneous deficiency of Apoe and the integrin chain Itga8. *Biology of Sex Differences*. 2017;8(1):1–13.
174. Lu C, Donners M, Karel J, de Boer H, van Zonneveld AJ, den Ruijter H, Jukema JW, Kraaijeveld A, Kuiper J, Pasterkamp G, Cavill R, Perales-Patón J, Ferrannini E, Goossens P, Biessen EAL. Sex-specific differences in cytokine signaling pathways in circulating monocytes of cardiovascular disease patients. *Atherosclerosis*. 2023:104908.
175. Niwa T, Wada H, Ohashi H, Iwamoto N, Ohta H, Kirii H, Fujii H, Saito K, Seishima M. Interferon-gamma produced by bone marrow-derived cells attenuates atherosclerotic lesion formation in LDLR-deficient mice. *Journal of atherosclerosis and thrombosis*. 2004;11(2):79–87.
176. Freeman GJ, Gribben JG, Boussiotis VA, Ng JW, Restivo VA, Lombard LA, Gray GS, Nadler LM. Cloning of B7-2: a CTLA-4 Counter-Receptor That Costimulates Human T Cell Proliferation. *Science*. 1993;262(5135):909–911.
177. Glass CK, Witztum JL. Atherosclerosis. the road ahead. *Cell*. 2001;104(4):503–16.
178. Lopes-Virella MF, Hunt KJ, Baker NL, Virella G, Moritz T. The levels of MDA-LDL in circulating immune complexes predict myocardial infarction in the VADT study. *Atherosclerosis*. 2012;224(2):526–531.
179. Palinski W, Tangirala RK, Miller E, Young SG, Witztum JL. Increased autoantibody titers against epitopes of oxidized LDL in LDL receptor-deficient mice with increased atherosclerosis. *Arteriosclerosis, Thrombosis, and Vascular Biology*. 1995;15(10):1569–1576.
180. Kolbus D, Ramos OH, Berg KE, Persson J, Wigren M, Björkbacka H, Fredrikson GN, Nilsson J. CD8+T cell activation predominate early immune responses to hypercholesterolemia in Apoe-/-mice. *BMC Immunology*. 2010;11.
181. Mustafa A, Nityanand S, Berglund L, Lithell H, Lefvert AK. Circulating immune complexes in 50-year-old men as a strong and independent risk factor for myocardial infarction. *Circulation*. 2000;102(21):2576–2581.
182. Cvetkovic JT. Increased levels of autoantibodies against copper-oxidized low density lipoprotein, malondialdehyde-modified low density lipoprotein and cardiolipin in patients with rheumatoid arthritis. *Rheumatology*. 2002;41(9):988–995.
183. Gómez-Zumaquero JM, Tinahones FJ, de Ramón E, Camps M, Garrido L, Soriguer FJ. Association of biological markers of activity of systemic lupus erythematosus with levels of anti-oxidized low-density lipoprotein antibodies. *Rheumatology*. 2004;43(4):510–513.
184. Netea MG, Quintin J, Van Der Meer JWM. Trained immunity: A memory for innate host defense. *Cell Host and Microbe*. 2011;9(5):355–361.

185. Quintin J, Saeed S, Martens JHA, Giamarellos-Bourboulis EJ, Ifrim DC, Logie C, Jacobs L, Jansen T, Kullberg B-J, Wijmenga C, Joosten LAB, Xavier RJ, van der Meer JWM, Stunnenberg HG, Netea MG. Candida albicans Infection Affords Protection against Reinfection via Functional Reprogramming of Monocytes. *Cell Host & Microbe*. 2012;12(2):223–232.
186. Cheng SC, Quintin J, Cramer RA, Shepardson KM, Saeed S, Kumar V, Giamarellos-Bourboulis EJ, Martens JHA, Rao NA, Aghajanirefah A, Manjeri GR, Li Y, Ifrim DC, Arts RJW, Van Der Meer BMJW, et al. MTOR- and HIF-1α-mediated aerobic glycolysis as metabolic basis for trained immunity. *Science*. 2014;345(6204).
187. Arts RJW, Novakovic B, ter Horst R, Carvalho A, Bekkering S, Lachmandas E, Rodrigues F, Silvestre R, Cheng SC, Wang SY, Habibi E, Gonçalves LG, Mesquita I, Cunha C, van Laarhoven A, et al. Glutaminolysis and Fumarate Accumulation Integrate Immunometabolic and Epigenetic Programs in Trained Immunity. *Cell Metabolism*. 2016;24(6):807–819.
188. Yang H, He H, Dong Y. CARD9 Syk-dependent and Raf-1 Syk-independent signaling pathways in target recognition of Candida albicans by Dectin-1. *European Journal of Clinical Microbiology and Infectious Diseases*. 2011;30(3):303–305.
189. Bekkering S, Quintin J, Joosten LAB, Van Der Meer JWM, Netea MG, Riksen NP. Oxidized low-density lipoprotein induces long-term proinflammatory cytokine production and foam cell formation via epigenetic reprogramming of monocytes. *Arteriosclerosis, Thrombosis, and Vascular Biology*. 2014;34(8):1731–1738.
190. Christ A, Günther P, Lauterbach MAR, Duewell P, Biswas D, Pelka K, Scholz CJ, Oosting M, Haendler K, Baßler K, Klee K, Schulte-Schrepping J, Ulas T, Moorlag SJCFM, Kumar V, et al. Western Diet Triggers NLRP3-Dependent Innate Immune Reprogramming. *Cell*. 2018;172(1–2):162-175.e14.
191. Sheedy FJ, Grebe A, Rayner KJ, Kalantari P, Ramkhelawon B, Carpenter SB, Becker CE, Ediriweera HN, Mullick AE, Golenbock DT, Stuart LM, Latz E, Fitzgerald KA, Moore KJ. CD36 coordinates NLRP3 inflammasome activation by facilitating intracellular nucleation of soluble ligands into particulate ligands in sterile inflammation. *Nature Immunology*. 2013;14(8):812–820.
192. Gamberale R, Giordano M, Trevani AS, Andonegui G, Geffner JR. Modulation of human neutrophil apoptosis by immune complexes. *Journal of immunology (Baltimore, Md. : 1950)*. 1998;161(7):3666–74.
193. Miller YI, Shyy JY-J. Context-Dependent Role of Oxidized Lipids and Lipoproteins in Inflammation. *Trends in Endocrinology & Metabolism*. 2017;28(2):143–152.
194. Ifrim DC, Quintin J, Joosten LAB, Jacobs C, Jansen T, Jacobs L, Gow NAR, Williams DL, Van Der Meer JWM, Netea MG. Trained immunity or tolerance: Opposing functional programs induced in human monocytes after engagement of various pattern recognition receptors. *Clinical and Vaccine Immunology*. 2014;21(4):534–545.
195. Sarrazy V, Viaud M, Westerterp M, Ivanov S, Giorgetti-Peraldi S, Guinamard R, Gautier EL, Thorp EB, De Vivo DC, Yvan-Charvet L. Disruption of Glut1 in Hematopoietic Stem Cells Prevents Myelopoiesis and Enhanced Glucose Flux in Atheromatous Plaques of ApoE -/- Mice. *Circulation Research*. 2016;118(7):1062–1077.
196. Seijkens T, Hoeksema MA, Beckers L, Smeets E, Meiler S, Levels J, Tjwa M, De Winther MPJ, Lutgens E. Hypercholesterolemia-induced priming of hematopoietic stem and progenitor cells aggravates atherosclerosis. *FASEB Journal*. 2014;28(5):2202–2213.

197. Cao W, Manicassamy S, Tang H, Kasturi SP, Pirani A, Murthy N, Pulendran B. Toll-like receptor-mediated induction of type I interferon in plasmacytoid dendritic cells requires the rapamycin-sensitive PI(3)K-mTOR-p70S6K pathway. *Nature Immunology*. 2008;9(10):1157–1164.
198. Shortman K, Heath WR. The CD8 + dendritic cell subset. *Immunological Reviews*. 2010;234(1):18–31.
199. Satpathy AT, Wu X, Albring JC, Murphy KM. Re(de)fining the dendritic cell lineage. *Nature Immunology*. 2012;13(12):1145–1154.
200. Katz JD, Ondr JK, Opoka RJ, Garcia Z, Janssen EM. Cutting Edge: Merocytic Dendritic Cells Break T Cell Tolerance to Cell Antigens in Nonobese Diabetic Mouse Diabetes. *The Journal of Immunology*. 2010;185(4):1999–2003.
201. Keating ST, Groh L, Thiem K, Bekkering S, Li Y, Matzaraki V, van der Heijden CDCC, van Puffelen JH, Lachmandas E, Jansen T, Oosting M, de Bree LCJ, Koeken VACM, Moorlag SJCFM, Mourits VP, et al. Rewiring of glucose metabolism defines trained immunity induced by oxidized low-density lipoprotein. *Journal of Molecular Medicine*. 2020;98(6):819–831.
202. Helft J, Böttcher J, Chakravarty P, Zelenay S, Huotari J, Schraml BU, Goubau D, Reis e Sousa C. GM-CSF Mouse Bone Marrow Cultures Comprise a Heterogeneous Population of CD11c+MHCII+ Macrophages and Dendritic Cells. *Immunity*. 2015;42(6):1197–1211.
203. Hole CR, Wager CML, Castro-Lopez N, Campuzano A, Cai H, Wozniak KL, Wang Y, Wormley FL. Induction of memory-like dendritic cell responses in vivo. *Nature Communications*. 2019;10(1):1–13.
204. Trottier MD, Naaz A, Li Y, Fraker PJ. Enhancement of hematopoiesis and lymphopoiesis in diet-induced obese mice. *Proceedings of the National Academy of Sciences of the United States of America*. 2012;109(20):7622–7629.
205. Edgar L, Akbar N, Braithwaite AT, Krausgruber T, Gallart-Ayala H, Bailey J, Corbin AL, Khoyratty TE, Chai JT, Alkhalil M, Rendeiro AF, Ziberna K, Arya R, Cahill TJ, Bock C, et al. Hyperglycaemia Induces Trained Immunity in Macrophages and Their Precursors and Promotes Atherosclerosis. *Circulation*. 2021;44(0).
206. Dobner J, Kaser S. Body mass index and the risk of infection - from underweight to obesity. *Clinical Microbiology and Infection*. 2018;24(1):24–28.
207. Van Der Valk FM, Bekkering S, Kroon J, Yeang C, Van Den Bossche J, Van Buul JD, Ravandi A, Nederveen AJ, Verberne HJ, Scipione C, Nieuwdorp M, Joosten LAB, Netea MG, Koschinsky ML, Witztum JL, et al. Oxidized phospholipids on Lipoprotein(a) elicit arterial wall inflammation and an inflammatory monocyte response in humans. *Circulation*. 2016;134(8).
208. Bekkering S, Arts RJW, Novakovic B, Kourtzelis I, van der Heijden CDCC, Li Y, Popa CD, ter Horst R, van Tuijl J, Netea-Maier RT, van de Veerdonk FL, Chavakis T, Joosten LAB, van der Meer JWM, Stunnenberg H, et al. Metabolic Induction of Trained Immunity through the Mevalonate Pathway. *Cell*. 2018;172(1–2):135-146.e9.
209. Bekkering S, Stiekema LCA, Bernelot Moens S, Verweij SL, Novakovic B, Prange K, Versloot M, Roeters van Lennep JE, Stunnenberg H, de Winther M, Stroes ESG, Joosten LAB, Netea MG, Riksen NP. Treatment with Statins Does Not Revert Trained Immunity in Patients with Familial Hypercholesterolemia. *Cell Metabolism*. 2019;30(1):1–2.

210. Tian M, Hao F, Jin X, Sun X, Jiang Y, Wang Y, Li D, Chang T, Zou Y, Peng P, Xia C, Liu J, Li Y, Wang P, Feng Y, et al. ACLY ubiquitination by CUL3-KLHL25 induces the reprogramming of fatty acid metabolism to facilitate iTreg differentiation. *eLife*. 2021;10:1–27.
211. Barrett TJ. Macrophages in Atherosclerosis Regression. *Arteriosclerosis, Thrombosis, and Vascular Biology*. 2020;40(1):20–33.
212. Bardin M, Pawelzik SC, Lagrange J, Mahdi A, Arnardottir H, Regnault V, Fève B, Lacolley P, Michel JB, Mercier N, Bäck M. The resolvin D2 – GPR18 axis is expressed in human coronary atherosclerosis and transduces atheroprotection in apolipoprotein E deficient mice. *Biochemical Pharmacology*. 2022;201(March):1–9.
213. Lee CH, Kim HJ, Lee YS, Kang GM, Lim HS, Lee S hwan, Song DK, Kwon O, Hwang I, Son M, Byun K, Sung YH, Kim S, Kim JB, Choi EY, et al. Hypothalamic Macrophage Inducible Nitric Oxide Synthase Mediates Obesity-Associated Hypothalamic Inflammation. *Cell Reports*. 2018;25(4):934-946.e5.
214. Bobryshev Y V., Ivanova EA, Chistiakov DA, Nikiforov NG, Orekhov AN. Macrophages and Their Role in Atherosclerosis: Pathophysiology and Transcriptome Analysis. *BioMed Research International*. 2016;2016(Figure 1).
215. Gencer S, Evans BR, Van Der Vorst EPC, Döring Y, Weber C. Inflammatory chemokines in atherosclerosis. *Cells*. 2021;10(2):1–26.
216. Virani SS, Alonso A, Benjamin EJ, Bittencourt MS, Callaway CW, Carson AP, Chamberlain AM, Chang AR, Cheng S, Delling FN, Djousse L, Elkind MSV, Ferguson JF, Fornage M, Khan SS, et al. *Heart disease and stroke statistics—2020 update a report from the American Heart Association*.; 2020.
217. Shabbir A, Rathod KS, Khambata RS, Ahluwalia A. Sex Differences in the Inflammatory Response: Pharmacological Opportunities for Therapeutics for Coronary Artery Disease. *Annual Review of Pharmacology and Toxicology*. 2021;61:333–359.
218. Hanke H, Kamenz J, Hanke S, Spiess J, Lenz C, Brehme U, Bruck B, Finking G, Hombach V. Effect of 17-β estradiol on pre-existing atherosclerotic lesions: Role of the endothelium. *Atherosclerosis*. 1999;147(1):123–132.
219. Rosenfeld ME, Kauser K, Martin-McNulty B, Polinsky P, Schwartz SM, Rubanyi GM. Estrogen inhibits the initiation of fatty streaks throughout the vasculature but does not inhibit intra-plaque hemorrhage and the progression of established lesions in apolipoprotein E deficient mice. *Atherosclerosis*. 2002;164(2):251–259.
220. Haarbo J, Christiansen C. The impact of female sex hormones on secondary prevention of atherosclerosis in ovariectomized cholesterol-fed rabbits. *Atherosclerosis*. 1996;123(1–2):139–144.
221. Luyer MDP, Khosla S, Owen WG, Miller VM. Prospective randomized study of effects of unopposed estrogen replacement therapy on markers of coagulation and inflammation in postmenopausal women. *Journal of Clinical Endocrinology and Metabolism*. 2001;86(8):3629–3634.
222. Manson JE, Allison MA, Rossouw JE, Carr JJ, Langer RD, Hsia J, Kuller LH, Cochrane BB, Hunt JR, Ludlam SE, Pettinger MB, Gass M, Margolis KL, Nathan L, Ockene JK, et al. Estrogen Therapy and Coronary-Artery Calcification. *New England Journal of Medicine*. 2007;356(25):2591–2602.

223. Nathan L, Shi W, Dinh H, Mukherjee TK, Wang X, Lusis AJ, Chaudhuri G. Testosterone inhibits early atherogenesis by conversion to estradiol: Critical role of aromatase. *Proceedings of the National Academy of Sciences of the United States of America*. 2001;98(6):3589–3593.
224. Grumbach MM, Auchus RJ. Estrogen: Consequences and implications of human mutations in synthesis and action. *Journal of Clinical Endocrinology and Metabolism*. 1999;84(12):4677–4694.
225. Xiong Y, Zhong Q, Palmer T, Benner A, Wang L, Suresh K, Damico R, D'Alessio FR. Estradiol resolves pneumonia via ERβ in regulatory T cells. *JCI Insight*. 2021;6(3).
226. Goodman WA, Bedoyan SM, Havran HL, Richardson B, Cameron MJ, Pizarro TT. Impaired estrogen signaling underlies regulatory T cell loss-of-function in the chronically inflamed intestine. *Proceedings of the National Academy of Sciences of the United States of America*. 2020;117(29):17166–17176.
227. Nakaya M, Tachibana H, Yamada K. Effect of estrogens on the interferon-γ producing cell population of mouse splenocytes. *Bioscience, Biotechnology and Biochemistry*. 2006;70(1):47–53.
228. Maret A, Coudert JD, Garidou L, Foucras G, Gourdy P, Krust A, Dupont S, Chambon P, Druet P, Bayard F, Guéry JC. Estradiol enhances primary antigen-specific CD4 T cell responses and Th1 development in vivo. Essential role of estrogen receptor α expression in hematopoietic cells. *European Journal of Immunology*. 2003;33(2):512–521.
229. Fijak M, Schneider E, Klug J, Bhushan S, Hackstein H, Schuler G, Wygrecka M, Gromoll J, Meinhardt A. Testosterone Replacement Effectively Inhibits the Development of Experimental Autoimmune Orchitis in Rats: Evidence for a Direct Role of Testosterone on Regulatory T Cell Expansion. *The Journal of Immunology*. 2011;186(9):5162–5172.
230. Gandhi VD, Cephus JY, Norlander AE, Chowdhury NU, Zhang J, Ceneviva ZJ, Tannous E, Polosukhin V V., Putz ND, Wickersham N, Singh A, Ware LB, Bastarache JA, Shaver CM, Chu HW, et al. Androgen receptor signaling promotes Treg suppressive function during allergic airway inflammation. *Journal of Clinical Investigation*. 2022;132(4):1–15.
231. Kissick HT, Sanda MG, Dunn LK, Pellegrini KL, On ST, Noel JK, Arredouani MS. Androgens alter T-cell immunity by inhibiting T-helper 1 differentiation. *Proceedings of the National Academy of Sciences of the United States of America*. 2014;111(27):9887–9892.
232. Zhu Y, Bian Z, Lu P, Karas RH, Bao L, Cox D, Hodgin J, Shaul PW, Thorén P, Smithies O, Gustafsson JÅ, Mendelsohn ME. Abnormal vascular function and hypertension in mice deficient in estrogen receptor β. *Science*. 2002;295(5554):505–508.
233. Sudhir K, Komesaroff PA. Clinical review 110: Cardiovascular actions of estrogens in men. *Journal of Clinical Endocrinology and Metabolism*. 1999;84(10):3411–3415.
234. Mendelsohn ME, Rosano GMC. Hormonal Regulation of Normal Vascular Tone in Males. *Circulation Research*. 2003;93(12):1142–1145.
235. Tai P, Wang J, Jin H, Song X, Yan J, Kang Y, Zhao L, An X, Du X, Chen X, Wang S, Xia G, Wang B. Induction of regulatory T cells by physiological level estrogen. *Journal of Cellular Physiology*. 2008;214(2):456–464.
236. Polanczyk MJ, Hopke C, Vandenbark AA, Offner H. Treg suppressive activity involves estrogen-dependent expression of programmed death-1 (PD-1). *International Immunology*. 2007;19(3):337–343.

237. Porbahaie M, Savelkoul HFJ, de Haan CAM, Teodorowicz M, van Neerven RJJ. Direct Binding of Bovine IgG-Containing Immune Complexes to Human Monocytes and Their Putative Role in Innate Immune Training. *Nutrients*. 2022;14(21).
238. Zhong Q, Gong F-Y, Gong Z, Hua S-H, Zeng K-Q, Gao X-M. IgG Immunocomplexes Sensitize Human Monocytes for Inflammatory Hyperactivity via Transcriptomic and Epigenetic Reprogramming in Rheumatoid Arthritis. *The Journal of Immunology*. 2018;200(12):3913–3925.
239. Dai X, Dai X, Gong Z, Yang C, Zeng K, Gong FY, Zhong Q, Gao XM. Disease-Specific Autoantibodies Induce Trained Immunity in RA Synovial Tissues and Its Gene Signature Correlates with the Response to Clinical Therapy. *Mediators of Inflammation*. 2020;2020.
240. Funes SC, Rios M, Fernández-Fierro A, Di Genaro MS, Kalergis AM. Trained Immunity Contribution to Autoimmune and Inflammatory Disorders. *Frontiers in Immunology*. 2022;13(April):1–15.
241. Yasuda K, Richez C, Maciaszek JW, Agrawal N, Akira S, Marshak-Rothstein A, Rifkin IR. Murine Dendritic Cell Type I IFN Production Induced by Human IgG-RNA Immune Complexes Is IFN Regulatory Factor (IRF)5 and IRF7 Dependent and Is Required for IL-6 Production. *The Journal of Immunology*. 2007;178(11):6876–6885.
242. Bonegio RG, Lin JD, Beaudette-Zlatanova B, York MR, Menn-Josephy H, Yasuda K. Lupus-Associated Immune Complexes Activate Human Neutrophils in an FcγRIIA-Dependent but TLR-Independent Response. *The Journal of Immunology*. 2019;202(3):675–683.
243. Grigoriou M, Banos A, Filia A, Pavlidis P, Giannouli S, Karali V, Nikolopoulos D, Pieta A, Bertsias G, Verginis P, Mitroulis I, Boumpas DT. Transcriptome reprogramming and myeloid skewing in haematopoietic stem and progenitor cells in systemic lupus erythematosus. *Annals of the Rheumatic Diseases*. 2019:242–253.
244. Witztum JL, Steinberg D. The oxidative modification hypothesis of atherosclerosis: Does it hold for humans? *Trends in Cardiovascular Medicine*. 2001;11(3–4):93–102.
245. Tulsyan N, Ouriel K, Kashyap VS. Emerging drugs in peripheral arterial disease. *Expert Opinion on Emerging Drugs*. 2006;11(1):75–90.
246. Liu F, Wang Y, Yu J. Role of inflammation and immune response in atherosclerosis: Mechanisms, modulations, and therapeutic targets. *Human Immunology*. 2023;(May).
247. Ridker PM, Everett BM, Thuren T, MacFadyen JG, Chang WH, Ballantyne C, Fonseca F, Nicolau J, Koenig W, Anker SD, Kastelein JJP, Cornel JH, Pais P, Pella D, Genest J, et al. Antiinflammatory therapy with canakinumab for atherosclerotic disease. *New England Journal of Medicine*. 2017;377(12):1119–1131.
248. Dunn J, Thabet S, Jo H. Flow-dependent epigenetic DNA methylation in endothelial gene expression and atherosclerosis. *Arteriosclerosis, Thrombosis, and Vascular Biology*. 2015;35(7):1562–1569.
249. Xu Y, Xu S, Liu P, Koroleva M, Zhang S, Si S, Jin ZG. Suberanilohydroxamic acid as a pharmacological Kruppel-like factor 2 activator that represses vascular inflammation and atherosclerosis. *Journal of the American Heart Association*. 2017;6(12).
250. Gatla HR, Muniraj N, Thevkar P, Yavvari S, Sukhavasi S, Makena MR. Regulation of chemokines and cytokines by histone deacetylases and an update on histone decetylase inhibitors in human diseases. *International Journal of Molecular Sciences*. 2019;20(5):1–27.

251. Michell DL, Faust A, Moore JL, Appleton BD, Ormseth M, Ramirez-Solano M, Sheng Q, Solus JF, Stein CM, Vickers KC, Major AS. Inhibition of miR-22-3p reduces kidney disease associated with systemic lupus erythematosus. *bioRxiv*. 2019.
252. Yurasov S, Wardemann H, Hammersen J, Tsuiji M, Meffre E, Pascual V, Nussenzweig MC. Defective B cell tolerance checkpoints in systemic lupus erythematosus. *Journal of Experimental Medicine*. 2005;201(5):703–711.
253. Bombardier C, Gladman DD, Urowitz MB, Caron D, Chang CH, Austin A, Bell A, Bloch DA, Corey PN, Decker JL, Esdaile J, Fries JF, Ginzler EM, Goldsmith CH, Hochberg MC, et al. Derivation of the sledai. A disease activity index for lupus patients. *Arthritis & Rheumatism*. 1992;35(6):630–640.
254. Bartel DP. MicroRNAs: Genomics, Biogenesis, Mechanism, and Function. *Cell*. 2004;116(2):281–297.
255. Bartel DP. MicroRNAs: Target Recognition and Regulatory Functions. *Cell*. 2009;136(2):215–233.
256. Shen N, Liang D, Tang Y, De Vries N, Tak PP. MicroRNAs-novel regulators of systemic lupus erythematosus pathogenesis. *Nature Reviews Rheumatology*. 2012;8(12):701–709.
257. Curtale G, Citarella F, Carissimi C, Goldoni M, Carucci N, Fulci V, Franceschini D, Meloni F, Barnaba V, Macino G. An emerging player in the adaptive immune response: MicroRNA-146a is a modulator of IL-2 expression and activation-induced cell death in T lymphocytes. *Blood*. 2010;115(2):265–273.
258. Tang Y, Luo X, Cui H, Ni X, Yuan M, Guo Y, Huang X, Zhou H, de Vries N, Tak PP, Chen S, Shen N. MicroRNA-146a contributes to abnormal activation of the type I interferon pathway in human lupus by targeting the key signaling proteins. *Arthritis & Rheumatism*. 2009;60(4):1065–1075.
259. Fayyad-Kazan H, Rouas R, Fayyad-Kazan M, Badran R, El Zein N, Lewalle P, Najar M, Hamade E, Jebbawi F, Merimi M, Romero P, Burny A, Badran B, Martiat P. MicroRNA profile of circulating CD4-positive regulatory T cells in human adults and impact of differentially expressed microRNAs on expression of two genes essential to their function. *Journal of Biological Chemistry*. 2012;287(13):9910–9922.
260. Xiao C, Srinivasan L, Calado DP, Patterson HC, Zhang B, Wang J, Henderson JM, Kutok JL, Rajewsky K. Lymphoproliferative disease and autoimmunity in mice with increased miR-17-92 expression in lymphocytes. *Nature Immunology*. 2008;9(4):405–414.
261. Jiang S, Li C, Olive V, Lykken E, Feng F, Sevilla J, Wan Y, He L, Li Q. Molecular dissection of the miR-17-92 cluster's critical dual roles in promoting Th1 responses and preventing inducible Treg differentiation. *Blood*. 2011;118(20):5487–5497.
262. Kim B-S, Jung J-Y, Jeon J-Y, Kim H-A, Suh C-H. Circulating hsa-miR-30e-5p, hsa-miR-92a-3p, and hsa-miR-223-3p may be novel biomarkers in systemic lupus erythematosus. *HLA*. 2016;88(4):187–193.
263. Carlsen AL, Schetter AJ, Nielsen CT, Lood C, Knudsen S, Voss A, Harris CC, Hellmark T, Segelmark M, Jacobsen S, Bengtsson AA, Heegaard NHH. Circulating MicroRNA Expression Profiles Associated With Systemic Lupus Erythematosus. *Arthritis & Rheumatism*. 2013;65(5):1324–1334.

264. Chung CP, Oeser A, Raggi P, Gebretsadik T, Shintani AK, Sokka T, Pincus T, Avalos I, Stein CM. Increased coronary-artery atherosclerosis in rheumatoid arthritis: Relationship to disease duration and cardiovascular risk factors. *Arthritis & Rheumatism*. 2005;52(10):3045–3053.
265. Asanuma Y, Oeser A, Shintani AK, Turner E, Olsen N, Fazio S, Linton MF, Raggi P, Stein CM. Premature coronary-artery atherosclerosis in systemic lupus erythematosus. *The New England journal of medicine*. 2003;349(25):2407–15.
266. Bombardier C, Gladman DD, Urowitz MB, Caron D, Chang CH, Austin A, Bell A, Bloch DA, Corey PN, Decker JL, Esdaile J, Fries JF, Ginzler EM, Goldsmith CH, Hochberg MC, et al. Derivation of the sledai. A disease activity index for lupus patients. *Arthritis & Rheumatism*. 1992;35(6):630–640.
267. Gladman D, Ginzler E, Goldsmith C, Fortin P, Liang M, Sanchez-Guerrero J, Urowitz M, Bacon P, Bombardieri S, Hanly J, Jones J, Hay E, Symmons D, Isenberg D, Kalunion K, et al. The development and initial validation of the systemic lupus international collaborating clinics/American college of rheumatology damage index for systemic lupus erythematosus. *Arthritis & Rheumatism*. 1996;39(3):363–369.
268. Michell DL, Allen RM, Landstreet SR, Zhao S, Toth CL, Sheng Q, Vickers KC. Isolation of high-density lipoproteins for non-coding small RNA quantification. *Journal of Visualized Experiments*. 2016;2016(117):1–9.
269. Allen RM, Zhao S, Ramirez Solano MA, Zhu W, Michell DL, Wang Y, Shyr Y, Sethupathy P, Linton MF, Graf GA, Sheng Q, Vickers KC. Bioinformatic analysis of endogenous and exogenous small RNAs on lipoproteins. *Journal of Extracellular Vesicles*. 2018;7(1).
270. Love MI, Huber W, Anders S. Moderated estimation of fold change and dispersion for RNA-seq data with DESeq2. *Genome Biology*. 2014;15(12):550.
271. Morel L, Croker BP, Blenman KR, Mohan C, Huang G, Gilkeson G, Wakeland EK. Genetic reconstitution of systemic lupus erythematosus immunopathology with polycongenic murine strains. *Proceedings of the National Academy of Sciences*. 2000;97(12):6670–6675.
272. Steiner DF, Thomas MF, Hu JK, Yang Z, Babiarz JE, Allen CDC, Matloubian M, Blelloch R, Ansel KM. MicroRNA-29 Regulates T-Box Transcription Factors and Interferon-γ Production in Helper T Cells. *Immunity*. 2011;35(2):169–181.
273. Wu X, Ye Y, Niu J, Li Y, Li X, You X, Chen H, Zhao L, Zeng X, Zhang F, Tang F, He W, Cao X, Zhang X, Lipsky PE. Defective PTEN regulation contributes to B cell hyperresponsiveness in systemic lupus erythematosus. *Science Translational Medicine*. 2014;6(246).
274. Zhang Y, Zhao S, Wu D, Liu X, Shi M, Wang Y, Zhang F, Ding J, Xiao Y, Guo B. MicroRNA-22 promotes renal tubulointerstitial fibrosis by targeting PTEN and suppressing autophagy in diabetic nephropathy. *Journal of Diabetes Research*. 2018;2018.
275. Palacios F, Prieto D, Abreu C, Ruiz S, Morande P, Fernández-Calero T, Libisch G, Landoni AI, Oppezzo P. Dissecting chronic lymphocytic leukemia microenvironment signals in patients with unmutated disease: MicroRNA-22 regulates phosphatase and tensin homolog/AKT/FOXO1 pathway in proliferative leukemic cells. *Leukemia and Lymphoma*. 2015;56(5):1560–1565.
276. Budagyan VM, Bulanova EG, Sharova NI, Nikonova MF, Stanislav ML, Yarylin AA. The resistance of activated T-cells from SLE patients to apoptosis induced by human thymic stromal cells. *Immunology Letters*. 1998;60(1):1–5.
277. Liarski VM, Kaverina N, Chang A, Brandt D, Yanez D, Talasnik L, Carlesso G, Herbst R, Utset TO, Labno C, Peng Y, Jiang Y, Giger ML, Clark MR. Cell distance mapping identifies

functional T follicular helper cells in inflamed human renal tissue. *Science Translational Medicine*. 2014;6(230):1–12.
278. Bubier JA, Sproule TJ, Foreman O, Spolski R, Shaffer DJ, Morse HC, Leonard WJ, Roopenian DC. A critical role for IL-21 receptor signaling in the pathogenesis of systemic lupus erythematosus in BXSB-Yaa mice. *Proceedings of the National Academy of Sciences of the United States of America*. 2009;106(5):1518–1523.
279. Choi JY, Ho JHE, Pasoto SG, Bunin V, Kim ST, Carrasco S, Borba EF, Gonçalves CR, Costa PR, Kallas EG, Bonfa E, Craft J. Circulating follicular helper-like T cells in systemic lupus erythematosus: Association with disease activity. *Arthritis and Rheumatology*. 2015;67(4):988–999.
280. Choi S-C, Hutchinson TE, Titov AA, Seay HR, Li S, Brusko TM, Croker BP, Salek-Ardakani S, Morel L. The Lupus Susceptibility Gene Pbx1 Regulates the Balance between Follicular Helper T Cell and Regulatory T Cell Differentiation. *The Journal of Immunology*. 2016;197(2):458–469.
281. Linterman MA, Pierson W, Lee SK, Kallies A, Kawamoto S, Rayner TF, Srivastava M, Divekar DP, Beaton L, Hogan JJ, Fagarasan S, Liston A, Smith KGC, Vinuesa CG. Foxp3+ follicular regulatory T cells control the germinal center response. *Nature Medicine*. 2011;17(8):975–982.
282. Pisetsky DS. Anti-DNA antibodies - Quintessential biomarkers of SLE. *Nature Reviews Rheumatology*. 2016;12(2):102–110.
283. Cervera R, Khamashta MA, Font J, Sebastiani GD, Gil A, Lavilla P, Mejía JC, Aydintug AO, Chwalinska-Sadowska H, De Ramón E, Fernández-Nebro A, Galeazzi M, Valen M, Mathieu A, Houssiau F, et al. Morbidity and mortality in systemic lupus erythematosus during a 10-year period: A comparison of early and late manifestations in a cohort of 1,000 patients. *Medicine*. 2003;82(5):299–308.
284. Lee SK, Silva DG, Martin JL, Pratama A, Hu X, Chang PP, Walters G, Vinuesa CG. Interferon-γ Excess Leads to Pathogenic Accumulation of Follicular Helper T Cells and Germinal Centers. *Immunity*. 2012;37(5):880–892.
285. Masutani K, Akahoshi M, Tsuruya K, Tokumoto M, Ninomiya T, Kohsaka T, Fukuda K, Kanai H, Nakashima H, Otsuka T, Hirakata H. Predominance of Th1 Immune Response in Diffuse Proliferative Lupus Nephritis. *Arthritis and Rheumatism*. 2001;44(9):2097–2106.
286. Wadwa M, Klopfleisch R, Adamczyk A, Frede A, Pastille E, Mahnke K, Hansen W, Geffers R, Lang KS, Buer J, Büning J, Westendorf AM. IL-10 downregulates CXCR3 expression on Th1 cells and interferes with their migration to intestinal inflammatory sites. *Mucosal Immunology*. 2016;9(5):1263–1277.
287. Enghard P, Langnickel D, Riemekasten G. T cell cytokine imbalance towards production of IFN-γ and IL-10 in NZB/W F1 lupus-prone mice is associated with autoantibody levels and nephritis. *Scandinavian Journal of Rheumatology*. 2006;35(3):209–216.
288. Gaublomme JT, Yosef N, Lee Y, Gertner RS, Yang L V., Wu C, Pandolfi PP, Mak T, Satija R, Shalek AK, Kuchroo VK, Park H, Regev A. Single-Cell Genomics Unveils Critical Regulators of Th17 Cell Pathogenicity. *Cell*. 2015;163(6):1400–1412.
289. Facciotti F, Larghi P, Bosotti R, Vasco C, Gagliani N, Cordiglieri C, Mazzara S, Ranzani V, Rottoli E, Curti S, Penatti A, Karnani B, Kobayashi Y, Crosti M, Bombaci M, et al. Evidence for a pathogenic role of extrafollicular, IL-10-producing CCR6+B helper T cells in systemic lupus erythematosus. *Proceedings of the National Academy of Sciences of the United States of America*. 2020;117(13):7305–7316.

290. Kühn R, Löhler J, Rennick D, Rajewsky K, Müller W. Interleukin-10-deficient mice develop chronic enterocolitis. *Cell*. 1993;75(2):263–274.
291. Roers A, Siewe L, Strittmatter E, Deckert M, Schlüter D, Stenzel W, Gruber AD, Krieg T, Rajewsky K, Müller W. T cell-specific inactivation of the interleukin 10 gene in mice results in enhanced T cell responses but normal innate responses to lipopolysaccharide or skin irritation. *Journal of Experimental Medicine*. 2004;200(10):1289–1297.
292. Rojas OL, Pröbstel AK, Porfilio EA, Wang AA, Charabati M, Sun T, Lee DSW, Galicia G, Ramaglia V, Ward LA, Leung LYT, Najafi G, Khaleghi K, Garcillán B, Li A, et al. Recirculating Intestinal IgA-Producing Cells Regulate Neuroinflammation via IL-10. *Cell*. 2019;176(3):610-624.e18.
293. Baglaenko Y, Manion KP, Chang NH, Gracey E, Loh C, Wither JE. IL-10 production is critical for sustaining the expansion of CD5+ B and NKT cells and restraining autoantibody production in congenic lupus-prone mice. *PLoS ONE*. 2016;11(3):1–16.
294. Mei H-Y, Liu J, Shen X-P, Wu R. A novel circRNA, circRACGAP1, hampers the progression of systemic lupus erythematosus via miR-22-3p-mediated AKT signalling. *Autoimmunity*. 2022;55(6):360–370.
295. Su Y-J, Tsai N-W, Kung C-T, Wang H-C, Lin W-C, Huang C-C, Chang Y-T, Su C-M, Chiang Y-F, Cheng B-C, Lin Y-J, Lu C-H. Investigation of MicroRNA in Mitochondrial Apoptotic Pathway in Systemic Lupus Erythematosus. *BioMed Research International*. 2018;2018:1–8.
296. Selbach M, Schwanhäusser B, Thierfelder N, Fang Z, Khanin R, Rajewsky N. Widespread changes in protein synthesis induced by microRNAs. *Nature*. 2008;455(7209):58–63.
297. Baek D, Villén J, Shin C, Camargo FD, Gygi SP, Bartel DP. The impact of microRNAs on protein output. *Nature*. 2008;455(7209):64–71.
298. Garchow BG, Bartulos Encinas O, Leung YT, Tsao PY, Eisenberg RA, Caricchio R, Obad S, Petri A, Kauppinen S, Kiriakidou M. Silencing of microRNA-21 in vivo ameliorates autoimmune splenomegaly in lupus mice. *EMBO Molecular Medicine*. 2011;3(10):605–615.
299. Xia Y, Tao JH, Fang X, Xiang N, Dai XJ, Jin L, Li XM, Wang YP, Li XP. MicroRNA-326 Upregulates B Cell Activity and Autoantibody Production in Lupus Disease of MRL/lpr Mice. *Molecular Therapy - Nucleic Acids*. 2018;11(17):284–291.
300. Lech M, Anders HJ. The pathogenesis of lupus nephritis. *Journal of the American Society of Nephrology*. 2013;24(9):1357–1366.
301. Bao L, Cunningham PN, Quigg RJ. Complement in Lupus Nephritis: New Perspectives. *Kidney Diseases*. 2015;1(2):91–99.
302. Coxon A, Cullere X, Knight S, Sethi S, Wakelin MW, Stavrakis G, Luscinskas FW, Mayadas TN. FcγRIII mediates neutrophil recruitment to immune complexes: A mechanism for neutrophil accumulation in immune-mediated inflammation. *Immunity*. 2001;14(6):693–704.
303. Allam R, Lichtnekert J, Moll AG, Taubitz A, Vielhauer V, Anders HJ. Viral RNA and DNA trigger common antiviral responses in mesangial cells. *Journal of the American Society of Nephrology*. 2009;20(9):1986–1996.
304. Piantoni S, Regola F, Zanola A, Andreoli L, Dall'Ara F, Tincani A, Airo' P. Effector T-cells are expanded in systemic lupus erythematosus patients with high disease activity and damage indexes. *Lupus*. 2018;27(1):143–149.

305. Fritsch RD, Shen X, Illei GG, Yarboro CH, Prussin C, Hathcock KS, Hodes RJ, Lipsky PE. Abnormal differentiation of memory T cells in systemic lupus erythematosus. *Arthritis & Rheumatism*. 2006;54(7):2184–2197.
306. Schneider WM, Chevillotte MD, Rice CM. Interferon-stimulated genes: A complex web of host defenses. *Annual Review of Immunology*. 2014;32:513–545.
307. Afkarian M, Sedy JR, Yang J, Jacobson NG, Cereb N, Yang SY, Murphy TL, Murphy KM. T-bet is a STATI-induced regulator for IL-12R expression in naïve CD4+ T cells. *Nature Immunology*. 2002;3(6):549–557.
308. Szabo SJ, Kim ST, Costa GL, Zhang X, Fathman CG, Glimcher LH. A novel transcription factor, T-bet, directs Th1 lineage commitment. *Cell*. 2000;100(6):655–669.
309. Theofilopoulos AN, Koundouris S, Kono DH, Lawson BR. The role of IFN-gamma in systemic lupus erythematosus: a challenge to the Th1/Th2 paradigm in autoimmunity. *Arthritis research*. 2001;3(3):136–41.
310. Seery JP, Carroll JM, Cattell V, Watt FM. Antinuclear autoantibodies and lupus nephritis in transgenic mice expressing interferon γ in the epidermis. *Journal of Experimental Medicine*. 1997;186(9):1451–1459.
311. Rossi RL, Rossetti G, Wenandy L, Curti S, Ripamonti A, Bonnal RJP, Birolo RS, Moro M, Crosti MC, Gruarin P, Maglie S, Marabita F, Mascheroni D, Parente V, Comelli M, et al. Distinct microRNA signatures in human lymphocyte subsets and enforcement of the naive state in CD4+ T cells by the microRNA miR-125b. *Nature Immunology*. 2011;12(8):796–803.
312. Steiner DF, Thomas MF, Hu JK, Yang Z, Babiarz JE, Allen CDC, Matloubian M, Blelloch R, Ansel KM. MicroRNA-29 Regulates T-Box Transcription Factors and Interferon-γ Production in Helper T Cells. *Immunity*. 2011;35(2):169–181.
313. Miyara M, Amoura Z, Parizot C, Badoual C, Dorgham K, Trad S, Nochy D, Debre P, Piette J-C, Gorochov G. Global Natural Regulatory T Cell Depletion in Active Systemic Lupus Erythematosus. *The Journal of Immunology*. 2005;175(12):8392–8400.
314. Lee JH, Wang LC, Lin YT, Yang YH, Lin DT, Chiang BL. Inverse correlation between CD4+ regulatory T-cell population and autoantibody levels in paediatric patients with systemic lupus erythematosus. *Immunology*. 2006;117(2):280–286.
315. Valencia X, Yarboro C, Illei G, Lipsky PE. Deficient CD4+CD25high T Regulatory Cell Function in Patients with Active Systemic Lupus Erythematosus. *The Journal of Immunology*. 2007;178(4):2579–2588.
316. Divekar AA, Dubey S, Gangalum PR, Singh RR. Dicer Insufficiency and MicroRNA-155 Overexpression in Lupus Regulatory T Cells: An Apparent Paradox in the Setting of an Inflammatory Milieu. *The Journal of Immunology*. 2011;186(2):924–930.
317. Scalapino KJ, Tang Q, Bluestone JA, Bonyhadi ML, Daikh DI. Suppression of disease in New Zealand Black/New Zealand White lupus-prone mice by adoptive transfer of ex vivo expanded regulatory T cells. *Journal of Immunology*. 2006;177(3):1451–1459.
318. Bagavant H, Tung KSK. Failure of CD25+ T cells from lupus-prone mice to suppress lupus glomerulonephritis and sialoadenitis. *Journal of immunology (Baltimore, Md. : 1950)*. 2005;175(2):944–50.
319. Cobb BS, Hertweck A, Smith J, O'Connor E, Graf D, Cook T, Smale ST, Sakaguchi S, Livesey FJ, Fisher AG, Merkenschlager M. A role for Dicer in immune regulation. *Journal of Experimental Medicine*. 2006;203(11):2519–2527.

320. De Santis G, Ferracin M, Biondani A, Caniatti L, Rosaria Tola M, Castellazzi M, Zagatti B, Battistini L, Borsellino G, Fainardi E, Gavioli R, Negrini M, Furlan R, Granieri E. Altered miRNA expression in T regulatory cells in course of multiple sclerosis. *Journal of Neuroimmunology*. 2010;226(1–2):165–171.
321. Lu W, You R, Yuan X, Yang T, Samuel ELG, Marcano DC, Sikkema WKA, M. Tour J, Rodriguez A, Kheradmand F, Corry DB. The microRNA miR-22 inhibits the histone deacetylase HDAC4 to promote TH17 cell-dependent emphysema. *Nature Immunology*. 2015;16(11):1185–1194.
322. Zhang L, Yang P, Wang J, Liu Q, Wang T, Wang Y, Lin F. MiR-22 regulated T cell differentiation and hepatocellular carcinoma growth by directly targeting Jarid2. *American journal of cancer research*. 2021;11(5):2159–2173.
323. Wang L, Qiu R, Zhang Z, Han Z, Yao C, Hou G, Dai D, Jin W, Tang Y, Yu X, Shen N. The MicroRNA miR-22 Represses Th17 Cell Pathogenicity by Targeting PTEN-Regulated Pathways. Xu Z, ed. *ImmunoHorizons*. 2020;4(6):308–318.
324. Hu Y, Setayesh T, Vaziri F, Wu X, Hwang ST, Chen X, Yvonne Wan YJ. miR-22 gene therapy treats HCC by promoting anti-tumor immunity and enhancing metabolism. *Molecular Therapy*. 2023;31(6):1829–1845.
325. McGeachy MJ, Bak-Jensen KS, Chen Y, Tato CM, Blumenschein W, McClanahan T, Cua DJ. TGF-β and IL-6 drive the production of IL-17 and IL-10 by T cells and restrain TH-17 cell-mediated pathology. *Nature Immunology*. 2007;8(12):1390–1397.
326. Ghoreschi K, Laurence A, Yang X-P, Tato CM, McGeachy MJ, Konkel JE, Ramos HL, Wei L, Davidson TS, Bouladoux N, Grainger JR, Chen Q, Kanno Y, Watford WT, Sun H-W, et al. Generation of pathogenic TH17 cells in the absence of TGF-β signalling. *Nature*. 2010;467(7318):967–971.
327. Lee Y, Awasthi A, Yosef N, Quintana FJ, Xiao S, Peters A, Wu C, Kleinewietfeld M, Kunder S, Hafler DA, Sobel RA, Regev A, Kuchroo VK. Induction and molecular signature of pathogenic TH17 cells. *Nature Immunology*. 2012;13(10):991–999.
328. Lewis BP, Burge CB, Bartel DP. Conserved seed pairing, often flanked by adenosines, indicates that thousands of human genes are microRNA targets. *Cell*. 2005;120(1):15–20.
329. Agarwal V, Bell GW, Nam JW, Bartel DP. Predicting effective microRNA target sites in mammalian mRNAs. *eLife*. 2015;4(AUGUST2015):1–38.
330. Shrestha S, Yang K, Guy C, Vogel P, Neale G, Chi H. Treg cells require the phosphatase PTEN to restrain TH1 and TFH cell responses. *Nature Immunology*. 2015;16(2):178–187.
331. Kamitani S, Togi S, Ikeda O, Nakasuji M, Sakauchi A, Sekine Y, Muromoto R, Oritani K, Matsuda T. Kruppel-Associated Box-Associated Protein 1 Negatively Regulates TNF- -Induced NF- B Transcriptional Activity by Influencing the Interactions among STAT3, p300, and NF- B/p65. *The Journal of Immunology*. 2011;187(5):2476–2483.
332. Tanaka S, Pfleger C, Lai JF, Roan F, Sun SC, Ziegler SF. KAP1 Regulates Regulatory T Cell Function and Proliferation in Both Foxp3-Dependent and -Independent Manners. *Cell Reports*. 2018;23(3):796–807.